An Experimental Study on Exhaust Emissions Abatement in Marine Diesel Engines with a Wet Scrubber System

School of Engineering

Thesis submitted by

Terence, Yuen Yeen Chin

For the Degree of Doctor of Philosophy

Newcastle University

Mar 2023

Abstract

Experimental studies were performed for the simultaneous removal of SO_2 and NO_x from simulated exhaust gas using a laboratory-based custom-designed wet scrubber, with detailed analysis on both the gaseous and aqueous components. In the initial phase, a range of chemical compounds with potential for commercial application, namely, seawater, NaOH, NaClO, $NaClO_2$, H_2O_2 and $KMnO_4$, were studied to establish the various reaction mechanisms at play. It was found that the absorption of SO_2 in the aqueous phase was influenced by three prominent factors: pH, ionic concentration and redox potential. Experimental results showed that for NO_x removal, effectiveness of the various substances studied can be ranked from least to most effective as follows: Seawater, NaOH, H_2O_2 < NaClO < $KMnO_4$ < $NaClO_2$. This effectiveness was found to be influenced by the substance's ability to oxidize NO to NO_2, absorb the NO_2 that was formed and retaining the nitrogen in the aqueous phase. High oxidation potential promoted the oxidation of NO to NO_2 but hindered the absorption of NO_2.

The initial phase showed that $NaClO_2$ was most viable and subsequent work focused on this compound. When used for NO_x removal, it was shown that the first step of the removal mechanism involving the oxidation of NO to NO_2 was the fast step while the second step involving the absorption of NO_2 was the rate determining step. Alternative pathways to enhance NO_2 removal were considered and the usage of a reducing agent was shown to be the most promising. Various sulfur-based reducing agents were reviewed from literature before narrowing to sodium sulfite and sodium thiosulfate. It was shown that although sulfite was around 15% more effective than thiosulfate in NO_2 removal, its consumption rate was more by a factor of 100 when compared to thiosulfate – this was because sulfite was unstable in a high oxygen environment and a significant amount was lost through oxidation to form sulfate. Usage of formaldehyde (1% v/v) as a stabilizing agent reduced sulfite consumption significantly, from 14.2 to 3.2 mol of reactant consumed per mol of NO_x pollutant removed. However, this was still poor compared to thiosulfate where only around 0.10 to 0.20 mol were consumed per mole of pollutant removed.

A novel wet scrubbing system comprising of an oxidation and a reducing section arranged in series proposed in this study demonstrated significant improvement over a conventional wet scrubbing system of equivalent specifications with just oxidation/absorption. At a *L/G* ratio of 15, NO_x removal was improved up to 20%, reactants consumed were reduced by up to 25%, and the formation of nitrite and nitrates in the aqueous phase were lowered by about 30% due to more of the NO_2 being reduced to N_2. The optimal pH values in the oxidizing and reducing sections of the wet scrubber in order to achieve the least aqueous nitrogen formation, lowest

reaction consumption rate and avoidance of precipitation were determined to be pH 10 to 12. At pH 12, the high alkaline condition in the reducing section of the wet scrubber was able to convert CO_2 to carbonates through absorption and neutralization, thereby enabling a partial CO_2 capture of approximately 4 – 5% being achieved in the system. Finally, results from thermodynamic models derived from the Metso Outotec HSC Chemistry software showed good agreement with the various experimental results shown here.

Acknowledgements

I would first like to thank my supervisors, Dr. Ivan Tam and Dr. Chun-Yang Yin. This endeavour would not have happened if my supervisor, Ivan, had not taken the trouble to meet with me over lunch to share about the process and journey of a part-time PhD student for a full-time working adult. Over the years, he has proven to be an excellent facilitator in helping me complete this journey. Not forgetting Yin, whom with over many late-night email exchanges, has taught me the correct mindset to adopt in order to navigate through the journal publication process, and also for giving me encouragement and confidence through dark and uncertain days.

I would not be able to do this without the support of my school management and colleagues at Nanyang Polytechnic, in particular Alvin, Zul, and Jeffrey for their constant encouragement and understanding. Also not forgetting Joshua, for the gas cylinders purchasing support and providing company around the lab through many impromptu chats, and Gia Wen who has always been generous with the her equipment and consumables! A big thank you to Mia Eng too, for being my big sister on campus all these years.

Like the many blessings I've received in life, I also owe this to my mum for her constant encouragement and prayers, especially through difficult times. A big thank you to Leia and Zac for your prayers and encouragement too – although I know the two of you are probably too young now to really understand this journey that Papa has taken. Lastly, I dedicate this to my wife, Elsa, for giving me her blessings to embark on this journey and for all her sacrifices all these years to keep to the family going. Thank you for journeying with me all the way.

To the author and perfector of my faith, may I never forget that all I have comes from you, and that my heart will be forever restless till it finds its rest in you.

List of publications

Chin, T., Tam, I. and Yin, C.Y. (2023), Wet Scrubbing Process with Oxidation and Reduction in Series for Removal of SO_2 and NO from Marine Diesel Engine Exhaust. *Chemical Engineering Journa*l, 464, 142299.

Chin, T., Tam, I.C. and Yin, C.Y. (2022), Comparison of various chemical compounds for the removal of SO_2 and NO_x with wet scrubbing for marine diesel engines. *Environmental Science and Pollution Research*, 29 (6), pp. 8873–8891.

List of presentations

Reducing Marine Emissions with the Simultaneous Removal of SO_x and NO_x using a Wet Scrubber, *Postgraduate Research Conference*, Newcastle Research & Innovation Institute, Singapore, 28 Jun 2018.

Project proposal: Reducing Shipping Emissions with an Integrated Wet Scrubbing Process, *Postgraduate Research Retreat*, Newcastle Research & Innovation Institute, Singapore, 14 Jun 2016 (Received Best Presentation Award).

Reducing Shipping Emissions with an Integrated Wet Scrubbing Process, *Postgraduate Immersion Programme,* Newcastle University, United Kingdom, 18 Mar 2016.

Table of Content

Abstract i

Acknowledgements iii

List of publications iv

Table of Content v

List of Figures x

List of Tables xvii

Nomenclature xix

Symbols xix

Chapter 1. Introduction 1

1.1. Background 1

1.2. Research motivations 2

1.3. Aims and Objectives 3

Chapter 2. Literature Review 4

2.1. Regulations for marine emissions 4

2.1.1. Regulations concerning SO_x and PM emissions 4

2.1.2. Regulations concerning NO_x emission 5

2.1.3. Regulations concerning washwater discharge from ships 6

2.2. Existing solutions in the marine sector 8

2.2.1. Existing solutions for sulfur oxides 8

2.2.2. Existing solutions for nitrogen oxides 9

2.3. Emerging technologies for simultaneous removal of SO_x and NO_x 11

2.3.1. Usage of dry sorbents 11

2.3.2. Usage of catalysis 12

2.3.3. Engine-Modifications 12

2.3.4. Gas-Liquid Reaction Approach 13

2.4. Usage of alternative fuel 15

2.4.1. Liquified natural gas (LNG) 15

2.4.2. Liquified Petroleum Gas (LPG) 16
2.4.3. Methanol 16
2.4.4. Biodiesel 16
2.4.5. Hydrogen 17
2.4.6. Ammonia 17
Chapter 3. Experimental Setup and Procedures 19
3.1. Materials 19
3.1.1. Chemicals used 19
3.1.2. Calibration standards 19
3.1.3. Gases 19
3.2. Equipment 20
3.2.1. Gas-liquid reactors used for wet scrubbing 20
3.2.2. Gas handling equipment 21
3.2.3. Liquid handling equipment 23
3.2.4. Equipment for aqueous analysis 23
3.3. Calculations 24
Chapter 4. Comparison of various chemical compounds for SO_2 and NO removal 25
4.1. A preliminary setup using a gas bubbling reactor 25
4.1.1. Experimental procedure 26
4.1.2. Mixing study of the gas bubbling reactor 28
4.1.3. Variation of liquid volume used for reaction 29
4.1.4. Variation of chemical compounds for NO removal 29
4.1.5. Variation of $NaClO_2$ concentration 31
4.1.6. Variation of $NaClO_2$ pH 34
4.1.7. Variation of $KMnO_4$ concentration 34
4.1.8. Variation of $KMnO_4$ pH 36
4.1.9. Double train gas bubbling reactors using $NaClO_2$ 37
4.2. Gas-liquid reaction using a counter-current wet scrubber 39

4.2.1. Experimental Procedure 39
4.2.2. Removal of sulfur dioxide (SO_2) 42
4.2.3. Removal of nitrogen oxides (NO_x) 45
4.2.4. Aqueous analysis of the wet scrubbing liquid 57
4.2.5. Scalability 62
4.3. Summary 63
Chapter 5. Counter current wet scrubber with sodium chlorite 66
5.1. Effect of carbon dioxide presence in the exhaust gas 66
5.2. Effect of pH adjustment with sodium hydroxide 71
5.3. Improving the removal of NO_2 in the counter-current wet scrubber 74
5.3.1. Removal of NO_2 using various types of chemical compounds 75
5.3.2. Reaction mechanisms of NO_2 in the presence of reducing agents 79
5.3.3. Removal of NO_2 with variation of sodium thiosulfate concentration 81
5.3.4. Variation of NO to NO_2 ratio in the exhaust gas 84
5.4. Summary 87
Chapter 6. Wet scrubbing with oxidation and reduction in series 88
6.1. Experimental procedure 88
6.2. Thermodynamic Analysis 93
6.2.1. Oxidation reduction potential versus pH diagrams 93
6.2.2. Sulfur system 94
6.2.3. Nitrogen system 96
6.2.4. Chlorine System 98
6.2.5. Carbon system 99
6.3. Oxidation in a half-height wet scrubber 100
6.3.1. Variation in pH 100
6.3.2. Variation of oxidant concentration 103
6.3.3. Variation of oxidation reduction potential (ORP) 105
6.4. Reduction with a half-height scrubber 106

6.4.1. Variation on reductant concentration 106
6.4.2. Variation of pH 109
6.4.3. Effect of using a packed column configuration 112
6.4.4. Comparison between thiosulfate and sulfite as reducing agents 114
6.4.5. Absorption of carbon dioxide 115
6.5. Reaction in a full height wet scrubber with oxidation only 116
6.5.1. Gaseous pollutant removal 116
6.5.2. Aqueous Analysis 117
6.6. Reaction in a full height wet scrubber with oxidation and reduction in series 119
6.6.1. Gaseous pollutant removal 119
6.6.2. Aqueous analysis 120
6.6.3. Improving the removal efficiency of the oxidation and reduction system 122
6.6.4. Absorption of carbon dioxide 123
6.7. Effect of temperature 124
6.8. Considerations for scrubber washwater discharge in the ocean 129
6.9. Mass balance considerations 130
6.9.1. Chlorine balance 130
6.9.2. Nitrogen balance 132
6.9.3. Sulfur balance 133
6.10. Summary 133
Chapter 7. Reaction kinetics and mass transfer considerations 135
7.1. Reaction kinetics considerations 135
7.1.1. Wet scrubbing with oxidation 135
7.1.2. Wet scrubbing with reduction 143
7.2. Mass transfer considerations 151
7.2.1. Full height scrubber with oxidation only 152
7.2.2. Full height scrubber with oxidation and reduction in series 157
7.3. Summary 159

Chapter 8. Conclusions and Recommendations 160

8.1. Conclusions 160

8.2. Recommendations for future work 163

References 164

Appendices 173

Appendix A: Conversion of NO_x emission limits from g/kWh to NO_x concentration based on ship engine type 173

Appendix B: Estimation of potential CO_2 that can be removed on a two-week journey based on a typical slow-speed, large diesel engine 176

Appendix C: Calculation related to discharge of washwater containing nitrate, based on a typical slow-speed large diesel ship engine 177

Appendix D: Calculation of rate of change of SO_2, NO and NO_2 removal during wet scrubbing 179

Appendix E: Calculation of rate of change of SO_2, NO and NO_2 gases during wet scrubbing 179

Appendix F: Calculation of concentration of species A in the aqueous phase based on the equilibrium with its partial pressure using Henry's Law 180

List of Figures

Figure 3-1: The gas bubbling reactor used in this study. 20
Figure 3-2: The schematic diagram of the counter-current glass wet scrubber with adjustable height. 22
Figure 4-1: Schematic diagram of the experimental setup using the gas bubbling reactor. 26
Figure 4-2: Mixing of dye with water under various timings. The liquid volume shown here was 150ml. 28
Figure 4-3: Outlet concentrations of NO exiting the gas bubbling reactor with variation of liquid volume (using $NaClO_2$). 29
Figure 4-4: Outlet concentrations of NO (top), NO_2 (middle) and NO_x (bottom) exiting the gas bubbling reactor, with variation in scrubbing chemicals used. 30
Figure 4-5: Outlet concentrations of SO_2 exiting the gas bubbling reactor with variation of $NaClO_2$ concentration. 31
Figure 4-6: Outlet concentrations of NO (top), NO_2 (middle) and NO_x (bottom) exiting the gas bubbling reactor with variation of $NaClO_2$ concentration. 32
Figure 4-7: Outlet concentrations of NO (top), NO_2 (middle) and NO_x (bottom) exiting the gas bubbling reactor with variation of $NaClO_2$ pH. 33
Figure 4-8: Outlet concentrations of SO_2 exiting the gas bubbling reactor with variation of $KMnO_4$ concentration. 34
Figure 4-9: Outlet concentrations of NO (top), NO_2 (middle) and NO_x (bottom) exiting the gas bubbling reactor with variation of $KMnO_4$ concentration. 35
Figure 4-10: Outlet concentrations of SO_2 exiting the gas bubbling reactor with variation of the pH of $KMnO_4$. 36
Figure 4-11: Outlet concentrations of NO (top), NO_2 (middle) and NO_x (bottom) exiting the gas bubbling reactor with variation of the pH of $KMnO_4$. 37
Figure 4-12: Outlet concentrations of NO (top), NO_2 (middle) and NO_x (bottom) exiting the gas bubbling reactor (impinger) with a single or double reactor arranged in series. 38
Figure 4-13: Schematic diagram using a counter current wet scrubber: 40
Figure 4-14: Counter-current wet scrubber in operation (400mm scrubber height configuration, with a QPHA-3 spray nozzle). 41
Figure 4-15: Sulfur dioxide (SO_2) removal from the simulated exhaust gas with various scrubbing liquids in the counter-current wet scrubber. 43
Figure 4-16: pH of the scrubbing liquid in the tank during SO_2 removal. 44
Figure 4-17: The ORP of the scrubbing liquid in the tank during the reaction to remove SO_2. 44

Figure 4-18: Nitric Oxide (NO) removal from the simulated exhaust gas with various scrubbing liquids in the counter-current wet scrubber. 47
Figure 4-19: pH of the scrubbing liquid in the tank during NO removal. 48
Figure 4-20: ORP of the scrubbing liquid in the tank during NO removal. 48
Figure 4-21: The counter-current wet scrubber with $KMnO_4$ as the scrubbing liquid. Etching of MnO_2 precipitates encountered on glass, tubings, nozzle and mist eliminator. 52
Figure 4-22: NO_x ($NO+NO_2$) removal from the simulated exhaust gas using various scrubbing liquids in the counter-current wet scrubber. 53
Figure 4-23: Ratio of NO_2 absorbed over the total NO_2 that was formed (converted to %) versus reaction time, using various types of scrubbing liquid in the counter-current wet scrubber.... 54
Figure 4-24: Ratio of NO_2 absorbed over the total NO_2 that was formed (converted to %) versus reaction time, using various types of scrubbing liquid in the counter-current wet scrubber.... 54
Figure 4-25: NO_2 gas removal from the simulated exhaust gas using DI water versus scrubbing mixtures of increasing alkalinity (NaOH: 0.05 – 0.40M), carried out in the counter-current wet scrubber. 57
Figure 4-26: NO_2 gas removal from the simulated exhaust gas using DI water versus scrubbing liquids of increasing oxidation potential ($NaClO_2$/pH10.9 < $NaClO_2$/pH8 < $NaClO_2$/pH7), carried out in the counter-current wet scrubber. 57
Figure 4-27: Amount of soluble nitrogen of various reactions using NaClO and $NaClO_2$ quantified by ion chromatography. The reactions were carried out in the counter-currrent wet scrubber. 58
Figure 4-28: The mole ratio of the reactant consumed per mole of NO_x removed. 60
Figure 4-29: The estimated chemical cost of various reactant per mole of NO_x removed..... 61
Figure 4-30: Nitric Oxide (NO) removal from the simulated exhaust gas with various scrubbing liquids at L/G ratios of 100 L/m^3 vs. 15 L/m^3 respectively. 63
Figure 4-31: NO_x ($NO+NO_2$) removal from the simulated exhaust gas using various scrubbing liquids 63
Figure 5-1: Removal (%) for SO_2 (top), NO (middle) and NO_x (bottom) using sodium chlorite in a counter-current wet scrubber, with and without CO_2 in the exhaust gas..... 68
Figure 5-2: Change in aqueous phase ORP and pH values as the reaction progressed, for the simultaneous removal of SO_2 and NO with sodium chlorite in a counter-current wet scrubber. 69
Figure 5-3: An illustration of the Bjerrum plot showing the carbonic acid equilibrium in water. 70

Figure 5-4: Removal (%) for CO_2 using sodium chlorite in a counter-current wet scrubber, with CO_2 in the exhaust gas. 71
Figure 5-5: Removal of CO_2 from the simulated exhaust gas during the reaction between sodium chlorite with SO_2 and NO in the counter-current wet scrubber. Experimental conditions shown in Table 5-1, No. 1, 4-7. 72
Figure 5-6: Removal (%) of SO_2 using sodium chlorite in a counter-current wet scrubber, with variation in NaOH addition. 73
Figure 5-7: Removal (%) for NO using sodium chlorite in a counter-current wet scrubber, with variation in NaOH addition. 73
Figure 5-8: Outlet concentrations of NO (top), NO_2 (middle) and NO_x (bottom) exiting the gas bubbling reactor with variation of chemical compounds, ... 76
Figure 5-9: Outlet concentrations of NO (top), NO_2 (middle) and NO_x (bottom) exiting the gas bubbling reactor with variation of NaOH addition to sodium thiosulfate. 77
Figure 5-10: The mole ratios of soluble nitrogen formed over total NO_x removed, and reactant consumed over gaseous pollutant (NO_x) removed, with variation of reactant used in the glass bubbling reactor. 78
Figure 5-11: Removal of NO_2 with variation of sodium thiosulfate concentration using the counter-current wet scrubber, ... 82
Figure 5-12: Removal of NO_2 with variation of sodium thiosulfate (average values without reaction time shown) using the counter current wet scrubber. 82
Figure 5-13: pH of scrubbing liquid used for NO_2 removal with variation of sodium thiosulfate using a counter-current wet scrubber 83
Figure 5-14: ORP of scrubbing liquid used for NO_2 removal with variation of sodium thiosulfate using a counter-current wet scrubber 83
Figure 5-15: Removal of NO_x in the counter-current wet scrubber with variation of $xNO2$, the mole fraction of NO_2. 84
Figure 5-16: Overall NO_x removal with variation of $xNO2$, the mole fraction of NO_2 85
Figure 5-17: Possible conceptual design for a wet scrubber incorporating the partial recirculation of exhaust gas to increase NO removal. Bottom section of wet scrubber is oxidising while the top section is reducing. 86
Figure 6-1: Schematic diagram for Configuration 1: 89
Figure 6-2: Schematic diagram for Configuration 2: 89
Figure 6-3: The E_h – pH diagram of the sulfur system at 25°C. 95
Figure 6-4: Comparison of the E_h – pH diagram of the sulfur system at 25°C and 55°C. 95
Figure 6-5: The E_h – pH diagram of the nitrogen system at 25°C. 96

Figure 6-6: Comparison of the E_h – pH diagram of the nitrogen system at 25°C and 55°C. ...97
Figure 6-7: The E_h – pH diagram of the chlorine system at 25°C. ...98
Figure 6-8: Comparison of the E_h – pH diagram of the chlorine system at 25°C and 55°C. ...98
Figure 6-9: The E_h – pH diagram of the chlorine system at 25°C. ...99
Figure 6-10: Comparison of the E_h – pH diagram of the chlorine system at 25°C and 55°C. 100
Figure 6-11: Removal of SO_2, NO, NO_x and the amount of N escaping the scrubber in the form of NO_2, with variation in the sodium chlorite oxidant pH in the oxidation half-height wet scrubber. ...101
Figure 6-12: Formation of soluble nitrogen in the form of nitrites (NO_2^-) and nitrates (NO_3^-) in the aqueous scrubbing liquid of the oxidation half-height wet scrubber, with variation in pH. ...101
Figure 6-13: The mole ratios of soluble nitrogen formed over total NO_x removed, and reactant (chlorite) consumed over gaseous pollutant (SO_2 and NO_x) removed, as the pH of the chlorite oxidant was varied in the oxidation half-height wet scrubber. ...102
Figure 6-14: Removal of SO_2, NO, NO_x and the amount of N escaping the scrubber in the form of NO_2, with variation in the sodium chlorite oxidant concentration in the oxidation half-height wet scrubber. ...104
Figure 6-15: The mole ratios of soluble nitrogen formed over total NO_x removed, and reactant (chlorite) consumed over pollutant (SO_2 and NO_x) removed, as the concentration of the oxidant was varied in the oxidation half-height wet scrubber. ...105
Figure 6-16: Removal of SO_2, oxidation of NO to NO_2, overall removal of NO_x, and the amount of N escaping as NO_2 with variation of the scrubbing liquid's oxidation potential in the oxidation half-height wet scrubber. ...106
Figure 6-17: Removal of NO, NO_2 and NO_x with variation of sodium thiosulfate concentration in the reducing half-height wet scrubber. ...107
Figure 6-18: Turbidity of the scrubbing liquid in the reducing half-height wet scrubber at the end of the experiment (30 mins), with variation of thiosulfate concentration. ...107
Figure 6-19: Formation of nitrites (NO_2^-) and nitrates (NO_3^-) and its corresponding ORP values in the aqueous scrubbing liquid, with variation in thiosulfate concentration, in the reducing half-height wet scrubber. ...108
Figure 6-20: The mole ratios of soluble nitrogen formed over total NO_x removed, and reactant (thiosulfate) consumed over gaseous pollutant (NO_x) removed, as thiosulfate concentration was varied in the reducing half-height wet scrubber. ...109

Figure 6-21: Removal of NO, NO_2 and NO_x with variation in pH, in a reducing half-height wet scrubber. 110
Figure 6-22: The mole ratios of soluble nitrogen formed over total NO_x removed, and reactant (thiosulfate) consumed per mole of gaseous pollutant (NO_x) removed, with variation of pH in a reducing half-height wet scrubber. 111
Figure 6-23: Turbidity of the scrubbing liquid in the reducing half-height wet scrubber at pH 6 and 12 respectively, with variation of reaction time. 112
Figure 6-24: Comparison of NO, NO_2 and NO_x removal in the reducing half-height wet scrubber using 0.05M of thiosulfate (with and without packing) and 0.05M sulfite (with and without stabilisation using 1% (v/v) formaldehyde). 113
Figure 6-25: The mole ratios of soluble nitrogen formed over total NO_x removed, and reactant consumed over gaseous pollutant (NO_x) removed, in the reducing half-height wet scrubber, using 0.05M of thiosulfate (with and without packing) and 0.05M sulfite (with and without stabilisation using 1% (v/v) formaldehyde)..... 113
Figure 6-26: Formation of nitrites (NO_2^-) and nitrates (NO_3^-) in the aqueous scrubbing liquid at the end of the experiment, in the reducing half-height wet scrubber using 0.05M of thiosulfate (with and without packing) and 0.05M sulfite (with and without stabilisation using 1% (v/v) formaldehyde). The ORP values of the scrubbing liquid are also shown here. 114
Figure 6-27: Removal of CO_2 with the variation of pH of 0.05M of thiosulfate in the reducing half-height wet scrubber. 115
Figure 6-28: Removal of SO_2, NO, NO_x, and the amount of N escaping the scrubber in the form of NO_2, with variation of the L/G ratio in a full height wet scrubber. 117
Figure 6-29: Formation of nitrites (NO_2^-) and nitrates (NO_3^-) in the aqueous scrubbing liquid at the end of the experiment, in the full height wet scrubber with oxidation only. The ORP values of the scrubbing liquid are also shown here. 118
Figure 6-30: The mole ratios of soluble nitrogen formed over total NO_x removed in the full height wet scrubber, with variation of the L/G ratio. In the full height [O] only scrubber, chlorite was used as the oxidant. In the oxidant and reduction wet scrubber, the full height scrubber was split into an oxidation half and reduction half. 118
Figure 6-31: The mole ratios of the reactant consumed per mole of gaseous pollutant removed the full height wet scrubber, with variation of the *L/G* ratio. In the full height [O] only scrubber, chlorite was used as the oxidant. In the oxidant and reduction wet scrubber, the full height scrubber was split into an oxidation half and reduction half. 119
Figure 6-32: Formation of nitrites (NO_2^-) and nitrates (NO_3^-) in the aqueous scrubbing liquid at the end of the experiment, in the full height wet scrubber consisting of an oxidation half and a

reducing half arranged in series. The ORP values of the scrubbing liquid in both halves are also shown here. 121
Figure 6-33: Reactants consumed in the oxidation and reduction halves of the full height wet scrubber with the oxidation/reduction configuration, with variation of L/G ratio. 121
Figure 6-34: Gaseous pollutant removal carried out by the oxidation/reduction full height wet scrubber, enhanced with higher oxidant concentration in the first half or using a packed column the second half. 122
Figure 6-35: The mole ratios of soluble nitrogen formed over total NO_x removed, and reactant consumed over gaseous pollutant (SO_2 & NO_x) removed, using the full height wet scrubber with oxidation and reduction configuration with further enhancements made. 123
Figure 6-36: Removal of SO_2, NO, NO_x and the amount of N escaping the scrubber in the form of NO_2, with variation of reaction temperature in the oxidation half-height wet scrubber. ... 125
Figure 6-37: The mole ratios of soluble nitrogen formed over total NO_x removed, and reactant (chlorite) consumed over pollutant (SO_2 and NO_x) removed, as the reaction temperature was varied in the oxidation half-height wet scrubber. 126
Figure 6-38: Removal of NO, NO_2, NO_x and CO_2 with variation of reaction temperature in the reducing half-height wet scrubber. 126
Figure 6-39: The mole ratios of soluble nitrogen formed over total NO_x removed, and reactant (thiosulfate) consumed over pollutant (NO_x) removed, as the reaction temperature was varied in the reducing half-height wet scrubber. 127
Figure 6-40: Formation of sulfites and sulfates during reaction in the reducing half-height wet scrubber, with variation in reaction temperature. 127
Figure 6-41: Gaseous pollutant removal carried out by the oxidation/reduction full height wet scrubber, with comparison between reaction temperatures of 25°C and 55°C. 128
Figure 6-42: The mole ratios of soluble nitrogen formed over total NO_x removed, and reactant consumed over gaseous pollutant (SO_2 & NO_x) removed, using the full height wet scrubber with oxidation and reduction configuration, with comparison between reaction temperatures of 25°C and 55°C. 129
Figure 6-43: Chlorite consumed (in) versus soluble chlorine compounds formed in the aqueous phase (out). 131
Figure 6-44: NO_x removed (in) versus soluble nitrogen compounds formed in the aqueous phase (out). 132
Figure 6-45: SO_2 removed (in) versus soluble sulfur compounds formed in the aqueous phase (out). 133

Figure 7-1: Chlorite concentration in the aqueous phase with time, in the half height oxidation wet scrubber, with variation in chlorite starting concentration. 136
Figure 7-2: Concentration of ClO_2 in the scrubbing liquid with time, in the half-height oxidation wet scrubber, with variation in pH. 138
Figure 7-3: Overall reaction rate obtained from the rate constant, k_1, with variation in starting chlorite concentration, assuming zero-order reaction..... 139
Figure 7-4: The rate of change of NO, NO_2 and SO_2, compared with the calculated reaction rate, with variation of starting chlorite concentration..... 140
Figure 7-5: Chlorite concentration in the aqueous phase with time, in the half height oxidation wet scrubber, with variation in pH. 141
Figure 7-6: The rate of change of NO, NO_2 and SO_2 compared with the calculated reaction rate, with variation of pH..... 143
Figure 7-7: Thiosulfate concentration in the aqueous phase with time, in the half height reduction wet scrubber, with variation in thiosulfate starting concentration (M). 145
Figure 7-8: The rate of change of NO and NO_2 removal compared with the calculated reaction rate, with variation thiosulfate concentration. 147
Figure 7-9: Sulfite concentration in the aqueous phase with time, in the half height reduction wet scrubber, with and without formaldehyde stabilisation. 148
Figure 7-10: The natural logarithm of sulfite concentration in the aqueous phase with time, in the half height reduction wet scrubber. 149
Figure 7-11: Comparison between the calculated reaction rate from sulfite consumption and the rate of change of NO and NO_2 gases, with and without formaldehyde stabilisation. 151
Figure 7-12: Change in amount of gas pollutant removed with time (averaged value) at different L/G ratio, using the full height oxidation only wet scrubber..... 152
Figure 7-13: The relationship between the overall gas phase mass transfer coefficient for SO_2 and *L/G* ratio,with variation in the full height wet scrubber arrangement. 154
Figure 7-14: The relationship between the overall liquid phase mass transfer coefficient for NO and *L/G* ratio,with variation in the full height wet scrubber arrangement. 155
Figure 7-15: The relationship between the overall liquid phase mass transfer coefficient for NO_2 and *L/G* ratio, with variation in the full height wet scrubber arrangement. 156
Figure 7-16: Change in amount of gas pollutant removed with time (averaged value) at different *L/G* ratio, using the full height wet scrubber with oxidation and reduction in series..... 158

List of Tables

Table 2-1: Allowable SO_x emission limits based on the equivalent sulfur content in fuel (Sulphur oxides (SOx) and Particulate Matter (PM) – Regulation 14, 2022) 5
Table 2-2: Fuel oil sulfur content and the equivalent SO_2/CO_2 ratio (MEPC.259(68), 2015) ... 5
Table 2-3: NO_x emission limit based on ship engine's speed (Nitrogen Oxides (NO_x) – Regulation 13, 2022) 6
Table 2-4: Discharge limit for polycyclic aromatic hydrocarbons in the scrubber washwater (MEPC.259(68), 2015) 7
Table 2-5: NO_x emissions reduction methods that are commercially available (Deng et al., 2021) 10
Table 2-6: Summary of alternative fuels for ships. 18
Table 4-1: A summary of experimental conditions for studies carried out using the gas bubbling reactor. Temperature was ambient and O_2 in excess (>5%). 27
Table 4-2: Summary of the simulated exhaust gas properties used to study the removal of SO_2 and NO by various chemical compounds using a counter current wet scrubber. 41
Table 4-3: Composition and properties of the scrubbing liquid used to react with the exhaust gas in the wet scrubber for the SO_2 and NO studies respectively, using the counter-current wet scrubber. 42
Table 4-4: The Henry's Law constant for several gases of interest, at 1atm and 25°C (Sander, 2015) 45
Table 4-5: The oxidation potential of various chemical compounds of relevance in this study (Tchobanoglous et al. 2013). 49
Table 4-6: Amount of NO_x removed by the various scrubbing liquids and the amount eventually converted to nitrate ions in the aqueous phase 59
Table 4-7: Cost estimation of the various scrubbing liquid systems used. 61
Table 5-1: A summary of experimental conditions for SO_2 and NO removal with the presence of CO_2 in the exhaust gas, carried out using the counter-current wet scrubber. 67
Table 5-2: A summary of potential reducing agents and their associated stabilizing agents for reaction with NO_2 gas. 74
Table 5-3: A summary of experimental conditions for NO_2 removal carried out using the gas bubbling reactor. 75
Table 5-4: Reaction mechanisms of sodium thiosulfate in the aqueous phase with NO_2 and their associated Gibbs Free Energy values, based on thermodynamic modelling software (Metso Outotec HSC Chemistry Version 7). 79

Table 5-5: A summary of experimental conditions for NO_2 removal carried out using the counter-current wet scrubber. 81
Table 6-1: The composition of the simulated exhaust gas used in this study, unless otherwise indicated. 88
Table 6-2: A summary of the experimental parameters used in this study. Unless otherwise indicated, the duration for all experimental runs in this study was 30 minutes. 92
Table 6-3: Species included in the sulfur, nitrogen, carbon and chlorine systems used for the E_h-pH diagram model. 94
Table 6-4: The CO_2 absorbed from the simulated exhaust gas between the two full height scrubber configurations – oxidation only configuration versus the oxidation and reduction in series configuration. 124
Table 7-1: The linear equations, linear regression values (R^2) and reaction rate constants obtained from adding a linear trendline to the chlorite concentration versus time graph in Figure 7-1, with variation in starting chlorite concentration. 137
Table 7-2: The rate of change of NO, NO_2 and SO_2 removal with variation of starting chlorite concentration. 139
Table 7-3: The linear equations, linear regression values (R^2) and reaction rate constants obtained from adding a linear trendline to the chlorite concentration versus time graph in Figure 7-5, with variation in pH. 142
Table 7-4: The rate of change of NO and SO_2 removal with variation of liquid pH. 142
Table 7-5: The linear equations, linear regression values (R^2) and reaction rate constants obtained from adding a linear trendline to the thiosulphate concentration versus time graph in Figure 7-7, with variation in starting thiosulfate concentration. 145
Table 7-6: The rate of change of NO and NO_2 removal, with variation of thiosulfate starting concentration. 146
Table 7-7: The equation, linear regression value (R^2) and reaction rate constant obtained from adding a linear trendline to the natural logarithmic value of sulfite concentration versus time graph in Figure 7-10. 149
Table 7-8: Calculation of the reaction rate of sulfite, obtained by the multiplication of the rate constant that was obtained with the $[SO_3^{2-}]_t$. 150
Table 7-9: The rate of change of NO and NO_2 removal for sulfite reducing agent with and without formaldehyde stabilisation. 150

Nomenclature

aq	Aqueous phase
ECA	Emissions Control Area
EGR	Exhaust gas recirculation
ESP	Electrostatic precipitator
GHG	Greenhouse gas
HFO	Heavy Fuel Oil
IMO	International Maritime Organisation
$KMnO_4$	Potassium permanganate
LNG	Liquified natural gas
LPG	Liquified petroleum gas
MEPC	Maritime Environment Protection Committee
MGO	Marine Gas Oil
NDIR	Nondispersive infrared
NO_x	Nitrogen oxides
ORP	Oxidation reduction potential or Redox potential
SCR	Selective Catalytic Reduction
SO_x	Sulfur oxides
x_{NO2}	mol fraction of NO_2

Symbols

µm	micrometre
A	Area
C_{Ae}	Concentration of A in liquid in equilibrium with P_{AG}
C_{AL}	Concentration of A in the bulk liquid
$C_{i,inlet}$	Concentration of gas i in the inlet
$C_{i,outlet}$	Concentration of gas i in the outlet
E_h	Redox potential or Oxidation Reduction Potential
H_i	Henry's Law constant for substance *i*
k	Reaction rate constant
K_G	Overall gas phase coefficient of mass transfer
kJ	Kilojoules

K_L	Overall liquid phase coefficient of mass transfer
kmol	kilomole
KWh	Kilowatts per hour
L/G	Liquid flowrate over gas flowrate ratio
L/min	Litres per minute
ln	natural logarithm
M	molarity or mol per litre
mg/L	milligram per litre
min	minutes
ml	millilitre
mV	millivolt
MWh	Megawatts per hour
n	mol
N_A'	Overall rate of mass transfer of gas A
η_i	Efficiency of the removal of pollutant i
P	Pressure
P_{Ae}	Partial pressure of gas A in the equilibrium with C_{AL}
P_{AG}	Partial pressure of gas A in the bulk gas
pKa	The logarithmic value (negative, base 10) of the acid dissociation constant
ppm	parts per million
ppm(v)	parts per million with volume basis
R	Ideal gas constant
R^2	Regression value
s	seconds
T	Temperature
V	Volume
V	Volt
ΔG	Gibbs Free Energy change

Chapter 1. Introduction

1.1. Background

It is well known that the combustion of fossil fuels in power plants, boilers and diesel engines generate large amounts of air pollutants in the form of sulfur oxides (SO_x) and nitrogen oxides (NO_x), amongst other polluting substances. Traditional end-of-pipe technologies for treatment of these air pollutants have been largely effective in large facilities such as power plants but fall short for when it comes to small-to-medium sized boilers and large 2-stroke diesel engines use on-board ships (Li *et al.*, 2019). In the former, the volume of the exhaust gas may not be large enough to justify the various equipment needed for treatment of SO_x and NO_x, which are typically treated separately. In the latter, ocean plying vessels face even more limitations, including space, weight and various logistical challenges. Also, consistent growth in the shipping industry over the decades have led to ever-increasing fossil fuel consumption and subsequent increases in SO_x and NO_x emissions. From 2014 to 2018, NO_x emissions climbed from 19 million tons to 20.9 million tons while the SO_x emissions rose from 10.2 million tons to 11.3 million tons annually (Deng *et al.*, 2021). These increases occurred despite the gradual introduction of new emissions control regulations by the International Maritime Organisation (IMO) during that period of time (Zannis *et al.*, 2022).

Control of air polluting substances on global shipping has come into effect through the 'Annex VI - Prevention of Air Pollution from Ships' of the International Convention for the Prevention of Pollution from Ships (Regulation 13 and 14), under the auspices of the International Maritime Organisation. Through this convention, SO_x and NO_x emissions were reduced in tiers, with the strictest tier coming into effect on 01 January 2020 (more details in Section 2.1).

For SO_x control, usage of low sulfur fuel is currently considered the main solution as it does not require any modifications on the ship. However, this is not a viable long-term solution on its own due to high cost and supply issues with low sulfur fuels. End-of-pipe treatment methods such as the installation of a wet scrubber on-board the vessel is accepted as a viable alternative for controlling SO_x emissions. Although such systems are already commercially available, they are only effective for SO_x removal but not for NO_x.

The control of NO_x has always been more challenging as most of it are generated in the engine itself due to the high temperatures of the combustion process (thermal NO_x). Hence, it can be formed even if the fuel does not contain any nitrogen (Nevers, 2000). Also, NO_x from engine combustion comprises of approximately 90% of nitric oxide (NO), which is highly insoluble in the aqueous phase and cannot simply be scrubbed or solubilized from the gas to aqueous phase

like SO_x. Therefore, engine medication techniques are mainly used to reduce the combustion temperature in the engine to reduce NO_x formation. However, such methods also reduce the engine efficiency, thereby leading to higher fuel consumption (Deng *et al.*, 2021). Apart from engine modification techniques, the only established end-of-pipe treatment method is Selective Catalytic Reduction (SCR) (*ABS Advisory On Exhaust Gas Scrubber Systems*, 2018). Although this method is quite effective in removing NO by itself, the catalyst used have a tendency to get poisoned by soot, particulate matter and SO_x. Excess urea that are not utilised in the reaction gets converted into ammonia, which is poisonous. The SO_x present in the exhaust gas also reacts with ammonia, forming a white precipitate which can poison the catalyst.

The usage of alternative fuels such as Liquified Natural Gas (LNG), Liquified Petroleum Gas (LPG), biodiesel, methanol, hydrogen and ammonia, has generated a significant amount of attention and excitement of late as shifting to those fuels will bypass the use of fossil fuels altogether. This will not only eliminate SO_x emissions (though not NO_x) but will also reduce the amount of greenhouse gases (GHG) generated. However, this area has major logistical, technological and economic hurdles that have yet to be overcome (Wang *et al.*, 2022). Because of that, the dependency on fossil fuels for ship propulsion will remain at least from the short to medium term, if not longer.

1.2. Research motivations

The acceptance of wet scrubbers on-board ships has already gained much traction because it is not only technologically feasible but also economically viable – Wärtsilä itself has already built more than 700 units before 2019 (Ni et al. 2020). Apart from the installation of wet scrubbers in newly commissioned ships, many shipyards are also becoming more familiar with retrofitting old ships with it. It is therefore justifiable to explore its potential to remove NO_x on top of SO_x. In the R&D scene, there has been substantial groundwork carried out for the simultaneous removal of SO_x and NO_x, with the majority of them taking place within the last two decades (to be discussed in Chapter 2: Literature Review). However, up to the point of the writing of this thesis, none of them has been successfully commercialized.

There are several barriers to commercialization that has not been overcome including cost, logistics and environmental concerns. Examples include chemical compounds that are too expensive, too unstable, too dangerous to be handled on ships, too heavy (solid adsorbents), or may generate washwater that is unsuitable for discharge in the ocean. A majority of work that has been published also relied on convenient experiment setups, such as using a gas bubbling

reactor to conduct the wet scrubbing reaction and not including carbon dioxide in the exhaust gas (Li *et al.*, 2019; Xi *et al.*, 2020; Zhang *et al.*, 2022b; Zhou *et al.*, 2022). Gas bubbling reactors, where the gas-liquid contact occurs in gas bubbles formed in liquid, has a very high mass transfer rate, making many types of reactions feasible but it has a very different mass transfer characteristic compared to the counter-current wet scrubber and it cannot be scaled up. As carbon dioxide is not only reactive but present in large quantities in the exhaust gas, ignoring its presence may cause the system to behave differently from reality.

1.3. Aims and Objectives

The main objective of this study is to develop a wet scrubbing method for the simultaneous removal of SO_x and NO_x from marine exhaust emissions, using an experimental approach. The work here started with the usage of a simple gas bubbling reactor to carry out the wet scrubbing reaction and progressed to a custom-made commercially scalable counter-current system with spray tower or packed tower configurations. Efforts were made to adopt experimental conditions that are close to operating conditions, such as using a more representative exhaust gas composition which includes carbon dioxide.

In the first phase of this study, a broad range of widely reported substances, namely, seawater, sodium hydroxide (NaOH), sodium hypochlorite (NaClO), sodium chlorite ($NaClO_2$), hydrogen peroxide (H_2O_2) and potassium permanganate ($KMnO_4$) were systematically compared for their capacity to remove SO_x and NO_x and new insights were gained. These chemicals were selected for this study because they either showed potential in NO_x removal, are widely available in the industry at a reasonable cost or are already currently used on ship-based wet scrubbers.

From this initial phase, the most promising chemical compound would be selected for further development in a counter-current wet scrubbing system in the subsequent phase. With commercialization potential in mind, the results will include the optimisation of reactant consumption rate for lowering operating cost and examine the viability of wastewater (scrubber washwater waste) discharge to ocean, with particular focus on the nitrogen levels in the wastewater.

In the final phase, a software will be used to generate thermodynamic models based on the wet scrubber system that will be developed, for comparison with the experimental results. The experimental data will also be analysed from the chemical reaction kinetics, mass transfer and mass balance aspects in order to gain a better understanding of this gas-liquid system.

Chapter 2. Literature Review

A broad literature review on areas related to topic was carried out and presented here. The range included regulatory control, existing solutions being employed to control shipping emission, emerging solutions currently being developed, and also the approach of using alternative fuels.

2.1. Regulations for marine emissions

The *International Convention for the Prevention of Pollution from Ships* (MARPOL) is a protocol established by the *International Maritime Organisation* (IMO) back in 1973 to regulate all kinds of pollution from ships that are plying the oceans. It consists of six annexes, each of them focusing on the various polluting discharges that can come from ships. Annex VI, also known as 'Prevention of Air Pollution from Ships' was the latest to be introduced and it focuses on the various air pollutants that are generated from ships due to the combustion of fossil fuel in its various engines, boilers and also its incinerators.

Chief among the focus of this annex are the two main polluting gases from combustion engines– Sulfur Oxides (SO_x) and Nitrogen Oxides (NO_x). The former comes from the sulfur content in fossil fuel, which is typically high in some types of fuel oil used by ships. The latter mainly comes from the thermal reaction when N_2 is oxidised by high temperatures in the combustion engine (thermal NO_x). A small amount also comes from the nitrogen content in the fuel (fuel NO_x). Another common air pollutant in combustion flue gas, particulate matter (PM), does not have a specific regulation on its own since its concentration is contributed indirectly by the presence of SO_x and NO_x.

2.1.1. Regulations concerning SO_x and PM emissions

Sulfur oxides emission from ships is defined under Regulation 14 (*Sulphur oxides (SOx) and Particulate Matter (PM) – Regulation 14*, 2022). The regulation differentiates between normal areas and special areas called *Emission Controlled Areas* (ECAs) where the discharge limits are much tighter. ECAs consist of certain territories along coastal areas in Europe and USA with a high population density. The allowable SO_2 emissions are based on the maximum allowable sulfur content in the fuel oil expressed in weight percentage (refer to Table 2-1).

The maximum sulfur content in fuel oils currently allowed in non-ECA has dropped from 3.50% m/m to 0.50% m/m in 2020. Within ECAs, the sulfur limit in fuel is already at 0.10% m/m. If the sulfur content does not meet the limit, end of pipe treatment methods such as exhaust gas scrubbing can also be used as long as the SO_2 concentrations are reduced to the level that would have been released when using fuel oil with sulfur content within the maximum stipulated limit.

Table 2-1: Allowable SO_x emission limits based on the equivalent sulfur content in fuel (Sulphur oxides (SOx) and Particulate Matter (PM) – Regulation 14, 2022)

SO_x Emissions Limit	
Outside ECA	**Within ECA**
Before 1 Jan 2012	Before 1 Jul 2010
4.50% m/m	1.50% m/m
After 1 Jan 2012	After 1 July 2010
3.50% m/m	1.00% m/m
After 1 Jan 2020	After 1 Jan 2015
0.50% m/m	0.10% m/m

If end-of-pipe treatment methods are used, the SO_2 concentration at the exhaust needs to be measured in order to know if compliance has been met. It can be somewhat tedious to calculate the SO_2 allowable discharge limit of a given the sulfur content in fuel oil – as ships uses various types of engines with varying exhaust gas flowrates. Two different engines can emit exhaust with very different SO_2 concentrations although they are using fuel with exactly the same sulfur content. In order to simplify monitoring, the fuel oil sulfur content is converted to an equivalent SO_2/CO_2 ratio (see Table 2-2) since both SO_2 and CO_2 can be measured easily from the exhaust gas stack (MEPC.259(68), 2015).

Table 2-2: Fuel oil sulfur content and the equivalent SO_2/CO_2 ratio (MEPC.259(68), 2015)

Fuel Oil Sulfur Content (%m/m)	**Ratio Emission SO_2 (ppm)/CO_2 (%v/v)**
4.5	195.0
3.5	151.7
1.5	65.0
1.0	43.3
0.5	21.7
0.1	4.3

2.1.2. Regulations concerning NO_x emission

Nitrogen oxides emission from ship exhaust is defined under Regulation 13 in the MARPOL Annex VI (*Nitrogen Oxides (NOx) – Regulation 13*, 2022), applicable for engine power exceeding 130 kW. Since NO_x is mostly generated from the oxidation of atmospheric N_2 under high combustion temperatures (thermal NO_x), its control has very little to do with the quality of fuel used. The amount of NO_x that ships are allowed to emit is determined by the speed of

its engines (in RPM) and expressed as the weight of NO_x per unit kWh of engine power (see Table 2-3). In general, the larger the ship engines are, the slower the engine speed.

Table 2-3: NO_x emission limit based on ship engine's speed (Nitrogen Oxides (NO_x) – Regulation 13, 2022)

Tier	Ship construction date on or after	Total weighted cycle emission limit (g/kWh) n = engine's rated speed (rpm)		
		n < 130	n = 130 - 1999	n ≥ 2000
I	1 January 2000	17.0	$45 \cdot n^{(-0.2)}$ e.g., 720 rpm – 12.1	9.8
II	1 January 2011	14.4	$44 \cdot n^{(-0.23)}$ e.g., 720 rpm – 9.7	7.7
III	1 January 2016	3.4	$9 \cdot n^{(-0.2)}$ e.g., 720 rpm – 2.4	2.0

Three types of ship diesel engine specifications (small, medium and large) were used as examples to calculate the actual NO_x discharge concentration allowed based on the table here (see calculation in Appendix A). It can be seen that the actual NO_x allowed in the corresponding ship exhaust ranged from 2.0 g/kWh for small engines to 3.4 g/kWh for large engines. In the three examples used there, the actual concentration of NO_x allowed in the ship exhaust ranged from around 370 to 450 ppmv.

2.1.3. Regulations concerning washwater discharge from ships

Washwater discharge concerns the disposal of wastewater from the wet scrubbing process into the ocean. If wet scrubbing is used to remove SO_x, care has to be taken on the water quality of any discharge of the scrubber washwater to the sea. IMO guidelines require the washwater discharge to be monitored and within stipulated limits. Discharge of any scrubbing liquid to the sea has to be monitored for pH, polycyclic aromatic hydrocarbons (PAH), turbidity and nitrate content (MEPC.259(68), 2015).

i) pH

As SO_x and NO_x are acidic gases and causes the scrubber washwater in the wet scrubber to be acidic as well, the main concern here is the discharge of acidic wastewater into the ocean and thereby contributing to ocean acidification. Therefore, any scrubber washwater discharge to the ocean should be below pH 6.5. Exceptions are given during transit and manoeuvring – in such cases, the pH of the wastewater discharge should not be less than the pH of the water surrounding seawater by 2 pH units.

The guidelines do not seem to have any mention on a maximum pH discharge limit. Since ocean acidification and consumption of ocean alkalinity is such a concern, any addition of alkalinity to the ocean should be doing good instead of harm.

ii) Turbidity and Suspended Solids

In general, suspended solids are undesirable as it causes water bodies not only to be unsightly but also does harm to the ecology. The turbidity of the washwater discharge should not exceed 25 NTU (nephlometric turbidity units), measured on a continuous basis.

iii) Polycyclic Aromatic Hydrocarbons (PAH)

Polycyclic Aromatic Hydrocarbons (PAH) are a product of incomplete combustion of the fuel and is highly carcinogenic. Therefore, the discharge limits are very stringent and must not exceed 50µg/L if the washwater discharge rate from the ship is 45 tonnes of wastewater per MWh of the ship engine power. The discharge limit for different wastewater discharge flowrates has to be normalised accordingly, as illustrated in Table 2-4.

Table 2-4: Discharge limit for polycyclic aromatic hydrocarbons in the scrubber washwater (MEPC.259(68), 2015)

Washwater discharge flowrate (t/MWh)	**Discharge limit (µg/L PAH equivalents)**
0 – 1	2250
2.5	900
5	450
11.25	200
22.5	100
45	50
90	25

iv) Nitrates (NO_3^-)

Nitrates are a component of concern as it is a nutrient needed for plant growth and its presence in water bodies contributes to algae blooms (eutrophication), which may lead to depletion of dissolved oxygen and hypoxic conditions when the algae decompose. No mention is given to nitrites (NO_2^-) in the washwater discharge. However, since most nitrites will be oxidised to nitrates in the natural environment, it can be assumed that all nitrites will eventually end up as nitrates over time.

Two different limits for nitrate discharge are provided. In the first, no more that 12% of the NO_x in the exhaust should end up in the washwater discharge. In the second, the washwater

discharge nitrate level should not exceed 60 mg/L if the washwater discharge flowrate is at 45 tons/MWh. The nitrate limit will vary according to discharge flowrate and has to be normalised in a similar way with the PAH according to Table 3.

Concern for nitrate discharge may be overstated in the open seas as phosphorus is usually the limiting nutrient there (*EGCSA Handbook 2012: A practical guide to exhaust gas cleaning systems for the maritime industry*, 2012). While phosphorus is generally present in the sea in areas closer to the shore, control of nitrate levels in washwater discharged in the open seas further from the shore is arguable.

2.2. Existing solutions in the marine sector

In this section, commercially available solutions for the mitigation of SO_x and NO_x are reviewed. These market-ready solutions can come within any of these three categories: fuel optimisation, pre-combustion control or exhaust gas treatment (Deng *et al.*, 2021). Here below, they are presented according to the type of pollutant being controlled.

2.2.1. Existing solutions for sulfur oxides

In the marine sector, the usage of low sulfur fuels is still considered to be the main solution for reducing SO_x emissions as this does not require any ship modifications. Alternative solutions include converting existing engines to run on very low sulfur fuel such as Liquefied Natural Gas (LNG) or installing exhaust gas cleaning equipment such as a wet scrubber.

Even before the COVID-19 pandemic, switching to low sulfur fuel was estimated to cost the industry billions of dollars per year. Switching to low sulfur fuel is the easiest solution to implement because it does not require any modifications on the ship even though this increases the operating cost significantly. While this may be convenient and immediate, the operation cost will constantly be subjected to fluctuations due to oil price volatility.

Apart from switching to low sulfur fuel, end-of-pipe treatment methods such as the installation of a wet scrubber on-board the vessel is also a viable alternative for controlling SO_x emissions. This is also known as the Exhaust Gas Cleaning System (EGCS). Although both wet and dry scrubber commercial systems exist, the wet scrubber system is by far more established than the dry system. There are many different marine wet scrubbers already available in the market and this approach is also fast gaining in popularity (*ABS Advisory On Exhaust Gas Scrubber Systems*, 2018). In 2013, only 67 ship exhaust gas scrubber units were installed in ships for SO_x control (*Global Exhaust Gas Scrubber Market 2020 Industry Future Trends, Growth,*

Strategies, Size, Share, Segmentation, In-depth Analysis Research Report by Foresight to 2025). This number increased to 468 in 2016 and is estimated to reach 3,254 in year 2023. As of 03 March 2019, Wärtsilä itself had already delivered installed 704 wet scrubbing units (Ni *et al.*, 2020). The market size for ship exhaust gas scrubbers was estimated to be at USD 1.3 billion in 2019 and is expected to reach USD 9 billion by year 2027 (*Marine Scrubber Market Research Report*, 2022).

Existing wet scrubbers in the market for SO_x removal comes in three forms, open-loop, closed-loop and hybrid systems (*ABS Advisory On Exhaust Gas Scrubber Systems*, 2018). Open-loop wet scrubbers utilises large amounts of seawater for the absorption of SO_x in the exhaust gas. Utilised seawater is discharged back into the ocean after a simple washwater treatment such as removing suspended solids and oil. Closed-loop wet scrubbers typically uses chemicals such as sodium hydroxide to absorb the SO_x pollutant and neutralise the acid formed. A much smaller amount of washwater is then discharged into the ocean. Hybrid systems, as the name implies, are systems that can switch between open and closed loop operation. In a review of various types of EGCS for SO_x abatement, Zannis and co-researchers concluded that closed-loop wet scrubbers with NaOH as the scrubbing liquid is likely the most effective system (Zannis *et al.*, 2022).

Although desulfurization using wet scrubbers onboard vessels can already be considered established, there has been several interesting developments that has taken place recently. One of them involved the use of a cascading design in a wet scrubber that allowed for higher *L/G* ratio without the risk of flooding, thereby achieving higher sulfur removal, lower pressure drop and with lower alkalinity requirements when compared with a straight-through traditional open-loop scrubber (Kuang *et al.*, 2020; Zhao *et al.*, 2021). Additionally, a square-shaped spray column which allowed for a smaller footprint, smaller pressure-drop and higher efficiency was also proposed (Van Duc Long *et al.*, 2021). Although only focused on desulfurization, these studies are interesting as some of their innovations may be applicable for simultaneous SO_2 and NO_x removal.

2.2.2. Existing solutions for nitrogen oxides

Removal of NO_x has always been more challenging due to the way they are generated and the nature of the molecule itself. Most of the NO_x produced from combustion are thermal NO_x – unlike sulfur, they are not present in the fuel and cannot be removed through a process (*Your options for emissions compliance: Guidance for shipowners and operators on the Annex VI SOx and NOx regulations*, 2015). Also, NO_x from engine combustion comprises of around 90%

of nitric oxide (NO), which is highly insoluble in the aqueous phase can cannot be simply scrubbed through a wet process unlike SO_x. Although NO can be oxidised to its more soluble NO_2 form in the atmosphere under natural conditions, this oxidation process is not sufficiently fast enough as the exhaust gas in any wet scrubbing typically only have seconds before the exhaust gas leaves the system to the atmosphere.

Reduction of NO_x onboard ships can be accomplished by modifying the fuel or the combustion process to lower the temperature of combustion in the engine. This is because thermal NO_x can be reduced significantly if the combustion temperature is lowered below 1200°C. In the shipping industry, such proven examples can range from changing the timing of the piston's cycle movement in tandem with the inlet valve (Miller Timing) to injection of water directly into the combustion chamber (Direct Water Injection, DWI) (see Table 2-5).

Table 2-5: NO_x emissions reduction methods that are commercially available (Deng et al., 2021)

Method	**Description**	**Effectiveness**
Fuel Additive	*Mixing of additives such as cerium oxide (CeO_2) to HFO*	+
Fuel Emulsification	*Mixing of water with fuel before injection into engine*	++
Miller Cycle	*Changing the timing of the piston's cycle with the aim or reducing the engine cylinder temperature at the end of compression*	++
Humid Air Motor (HAM)	*Addition of water vapour into the air intake at the beginning of the compression cycle*	+++
Direct Water Injection	*A separate nozzle is used to directly inject water into the engine combustion chamber*	+++
Exhaust Gas Recirculation (EGR)	*A portion of flue gas being recirculated back to the engine to reduce peak in-cylinder combustion temperature*	++++
Selective Catalytic Reduction (SCR)	*A catalyst is used to reduce the NO_x formed to harmless N_2 gas*	+++++

One of these methods involve a portion of exhaust gas being recirculated back to the engine in order to reduce peak in-cylinder combustion temperature, in a technique known as Exhaust Gas Recirculation (EGR). Unfortunately, all these methods incur a penalty of lowering the efficiency of engines, leading to higher fuel consumption (*Your options for emissions compliance: Guidance for shipowners and operators on the Annex VI SOx and NOx regulations*, 2015; *ABS Advisory On Exhaust Gas Scrubber Systems*, 2018).

When it comes to end-of-pipe treatment methods, the most established and market-available process is the Selective Catalytic Reduction (SCR) method. This process involves the usage of

a reducing agent, usually urea solution, to reduce NO to inert N_2 over a metal catalyst. Ships that have installed this system need to carry large amounts of urea on-board. Although this method is quite effective in removing NO by itself, the catalyst used tend to get poisoned by soot, particulate matter and SO_x. Excess urea that are not utilised in the reaction gets converted into ammonia (NH_3) which can be dangerous above a certain concentration. The presence of SO_x also tend to react with NH_3, forming a white precipitate which can poison the catalyst, so SCR is best used in tandem with lower sulfur fuels.

Current end-of-pipe solutions in the marine sector are still very inadequate and they tend to focus on either SO_x or NO_x. While this is entirely normal for land-based systems, it is impractical to install two separate systems on-board a vessel due to the lack of space. Furthermore, some of these SO_x and NO_x removal systems are not compatible. Case in point would be the wet scrubber for SO_x and SCR for NO_x removal *(Lloyd's Register Marine, Your options for emissions compliance: Guidance for shipowners and operators on the Annex VI SOx and NOx regulations*, 2015). If these two units are combined, SO_x removal would have to be carried out upstream of the SCR since its presence will form ammonium sulfate precipitates in the SCR, which will poison the catalyst. However, placing a wet scrubber before the SCR would significantly cool the exhaust gas before it reaches the SCR, causing it to be below the minimum operating temperatures required by the SCR. Exhaust gas exiting the wet scrubber can be cooled to as low as below 50°C while the SCR requires the exhaust gas to be above 300°C. A significant amount of energy would have to be used to re-heat the exhaust gas leaving the wet scrubber before it enters the SCR.

2.3. Emerging technologies for simultaneous removal of SO_x and NO_x

In this section, end-of-pipe treatment methods for the simultaneous removal of SO_2 and NO_x are discussed. For a more complete literature review, patent claims are included as well on top of journal publications.

2.3.1. Usage of dry sorbents

One of the earliest patents that claims to control both SO_x and NO_x in the exhaust uses dry injection of urea and nahcolite, which were sprayed directly into the exhaust gas (US 5,082,586) (Hooper, 1992). The dry powder reacts with the SO_x and NO_x through a gas-solid reaction and the pollutants are absorbed on the surface of the dry powder. In order to prevent the dry powder from escaping into the atmosphere, an electrostatic precipitator (ESP) has to be installed downstream to capture and collect the dry sorbents. This method requires a large footprint for

installing the ESP and generates large quantities of solid waste, which must be disposed as a toxic waste.

In another invention, an alumina-based solid absorbent is used to remove SO_x, followed by a chemisorption reduction catalyst which is used to reduce NO_x to N_2 (EP 0892159A2, US 6,272,848 B1) (Okude *et al.*, 1999; Okude *et al.*, 2001). However, saturation of the absorbent for SO_x removal will lead to the catalyst being poisoned. Yet another invention claims to have a NO_x trapping catalyst material that is tolerant to the presence of SO_x (US 6,699,448 B2) (Wu and Dettling, 2004). In WO 2015/176101 Al, it is claimed that a special sorbent containing certain transition metals supported on an activated charcoal base can be used to adsorb both SO_x and NO_x (Yu, 2015). Additionally, it was also claimed in WO 2013/033763 Al that a binding agent can be used to capture and solidify SO_x, NO_x and CO_2 (Silic *et al.*, 2013). However, all solid absorbents and adsorbents generate large amounts of solid waste which needs to be disposed, making it very challenging for ship-based applications.

2.3.2. Usage of catalysis

Apart from the commercially utilised Selective Catalytic Reduction (SCR) discussed in Section 2.2.2, other forms of catalysis-based solutions include an approach by Menon, et. al. (WO 2014/114735 Al) which uses a catalyst to oxides SO_x and NO_x to SO_3 and NO_2 gases (Menon and Ovrebo, 2014). This is followed by cooling the exhaust gas in a condenser below the dew point temperature of water so that SO_3 and NO_2 condenses the aqueous phase and end up as sulfate and nitrate ions. However, this would be difficult to work as the solubility of NO_2 in the aqueous phase is still limited. Although NO_2 is more soluble than NO, only part of the pollutant may end up in the aqueous phase while the rest will escape through the exhaust.

2.3.3. Engine-Modifications

Besides catalysis and solid absorbents/adsorbents, one approach claims that injecting hydrocarbon into the diesel engine's cylinder during the decompression cycle can lead to overall NO_x reduction when the exhaust is removed by a de-NOx catalyst (EP 1038099B1) (Weissman *et al.*, 2002). In WO 2007/045721 Al, water is injected into the engine in order to lower the combustion temperature and reduce the formation of NO_x (Ylinen 2007). In a very similar invention, the freshwater injected into the ship's engine is produced using a reverse osmosis (RO) system (EP 1,957,181B1) (Ylinen, 2009). The retentate from the RO system is then used as a scrubbing solution for SO_x removal in a wet scrubber. Yet another approach focuses on Exhaust Gas Recirculation (EGR), a method that recirculates a portion of exhaust gas back into the engine in order to reduce the overall combustion temperature and formation of NO_x (JP 6,188,033B2) (Ito and Naohiro, 2015). An EGR method was also combined with

wet scrubbing to remove SO_x apart from lowering the formation of NO_x, in WO 2014/041734 A1, EP 2,738,364A1 and EP 3,085,910A1 (Mölgaard, 2014; Toma, 2014; Furugen *et al.*, 2016). Methods such as these tend to lower the overall efficiency of the internal combustion engine.

2.3.4. Gas-Liquid Reaction Approach

In the field of oxidising the insoluble NO gas to its slightly more soluble NO_2 form, oxidants which were reported to be able to carry out the conversion have been well-documented, with varying degree of success. These includes oxidants such as permanganate (MnO_4^{2-}) (Brogren *et al.*, 1997; Chu *et al.*, 2001; Fang *et al.*, 2013), ozone (O_3) (Wang *et al.*, 2007), cobalt ethylenediamine solution (Long *et al.*, 2007), urea (Resnik *et al.*, 2004; Fang *et al.*, 2011), hydrogen peroxide (H_2O_2) (Liémans and Thomas, 2013; Liu *et al.*, 2014; Liu *et al.*, 2015; Zhao *et al.*, 2015a), the iron-based ferrate (IV) solution (Zhao *et al.*, 2014) and chlorine-based oxidants such as hypochlorite (ClO^-), chlorite (ClO_2^-), chlorate (ClO_3^-) and chlorine dioxide (ClO_2) gas (Chien and Chu, 2000; Chu *et al.*, 2003; Chien *et al.*, 2005; Jin *et al.*, 2006; Deshwal *et al.*, 2008; Wei *et al.*, 2009; Zhao *et al.*, 2010; Zhao *et al.*, 2011; Mondal and Chelluboyana, 2013; Park *et al.*, 2015; Zhao *et al.*, 2015c; Zhao *et al.*, 2016). Photocatalysis methods, involving the use of UV light to carry out the oxidation has also been tried out (Liu and Zhang, 2011; Xia *et al.*, 2015). Some of these studies included using electrolysis of seawater to generate chlorine-based oxidation compounds to oxidise NO to NO_2 (An and Nishida, 2003; Yang *et al.*, 2016; Yang *et al.*, 2018).

Similarly in the patent-sphere, oxidising NO to NO_2 before removing it by some sort of gas-liquid reaction can also be found and it includes the use of ozone injection into the exhaust gas, followed by wet scrubbing with NaOH to remove the NO_2 formed (US 5,206,002) (Skelley *et al.*, 1993). In a similar invention, a phosphorus-based oxidant in the form of P_4O_{10} is injected instead of ozone (US 6,063,348) (Hinke and Hinke, 2000). The phosphorus oxide will decompose to generate ozone, which will then facilitate the oxidation of NO to NO_2, followed by removal by wet scrubbing. Another similar invention uses ozone and hydrogen peroxide (CN 102463015A) (Pu and Li, 2012). Apart from this, it is also claimed in CN 101822937A that UV light can be used to promote ozonation to oxidise NO to NO_2 (Yu *et al.*, 2010). Yet another source of oxidising agent is iron (Fe) ions. According to US 8,383,074B2, adding Fe^{2+} or Fe^{3+} into seawater at low pH and under a magnetic field helped to catalyst the oxidation of NO gas to NO_2 and enables it to become soluble (Peng, 2011).

The studies and inventions mentioned so far generally assumed that the complete oxidation of NO to NO_2 solves the problem of NO_x removal as the latter is readily soluble in the aqueous phase. However, this is not true especially given the short contact time of the gas-liquid reaction

in an actual life-size scrubber, which is in the magnitude of seconds. Most of the studies mentioned also did not take into account the presence of CO_2 in the exhaust gas, which may have a significant influence on the reaction mechanisms.

Studies that take into account the partial solubility of NO_2 include US 5,328,673A, where oxidation of NO to NO_2 was first carried out using chloric acid ($HClO_3$), followed by NO_2 removal using a sulfur-based reducing agent in a separate reaction chamber (Kaczur *et al.*, 1994). The chloric acid used can be commercially purchased or from in-situ electrolysis of hypochlorous acid (HClO). However, chlorine in its chlorate form (ClO_3^-), where the Cl atom is in the oxidation state of +5, is generally known to be more unstable and harmful to health and the environment, compared to the more benign forms of hypochlorous (ClO^-) and chlorite (ClO_2^-), which are even available as household products. This invention also did not take into account any control or design parameters to avoid the formation of hydrogen sulfide (H_2S) in the second step although sulfur based reducing agents were used.

In another similar invention, in-situ electrolysis of seawater is used to generate active chlorine compounds to oxidise NO to NO_2 in the first stage, followed by the usage of a sulfur-based reducing agent to reduce NO_2 to N_2 in the second stage (WO 2012/128721) A2 (Liu *et al.*, 2012). To reduce the consumption of the sulfur-based reducing agent used, yet another electrolysis chamber is employed to regenerate it and keep the reducing potential as low as possible. This invention will occupy a large footprint as the vessel will have to house two separate electrolysis systems (one for electrolysing seawater in the first stage and another for regenerating the sulfur reducing agent in the second stage) on top of two distinct wet scrubbers. Additionally, it focuses on keeping the reducing potential at the second stage to as low as possible to ensure NO_2 is reduced N_2, without considering the formation of H_2S.

In another study by Chang and co-researchers, a Dielectric Barrier Discharge (DBD) was used to oxidised NO to NO_2, followed by a wet scrubber where the NO_2 is reduced to harmless N_2 gas using a sulfur-based reducing agent (Chang *et al.*, 2004). A DBD is a non-thermal plasma method where the exhaust gas is bombarded by electrons to generate free radicals, which causes the oxidation to take place. However, this group did not report the pH data of the wet scrubber and also did not take into account the absorption of CO_2 or the potential formation of H_2S due to the usage of sulfur-based reducing agents. Furthermore, when CO_2 is present in the exhaust gas, bombardment by electrons in the DBD section causes the formation of significant amounts carbon monoxide, which is poisonous.

2.4. Usage of alternative fuel

The consideration for using alternative fuels for shipping in oppose to traditional marine fuels is mostly driven the effort to reduce carbon dioxide emissions, and less so about reducing SO_x and NO_x. Under the 'Initial IMO Strategy on Reduction of GHG Emissions from Ships' adopted in 2018, the target is to reduce at least 50% of CO_2 emissions by 2050, based on 2008 levels (MEPC.72/17/Annex11, 2018). This target will help the shipping industry align itself to the Paris Agreement in keeping global temperature rise to within 1.5°C. The definition of alternative fuel is broad and includes other forms of fossil fuel as well as renewable energy – basically anything that is not the traditional marine fuel (HFO and MGO) is considered an alternative fuel. All types of alternative fuel currently being considered, including fossil-based alternatives, have very low sulfur content and their usage would eliminate the emissions of SO_x. However, NO_x, which is mostly made up of NO and is a product of high combustion temperature, would still be present in the exhaust gas.

2.4.1. Liquified natural gas (LNG)

Liquified natural gas or LNG is natural gas that has been cooled to -162°C, causing it to convert to liquid form and making it easier for transportation and storage. From the short to medium term timeline, the usage of fossil-based LNG can help to reduce GHG emissions because its combustion generates a much smaller amount of CO_2 due to the presence of only one carbon molecule in methane. The LNG supply chain is also very well established, making it a reliable fuel source. Usage of LNG would reduce SO_x and PM emissions to negligible levels and NO_x emissions by as much as 80% (Thepsithar, 2020; Feng *et al.*, 2022). However, the overall GHG reduction may be only in the range of 8 – 20%. This is because the benefits of CO_2 reduction from LNG combustion is usually offset by methane slip, where methane, which is also a GHG itself, unintentionally escapes into the atmosphere during the combustion process.

To utilise LNG, ships require a special dual-fuel propulsion system in oppose to the traditional diesel ship engines and also special fuel tanks and its associated support system. These systems are typically more complicated to construct, owing to the higher safety standards that are required, making LNG ships more expensive than conventional ships by up to 30%. Additional bunkering infrastructure will also have to be set up, requiring additional investment.

In order to further reduce GHG emissions, renewable LNG which is LNG produced from renewable pathways instead of fossil fuels, can be considered. These renewable pathways include the anaerobic digestion of organic matters. However, the supply of renewable LNG is expected to be small.

2.4.2. Liquified Petroleum Gas (LPG)

LPG is mainly made up of a mixture of propane and butane. Although both of these compounds are gaseous in ambient temperature, they have a much higher boiling point compared to methane (-42°C and -0.5°C respectively, versus -162°C of methane), making them much easier to liquify with just the application of higher pressure without the need for expensive cryogenic cooling. Similar to LNG, LPG also requires a dual-fuel engine to run and a special fuel tank for storage (Wang *et al.*, 2022). However, retrofitting of conventional ships to be LPG powered would be simpler than LNG's case as cryogenic auxiliary systems would not be required. From the environmental aspect, LPG are typically desulfurized during the production stage and will not generate any SO_x emissions when it undergoes combustion. It also generates up to 20% less GHG and NO_x emissions (WLPGA, 2021).

2.4.3. Methanol

Methanol, which is made up of a methyl and hydroxyl group combined together (CH_3-OH), is a common chemical feedstock with many industrial purposes. Its main draw to be used as a fuel is that it exists as a liquid in room temperature, making it much easier to store and transport, unlike hydrogen, and does not need to be liquefied at very low temperatures like LNG or pressurised like LPG. During combustion, no SO_x is emitted since there is no sulfur in methanol, and PM can be reduced to insignificant levels. Up to around 50% of reduction in NO_x emission is expected to be achieved as combustion using methanol occurs at a lower temperature (Thepsithar, 2020). However, fossil methanol does not contribute much to GHG reduction, up to only 7% (Wärtsilä, 2023)

Similar to LNG and LPG, methanol requires the use of a dual-fuel engine, but has a much simpler fuel storage requirements since it does not require cryogenic cooling or pressurisation to keep it in liquid state (Wang *et al.*, 2022). However, when it comes to the amount of fuel which can be stored, more space is required since its energy density is less than half compared with conventional fuels. Methanol is also toxic and corrosive to most metals, therefore requiring special safety requirements and construction material.

2.4.4. Biodiesel

Biodiesels, consist of fatty acid methyl esters (FAME) and are usually produced from vegetable oil. Because its quality closely resembles diesel fuel, it can be used directly by blending with traditional marine fuel. Unlike LNG which requires a different ship engine, biofuels can be used with traditional ship engines and its corresponding support systems (Mohd Noor *et al.*, 2018). It also does not require new bunkering infrastructure. However, the production capacity is small and most of the biofuels currently produced are from food-based sources such as palm oil, soya

oil or rapeseed oil instead of more sustainable sources such as animal fats or used cooking oil (Thepsithar, 2020).

When blended with traditional marine fuel, the resulting emissions would have lower amounts of SO_x and PM, depending on the level of blending. However, NO_x emissions may increase by up to 10% (Lin, 2013; Feng *et al.*, 2022).

2.4.5. Hydrogen

The usage of hydrogen (H_2) to replace conventional fuels has been discussed for decades but has only been taken more seriously lately due to intensifying GHG emissions and climate change. As the majority of currently produced H_2 comes from the usage of fossil fuel as feedstock (>90%), the impact on GHG reduction would not be significant unless it is produced by the electrolysis of water powered by renewables.

Hydrogen can be used as a fuel source via two routes – by internal combustion engine (ICE) or by proton exchange membrane fuel cells (PEMFC). For internal combustion, hydrogen fuel mainly utilises a dual-fuel engine design, similar to LNG, LPG and methanol (Wang *et al.*, 2022). In terms of emissions, SO_x and PM would be negligible but NO_x would still be generated due to the high combustion temperatures. For the fuel cell route, the emissions generated would be water only.

The main challenge of utilising hydrogen would be storage due to safety concerns and its low energy density. Current methods of storage include liquefaction and compression, like LNG and LPG respectively. However, hydrogen can also be stored in the form of methanol or ammonia, as each of these molecules contain four and three atoms of H respectively (Thepsithar, 2020).

2.4.6. Ammonia

Similar to hydrogen, ammonia does not contain any carbon in its molecule and its molecular formula is NH_3. It is a colourless gas under atmospheric conditions and when combusted, nitrogen gas and water vapour are formed. The vast majority of ammonia is produced from the Haber-Bosch process, where N_2 and H_2 gases are reacted at high temperatures with the aid of a catalyst, which is a very energy intensive process (McKinlay *et al.*, 2021). Although the carbon footprint of ammonia production is high, it can be significantly reduced if renewable energy is used to generate the heat for reaction during process and to produce the H_2 feedstock by electrolysis.

On board a vessel, ammonia has to be stored in a refrigerated tank below -33°C in order to keep it in liquid state, which makes it much simpler to store compared to LNG since no cryogenics is needed, but harder compared to methanol and LPG since refrigeration is required. Similar to other alternative fuels, it requires the use of a special dual-fuel engine to run. From the environmental aspect, combustion of ammonia produces negligible amounts of SO_x and PM due to the absence of sulfur. However, NO_x emissions are typically high since the combustion chambers have to maintain a high temperature to minimise ammonia slip ((Wang *et al.*, 2022).

Table 2-6: Summary of alternative fuels for ships.

Alternative Fuel Type	**LNG**[^]	**LPG**[^]	**Methanol**[^]	**Biodiesel**	**Hydrogen**	**Ammonia**
Content	Methane	Propane Butane	Methanol	FAME	Hydrogen	Ammonia
SO_x/PM emissions[*]	Negligible	Negligible	Negligible	Low, depends on blending ratio	Negligible	Negligible
NO_x emissions[*]	Up to 80% reduction	Up to 20% reduction	Up to 50% reduction	Up to 10% increase	Nil (PEMFC) Low (ICE)	High
GHG emissions[*]	Up to 20% reduction	Up to 20% reduction	Up to 7% reduction	Carbon neutral	Carbon free	Carbon free
Compati-bility[+]	Very Low	Low	Low	Good	Low	Low
EHS concerns	• Cryogenic hazard • Highly flammable • Health hazard	• Corrosive • Highly flammable • Health hazard	• Toxic • Corrosive	Nil	• Highly flammable	• Toxic •

[^] *Fossil source*

[*] *In comparison with conventional ship engines utilising traditional marine fuels*

[+] *Denotes compatibility with conventional ship engine and design of supporting systems*

On a long-term basis, there are opinions that the usage of LNG and LPG are expected to fade out of the market due to their limitations from the decarbonisation point of view (Wang *et al.*, 2022). Green ammonia and green hydrogen are expected to edge out biodiesel and methanol eventually over their ability for achieving a high degree of decarbonisation in their life-cycle and having a higher potential to be price competitive.

Chapter 3. Experimental Setup and Procedures

Details of the materials, equipment, procedures and method are described in this section.

3.1. Materials

3.1.1. Chemicals used

The sodium hydroxide (NaOH) solution and hydrochloric acid (HCl) used were from Merck Millipore (Titripur series), both at 1M concentration. The sodium chlorite ($NaClO_2$) (80% assay) and potassium permanganate (98% assay) were from Acros Organics. The hydrogen peroxide (H_2O_2) was purchased from VWR chemicals, with a concentration of 6% w/v in solution form. The sodium sulfite anhydrous (Na_2SO_3) (puriss, 98-100%), formaldehyde solution (ACS reagent, 37%wt in water) and sodium hypochlorite (NaClO) reagent grade solution were purchased from Sigma-Aldrich. The sodium hypochlorite had an available chlorine range of 4.00 – 4.99% and its actual concentration was determined by iodometric titration. The sodium thiosulfate pentahydrate ($Na_2S_2O_3.5H_2O$) was purchased from Sinopharm Chemical Reagent Co. Ltd.

The seawater used for experiments was collected from the Labrador Park jetty, Singapore. The collection point was approximately 120 meters from the beach and collection was done during high tide. The seawater sample was filtered (0.45μm pore size) first before usage to remove all suspended solids which may get clogged up in the spray nozzle.

3.1.2. Calibration standards

Calibration standards were needed for establishing calibration lines for anionic analysis using the ion chromatograph and UV-Vis Spectrophotometer. These included multi-element standards consisting of chloride, nitrate, and sulfate from Merck and nitrite ions, chlorite ions, and thiosulfate from Sigma Aldrich. The chlorate calibration standard was purchased from VWR Chemicals while the sulfite standard was prepared by weighing a freshly purchase high purity sodium sulfite solid powder. All the standards mentioned above had a concentration of 1000 mg/L.

For the calibration of pH meters, calibration standards of pH 4, 7 and 10 were purchased from Hanna. Oxidation Reduction Standards used to check the accuracy of the ORP probes were the 220mV and 420mV solutions, purchased from Titolchimica.

3.1.3. Gases

The sulfur dioxide (SO_2) and nitric oxide (NO) gases used in this experiment were specially blended with a concentration of 10,000 ppm(v) and 20,000 ppm(v) respectively, balanced with nitrogen. The oxygen (O_2) and nitrogen (N_2) gasses used were of high purity quality, with a

concentration of 99.99% and 99.995% respectively. The gas cylinders mentioned above were supplied by Singapore Oxygen Air Liquide Private Limited. The nitrogen dioxide (NO_2) gas at a concentration of 10,000 ppm(v) was supplied by Leedon National Oxygen Ltd.

3.2. Equipment

The equipment used for this study can be segregated into the gas-liquid reactors, the gas handling equipment, liquid handling equipment and the analysers for carrying out quantitative analysis of the aqueous samples.

3.2.1. Gas-liquid reactors used for wet scrubbing

Two types of gas-liquid reactors or wet scrubbers were used in this study and are describe below:

i) Gas bubbling reactor (impinger)

The gas bubbling reactor is a simple device for conducting gas-liquid reaction by bubbling gas in aqueous solution. This device was a product of Pyrex and has a capacity of 250ml (No. 31770, 29/42) (see Figure 3-1). Gas entering this device is passed through a glass fritted cylinder (coarse porosity, diameter approximately 12mm) where it is forced to form small bubbles in the liquid. Small bubble sizes increase the mass-transfer rate between the gas and liquid. This device was easy to use and clean, and experiments with it can be carried out using smaller amounts of gases and chemicals. However, the liquid in the reactor does not flow and remains stationary. Also, forcing gas through a fritted cylinder to bubble in a solution causes a significant pressure drop.

Figure 3-1: The gas bubbling reactor used in this study.

ii) Counter-current adjustable wet scrubber

The design of this custom-made wet scrubber was based on a cylindrical counter-current wet scrubber typically used in the industry, with a diameter of 99 mm (see Figure 3-2). The top, middle and bottom sections are individual modules which are all compatible with each other and can be separated or joined according to the configuration needed. The middle section between the spray nozzle and the base is the reaction zone where the gas-liquid reaction takes place and can be made up of modules which are either 100mm or 150mm in height. For brevity, this reaction zone at the middle section will simply be referred to as 'scrubber height'. These separate modules are locked together with a horse-shoe metal clamp, with PTFE O-rings in between modules to prevent any gas leaking from its joints. The spray section was designed to be fitted with existing industrial spray nozzles. A glass filter disc was fitted at the top of the scrubber before the gas exited to function as a mist eliminator to minimise the escape of liquid with the exhaust gas. This wet scrubber can be converted from a spray tower to a packed column configuration by the addition of packing materials to the reaction zone in the middle section.

3.2.2. Gas handling equipment

The flowrates of gases flowing from the pressure regulators were controlled by Brooks Instruments GF100 mass flow controllers (MFC). These MFCs were equipped with Hastelloy seal on the plunger side in order to provide the necessary corrosion resistance to acidic gases. Each MFC was in turned wired to a four-channel Brooks Instruments 0254 reader/controller. The MFCs used here were able to control the flowrate of gases coming from the gas cylinders at a much higher precision compared with traditional rotameters.

Various gases from the gas cylinders were mixed in the appropriate ratio and are hence referred to as '*simulated exhaust gas'*. Before going into the wet scrubber, the simulated exhaust gas was passed through a Swagelok stainless steel 316 double-ended gas mixing cylinder in order to enhance its mixing. When temperature control was required, the simulated exhaust gas was heated by passing it through an Omega Gas Heater (Model AHP-7562) with P&ID control. The mixed simulated flue gas was eventually channelled to a three-way ball valve that toggled the gas to either the flue gas analyser or wet scrubber.

Two different flue gas analysers were used for this study. In the initial stage of this study, it was discovered that the Testo 350XL flue gas analyser which utilised electrochemical sensors could not accurately measure the concentration of SO_2 and NO_2 gas under certain circumstances – the presence of small amounts of chlorine-based gases (likely ClO_2) interfered with its accuracy. Therefore, a second analyser was used, which was the MGA Luxx which utilised

nondispersive infrared (NDIR) sensors for measuring SO_2, NO, NO_2, CO_2 and H_2S, and an electrochemical cell for measuring O_2. These NDIR-based sensors are more accurate as they are not subjected to cross-sensitivity interferences experienced by electrochemical sensors. Data from both the exhaust gas analysers were data-logged with their respective software.

Moisture from the gas was removed by in-built moisture traps in both analysers. The MGA Luxx flue gas analyser contained an in-built dual gas cooler (Peltier) with dual condensate draining pumps operating at 5°C. The tube connecting the gas sampling probe to the gas analyser was kept heated at 150°C to prevent any condensation along the sampling line.

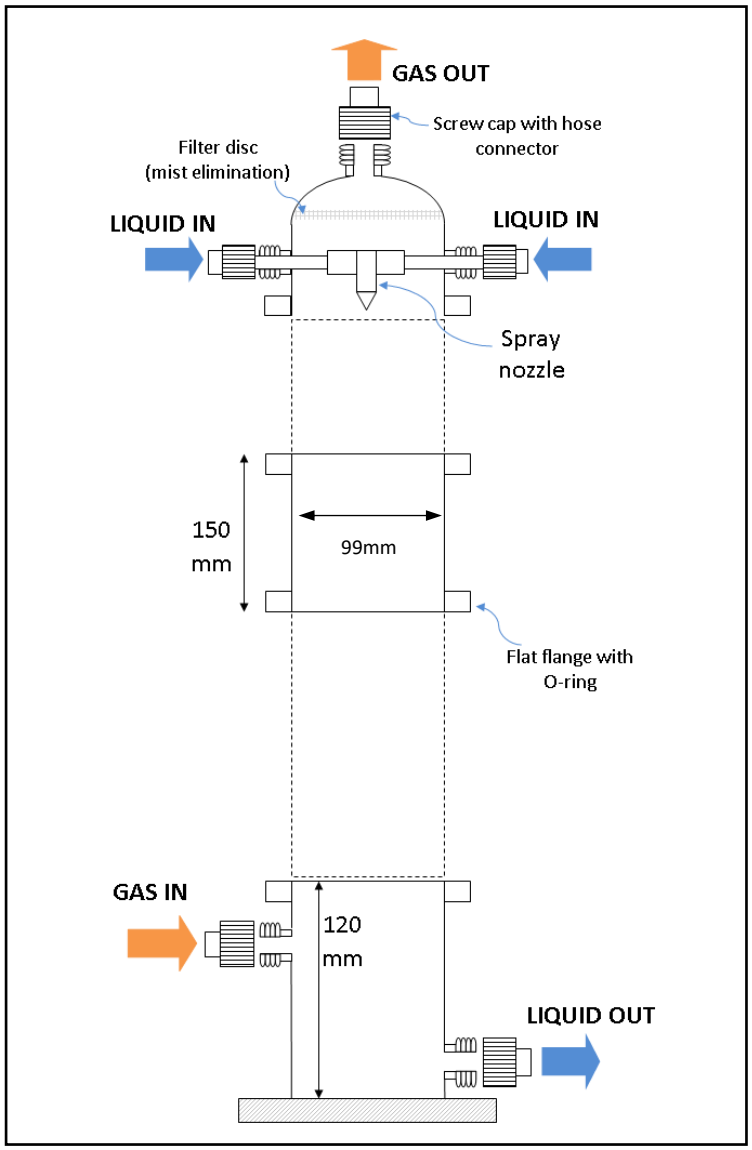

Figure 3-2: The schematic diagram of the counter-current glass wet scrubber with adjustable height.

3.2.3. Liquid handling equipment

All liquid pumping requirements in this experimental setup were carried out by the Masterflex L/S (Model 7523-80) peristaltic pump. These included continuous pumping of scrubbing liquid from the liquid holding tank into the wet scrubber which was then recirculated back from the wet scrubber to the liquid holding tank and also the dosing of acid or alkaline solution into the liquid holding tanks in order to control the pH. The pH, conductivity and oxidation reduction potential (ORP) probes used to measure the scrubbing liquid in the tank were from Thermo Fisher Scientific, with built-in temperature sensors for automatic temperature compensation (ATC). These were connected to the Orion Versa Pro multi-meter, with datalogging function. When temperature control was needed, the temperature of the scrubbing liquid was controlled by submerging the reaction tank into a large water bath, with a submersible magnetic stirrer placed at the bottom of the tank to ensure good mixing.

3.2.4. Equipment for aqueous analysis

Aqueous samples from the scrubbing liquid were collected from the liquid holding tank before the beginning of reaction, in between reaction at specific time intervals, and at the end of the reaction in the experiments carried out here. Analysis of the aqueous samples for chlorine dioxide (ClO_2) concentration was carried out immediately using the Hach DR900 colourimeter as this species is very unstable. The direct measurement method was used in this case (Method 73). Where turbidity measurement was required, the analysis was also carried out immediately using the Lovibond TB 210 IR as the presence of suspended solids may be unstable as well. The aqueous samples were then stored in an ice box to ensure stop the reaction and minimise further changes.

The Metrohm Basic IC ion chromatograph system was used for the quantitative analysis of chloride (Cl^-), chlorite (ClO_2^-), chlorate (ClO_3^-), nitrite (NO_2^-), nitrate (NO_3^-), sulfite (SO_3^-), sulfate (SO_4^{2-}) and thiosulfate ($S_2O_3^{2-}$) while the Biochrom Libra S22 UV-VIS Spectrophotometer was used for the analysis of hypochlorite (ClO^-) and permanganate (MnO_4^-). After dilution, the aqueous samples were filtered with a 0.45µm polypropylene syringe filter in order to remove any solid particles which may clog the ion chromatography column or interfere with the spectrophotometer results. In this study, Total Soluble Nitrogen was defined as the total soluble nitrogen that exists in the aqueous phase. This was calculated by adding the nitrite (NO_2^-) and nitrate (NO_3^-) anion concentrations obtained from the ion chromatography results.

3.3. Calculations

The removal efficiency (η_i) of gas pollutant *i* from the various gas-liquid reactions were calculated according to Equation 3.1:

$$\eta_i = \frac{[C_i]_{inlet} - [C_i]_{outlet}}{[C_i]_{inlet}} \times 100\% \qquad \ldots (3.1)$$

Where *i* refers to one of the gas pollutants SO_2, NO, NO_2 or NO_x, and $[C_i]_{inlet}$ or $[C_i]_{outlet}$ refers to the concentrations of the gas pollutant *i* at the inlets or outlets of the wet scrubber, as recorded by the flue gas analysers, in ppm(v).

The amount of gaseous pollutant *i* that was removed (in mol) during the wet scrubbing process by various scrubbing mixtures was calculated by taking the area under the curve in the graph of pollutant *i* removal vs. time. More specifically, amount of pollutant *i* removed during the experimental run can be calculated as follows:

Amount of gas pollutant *i* removed

$$= \sum([C_i]_{inlet} - [C_i]_t) \times 1{,}000{,}000 \times \mathrm{G} \times \frac{P}{RT} \times \Delta t \ (mol)$$

Where G refers to the gas flowrate, P is the atmospheric pressure at 101325 Pa, *T* is the temperature in kelvins and R is the universal constant at 8.3145 $m^3.Pa.K^{-1}.mol^{-1}$. The time interval, Δt, in this study refers to the time interval used by the flue gas analyser datalogger, which was 5 seconds. It was assumed that ideal gas law was followed.

Chapter 4. Comparison of various chemical compounds for SO_2 and NO removal

In this chapter, various types of chemical compounds were compared for their ability to remove SO_2 and NO from the exhaust gas by wet scrubbing. From the literature review, it was seen that there is a large variety of chemical compounds that has been studied so far. However, almost all of these were done as separate studies – there is very limited work carried out to compare various types of chemical compounds on a single experimental platform. The chemicals selected for this study were based on three criteria, namely, for their potential in NO_x removal, availability in the industry at a reasonable cost or existing usage on ship-based wet scrubbers.

This chapter is split into two sections, with the first involving the use of the gas bubbling reactor and the second involving the use of a counter-current wet scrubber. Although the former was carried out as an investigation on the preliminary stage, its results are included here as some of the observations seen are also important in supporting the overall findings.

4.1. A preliminary setup using a gas bubbling reactor

The gas bubbling reactor was first used during the initial setting-up phase of this experimental skit. The simplicity of this type of wet scrubber allowed more attention to be paid to other more complicated areas of this experimental skit, especially in the control of gas flow, gas mixing and flue gas analysis. Troubleshooting and correction could be carried out more easily at the initial stage without having to deal with the complexities of a counter-current wet scrubber with liquid flowing in a continuous loop at the initial stage. This also allowed crucial work to be done while waiting for the custom-made counter current wet scrubber to be fabricated.

Additionally, the setup using the gas bubbling reactor continued to be useful even till the later stages of the project. Since the gas bubbling reactor is much smaller in size compared to the counter-current wet scrubber, new gas-liquid reactions could be carried out quickly without the need of using large quantities of chemicals and gases, while the ease of setting up and cleaning allowed for more runs to be carried out in a short time.

It should be noted that the mechanism of mass transfer between the gas and liquid phases in a gas bubbling reactor is different from the counter current wet scrubber. In the former, gas is passed through a fritted cylinder submerged in liquid, forming bubbles which are then dispersed in the liquid. In the latter, small droplets of liquid are formed when it passes through the spray nozzle (in the case of a spray tower), forming tiny droplets which interacts with the gas in a counter-current manner. Although the gas bubbling reactor should have a higher mass-transfer rate compared to the counter- current wet scrubber, it is not practical for scaling up due to the large pressure drop in such systems. Although there are limitations when making comparisons

between the gas bubbling reactor and the counter-current wet scrubber due to their differences in mass transfer, the initial observations that could be obtained from the former can still provide important information.

In this section, the general reactions trends that were observed are discussed below but the more detailed reaction mechanisms and chemical equations have been consolidated in the section for the counter-current wet scrubber, in order to avoid duplication (Section 4.2).

4.1.1. Experimental procedure

In this section, the gas-liquid reaction was carried out using a gas bubbling reactor or impinger (shown in Figure 3-1 previously) and the experimental schematic setup is shown in Figure 4-1.

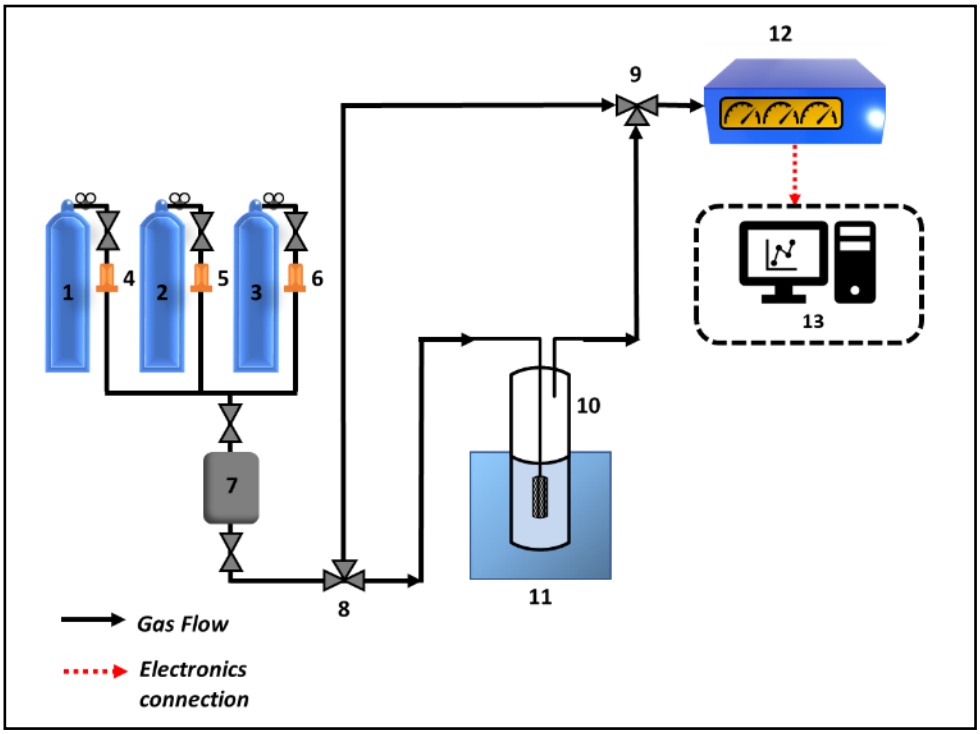

Figure 4-1: Schematic diagram of the experimental setup using the gas bubbling reactor.
(1 – 3) Gas cylinders; (4 – 6) mass flow controllers; (7) gas mixer; (8 – 9) three-way valves; (10) gas bubbling reactor; (11) water bath; (12) flue gas analyser; (13) computer.

The experiments carried out in this section using the gas bubbling reactor is summarised in Table 4-1. As can be seen in the table, more emphasis was given to NO rather than SO_2 since the former is a much more difficult gas to remove. The chemicals to be used as the scrubbing solution were prepared beforehand and diluted to the required concentration. The correct volume of the solution was measured with a glass measuring cylinder and poured into the gas bubbling reactor. The mass flow controllers were then set accordingly to channel the gas at the desired concentration. Before the reaction began, the simulated flue gas was channelled to the

flue gas analyser. Once the baseline reading was stabilised, the three-way valve was then switched to channel the flue gas into the gas bubbling reactor. The flue gas analyser used in this section was the Testo 350XL with electrochemical cells.

Table 4-1: A summary of experimental conditions for studies carried out using the gas bubbling reactor. Temperature was ambient and O_2 in excess (>5%).

No	Scrubbing solution	Conc. (M)	pH	ORP (mV)	Liq. Vol (ml)	Gas Flow rate (L/min)	Conc. (ppmv)		
							SO_2	NO	NO_2
1	Sodium chlorite ($NaClO_2$)	0.10	12.5	490	100-200	1.20	--	125	--
2	Sodium hydroxide (NaOH)	0.10	13.1	-16	150	1.20	--	150	--
3	Sodium hypochlorite (NaClO)	0.10	12.5	490	150	1.20	--	150	--
4	Sodium chlorite ($NaClO_2$)	0.10	10.7	450	150	1.20	--	150	--
5	Potassium permanganate ($KMnO_4$)	0.10	9.7	530	150	1.20	--	150	--
6	Sodium chlorite ($NaClO_2$)	0.05-0.20	--	--	150	1.20	150	--	--
7	Sodium chlorite ($NaClO_2$)	0.05-0.20	--	--	150	1.20	--	150	--
8	Sodium chlorite ($NaClO_2$)	0.10	6.8 – 10.7	--	150	1.20	--	150	--
9	Potassium permanganate ($KMnO_4$)	0.05-0.20	--	--	150	1.20	150	--	--
10	Potassium permanganate ($KMnO_4$)	0.05-0.20	--	--	150	1.20	--	150	--
11	Potassium permanganate ($KMnO_4$)	0.10	3.1 – 11.0	--	150	1.20	150	--	--
12	Potassium permanganate ($KMnO_4$)	0.10	3.2 – 11.1	--	150	1.20	--	150	--
13	Sodium chlorite ($NaClO_2$) + Sodium hydroxide (NaOH) *	0.10 0.10	--	--	150 150	1.20	--	150	--
14	Sodium chlorite ($NaClO_2$) + Sodium hydroxide (NaOH) *	0.10 0.20	--	--	150 150	1.20	--	150	--
15	Sodium chlorite ($NaClO_2$) + Sodium chlorite ($NaClO_2$) *	0.10 0.10	--	--	150 150	1.20	--	150	--

** Denotes a configuration where two gas bubbling reactors were arranged in series*

The stopwatch was simultaneously started to keep track of the reaction time. The simulated exhaust gas was bubbled in the scrubbing liquid and then exited the gas bubbling reactor into the flue gas analyser once again where its concentration after scrubbing was measured. The flue gas concentrations before and after scrubbing were then compared. As the computer system for data logging was still in the midst of being setup, some of the data were recorded by hand at regular time intervals. Data that were manually recorded are presented as individual points in the graphs in this study, in oppose to continuous lines for data that were automatically logged as these have a very short time interval of 5 seconds.

4.1.2. Mixing study of the gas bubbling reactor

A simple study was carried out to ensure that gas-liquid mixing in the gas bubbling reactor was homogenous and the conditions used avoided the occurrence of dead-zones which may impact the results. Both the range of gas flowrate and liquid volume had to be determined. With respect to the selection of gas flowrate, it was noted that the flue gas analyser required 1 L/min of inlet gas flow for gas analysis. If the amount of gas reaching the flue gas analyser was below this, ambient air will be sucked-in and mixed with the sample gas, causing it to be diluted and rendering the results inaccurate.

In order to ensure that the amount of gas reaching the flue gas analyser was at least 1 L/min, the chosen gas flowrate should be at least slightly in excess of this. However, since the gas bubbling reactor was small in size, it was also observed that overly high flowrates in excess of 2 L/min caused excessive turbulence and led to potential spillage of liquid from the reactor. Therefore, a more suitable range of 1.20 – 1.50 L/min was chosen as decent mixing was observed for the various liquid volumes tried out. As for the liquid volume, the range of 100 – 200ml was selected. Volumes exceeding 200ml was avoided as the liquid level should not be too close to the top of the gas bubbling reactor to avoid spillage during mixing.

Based on these conditions, a simple visual observation study was used to determine the mixing during reaction. A drop of saturated potassium permanganate dye was dropped into DI water of various volumes (100, 150 and 200ml) and bubbled with nitrogen gas at 1.20 L/min and the mixing was observed and timed. Without gas flow in the chamber, the mixing of the dye in water was slow, requiring more than a minute before achieving homogeneity (see Figure 4-2 [A], where the state of mixing at around 10 seconds was still far from homogenous).

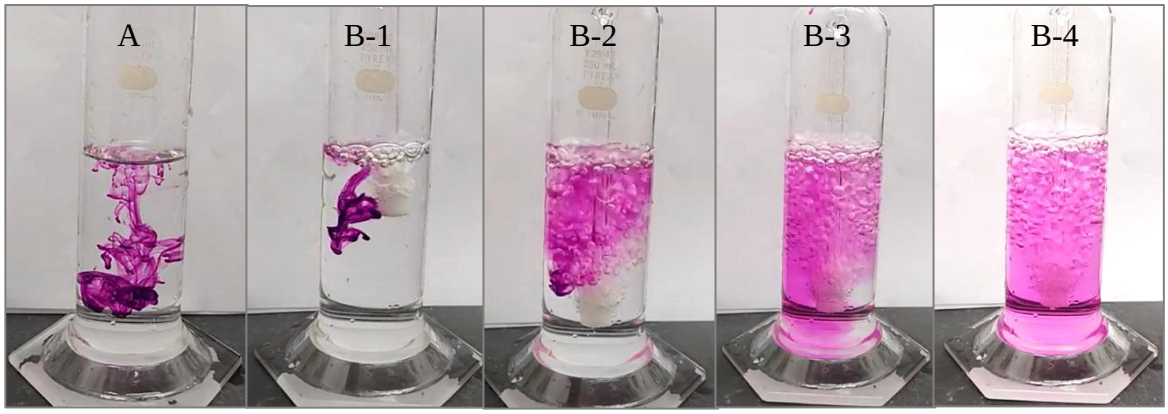

Figure 4-2: Mixing of dye with water under various timings. The liquid volume shown here was 150ml.
[A]: Without gas flow (at 10 seconds, still far from homogeneity).
[B-1] to [B-4]: With gas flowrate of 1.20 L/min. [B-1] is at 0 seconds, [B-2] and [B-3] between 0 to 2 seconds and [B-4] around 2 seconds.

When gas was bubbled the same time as the dye was introduced, a strong turbulent mixing pattern was observed even at the aqueous zone below the fritted cylinder and complete mixing was observed in less than 2 seconds for all the three aqueous volumes used. Although the gas bubbles flowed upwards when exiting the fritted cylinder and did not come into direct contact with the aqueous layer at the bottom, the strong mixing caused by the turbulent flow in the aqueous phase would likely compensate for any loss in mass transfer.

4.1.3. Variation of liquid volume used for reaction

It was established in the previous section that the volume of 100 – 200ml was suitable for use in the gas bubbling reaction. In this section, the liquid volume used in the gas bubbling reactor was varied between 100 – 200ml in order to determine the optimal volume to be used. Here, sodium chlorite ($NaClO_2$) was used for NO removal and the results are shown in Figure 4-3. It can be seen that sodium chlorite of 0.10M concentration were effective in the removal of NO at all liquid volumes used. Total removal of NO gas took between 8 to 20 minutes to achieved, with the highest volume taking the least time. The middle volume of 150ml was chosen for subsequent experiments as a balance between reducing chemical wastage and having sufficient sample volume for conducting aqueous analysis.

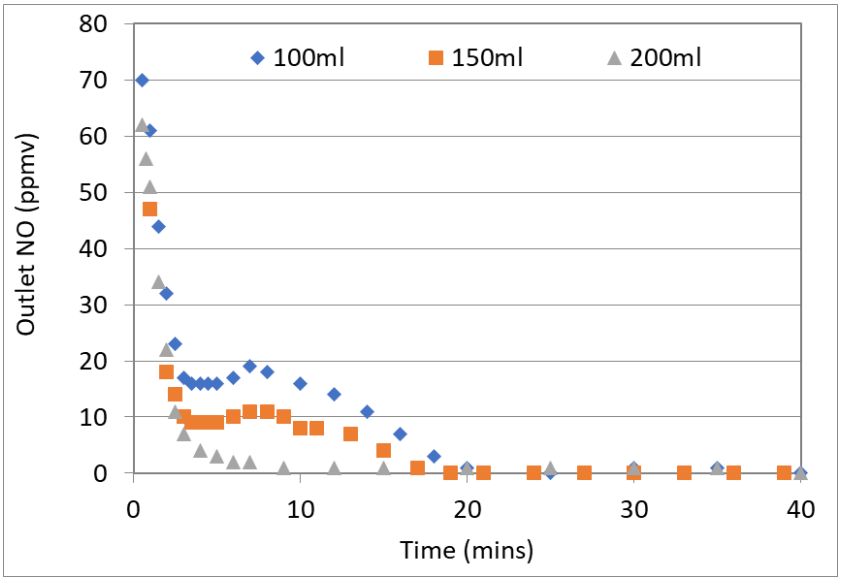

Figure 4-3: Outlet concentrations of NO exiting the gas bubbling reactor with variation of liquid volume (using $NaClO_2$).
Experimental conditions are shown in Table 4-1, no. 1.

4.1.4. Variation of chemical compounds for NO removal

In this section, sodium hydroxide (NaOH), sodium hypochlorite (NaClO), sodium chlorite ($NaClO_2$) and potassium permanganate ($KMnO_4$) were used as scrubbing solution for removing NO gas. Experimental details can be seen in Table 4-1, No. 2-5. As can be seen from the table, $KMnO_4$ had the highest oxidation reduction potential (ORP) or redox potential among all the

substances used, followed by NaClO, $NaClO_2$, and finally NaOH. From the results in Figure 4-4, the NaOH and NaClO scrubbing solutions had no effect on NO removal; the concentration of NO gas entering and leaving the scrubber is around the same using these two compounds. Both the runs for NaOH and NaClO was stopped after 10 mins since there were no reaction taking place. This was unsurprising for NaOH – although it is a highly alkaline solution, it does not have any oxidising power and was not able to react with any of the insoluble NO gas molecules.

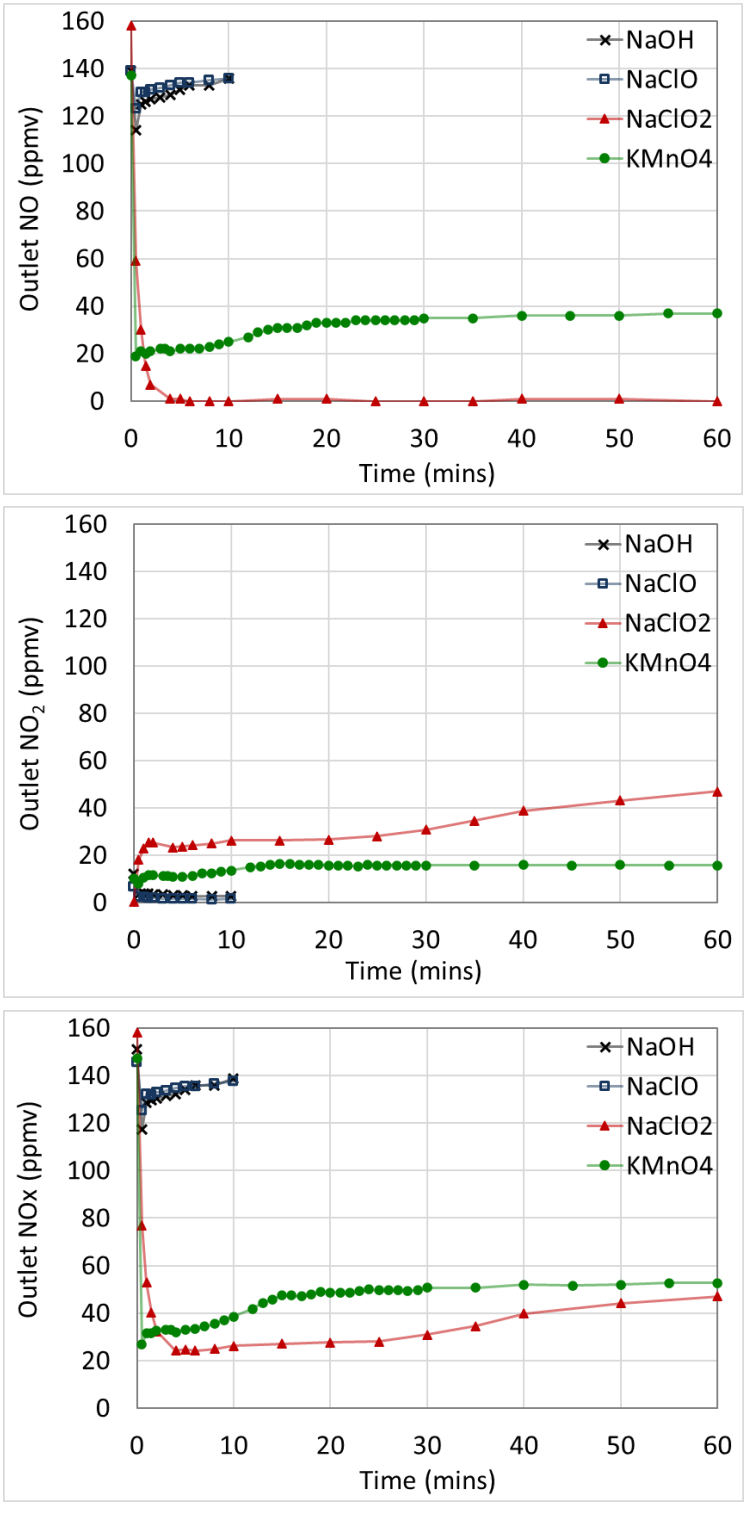

Figure 4-4: Outlet concentrations of NO (top), NO_2 (middle) and NO_x (bottom) exiting the gas bubbling reactor, with variation in scrubbing chemicals used. *Experimental conditions are shown in Table 4-1, No. 2-5.*

On the other hand, NaClO, which is a common oxidising agent used for bleaching and cleaning, also did not manage to oxidise or solubilise the NO gas molecules although it had a high ORP value. It is possible that the NaClO used was ineffective because of its very high pH, at 12.5, causing it to remain in its hypochlorite anion form (Black & Veatch Corporation, 2009). For subsequent experiments, a pH adjustment might be needed to enable it to partition from hypochlorite to hypochlorous acid – the latter exist in more acidic conditions and is known to be a stronger oxidant.

$KMnO_4$, which was the most powerful oxidising agent used in this set (according to redox potential) managed to remove around 80% of NO gas. $NaClO_2$, which had a slightly less oxidizing potential than $KMnO_4$, managed to oxidise NO gas completely. For the present study, it can be concluded that oxidising potential alone as indicated by ORP measurement is not sufficient to predict the effectiveness of NO removal. Observation of the NO_2 gas exiting the gas bubbling reactor showed that $KMnO_4$ and $NaClO_2$ could not completely absorb the NO_2 that was oxidised from NO gas. In terms of overall NO_x removal, $NaClO_2$ performed better compared to $KMnO_4$ in the gas bubbling reactor.

4.1.5. Variation of $NaClO_2$ concentration

The concentration of the sodium chlorite ($NaClO_2$) oxidant was varied for the removal of SO_2 and NO and the results are shown in Figure 4-5 and Figure 4-6 respectively. From Figure 4-5, it can be seen the removal of SO_2 was relatively straightforward and all concentrations of oxidants used could remove the gaseous pollutant completely using the gas bubbling reactor almost immediately with no observable difference.

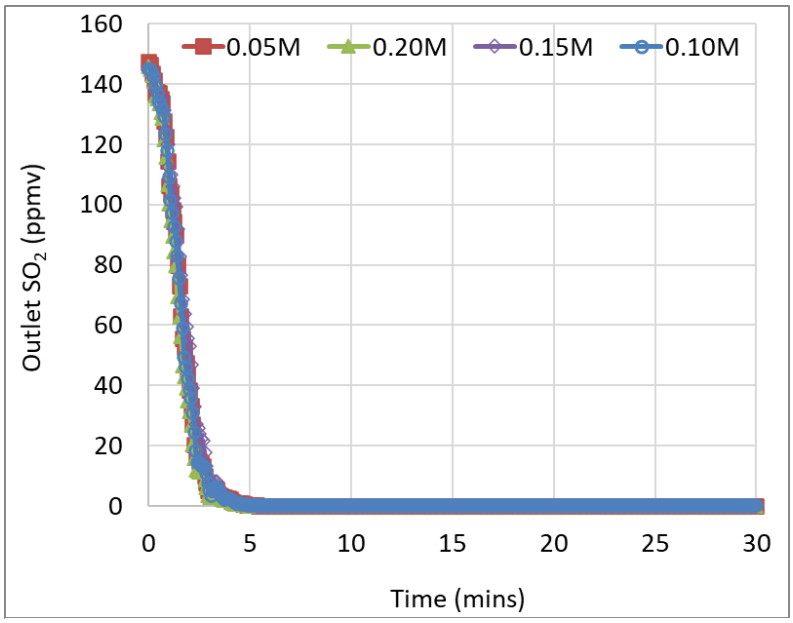

Figure 4-5: Outlet concentrations of SO_2 exiting the gas bubbling reactor with variation of $NaClO_2$ concentration.
Experimental conditions are shown in Table 4-1, No. 6.

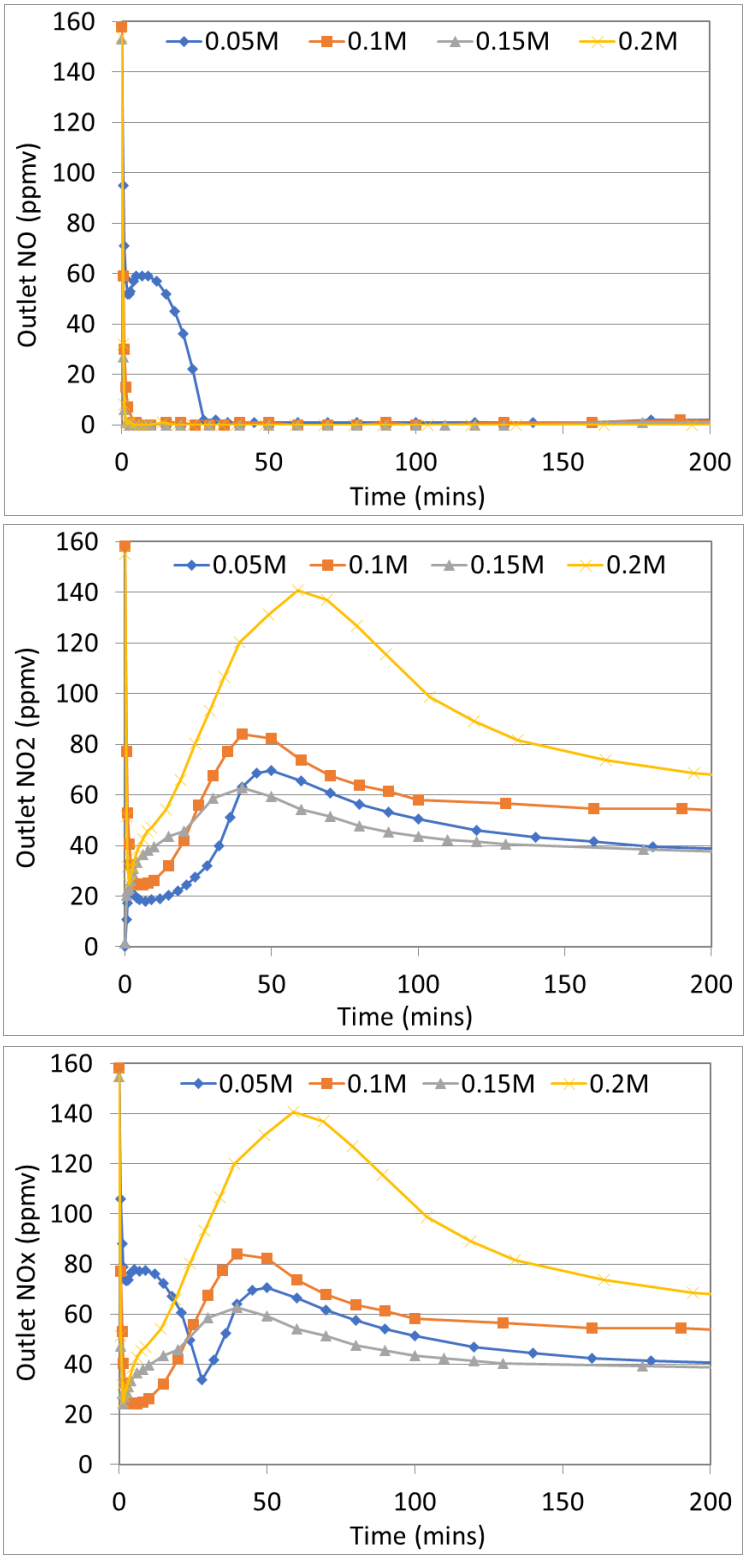

Figure 4-6: Outlet concentrations of NO (top), NO_2 (middle) and NO_x (bottom) exiting the gas bubbling reactor with variation of $NaClO_2$ concentration.
Experimental conditions found in Table 4-1, No. 7.

The removal of NO using the $NaClO_2$ oxidant was slightly more complex (Figure 4-6). Although all concentrations of oxidant could completely remove NO, the lowest oxidant concentration (0.05M) took a significantly longer time to achieve complete removal. This suggested that the aqueous phase was probably going through changes during the reaction that aided the removal of NO gas. One measurable change is the lowering of aqueous pH before and

after reaction (from 10.6 to 8.0), indicating that the oxidant used favoured a lower pH for NO removal.

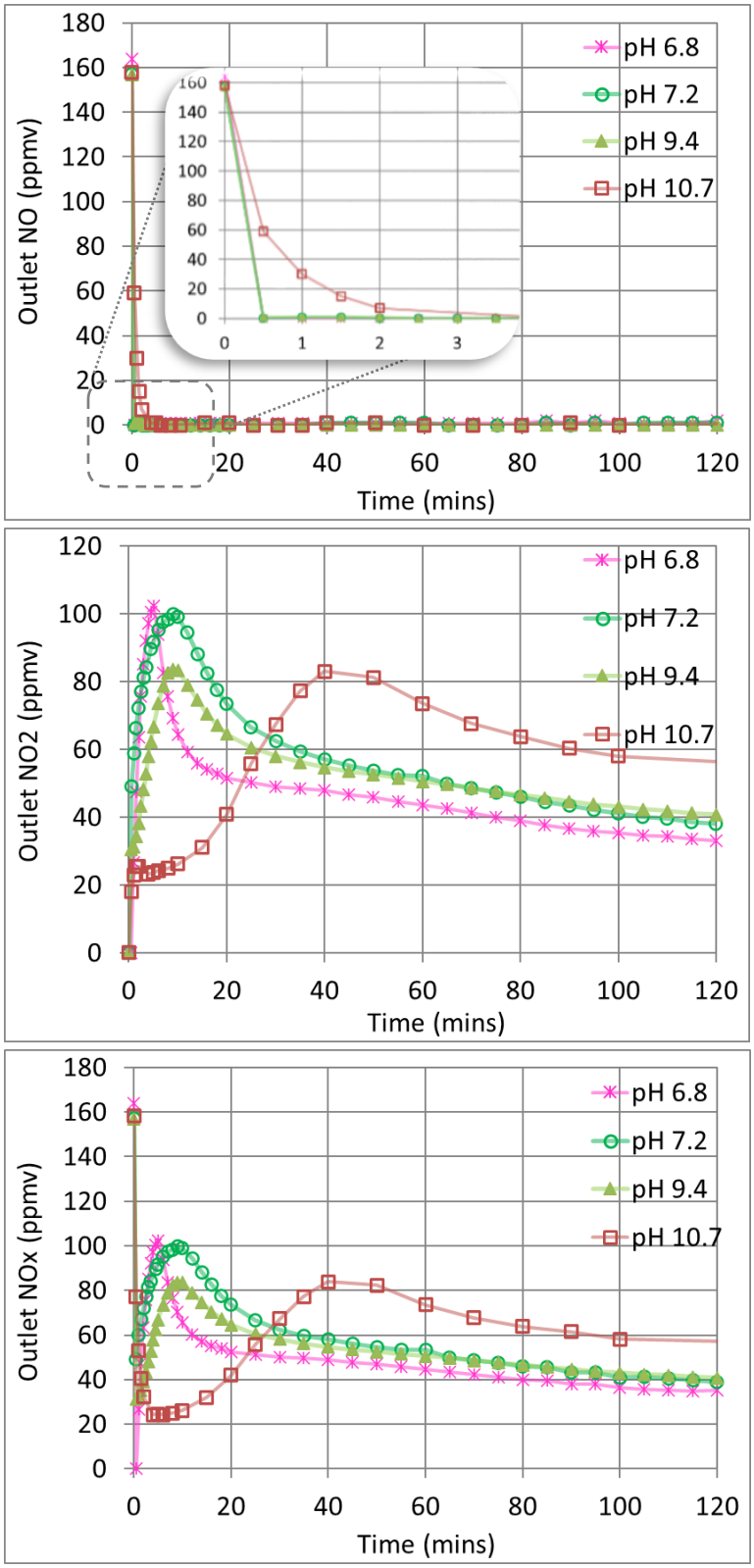

Figure 4-7: Outlet concentrations of NO (top), NO_2 (middle) and NO_x (bottom) exiting the gas bubbling reactor with variation of $NaClO_2$ pH.
Experimental conditions shown in Table 4-1, No. 8.

The removal of NO also coincided with the release of NO_2 gas exiting from the gas bubbling reactor, suggesting that the latter was formed when the former was removed (Figure 4-6, middle). This showed that the oxidant was likely oxidising NO to NO_2 gas. The NO_2 gas that

was formed could only be partially absorbed by the aqueous phase. Part of the NO_2 that was measured could also have been slightly contributed by cross-sensitivity due to the presence of ClO_2 in the exhaust gas. This could have been more pronounced for samples with higher chlorite concentration such as the 0.20M chlorite sample.

4.1.6. Variation of $NaClO_2$ pH

The starting pH of the $NaClO_2$ oxidant used was varied and the results can be seen in Figure 4-7. For NO removal, it can be seen that the highest pH at 10.7 took to longest time to achieve complete removal, at around 3.5 minutes. For pH 9.7 and below, complete removal of NO gas took around half a minute. This was consistent with previous observation that a lower pH favoured the removal of NO. The lowest pH, in this case at 6.8, was also the most effective in removing the NO_2 that was formed, thereby achieving the highest NO_x removal.

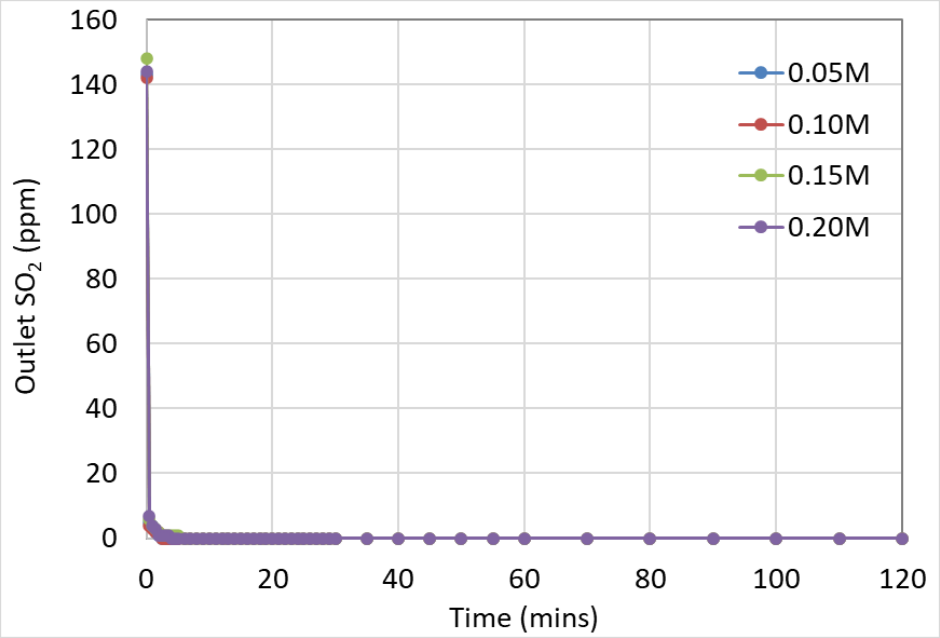

Figure 4-8: Outlet concentrations of SO_2 exiting the gas bubbling reactor with variation of $KMnO_4$ concentration.
Experimental conditions shown in Table 4-1, No. 9.

4.1.7. Variation of $KMnO_4$ concentration

Further runs were carried out using $KMnO_4$ since this chemical compound also showed potential for application, alongside sodium chlorite. In this section, the concentration of $KMnO_4$ was varied for the removal of SO_2 and NO respectively, using the gas bubbling reactor. The results can be seen in Figure 4-8 and Figure 4-9.

As expected, the removal of SO_2 by $KMnO_4$ was quick and complete for all concentrations of the reactant used, owing to the high solubility of SO_2 gas (Figure 4-8). This was similar to using

$NaClO_2$ as the oxidant for SO_2 removal in the previous section. As for NO, it can be seen that its removal was proportional to the concentration of $KMnO_4$ used. Complete removal of NO was close to complete when the concentration was 0.20M. The NO_2 that was formed from oxidation of NO was not completely absorbed by the aqueous phase and escaped from the gas bubbling reactor, indicating that NO_2 solubility is not as high as anticipated. This observation was consistent when $NaClO_2$ was used as the oxidant as well. In terms of overall NO_x, increasing of $KMnO_4$ concentration increased its removal (Figure 4-9, bottom).

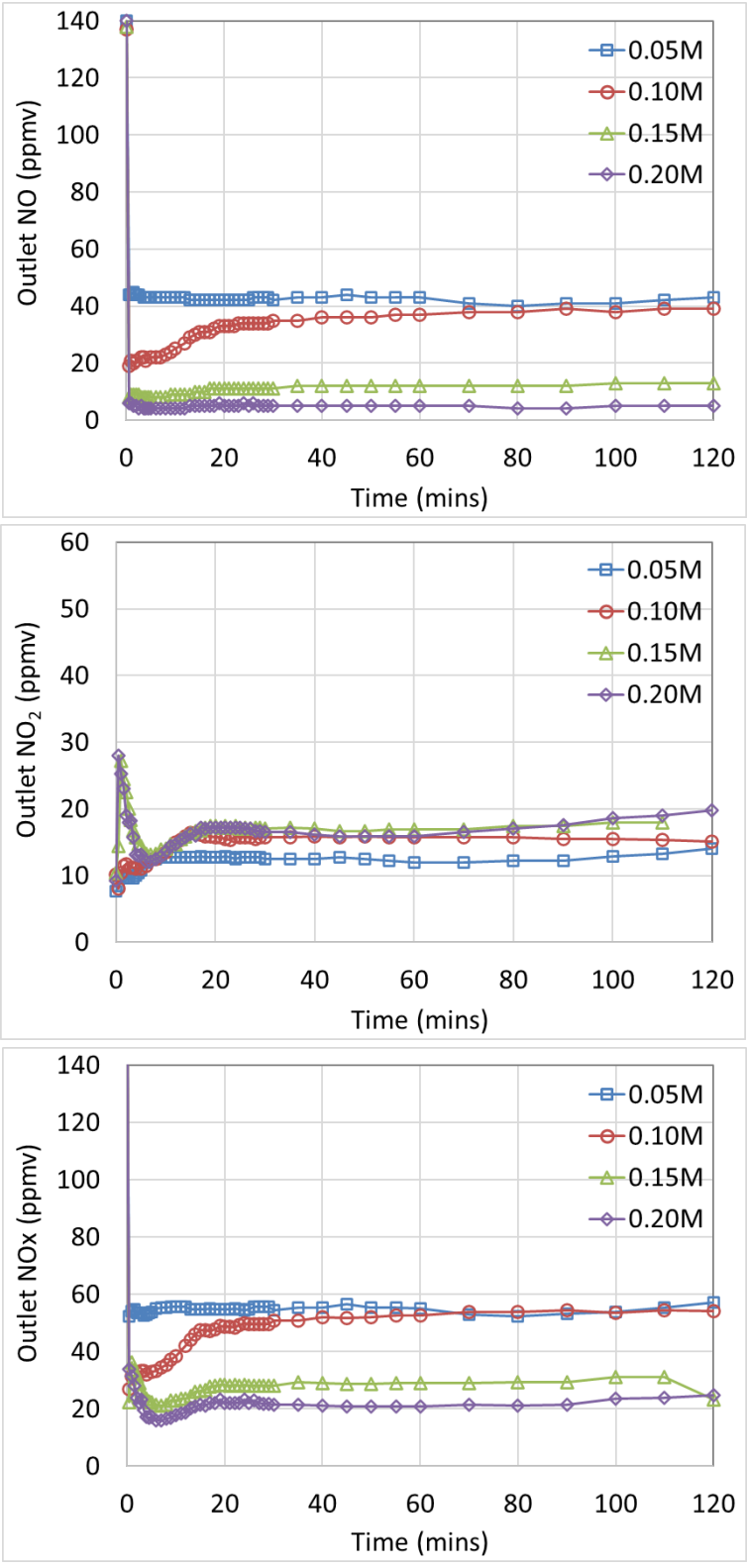

Figure 4-9: Outlet concentrations of NO (top), NO_2 (middle) and NO_x (bottom) exiting the gas bubbling reactor with variation of $KMnO_4$ concentration. *Experimental conditions are shown in Table 4-1, No. 10.*

4.1.8. Variation of $KMnO_4$ pH

The pH of the $KMnO_4$ oxidant was varied for the removal of SO_2 and NO respectively, and the results can be seen in Figure 4-10 and Figure 4-11. From Figure 4-10, it can be seen that the removal of SO_2 was again rapid and complete. Owing to the high solubility of SO_2, complete absorption was achieved even at a low pH of 3.1.

The variation of the pH of $KMnO_4$ solution did not seem to have a significant impact on the removal of NO. From Figure 4-11 (top), it can be seen that the removal achieved at various pH levels clustered together at around 10-30ppm of outlet NO concentration. This was different compared with the $NaClO_2$ oxidant, which was pH dependant, indicating that both operated on different mechanisms.

The removal of NO_2 that was formed from the oxidation of NO did show a pH trend – a higher pH seemed to have favoured NO_2 removal (Figure 4-11, middle). This indicated that NO_2 could have been absorbed in the aqueous phase to form nitrite or nitrate acid, thereby preferring a more alkaline solution for more complete absorption. Increase in pH resulted in an increase in overall NO_x removal (Figure 4-11, bottom). This was because higher pH aqueous solutions have an advantage in being able to absorb more of the NO_2 that was formed.

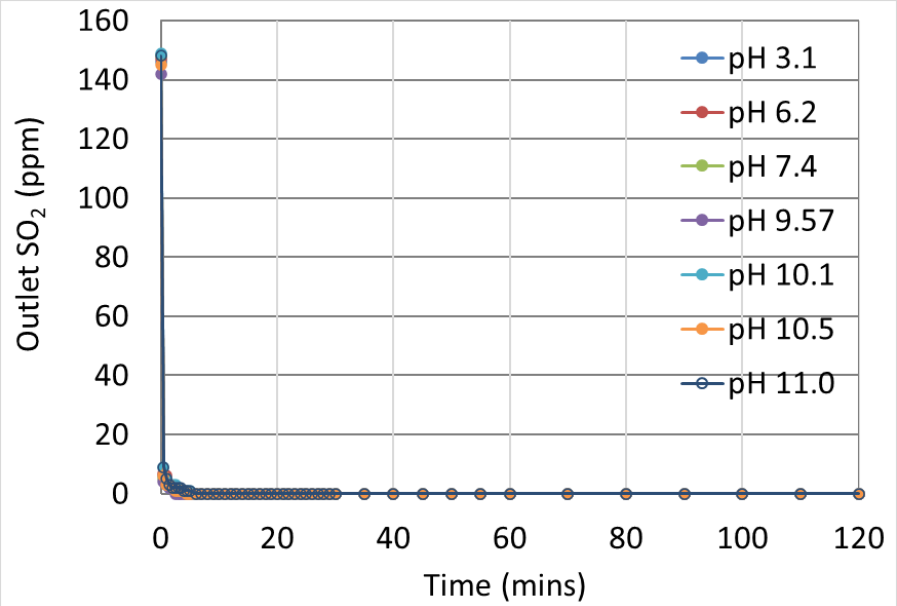

Figure 4-10: Outlet concentrations of SO_2 exiting the gas bubbling reactor with variation of the pH of $KMnO_4$.
Experimental conditions are shown in Table 4-1, No. 11.

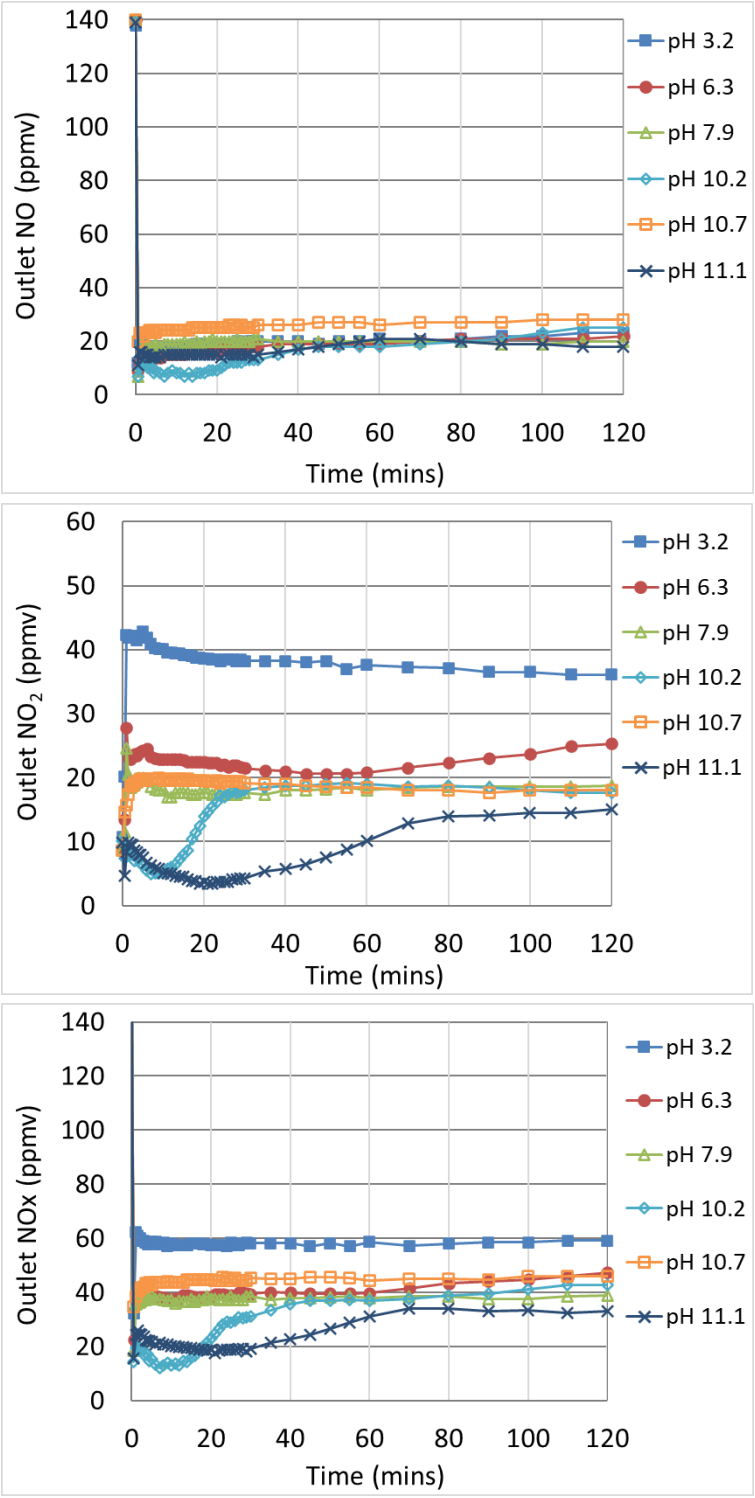

Figure 4-11: Outlet concentrations of NO (top), NO_2 (middle) and NO_x (bottom) exiting the gas bubbling reactor with variation of the pH of $KMnO_4$. *Experimental conditions are shown in Table 4-1, No. 12.*

4.1.9. Double train gas bubbling reactors using $NaClO_2$

Reactions were carried out using two gas bubbling reactors connected in series, with the first gas bubbling reactor using the sodium chlorite oxidant. The objective was to observe if the NO_2 gas that was formed as a result of NO oxidation could be removed with the addition of a second gas bubbling reactor. Experimental details can be seen in Table 4-1, No. 1, 13-15. As can be seen from Figure 4-12, all configurations, whether single or double train, could completely

remove the NO gas, as expected. The best result for NO removal was achieved by having a double train of gas bubbling reactors both containing $NaClO_2$, where total NO removal was achieved at a shorter time, but this improvement was only a minor one.

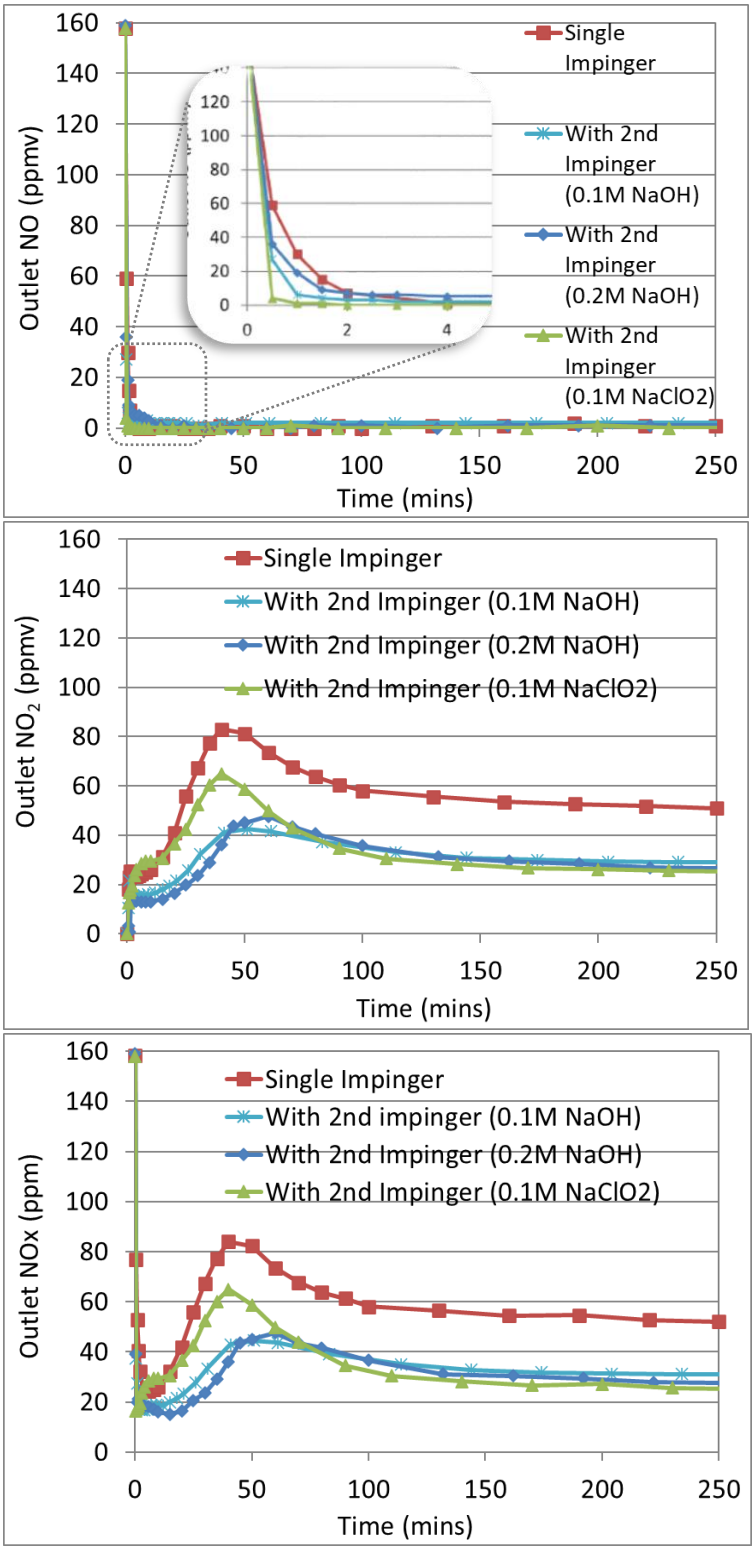

Figure 4-12: Outlet concentrations of NO (top), NO_2 (middle) and NO_x (bottom) exiting the gas bubbling reactor (impinger) with a single or double reactor arranged in series.
Experimental conditions are shown in Table 4-1, No. 1, 13-15.

It can be seen that having a second gas bubbling reactor helped to remove some of the NO_2 that was formed from the oxidation of NO. However, this improvement was limited as even a high

alkaline solution like 0.20M of NaOH could not completely remove the NO_2. This indicated the absorption of NO_2 may not be as high as expected.

4.2. Gas-liquid reaction using a counter-current wet scrubber

In this section, the study moved on from a gas bubbling reactor to a counter-current wet scrubber with a spray tower configuration. A broad range of widely reported substances, namely, seawater, sodium hydroxide (NaOH), sodium hypochlorite (NaClO), sodium chlorite ($NaClO_2$), hydrogen peroxide (H_2O_2) and potassium permanganate ($KMnO_4$) were systematically compared for their capacity to remove SO_x and NO_x and new insights were gained from comparing these reactions. These chemicals were selected for this study because they either showed potential in NO_x removal, are widely available in the industry at a reasonable cost or are already currently used on ship-based wet scrubbers. Previously in the reaction with the gas bubbling reactor, $NaClO_2$ and $KMnO_4$ were two chemical compounds that showed good results – both are therefore studied more in-depth here.

4.2.1. Experimental Procedure

The schematic representation of the experimental setup is shown in Figure 4-13. Due to the change from the gas bubbling reactor to a counter-current wet scrubber running on continuous loop, a liquid tank for holding the wet scrubbing liquid and the associated peristaltic pumps for pumping the scrubbing liquids in and out of the scrubber were added to the setup. A pH, oxidation reduction potential (ORP) and conductivity probe were attached to the liquid tank in order to monitor these parameters on a continuous basis during reaction. More details of the counter-current wet scrubber can be found in Figure 3-2 shown previously. The scrubber height used in this section was 400mm.

A three-way valve was used to manually switch the simulated exhaust gas directly to the flue gas analysers before reaction and from the exit of the wet scrubber during reaction. In this section, the Testo 350XL flue gas analyser was used for measuring O_2, SO_2 and NO while the MGA Luxx with NDIR sensor was used to measure NO_2. Overall NO_x was calculated by addition of NO and NO_2. The simulated exhaust gas used in this study are found in Table 4-2. Two separate reactions were planned for the scrubbing liquid mixtures being studied – the first for SO_2 removal and the second for NO removal. In each experiment, 2.5 litres of the scrubbing liquid were recirculated through the wet scrubber to react with the simulated exhaust gas for 60 minutes. The scrubbing liquid flowrate was kept at 1.0 litres per minute (using spray nozzle QPHA-3/ 1.0 L/min) for all experimental runs. A third study involving the removal of NO_2 was

added for selected scrubbing mixtures to obtain better clarity on the subject. In section 4.2.5 when the *L/G* ratio was reduced to 15 L/m^3, the total gas flowrate was increased to 25 L/min and the spray nozzle used was changed to the QPHA-1 (0.38 L/min) and the experiment time reduced to 30 mins. The rest of the parameters remained as stated in Table 4-2. All experiments were run using the spray chamber configuration.

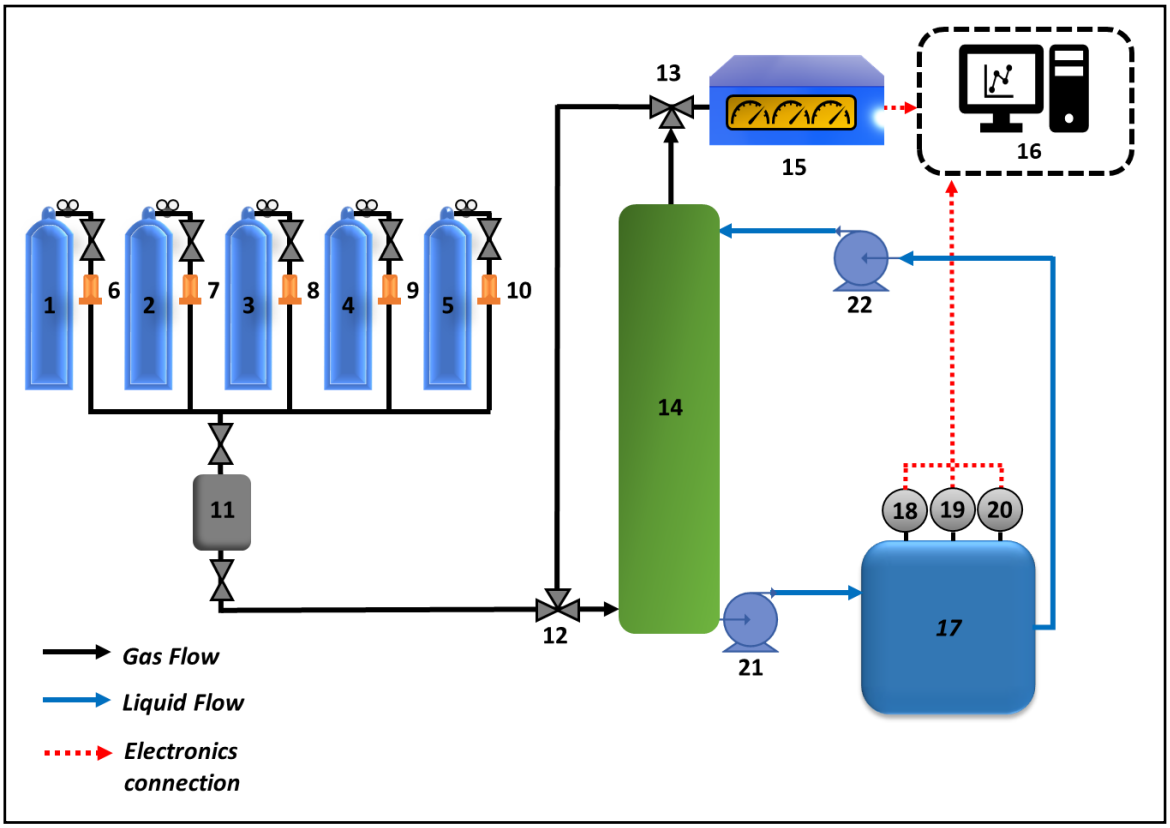

Figure 4-13: Schematic diagram using a counter current wet scrubber:
(1 – 5) Gas cylinders, N_2, O_2, SO_2, NO and NO_2; (6 – 10) mass flow controllers; (11) gas mixer; (12 – 13) three way valves; (14) counter-current wet scrubber; (15) flue gas analyzers; (16) computer (17) scrubbing liquid tank; (18) pH meter; (19) ORP meter; (20) conductivity meter; (21 – 22) peristaltic pumps for liquid in and out of scrubber.

The properties of the different types of chemicals used as scrubbing liquids for the gas-liquid reaction can be found in Table 4-3. Among the oxidizing agents used in the scrubbing liquid, it is known that the oxidation potential of both NaClO and $NaClO_2$ are greatly influenced by solution pH. Therefore, both the scrubbing liquids of these compounds were also adjusted to pH 6 and 8 before the start of the reaction using hydrochloric acid (0.1M). When prepared without any pH adjustments, the starting pH of NaClO and $NaClO_2$ were 10.9 and 10.6, so these liquid mixtures were designated as NaClO/pH10.9 and $NaClO_2$/pH10.6 respectively.

For reactions that were able to removal NO_x, aqueous samples were collected at the beginning, midpoint and the end of the experiments (0, 30, 60 mins respectively) for aqueous analysis which was carried out within 24 hours of the experimental run to minimize sample deterioration.

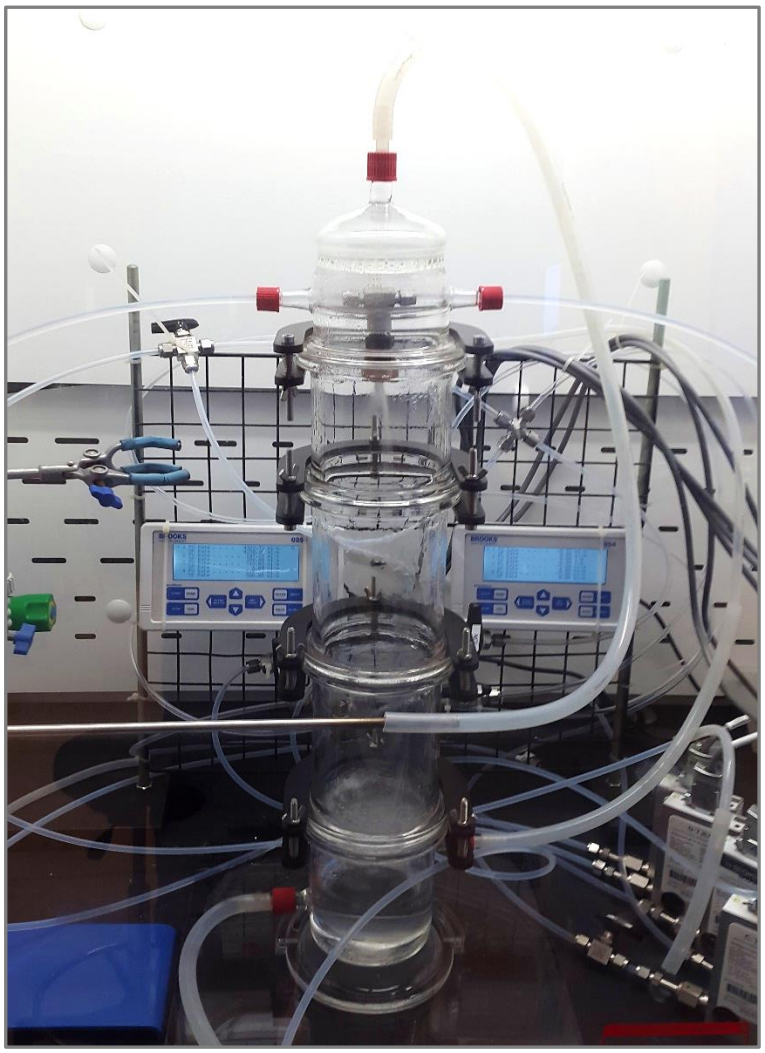

Figure 4-14: Counter-current wet scrubber in operation (400mm scrubber height configuration, with a QPHA-3 spray nozzle).

Table 4-2: Summary of the simulated exhaust gas properties used to study the removal of SO_2 and NO by various chemical compounds using a counter current wet scrubber.

Simulated exhaust gas properties	
Composition (for SO_2 study)	SO_2: 500ppmv / O_2: 14% / N_2 balance
Composition (for NO study)	NO: 500ppmv / O_2: 14% / N_2 balance
Gas flowrate	10 litres/min
Temperature	Ambient (~25^{o}C)

Table 4-3: Composition and properties of the scrubbing liquid used to react with the exhaust gas in the wet scrubber for the SO_2 and NO studies respectively, using the counter-current wet scrubber.

No	Scrubbing liquid composition	Concen-tration (M)	Total Alkalinity (mg/L $CaCO_3$)	Starting measurement			SO_2 study	NO study	NO_2 study
				pH	ORP (mV)	Cond. (mS/ cm)			
1	Seawater (SW)	NA	116	8.2	206	47.2	x	x	-
2	NaOH	0.05	2,468	12.4	-5	11.2	x	x	x
		0.10	-	12.9	-15	21.1	-	-	x
		0.40	-	13.4	-32	75.7	-	-	x
3	H_2O_2	0.05	6	4.4	352	-	x	x	-
4	NaClO/pH10.9	0.05	436	10.9	625	10.4	x	x	-
5	NaClO/pH 8	0.05	-	7.9	880	10.5	-	x	-
6	NaClO/pH 6	0.05	-	6.0	1013	11.4	-	x	-
7	$NaClO_2$/pH10.6	0.05	350	10.6	432	6.0	x	x	x
8	$NaClO_2$/pH 8	0.05	-	8.3	483	5.8	-	x	x
9	$NaClO_2$/pH7	0.05	-	7.3	-	5.8	-	-	x
10	$NaClO_2$/pH 6	0.05	-	6.2	523	5.8	-	x	-
11	$KMnO_4$	0.05	36	9.2	561	6.0	x	x	-
12	Deionised (DI) water	NA	4	6.2	353	0.006	x	-	x

4.2.2. Removal of sulfur dioxide (SO_2)

The reaction mechanisms for the absorption of SO_2 in the aqueous phase has been well documented and can be summarised as follows (Al-Enezi *et al.*, 2001; Tokumura *et al.*, 2006; Andreasen and Mayer, 2007):

$$SO_2(g) \rightarrow SO_2(aq) \quad \ldots (4.1)$$

$$SO_2(aq) + H_2O \rightarrow HSO_3^- + H^+ \quad \ldots (4.2)$$

$$HSO_3^- \rightarrow SO_3^{2-} + H^+ \quad \ldots (4.3)$$

$$HSO_3^- + \tfrac{1}{2}O_2(g) \rightarrow SO_4^{2-} + H^+ \quad \ldots (4.4)$$

$$SO_3^{2-} + \tfrac{1}{2}O_2(g) \rightarrow SO_4^{2-} \quad \ldots (4.5)$$

These series of equations can roughly be grouped into 2 categories, the first being the absorption of SO_2 into bisulfite or sulfite in the aqueous phase (Equations 4.1, 4.2 and 4.3), followed by oxidation to sulfate, its most stable aqueous form (Equations 4.4 and 4.5). From the reactions, it can be seen that the absorption of 1 mol of SO_2 in the aqueous phase results in the release of 1 to 2 moles of protons, thereby causing the pH to reduce over time.

The removal of SO_2 by the gas-liquid reaction in the wet scrubber by various scrubbing mixtures can be seen in Figure 4-15 while the corresponding pH and ORP values are shown in Figure 4-16 and Figure 4-17 respectively. It can be seen from Figure 4-15 that all compounds used achieved 100% SO_2 removal for the entire duration of the experiments except for DI water and Seawater.

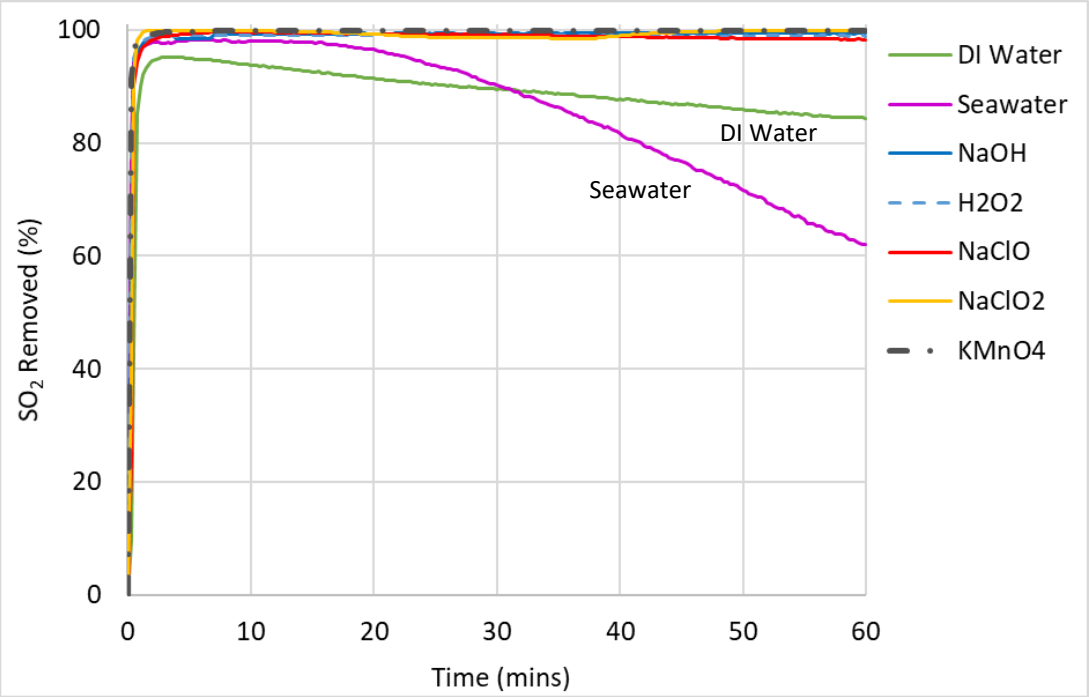

Figure 4-15: Sulfur dioxide (SO_2) removal from the simulated exhaust gas with various scrubbing liquids in the counter-current wet scrubber.

The reduction in SO_2 removed seen in DI water and seawater can be explained by the gradual reduction of pH over time as the reaction progressed. Further comparison between DI water and seawater showed that the performance of the seawater in removing SO_2 dipped below that of DI water at about the halfway point of the experiment although its pH still remained higher than the pH of DI water. This showed that other mechanisms could be at play for SO_2 removal besides pH.

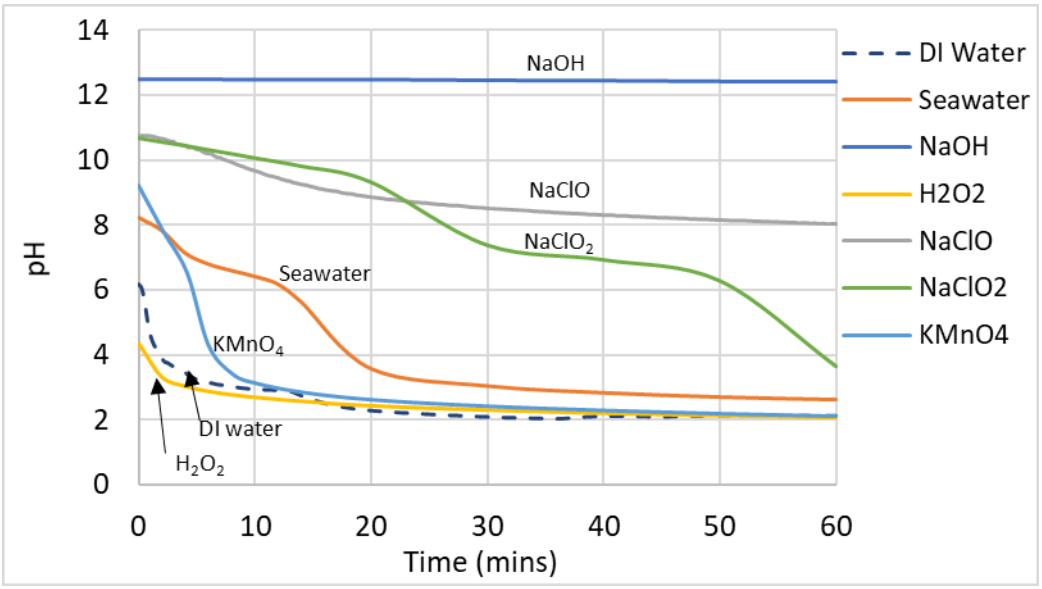

Figure 4-16: pH of the scrubbing liquid in the tank during SO_2 removal.

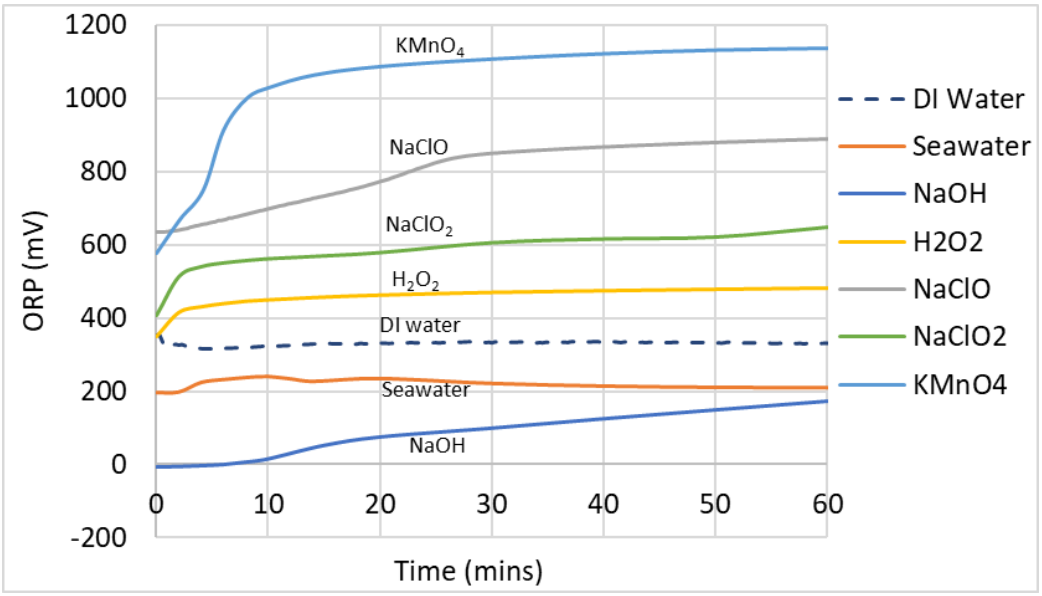

Figure 4-17: The ORP of the scrubbing liquid in the tank during the reaction to remove SO_2.

There are two possibilities for this. Firstly, DI water was more oxidative compared to seawater (Figure 4-17), which could have aided the oxidation of sulphite and bisulphite ions into sulphate ions (Equations 5 and 6) and helped in the overall removal of SO_2. Secondly, seawater is much more saturated with ions compared to DI water and this can extensively lessen the solubility of gases in the aqueous phase (Black & Veatch Corporation, 2009). This vast difference in ionic saturation can be seen it their conductivity values – the conductivity of seawater at 47.2 mS/cm, was more than 7,400 times higher than the conductivity of DI water (Table 4-3). Furthermore, as typical seawater already contains around 2,500 – 3,000 mg/L of sulfate ions (Al-Enezi *et al.*, 2001; Vidal B and Ollero, 2001; Andreasen and Mayer, 2007; Black & Veatch Corporation,

2009), the saturation level of sulfur-based ions in the aqueous phase will be reached more quickly due to the common ion effect compared with DI water, which was almost free of external ions.

Although the scrubbing mixtures of $KMnO_4$ and H_2O_2 were on par or even more acidic than DI water and seawater in terms of pH, they both performed better in terms of SO_2 removal. Again, this could be due to the higher oxidation potential of $KMnO_4$ and H_2O_2, giving them an advantage in the oxidation of sulfite and bisulfite ions into sulfates. It can be summarised that the full removal of SO_2 proceeded quite readily and was achieved by nearly all types of scrubbing mixtures that were tested here. This is because SO_2 gas is very soluble in the aqueous phase (Table 4-4) (Sander, 2015). It was observed that the absorption of SO_2 in the aqueous phase under the experimental conditions here were likely influenced by three factors, namely, pH/alkalinity, concentration of soluble sulfur ions already present in the solution, and oxidation potential (estimated by ORP). An effective scrubbing liquid for the removal of SO_2 gas should have a high pH or alkalinity, low in sulfate ions, and oxidative in nature. If equipment for the measurement and monitoring of sulfite or sulfate ions in the aqueous phase is not available, a conductivity meter could be used to determine the overall ionic content as a substitute of sorts to provide some indication.

Table 4-4: The Henry's Law constant for several gases of interest, at 1atm and 25°C (Sander, 2015)

Gas	**Henry's Law Constant, H_i (mol.m^{-3}/Pa)**	**Solubility compared to NO**
Carbon dioxide, CO_2	3.3×10^{-4}	17.4
Sulfur dioxide, SO_2	1.3×10^{-2}	684
Nitric oxide, NO	1.9×10^{-5}	1
Nitrogen dioxide, NO_2	9.9×10^{-5}	5.2

4.2.3. Removal of nitrogen oxides (NO_x)

Under natural conditions, the removal of NO when it is released into the atmosphere is a two-part mechanism, according to the following reactions (Nevers, 2000; Yang *et al.*, 2018):

$$\mathrm{NO(g)} + \frac{1}{2}\mathrm{O_2(g)} \rightarrow \mathrm{NO_2(g)} \qquad \ldots (4.6)$$

$$3NO_2(g) + H_2O(g) \leftrightarrow 2HNO_3(aq) + NO(g) \quad \ldots (4.7)$$

$$2NO_2(g) + H_2O(g) \leftrightarrow HNO_2(aq) + HNO_3(g) \quad \ldots (4.8)$$

In the first step, NO is naturally oxidized into a more soluble form, NO_2 (Equation 4.6) before it is subsequently solubilized in the form of nitrites and nitrates (Equations 4.7 and 4.8). Although the oxidation of NO to NO_2 takes place spontaneously under atmospheric conditions, the rate of reaction is relatively slow when compared to the movement of the exhaust gas and there is insufficient retention time for this to occur in the combustion process before the exhaust is discharged. Therefore, a substantial amount of research has focused on speeding up this oxidation process so that the absorption step in the aqueous phase can take place.

In addition to the reactions shown in Equations 4.7 and 4.8 for the absorption of NO_2, Brogren and Deshwal suggested additional pathways involving the formation of more soluble intermediate in N_2O_3 and N_2O_4 (Brogren *et al.*, 1998; Deshwal *et al.*, 2008):

$$NO(g) + NO_2(g) \leftrightarrow N_2O_3(g) \quad \ldots (4.9)$$

$$2NO_2(g) \leftrightarrow N_2O_4(g) \quad \ldots (4.10)$$

$$N_2O_3(g) + H_2O \leftrightarrow HNO_2(aq) \quad \ldots (4.11)$$

$$N_2O_4(g) + H_2O \leftrightarrow 2H^+ + NO_2^- + NO_3^- \quad \ldots (4.12)$$

It was further demonstrated by Sun, Lin and Shao that the formation of intermediate N_2O_5 was also very effective for the solubilization of nitrogen in the aqueous phase (Sun *et al.*, 2015; Lin *et al.*, 2016; Shao *et al.*, 2019). It is generally accepted that the solubility of gaseous nitrogen in the aqueous phase increases with increasing nitrogen valency (Lin *et al.*, 2016).

(A) Oxidation of nitric oxide (NO)

The results of the removal of nitric oxide (NO) from the simulated exhaust gas from the gas-liquid reaction in the wet scrubber can be seen in Figure 4-18. Since the removed NO could have been oxidised to NO_2 without the latter getting absorbed, it should be noted that NO removal does not necessarily translate to NO_x removal.

The outcome can be broadly categorised into three groups – ineffective, somewhat effective and effective. In the ineffective group, in can be seen that seawater, H_2O_2, NaOH and

NaClO/pH10.9 converted less than 5% of nitric oxide in the flue gas throughout the entire duration of the experiment. That is why existing commercial marine wet scrubbers which uses seawater and NaOH are able to remove SO_2 effectively but not NO.

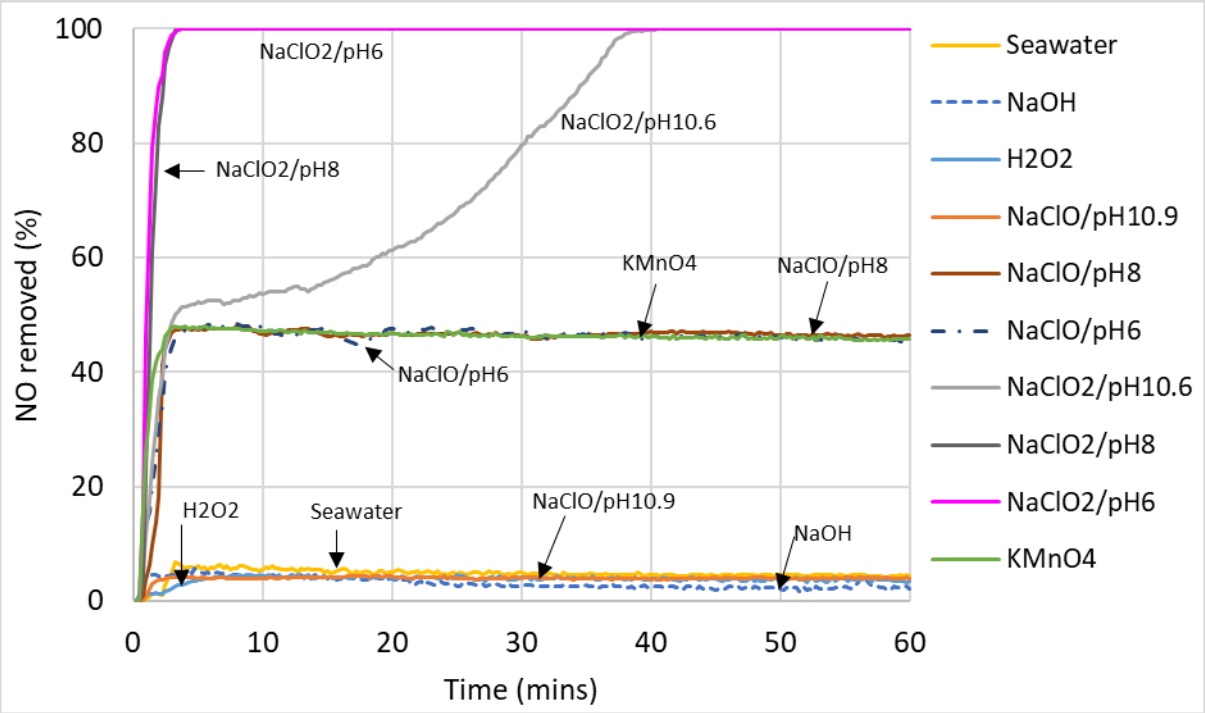

Figure 4-18: Nitric Oxide (NO) removal from the simulated exhaust gas with various scrubbing liquids in the counter-current wet scrubber.

In the somewhat effective group, $KMnO_4$, NaClO/pH6 and NaClO/pH8 removed around 50% of the nitric oxide in the simulated emission gas. In the effective group, $NaClO_2$/pH6 and $NaClO_2$/pH8 achieved 100% nitric oxide removal for the duration of the experiment. The $NaClO_2$/pH10.6 aqueous mixture could only remove around 50% of nitric at the beginning but its removal efficiency continued to increase as the reaction progressed until it eventually reached 100% removal.

As seen in the pH graph in Figure 4-19, high pH (NaOH) has no effect on the removal of NO gas as this gas-liquid reaction does not seem to follow an acid-alkaline absorption reaction owing to its very low solubility (Table 4-4). Observation of the ORP change (Figure 4-20) showed that NaClO mixtures had higher values than $NaClO_2$ and $KMnO_4$ but performed worse in the conversion of NO. This showed that solely using ORP values to predict the effectiveness of a liquid mixture to oxidize NO to NO_2 would be inaccurate. However, ORP values did give a good indication of NO conversion when predicting the effectiveness of the same chemical compounds under different mixing conditions (pH, concentration, etc).

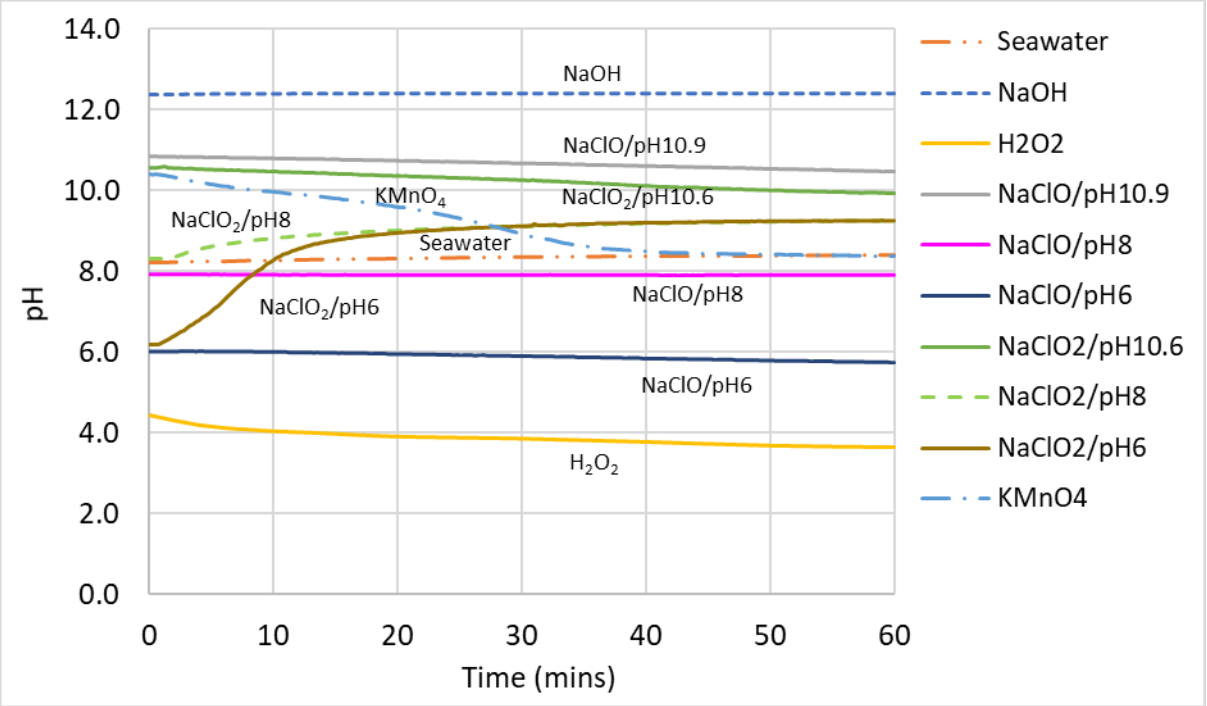

Figure 4-19: pH of the scrubbing liquid in the tank during NO removal.

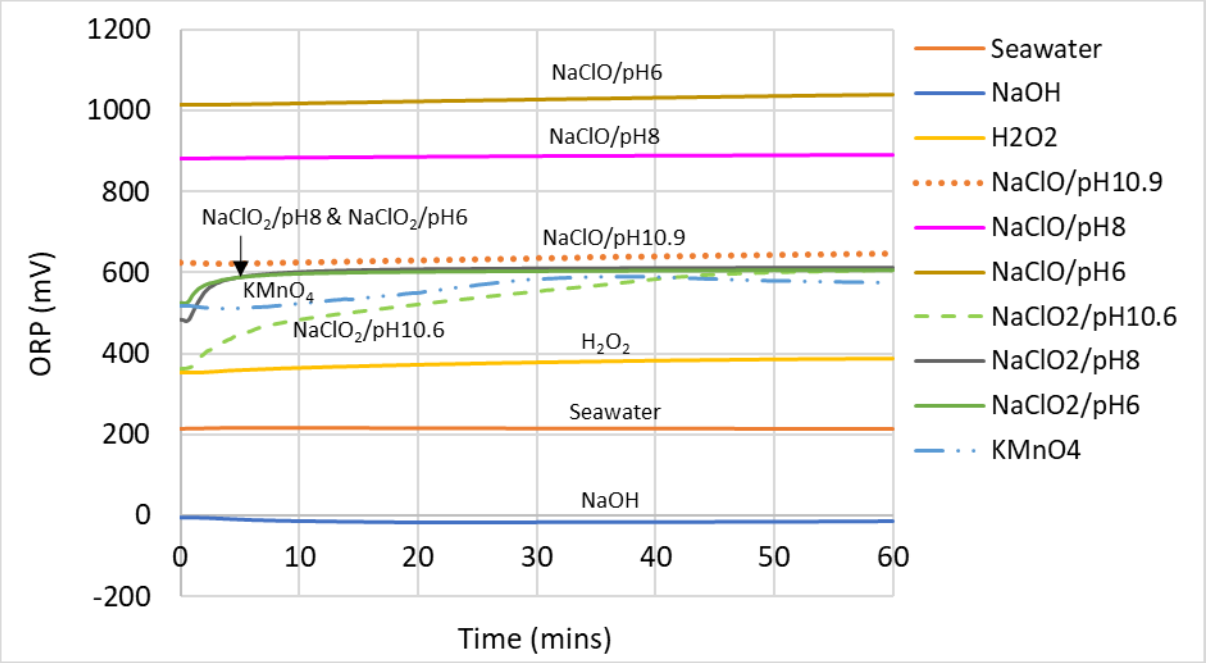

Figure 4-20: ORP of the scrubbing liquid in the tank during NO removal.

i. Oxidation of nitric oxide (NO) by hydrogen peroxide (H_2O_2)

H_2O_2 was not effective in oxidizing NO to NO_2 in this study. On top of using a high concentration, studies involving H_2O_2 usually required some sort of activation either with UV radiation or ozone (Wen *et al.*, 2019; Xie *et al.*, 2019). Without these, it can be seen that H_2O_2

was inferior compared to other types of chemical oxidants of the same concentration studied here.

ii. Oxidation of nitric oxide (NO) by sodium hypochlorite (NaClO)

NaClO was ineffective in removing NO gas in the wet scrubber in high pH but was more effective when the starting pH was lowered to 8 and 6 respectively. It is widely known that hypochlorite will partition itself between its ionic and hypochlorous acid form according to pH. It exists as hypochlorous acid (HOCl) below pH 6, as hypochlorite (ClO^-) above pH 10, and a mixture of two between pH 6 – 9 (Metcalf & Eddy *et al.*, 1991).

When NaClO was at pH 10.9, the chlorine existed in its hypochlorite form (ClO^-) where it is a less powerful oxidizing agent. As the pH was decreased to 8, partitioning into the hypochlorous acid form began and the oxidation potential increased as a result (Figure 4-20). This trend was also consistent with theoretical values shown in Table 4-5 – the half reaction of the oxidation of hypochlorous acid was +1.49V, much higher compared its hypochlorite at +0.90V (Tchobanoglous *et al.*, 2013). However, further lowering of pH from 8 to 6 did not show additional improvement in removal effectiveness, which was consistent with the findings of Yang et. al (Yang *et al.*, 2016).

Table 4-5: The oxidation potential of various chemical compounds of relevance in this study (Tchobanoglous et al. 2013).

Chemical compounds	**Half Reaction**	**Redox Potential, E_h (V)**
Hydrogen peroxide	$H_2O_2 + 2H^+ + 2e^- \leftrightarrow 2H_2O$	+1.78
Permanganate	$MnO_4^- + 4H^+ + 3e^- \leftrightarrow MnO_2 + 2H_2O$	+1.67
Chlorine dioxide	$ClO_2 + e^- \leftrightarrow ClO_2^-$	+1.50
Hypochlorous acid	$HOCl + H^+ + 2e^- \leftrightarrow Cl^- + H_2O$	+1.49
Hypochlorite	$ClO^- + H_2O + 2e^- \leftrightarrow Cl^- + 2OH^-$	+0.90
Chlorite	$ClO_2^- + H_2O + 4e^- \leftrightarrow Cl^- + 4OH^-$	+0.76

The reaction mechanism of nitric oxide conversion by sodium chlorite is likely via the following pathways (Mondal and Chelluboyana, 2013; Yang *et al.*, 2016; Yang *et al.*, 2018):

$$NO(g) + HOCl \rightarrow NO_2(aq) + H^+ + Cl^- \quad \ldots (4.13)$$

$$NO(g) + ClO^- \rightarrow NO_2(aq) + Cl^- \quad \ldots (4.14)$$

iii. Oxidation of nitric oxide (NO) by sodium chlorite ($NaClO_2$)

Chlorite's lower oxidation potential seen in the ORP readings (Figure 4-20) was consistent with theoretical values seen in Table 4-5, (+0.76 versus +0.90 to 1.49V of the hypochlorite/ hypochlorous combination). Yet, it outperformed hypochlorite in oxidizing NO to NO_2. This was likely due to the tendency of $NaClO_2$ to decompose into its more oxidative form, ClO_2, at more acidic pHs, according to the reactions shown in Equations 4.15 – 4.17 (Brogren *et al.*, 1998; Roy Choudhury, 2011; Zhao *et al.*, 2015b; Gong *et al.*, 2020). This decomposition will occur slowly when the pH is from 5 – 7 and accelerate when the pH is below 5.

$$5ClO_2^-(aq) + 4H^+ \rightarrow 4ClO_2(aq) + Cl^-(aq) + 2H_2O \quad \ldots (4.15)$$

$$4ClO_2^-(aq) + 2H^+ \rightarrow 2ClO_2(aq) + ClO_3^-(aq) + Cl^- + H_2O \quad \ldots (4.16)$$

$$ClO_2(aq) \rightarrow ClO_2(g) \quad \ldots (4.17)$$

Further evidence of this decomposition can be seen from Figure 4-19 where the pH for the scrubbing mixtures of $NaClO_2$/pH6 and $NaClO_2$/pH8 defied the common trend by increasing instead of decreasing as the reaction progressed even though reaction with NO_x generates proton ions. This was likely because the conversion of chlorite to chlorine dioxide absorbs proton ions, according to Equations 4.15 and 4.16.

When the pH was in the alkaline range, it was likely that any decomposition from ClO_2^- into ClO_2 gas was likely to have occurred mainly at the gas-liquid boundary layer when the chlorite ion came into contact with the NO gas instead of the bulk phase (Gong *et al.*, 2020). This mechanism enabled the chlorite solution to effectively oxidise NO to NO_2 without needing very high ORP values in the bulk solution.

It could be seen from Figure 4-19 and Figure 4-20 that in general, the ORP values increases with decreasing pH, due to the increasing decomposition of ClO_2^- to ClO_2. However, it can be seen that in the pH range of 6 to 8, the ORP values were quite similar, hovering at around 600mV. This suggested that further pH adjustment below 8 seemed unnecessary and as does not increase the oxidation potential of the solution. Higher than necessary formation of the more volatile ClO_2 would result in more reactants being lost to the exhaust, which is both wasteful and a potential safety hazard. The reaction mechanism for the conversion of NO to NO_2 by

sodium chlorite is likely to have taken place in the following manner (Brogren *et al.*, 1998; Deshwal *et al.*, 2008):

$$2NO(g) + ClO_2^-(aq) \rightarrow 2NO_2(g) + Cl^-(aq) \quad \ldots (4.18)$$

$$NO(g) + ClO_2^-(aq) \rightarrow NO_2(g) + ClO^-(aq) \quad \ldots (4.19)$$

On top of oxidising NO to NO_2, the following competing reactions to form nitrites in the aqueous phase can also take place (Brogren *et al.*, 1998):

$$4NO(g) + ClO_2^-(aq) + 4OH^- \rightarrow 4NO_2^-(aq) + Cl^-(aq) + 2H_2O \quad \ldots (4.20)$$

$$2NO(g) + ClO_2^-(aq) + 2OH^- \rightarrow 2NO_2^-(aq) + ClO^-(aq) + H_2O \quad \ldots (4.21)$$

iv. Oxidation of nitric oxide (NO) by potassium permanganate ($KMnO_4$)

It can be seen from Figure 4-18 that the $KMnO_4$ scrubbing mixture managed to convert about 45% of NO for the duration of the experimental run. The pH of the mixture reduced from 10.4 to 8.4 during the run but this did not affect the oxidative power of the liquid solution much, as seen by the ORP values which fluctuated within the 500 – 600mV range for the entire reaction. The drop in pH was probably due to the acidic nature of NO_2 when absorbed and the low buffering capacity of the $KMnO_4$ mixture. Unlike the chlorine-based oxidation agents, $KMnO_4$ did not seem as sensitive to pH change as both its ORP values and NO conversion remained relatively stable throughout the reaction. The reaction mechanism for the conversion of NO to NO_2 by $KMnO_4$ is likely to have been the following (Chu *et al.*, 2001; Fang *et al.*, 2013):

$$3NO + 2MnO_4^- + H_2O \rightarrow 3NO_2 + 2MnO_2(s) + 2OH^- \quad \ldots (4.22)$$

$$NO + MnO_4^- \rightarrow NO_3^- + MnO_2(s) \quad \ldots (4.23)$$

$$3NO + MnO_4^- + H_2O \rightarrow 3NO_2^- + MnO_2(s) + 2H^+ \quad \ldots (4.24)$$

As can be seen, all reactions resulted in the formation of MnO_2, which is a solid precipitate. In all the experiments involving $KMnO_4$ conducted here, a dark brown precipitate was observed from early in the experiments. This dark brown MnO_2 precipitate, was present everywhere in the setup and was etched in the tubings, the walls of the wet scrubber and within the crevices of the spray nozzle. Cleaning was very challenging as the apparatus had to be dismantled and soaked in concentrated acid solution.

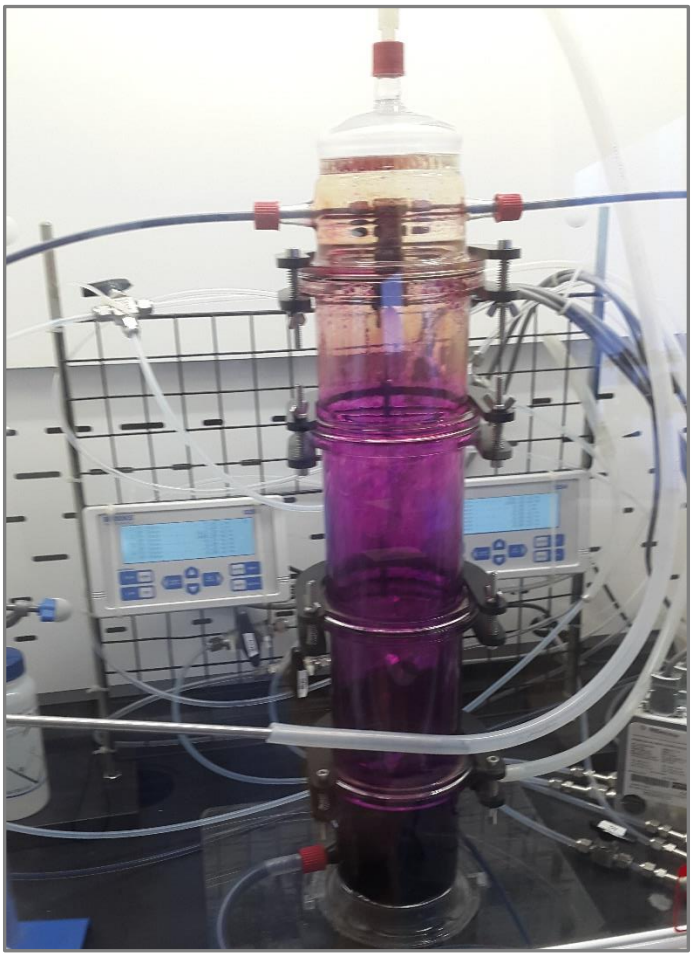

Figure 4-21: The counter-current wet scrubber with $KMnO_4$ as the scrubbing liquid. Etching of MnO_2 precipitates encountered on glass, tubings, nozzle and mist eliminator.

(B) Overall NO_x removal

The removal of overall NO_x, which is made up from NO and NO_2, is shown in Figure 4-22. Seawater, NaOH and H_2O_2 were omitted from the graphs here as these chemical compounds were ineffective in NO_x removal. For the overall removal of NO_x, the effectiveness of various oxidants or chemical compounds used under present experimental conditions can be ranked as follows, from least to most effective: Seawater, NaOH, H_2O_2 < NaClO < $KMnO_4$ < $NaClO_2$.

It can be seen that the NO_x removal by NaClO was very low at pH 10.9, peaked when pH was lowered to 8, but then reduced slightly when pH was further lowered to 6. These NO_x removal figures were much lower compared to the oxidation rates of NO to NO_2 that it achieved, suggesting that a significant amount of NO which were oxidized to NO_2 could not be absorbed in the wet scrubber. As for the chlorites, both $NaClO_2$/pH 8 and $NaClO_2$/pH 6 exhibited very similar performances, managing around 65 – 70% of NO_x removal for the duration of their experiments. The fluctuation seen for $NaClO_2$/pH10.6 aqueous mixture was likely to do with the lowering of the pH of the liquid mixture as the reaction progressed, leading to an increase in its oxidative properties.

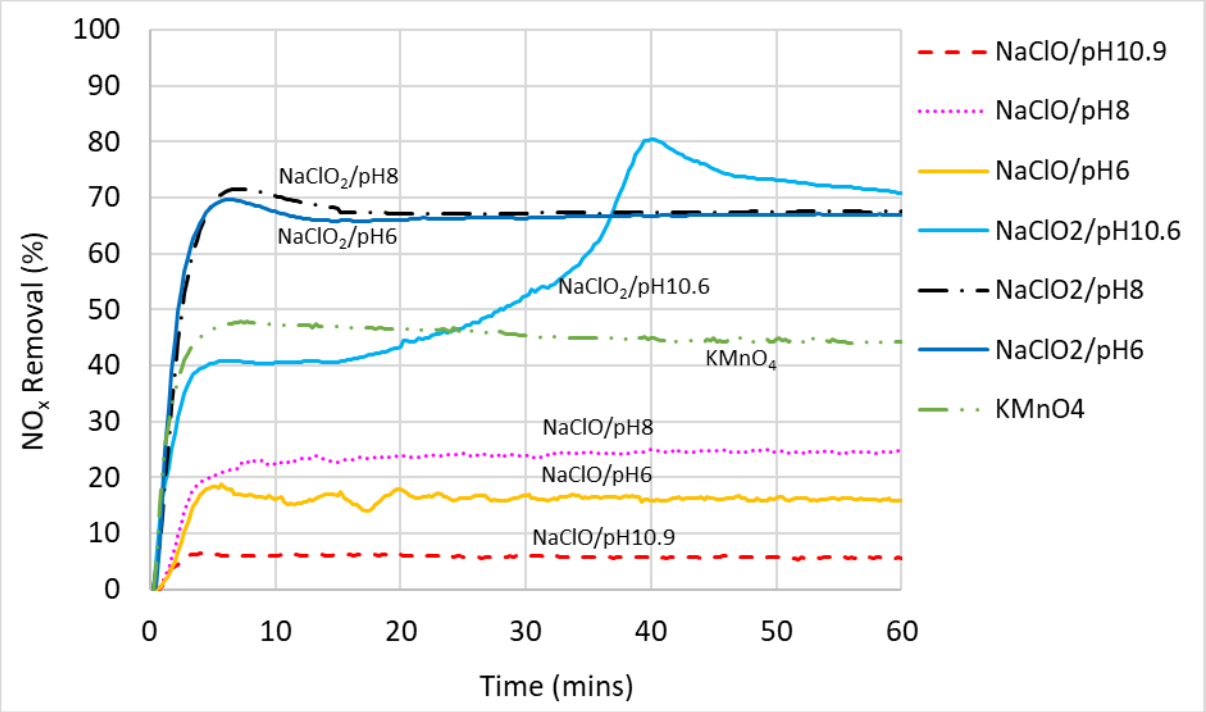

Figure 4-22: NO_x ($NO+NO_2$) removal from the simulated exhaust gas using various scrubbing liquids in the counter-current wet scrubber.

In order to get a better view of the NO_2 absorption ability, Figure 4-23 and Figure 4-24 were plotted to show the ratio of NO_2 absorbed over the amount of NO that was oxidized to NO_2 for the duration of the experiment.

i. Absorption and oxidation potential

From Figure 4-24, a clear inverse relationship between NO_2 absorption and oxidation potential of the various chemical compounds can be seen. NO_2 absorption by NaClO showed the strongest inverse linear correlation with oxidation potential, with the linear regression R^2 value at 0.99. However, it should not be expected that all the different points belonging to various compounds fit nicely into one linear trendline as different chemical compound have different reaction pathways even though they all broadly followed the linear trendline.

The observations here is consistent with the work by Chang, Xi and Zhang who used compounds which has very low oxidation potential such as Na_2SO_3, NaS and $NaHSO_3$ to improve the absorption of NO_2 (Chang *et al.*, 2004; Xi *et al.*, 2020; Zhang *et al.*, 2020). Chang and Xi further showed that in a low oxidation potential environment, NO_2 can even be directly reduced to N_2 gas, thereby avoiding the formation of nitrogen anions altogether (Chang *et al.*, 2004; Xi *et al.*, 2020).

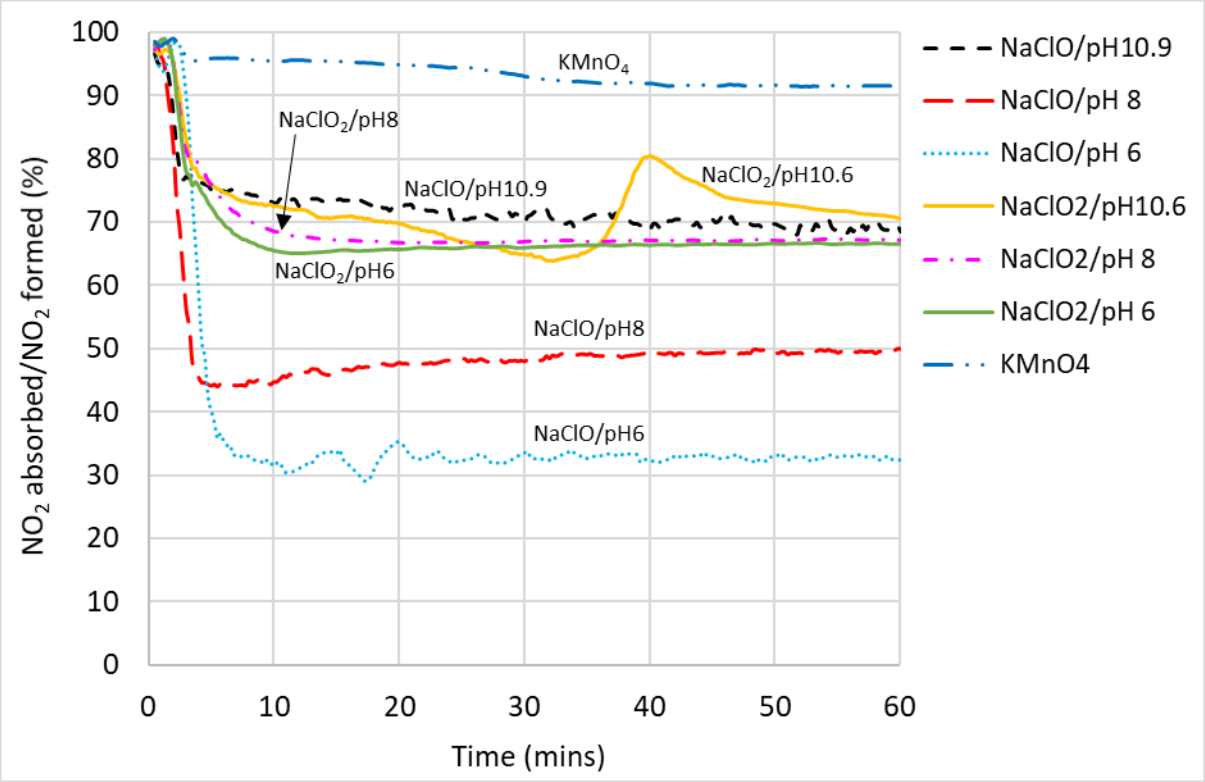

Figure 4-23: Ratio of NO_2 absorbed over the total NO_2 that was formed (converted to %) versus reaction time, using various types of scrubbing liquid in the counter-current wet scrubber.

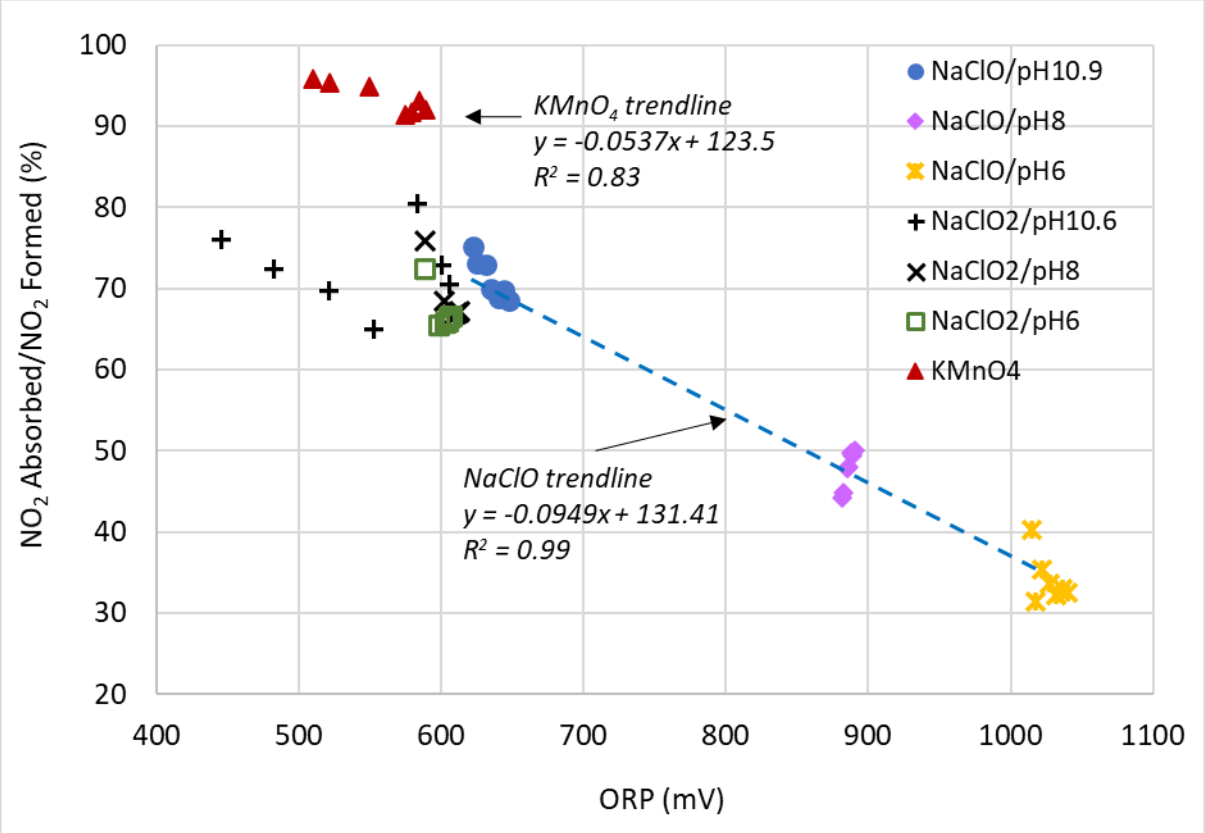

Figure 4-24: Ratio of NO_2 absorbed over the total NO_2 that was formed (converted to %) versus reaction time, using various types of scrubbing liquid in the counter-current wet scrubber.

It should also be pointed out here that these observations were in contradiction with the other school of thought which focused on increasing the oxidation potential in order to form high valency intermediates such as N_2O_3, N_2O_4 and N_2O_5 as these have higher solubility in aqueous solution (Brogren *et al.*, 1998; Sun *et al.*, 2015; Lin *et al.*, 2016; Shao *et al.*, 2019). The formation of these intermediates, especially N_2O_5, is heavily dependent on the residence time (Lin *et al.*, 2016; Shao *et al.*, 2019) and it was possible that the setup in this study could not provide sufficient residence time for these reactions to take place.

ii. Absorption by sodium hypochlorite (NaClO)

As shown in Figure 4-23 and Figure 4-24, NaClO's capacity to absorb NO_2 increased with decreasing oxidation potential values in the pH range of 6 – 11. If NaClO is to be the oxidant of choice, a balance would have to be struck between achieving high NO oxidation rate, favoured by high oxidation potential, versus absorbing the NO_2 that will be formed, favoured by a low oxidation potential. Compared with other oxidants, NaClO performed the poorest in terms of absorbing the NO_2 that it formed from the oxidation of NO. However, NaClO could be ideal if the process requires only oxidation but not absorption.

iii. Absorption by sodium chlorite ($NaClO_2$)

In general, $NaClO_2$ of various pH were more effective in absorbing the NO_2 compared to NaClO due to its lower oxidation potential, managing to remove between 65 – 80% of NO_2 that was formed during the reaction. Additionally, it could also be that $NaClO_2$ has additional reaction pathways for the absorption of NO_2 in the aqueous phase on top of the reactions shown in Eq. 8 and 9 (Brogren *et al.*, 1997):

$$4NO_2 + ClO_2^- + 4OH^- \rightarrow 4NO_3^- + Cl^- + 2H_2O \qquad \dots (4.25)$$

$$2NO_2 + ClO_2^- + 2OH^- \rightarrow 2NO_3^- + ClO^- + H_2O \qquad \dots (4.26)$$

iv. Absorption by potassium permanganate ($KMnO_4$)

It can be seen from Figure 4-23 that $KMnO_4$ was the most effective in the absorption of NO_2 – almost all the NO that was oxidised to NO_2 was subsequently absorbed into the aqueous phase. One possiblity was that $KMnO_4$ oxidised NO directly to nitrate ions in the aqueous phase as shown in Equations 4.23 and 4.24 instead of the other gaseous intermediates such as NO_2. Nevertheless, $KMnO_4$ still trailed chlorite ions in terms of overall NO_x removal and the staining of pipes, pumps and nozzles among the wet scrubbing equipment poses a significant problem

for it to be considered the oxidant of choice. Brogren reported that the formation of the MnO_2 precipitate can be avoided under very high alkaline conditions – when the solution contains more than 3 moles/L of hydroxide ions, MnO_4^- will be formed instead of MnO_2 (Brogren *et al.*, 1997) . However, it was also reported in the same study that NO_x removal will be suppressed under such high pH conditions. Futhermore, it will also be quite costly to maintain such a high pH in a large scale operation.

(C) Absorption of nitrogen dioxide (NO_2)

In this additional study, selected chemical compounds were reacted with NO_2 in the wet scrubber in order to gain a clearer understanding its absorption and removal in the gas-liquid reaction. From Figure 4-25, it can be seen that deionised (DI) water could only remove around 10% of the NO_2 in the exhaust gas in this scrubbing system. Addition of NaOH up to 0.40M to increase the alkalinity of the scrubbing liquid did not improve the absorption of NO_2 at all. The results seen here are in contrast with some of the previous reported literature which suggested significant levels of NO_2 absorption in the aqueous phase is possible after the oxidation of NO to NO_2 has been achieved (Brogren *et al.*, 1998; Kurpoka, 2011). In one such example, Brogren reported that around 50 – 60% of NO_2 was successfully removed by NaOH between pH 9 – 12 (Brogren *et al.*, 1998). However, it was consistent in the study by Chang et. al. which showed NaOH as high as pH 13 had no effect on absorbing NO_2 (Chang *et al.*, 2004).

Brogren also reported that the addition of sodium chlorite under alkaline conditions increased the absorption of NO_2, up to almost 80% removed when 0.6M was used. However, it can be seen from Figure 4-26 that the addition of $NaClO_2$ in the scrubbing mixture decreased amount of NO_2 absorbed. Since Figure 4-25 already showed that NO_2 absorption was not directly dependant on pH, it follows that the diminishing capacity to absorb NO_2 seen in Figure 4-26 when the pH of $NaClO_2$ was lowered from 10.6 to 6 likely has less to do with the increasing acidity of the aqueous solution but rather due to the increasing oxidation potential.

Although NO_2 gas is at least 5 times more soluble in the aqueous phase than NO (Table 4-4), its solubility was clearly still insufficient for the significant absorption and removal of NO_x from the exhaust. Absorption and removal of NO_2 required more than can be provided by an alkaline mixture such as NaOH. Increasing the oxidising potential in attempt to form higher valency nitrogen intermediates which have higher solubility such as N_2O_3, N_2O_4 and N_2O_5 did not improve the absorption but made it worse, contrary to reported literature (Brogren *et al.*,

1998; Sun *et al.*, 2015; Lin *et al.*, 2016; Shao *et al.*, 2019). This was consistent with the findings discussed in the previous section.

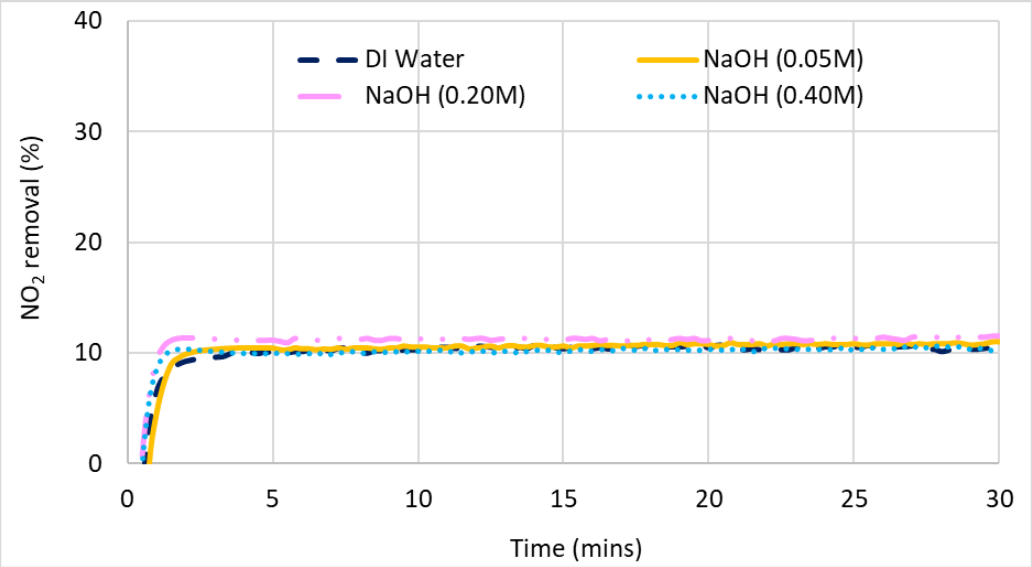

Figure 4-25: NO_2 gas removal from the simulated exhaust gas using DI water versus scrubbing mixtures of increasing alkalinity (NaOH: 0.05 – 0.40M), carried out in the counter-current wet scrubber.

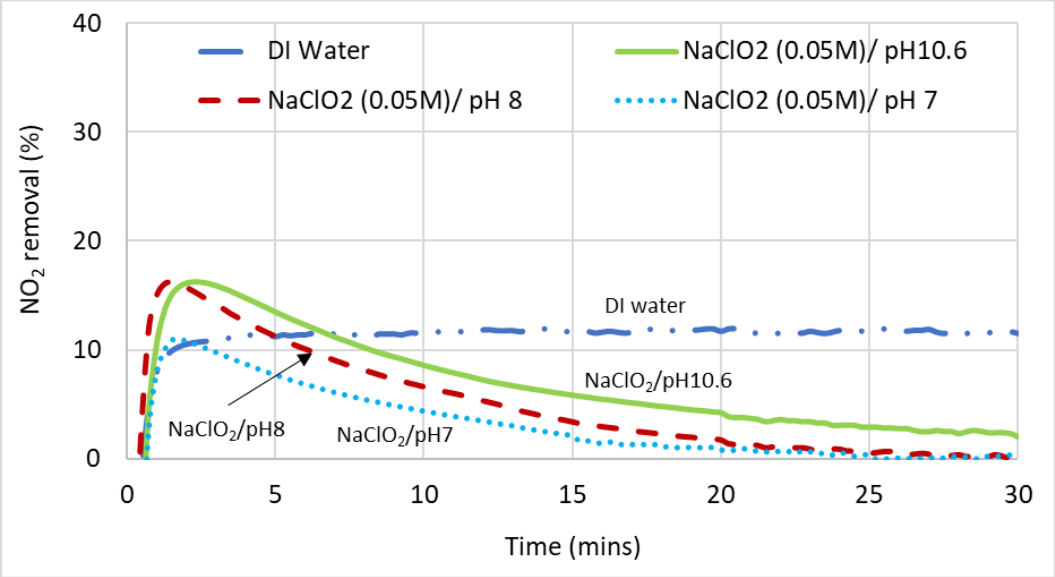

Figure 4-26: NO_2 gas removal from the simulated exhaust gas using DI water versus scrubbing liquids of increasing oxidation potential ($NaClO_2$/pH10.9 < $NaClO_2$/pH8 < $NaClO_2$/pH7), carried out in the counter-current wet scrubber.

4.2.4. Aqueous analysis of the wet scrubbing liquid

The analysis of aqueous samples from scrubbing mixtures which could remove NO_x at least partially are presented here. NO and NO_2 gases captured in the gas-liquid reaction in the wet scrubber should end up as either nitrites or nitrates in the aqueous phase. From Figure 4-27, it can be seen that the nitrogen existing in the aqueous phase were all in nitrate form. This was

because the residue oxidising agent in the liquid phase will oxidise all the nitrites into nitrates. This is advantageous as nitrates are the more stable in the aqueous phase. However, one area of concern is if part of the scrubbing liquid needs to be treated and discharged into the ocean during voyage. According to existing IMO guidelines for wastewater discharge from vessels to the ocean, high levels of nitrates may cause algae bloom, especially near the coastal areas, and are hence subjected to an upper discharge limit, in contrast to sulfates and chlorides which are considered to be naturally occurring in seawater and can be discharged freely (IMO, 2015).

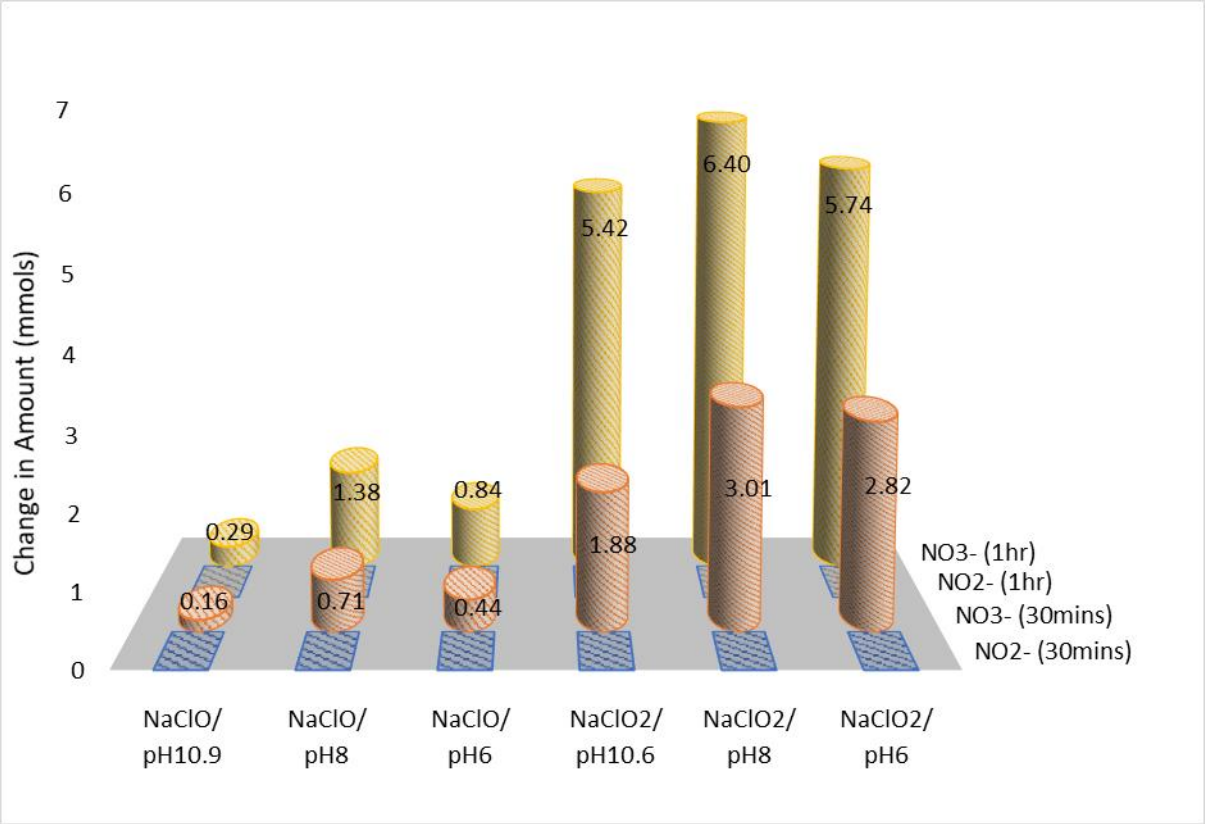

Figure 4-27: Amount of soluble nitrogen of various reactions using NaClO and $NaClO_2$ quantified by ion chromatography. The reactions were carried out in the counter-currrent wet scrubber.

In Table 4-6, the amount of nitrate in the aqueous system was compared to the calculated theoretical amount of NO_x that was removed based on the results from the flue gas analyser. It can be seen that for NaClO samples of various starting pH, only around 35 – 50% of the NO_x captured showed up as nitrates in the aqueous system. This range was around 70 – 80% for $NaClO_2$ samples.

The unaccounted nitrogen between the gaseous and aqueous phases could at least be partially attributed to the assumption that the system followed the ideal gas law when converting the gaseous concentration values from ppm(v) to mole. Secondly, it was also possible that the NO_2 that was absorbed by the aqueous mixture was unstable and a portion of it could have desorbed

from the scrubbing liquid before the quantitative analysis was carried out (within 24 hours), on account of Equations 4.7 and 4.8 being reversible reactions. These unstable absorbed nitrogen includes non-anionic aqueous forms such as NO_2 (aq) or HNO_2 (aq) (Yang *et al.*, 2016). Thirdly, they could simply have been reduced to N_2 gas especially when under low oxidation potential conditions (Chang *et al.*, 2004).

Table 4-6: Amount of NO_x removed by the various scrubbing liquids and the amount eventually converted to nitrate ions in the aqueous phase

Scrubbing liquid	**Total amount of Nitrates formed (mmol)**	**Total amount of NO_x Removed (mmol)**	**Percentage of removed NO_x converted to nitrates (%)**
NaClO	0.29	0.82	35.4
NaClO/pH 8	1.38	2.90	47.6
NaClO/pH 6	0.84	1.99	42.2
$NaClO_2$	5.42	7.06	76.8
$NaClO_2$/pH 8	6.40	8.32	76.9
$NaClO_2$/pH 6	5.74	8.23	69.7
$KMnO_4$	--	5.65	--

These results clearly showed that in the operating pH range from 6 – 11, $NaClO_2$ was more successful in not only oxidizing NO to NO_2 (Figure 4-18), but also in absorbing (Figure 4-23 and Figure 4-27) and retaining (Table 5) the NO_2 in the aqueous phase, compared to NaClO. It could effectively oxidize NO to NO_2 without needing a high ORP environment in the bulk phase likely due to its ability to decompose to its more oxidative form, ClO_2, at the gas-liquid interface, so the subsequent absorption of NO_2 which required a lower ORP environment was not inhibited.

For both NaClO and $NaClO_2$, the reaction at pH 8 registered the highest amount of nitrate in the aqueous system. The balance between the ability to oxidise NO to NO_2 and absorb the NO_2 formed was seen around this pH region. Deshwal speculated a similar concept of this balance when studying $NaClO_2$ but without arriving at an optimal pH as the work carried out was in the acidic pH range (Deshwal *et al.*, 2008). A study by Han et. al. on NO removal using $NaClO_2$ between the pH of 2.4 to 8.0 also showed that the absorption of NO_2 that was formed from the oxidation of NO was highest at pH 8.0 (Han *et al.*, 2019).

(A) Consumption of reactants

The mole ratio of the reactant consumed over the amount of NO_x that was removed is shown in Figure 4-28. It can be seen that for NaClO, the consumption of reactants for every mole of NO_x

removed increased with decreasing pH, for the pH range of 6 – 11. This was because as the pH shifted from 11 to 6, the dominant form of the chlorine oxidants also shifted from ClO^- to HOCl. The latter, while having a stronger oxidation strength, was also more volatile, leading to significant losses to the scrubber exhaust and a high reactant consumption rate. If NaClO is the oxidant of choice, the operating pH should be in the region of 8, as this range provided a balance between effectiveness of NO_x removal vs. reactant consumption rate. In this experimental setup, about 3 moles of ClO_2^- oxidant was consumed for every mole of NO_x removed at this operating pH.

Except for NaClO/pH10.9 and $NaClO_2$/pH10.6, all reactions showed similar reactant consumption rates at the midpoint and end of reaction, suggesting that the consumption rates of reactants were linear throughout the experimental duration. These two liquid mixtures saw increasing reactant consumption because their pH started high but gradually dropped throughout the reaction, leading to higher reactant losses to the gaseous phase.

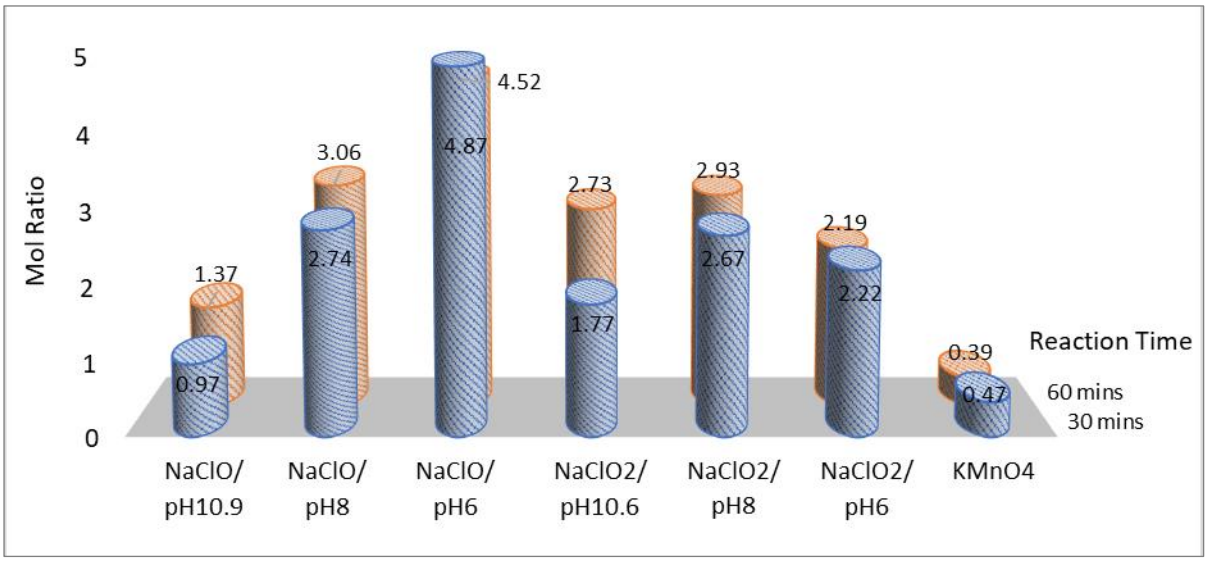

Figure 4-28: The mole ratio of the reactant consumed per mole of NO_x removed.

The various samples of $NaClO_2$ achieved between 2 – 3 moles of reactant consumed for every mole of NO_x removed; this was a better performance compared to NaClO, which ranged between 3 – 5 moles (with the exception of NaClO/pH10.9 as the NO_x removal for that sample was quite insignificant). Of all the reactants studied here, $KMnO_4$ had the lowest reactant consumption rate, achieving around half a mole of reactant consumed for every mole of NO_x removed. Unlike chlorine-based oxidants which tended to partition into more volatile forms especially at lower pH, the permanganate oxidant tends to precipitate out of the aqueous phase

as solid deposits instead when oxidised into its MnO_2 form. It is able to achieve this low reactant consumption rate since it is not volatilised and lost via the exhaust like chlorine-based oxidants.

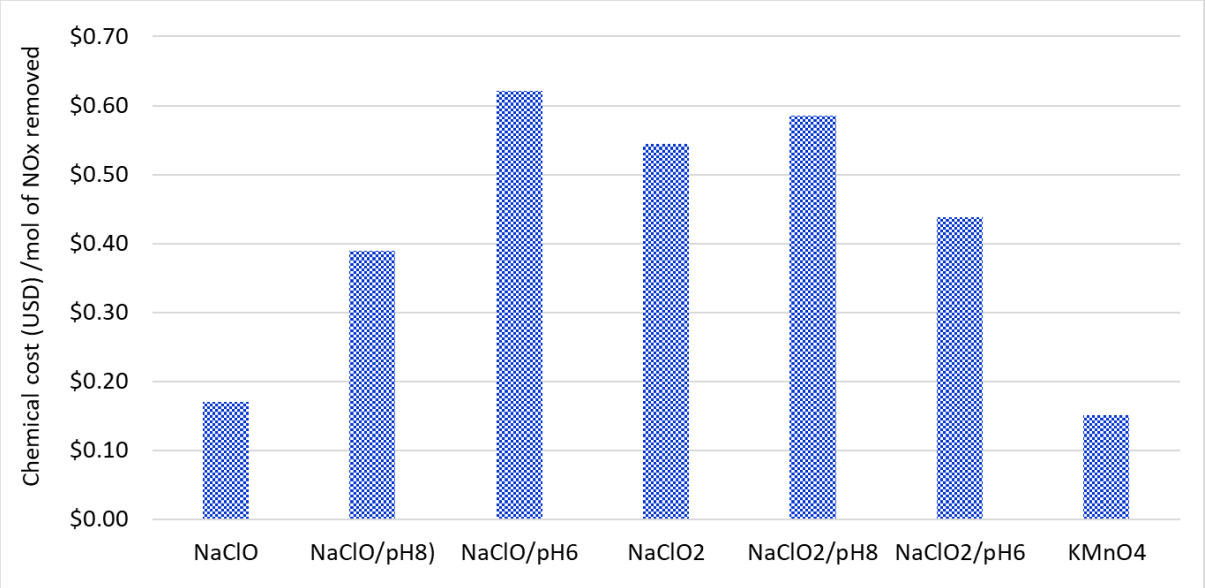

Figure 4-29: The estimated chemical cost of various reactant per mole of NO_x removed.

Table 4-7: Cost estimation of the various scrubbing liquid systems used.
Bulk cost of chemicals were estimated from industrial chemical aggregator sites, namely chembid.com, alibaba.com and diytrade.com. Assessed: 25 May 2021.

No	Scrubbing Liquid	Reactant cost (per mole)	Cost of HCl needed for pH adjustment (per mole)	Total cost (reactant + acid) (per mole)
1	NaClO	USD 0.124	USD 0.000	USD 0.124
2	NaClO/pH8	USD 0.124	USD 0.003	USD 0.127
3	NaClO/pH6	USD 0.124	USD 0.013	USD 0.137
4	$NaClO_2$	USD 0.199	USD 0.000	USD 0.199
5	$NaClO_2$/pH8	USD 0.199	USD 0.001	USD 0.200
6	$NaClO_2$/pH6	USD 0.199	USD 0.002	USD 0.201
7	$KMnO_4$	USD 0.392	USD 0.000	USD 0.392

Based on the amount of chemicals consumed in Figure 4-28 and the cost of chemicals in Table 4-7, the estimated chemical cost per mole of NO_x removed was estimated in Figure 4-29. It can be seen from Table 4-7 that the bulk cost of industrial chemicals from cheapest to most expensive is: NaClO < $NaClO_2$ < $KMnO_4$. Although $KMnO_4$ is the most expensive chemical, it is still the most cost effective after accounting for its high utilization rate, at approximately USD 0.15 per mole of NO_x removed. Although NaClO was less efficient than $NaClO_2$ in terms

of reactant consumption, they did not differ significantly after accounting their cost – both laid around the range of USD 0.39 – 0.62 per mole of NO_x removed. Therefore, if these two compounds are being considered for usage in a system, the choice would likely be decided by other factors instead of costs.

4.2.5. Scalability

The optimal conditions for the best three scrubbing compounds, namely $NaClO_2$, $KMnO_4$ and NaClO, were selected for further experimental runs at a significantly higher flowrate which are closer to industrial wet scrubbers. This was carried out to observe the behaviour of each of these compounds when scaled to a liquid-to-gas ratio that is closer to industrial norms. Focus was placed on NO removal as it is the more challenging pollutant compared to SO_2. The *L/G* ratio were decreased from 100 L/m^3 to 15 L/m^3 and the results are shown in Figure 4-30 and Figure 4-31.

It can be seen that the conversion of NO and removal of NO_x by $NaClO_2$ were very similar for both *L/G* ratios. However, this was not so for $KMnO_4$ and NaClO, which saw a reduction in capacity for the oxidation of NO and removal of NO_x when the *L/G* ratio were reduced to 15. $KMnO_4$ encountered a reduction of 40% in its capacity to oxidise NO to NO_2 and in the removal of NO_x. As for NaClO, this reduction of capacity was around 80% for both the oxidation of NO and removal of NO_x.

This limitation in the capacity of $KMnO_4$ and NaClO to oxidise NO and absorb NO_x when the *L/G* ratio was reduced (ie. gas flowrate was increased and liquid flowrate reduced) showed that these two compounds were more limited in their reaction kinetics or mass transfer capacities compared to $NaClO_2$. As $NaClO_2$ showed a maximum conversion (100%) of NO to NO_2 for both high and low *L/G* ratios studied here, it is likely that it has high chemical reaction rate or mass transfer capacity to remain effective at even lower *L/G* ratios. Therefore, $NaClO_2$ would likely be the most effective compound compared to $KMnO_4$ and NaClO when scaling up to industrial size requires much higher gas flowrates compared to liquid flowrates. The latter two compounds may still be used if a significant increase in concentration can improve their effectiveness, but further work is needed to verify this at low *L/G* ratios.

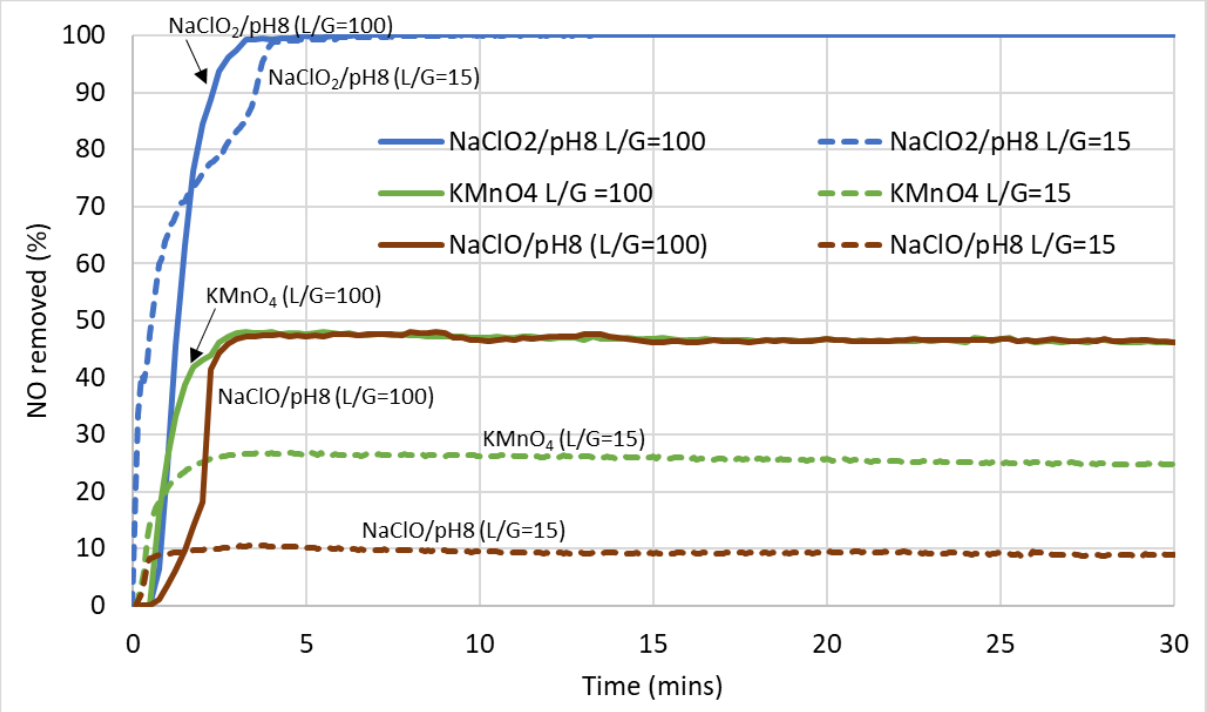

Figure 4-30: Nitric Oxide (NO) removal from the simulated exhaust gas with various scrubbing liquids at L/G ratios of 100 L/m^3 vs. 15 L/m^3 respectively.

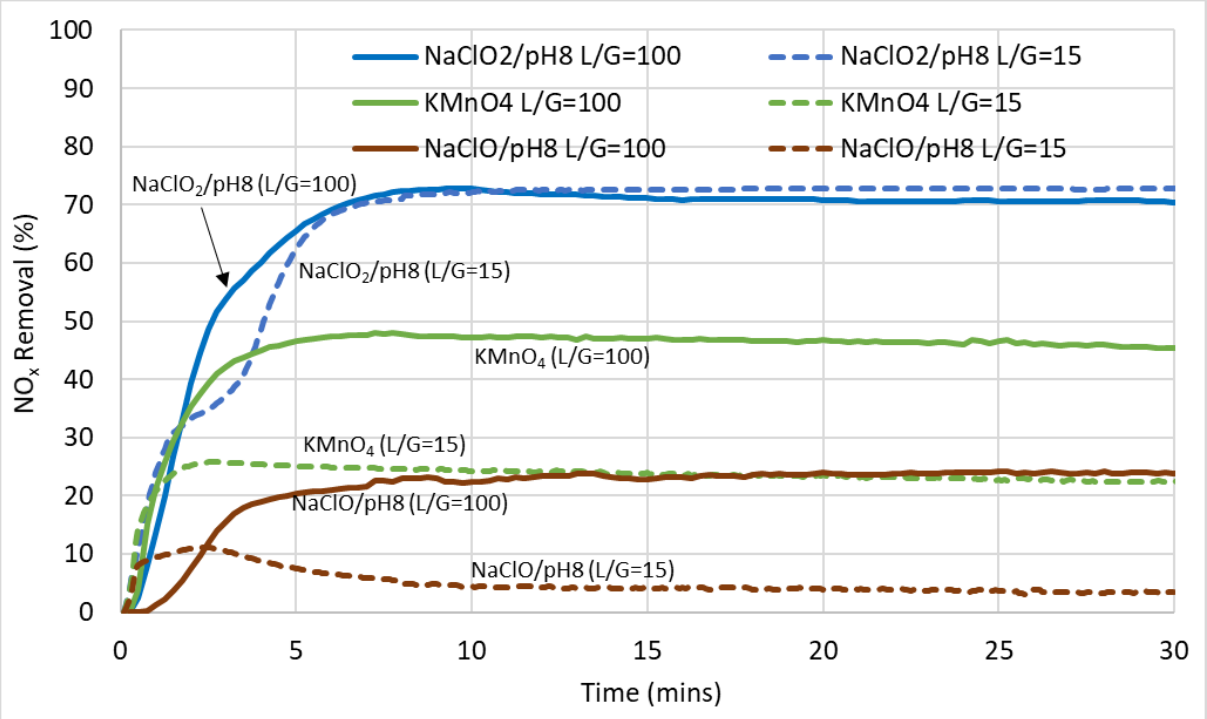

Figure 4-31: NO_x ($NO+NO_2$) removal from the simulated exhaust gas using various scrubbing liquids

4.3. Summary

For the reaction with SO_2, full removal of SO_2 proceeded quite readily and was achieved by nearly all the different types of scrubbing mixtures that were tested. This is because SO_2 gas is

very soluble in the aqueous phase. The absorption of SO_2 in the aqueous phase by the various gas-liquid reactions were likely influenced by three factors, namely pH, the ionic concentration in the scrubbing mixture in terms of both its overall ionic strength and concentration of sulphate ions, and oxidation potential. An effective scrubbing liquid for the effective removal of SO_2 gas should have high pH or alkalinity, low in ionic strength and sulphate ions, and oxidative in nature.

As for NO_x removal, the effectiveness of various chemical compounds used can be ranked as follows, from least to most effective: Seawater, NaOH, H_2O_2 < NaClO < $KMnO_4$ < $NaClO_2$. The first three, seawater, NaOH and H_2O_2 had little or no effect. NaClO was somewhat effective when the pH was lowered to 9 and below, when the hypochlorite ions shifted to its oxidative form, HOCl. Following that was $KMnO_4$ which was moderately effective, while $NaClO_2$ was the most effective, especially when the pH was below 10. When the *L/G* ratio was reduced from 100 L/m^3 to 15 L/m^3, $NaClO_2$ showed no change in its effectiveness for NO_x removal while NaClO and $KMnO_4$ showed a reduction in 80% and 40% respectively. This showed that $NaClO_2$ is the most reactive and suitable for scaling up to industrial size (higher gas flowrate, lower liquid flowrate conditions) while NaClO and $KMnO_4$ would probably require higher concentrations to make up for their kinetic and mass transfer limitations.

For achieving high NO_x removal, the scrubbing liquid mixture must be effective in:

i) oxidizing NO to NO_2,
ii) absorbing the NO_2 into the aqueous phase, and
iii) retaining the nitrogen in the aqueous phase as anions.

Seawater, NaOH and H_2O_2 were ineffective in NO_x removal because they had difficulty oxidizing NO to NO_2. NaClO was effective in oxidizing NO to NO_2 after it partitioned into its HOCl form when the pH was reduced below 9. However, it was not very effective in absorbing and retaining NO_2 in the aqueous phase, especially when the pH was lowered to below 9 – up to half of the NO_2 that was absorbed likely desorbed back into the atmosphere after a short period of time.

Successful oxidation of NO to NO_2 did not necessarily translate to high NO_x removal as the absorption of NO_2 proved to be a challenge although it is approximately 5 times more soluble than NO in the aqueous phase. Alkalinity was not a factor in the absorption of NO_2 into the aqueous phase as increasing the NaOH concentration had no effect on it. Rather, NO_2 absorption showed an inverse relationship with oxidation potential in this study. The seeming

relationship between NO_2 absorption and pH was likely coincidental since the oxidation potential of chlorine-based oxidants are also pH dependent.

$NaClO_2$ was superior compared to NaClO in all three categories of oxidizing, absorption and retention of NO in the pH range of 6 – 11. It could effectively oxidize NO to NO_2 without needing a high ORP environment in the bulk phase likely due to its ability to decompose to its more oxidative form, ClO_2, at the gas-liquid interface, so the subsequent absorption of NO_2 which required a lower ORP environment was not inhibited.

In the pH range of 6 – 11 studied here, the pH at around the region of 8 provided an optimal balance between oxidation versus both absorption/retention and reactant utilization for NaClO and $NaClO_2$, respectively. Operating at an optimal pH was important as to minimize reactant losses to the atmosphere as both $NaClO_2$ and NaClO partitioned into a gaseous state at lower pH.

Although $KMnO_4$ was less effective than $NaClO_2$ in terms of overall NO_x removal, it was very effective in absorbing and retaining the NO_2 in the aqueous phase. In fact, it was possible that this seemingly high NO_2 absorption could be because $KMnO_4$ was able to oxidize NO into the aqueous phase without forming gaseous intermediates such as NO_2. $KMnO_4$ also had the lowest reaction consumption rate, with only half a mole utilized for every mole of NO_x removed, compared to 2 – 3 moles of $NaClO_2$ or 3 – 5 moles of NaClO needed for every mole of NO_x removed. This was because unlike the chlorine-based oxidants, $KMnO_4$ does not partition into a more volatile form, leading to less reactant losses to the atmosphere. However, $KMnO_4$ has a tendency to precipitate in the form of MnO_2 which caused clogging and was very difficult to remove.

In terms of chemical cost per mole of NO_x removed, $KMnO_4$ is the most cost effective while NaClO and $NaClO_2$ were similar in range. As each of the chemical reactant compared here have their own advantages and disadvantages, the choice of the most suitable reactant will still depend on the actual design of the wet scrubbing system. Nevertheless, this comparison exercise enabled a deeper understanding of the reaction mechanisms and behaviour of the reactants during reaction.

Chapter 5. Counter current wet scrubber with sodium chlorite

In the previous chapter, it was established that sodium chlorite was the most effective for the gas-liquid reaction to remove SO_2 and NO simultaneously in the counter-current wet scrubber among the group of chemical compounds studied here. In this chapter, further development was carried out using this oxidant in the counter-current wet scrubber setup. Prior to this section, the simulated exhaust gas for all experiments conducted contained N_2 and O_2 in the background apart from the pollutant gases but not CO_2. In this section, CO_2 was introduced into the simulated exhaust gas and its effects were observed. Carbon dioxide concentration in the exhaust gas is typically quite high, at around 4% v/v (which corresponds to 40,000 ppmv), which made it significantly higher that the concentrations of SO_2 and NO. As carbon dioxide is also a weak acid and is absorbed in aqueous phase to a certain extent, its presence may influence the gas-liquid reaction taking place for SO_2 and NO removal. The pH of the sodium chlorite oxidant was also adjusted to observe for possible influences.

Although sodium chlorite showed potential in the simultaneous removal of SO_2 and NO, it is clear that one of the main challenges to achieving high NO_x removal is the difficulty in absorbing the NO_2 which was formed from NO oxidation. As discussed in the previous chapter, although NO_2 gas is at least 5 times more soluble in the aqueous phase than NO (Table 4-4), its solubility was clearly still insufficient for the significant absorption and removal of NO_x from the exhaust. Although NO_2 gas is acidic in nature, its absorption did not show any improvement when reacted with highly alkaline liquid. At this point, it has also been shown that NO_2 absorption worsened with increasing ORP. Therefore, increasing the oxidising potential in an attempt to form higher valency nitrogen intermediates which have higher solubility such as N_2O_3, N_2O_4 and N_2O_5 did not work at all. Therefore, the last part of this chapter is dedicated to making further improvement in NO_2 absorption, in particular, through the usage of reducing agents. The ratio of NO to NO_2 concentration in the exhaust gas was also varied to determine if any particular ratio to these two gases has an advantage in NO_x removal.

5.1. Effect of carbon dioxide presence in the exhaust gas

Prior to this section, the simulated exhaust gas for all experiments conducted contained N_2 and O_2 in the background apart from the pollutant gases but not CO_2. In this section, CO_2 was introduced into the simulated exhaust gas and its effects observed (see Table 5-1, No. 1-2). The oxidant sodium chlorite was chosen as it was shown to be the most promising chemical compound for NO_x removal in the group of chemicals studied here, as discussed in the previous

section. The experimental setup and the wet scrubber configuration remained unchanged from the previous setup shown in Figure 4-13 and described in the experimental procedure in Section 4.2.1.

Table 5-1: A summary of experimental conditions for SO_2 and NO removal with the presence of CO_2 in the exhaust gas, carried out using the counter-current wet scrubber.
Wet scrubber specifications – Liquid volume: 2.5L; liquid flowrate: 1.0 L/min; gas flowrate: 10 L/min; O_2: 14%; ambient temperature; Scrubber height: 400mm.

No	Scrubbing solution	$NaClO_2$ (M)	NaOH (M)	pH	ORP (mV)	Exhaust Gas Concentration		
						SO_2 (ppmv)	NO (ppmv)	CO_2 (%)
1	$NaClO_2$	0.05	0.000	10.5	601	500	500	0
2	$NaClO_2$	0.05	0.000	10.5	601	500	500	4%
3	$NaClO_2$	0.05	0.000	10.5	601	0	0	4%
4	$NaClO_2$ + NaOH	0.05	0.010	12.0	591	500	500	4%
5	$NaClO_2$ + NaOH	0.05	0.025	12.2	581	500	500	4%
6	$NaClO_2$ + NaOH	0.05	0.040	12.6	549	500	500	4%
7	$NaClO_2$ + NaOH	0.05	0.050	12.7	575	500	500	4%

The removal of SO_2, NO and overall NO_x with and without the presence of CO_2 in the exhaust gas is shown in Figure 5-1. At first glance, it would seem that the presence of CO_2 in the exhaust gas had no effect on the simultaneous removal of SO_2 and NO at all. Both SO_2 removal and oxidation of NO reached 100% after the initial unsteady state. Overall NO_x removal results experience more fluctuation but were also quite similar and remained in the range of 50 – 60% for both conditions throughout the experimental run. However, upon closer inspection, it would seem that the presence of CO_2 slightly favoured NO and NO_x removal as it reached its maximum removal plateau first compared to without CO_2 present. This showed that the rate of reaction for NO and NO_x removal were faster in the presence of CO_2. Conversely, the presence of CO_2 seemed to have slowed the reaction rate for SO_2 removal, but this effect was very small.

A look at the pH and redox potential values showed large changes occurring during reaction (Figure 5-2). In both conditions, the starting pHs of the aqueous phases were at around 10.5 at the beginning and dipped to around 3.4 at the end of the reaction. The condition with the presence of CO_2 showed a much sharper drop in pH from 10.5 to 7.0 compared to the condition without CO_2 and this was due to the absorption of CO_2. This acidification effect due to the presence of CO_2 likely caused the sodium chlorite oxidant to dissociate more quickly to form

ClO_2, its more powerful oxidation form, according to Equations 4.15 and 4.16. This effect can also be seen in the redox potential value of the aqueous phase with CO_2 presence, which rosed and plateaued at around 600mV more quickly that the condition without CO_2.

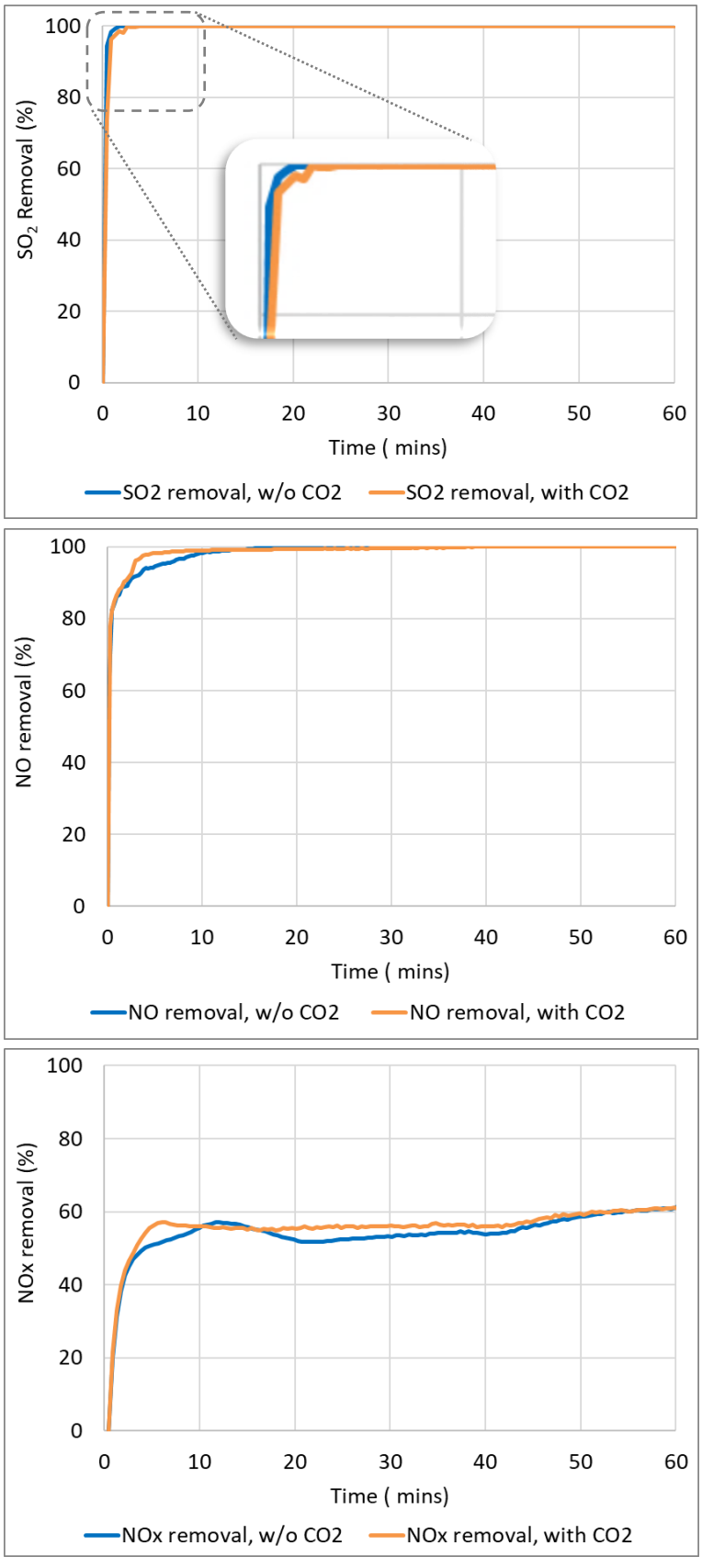

Figure 5-1: Removal (%) for SO_2 (top), NO (middle) and NO_x (bottom) using sodium chlorite in a counter-current wet scrubber, with and without CO_2 in the exhaust gas.
Experimental conditions shown in Table 5-1, No. 1-2.

A second sharp pH dip was also observed from around the pH of 6.4 till below 4.0, with both conditions with and without CO_2 dipping at the same rate this time. Similar with the first pH drop, this second occurrence which happened between 35 – 40 mins of reaction time also bumped the redox potential values up, causing a noticeable increase in the overall NO_x removal from the 40th min onwards.

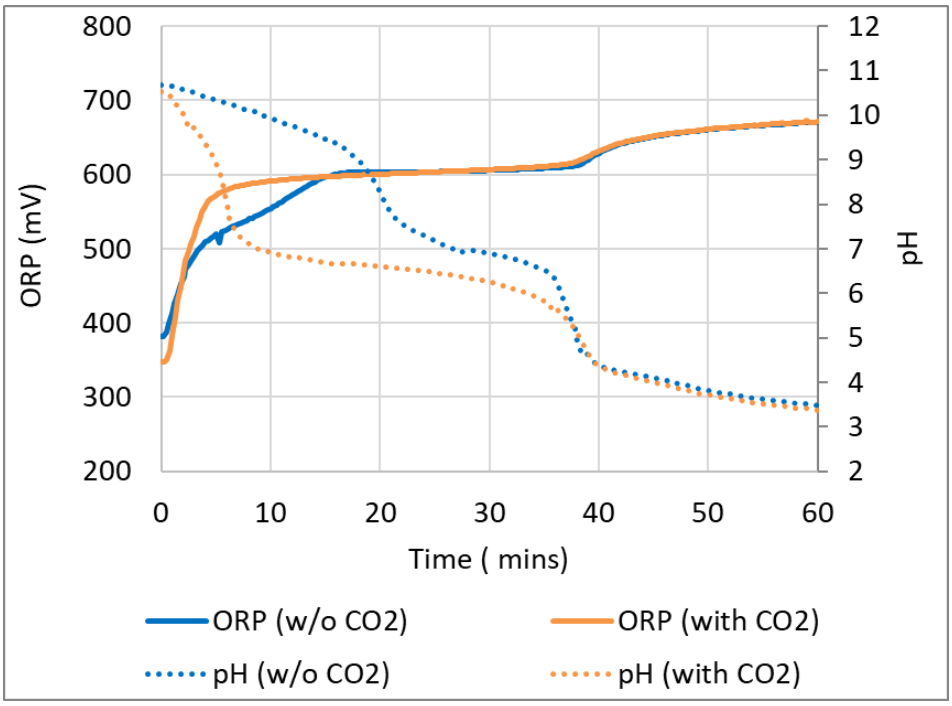

Figure 5-2: Change in aqueous phase ORP and pH values as the reaction progressed, for the simultaneous removal of SO_2 and NO with sodium chlorite in a counter-current wet scrubber.
Experimental conditions shown in Table 5-1, No. 1-2.

The manner of pH drop due to carbon dioxide absorption seen in Figure 5-2 can be better understood by looking at the behaviour of CO_2 in the aqueous phase, which will first dissolve in water as carbonic acid (H_2CO_3) in the beginning, followed by the formation of bicarbonates (HCO_3^-) and carbonates (CO_3^{2-}) (Snoeyink and Jenkins, 1980):

$$CO_2(g) + H_2O \leftrightarrow H_2CO_3(aq) \quad \dots (5.1)$$

$$H_2CO_3(aq) + OH^-(aq) \leftrightarrow HCO_3^-(aq) + H_2O \quad (pKa_1 = 6.35) \quad \dots (5.2)$$

$$HCO_3^-(aq) + OH^-(aq) \leftrightarrow CO_3^{2-}(aq) + H_2O \quad (pKa_2 = 10.33) \quad \dots (5.3)$$

When absorbed in water, carbon dioxide exists as carbonic acid, a diprotic acid which partitions into bicarbonate and carbonate according to the carbonic acid equilibrium system (Figure 5-3). The buffer system that is created here provides two buffer zones in the aqueous phase, the first

occurring at a high pH zone involving the transition between bicarbonates and carbonates (Equation 5.3) and the second taking place at a lower pH zone where the transition between carbonic acid and bicarbonates occurs (Equation 5.2). The two large pH drops seen in Figure 5-2 were associated with pH change that occurred outside these two buffer zones.

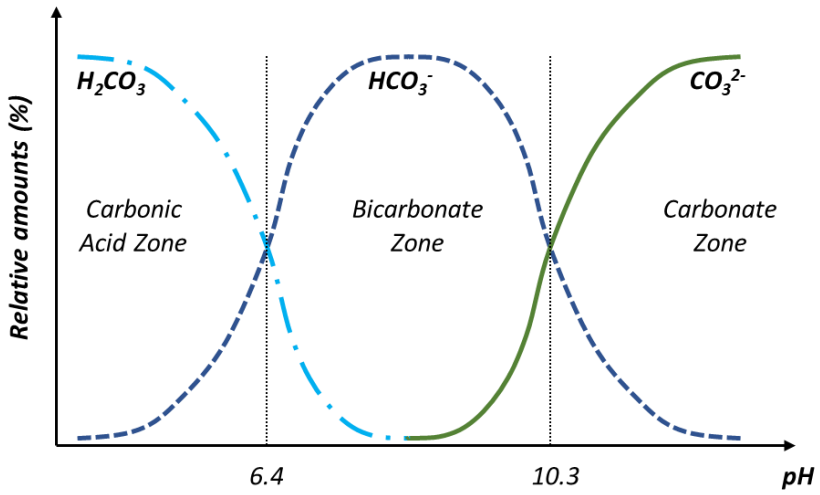

Figure 5-3: An illustration of the Bjerrum plot showing the carbonic acid equilibrium in water.
Derived from: (Snoeyink and Jenkins, 1980)

In the condition without the presence of CO_2 in the exhaust gas, the rate of pH drop was slower at the first half of the reaction but was similar and overlapped with the condition with CO_2 in the second half of the reaction (Figure 5-2). The pattern of pH drops for both conditions were also somewhat similar. Although no CO_2 was absorbed during the experiment for the condition without CO_2 in the exhaust gas, acidification of the aqueous system would still occur due to the absorption of SO_2 and NO and the shape of the pH change still followed the pattern of the bicarbonate buffer system. This was because all commercially available sodium chlorite powder contains a small amount of sodium carbonate that was added to stabilise the chlorite for storage. Therefore, when the chemical was diluted from its powder form, the bicarbonate buffer system describe above would also be present in its aqueous phase.

The removal of CO_2 during the wet scrubbing process was also observed and shown in Figure 5-4. The removal of CO_2 in the simulated exhaust gas containing SO_2, NO and CO_2 were compared with exhaust gas that contained only CO_2. For both cases, it can be seen that CO_2 stopped being absorbed in the aqueous phase after the pH dipped to around 7.0 – 7.1. In the case of the simulated exhaust gas containing SO_2, NO and CO_2, the pH continued to fall after CO_2 stopped being absorbed due to reaction with SO_2 and NO.

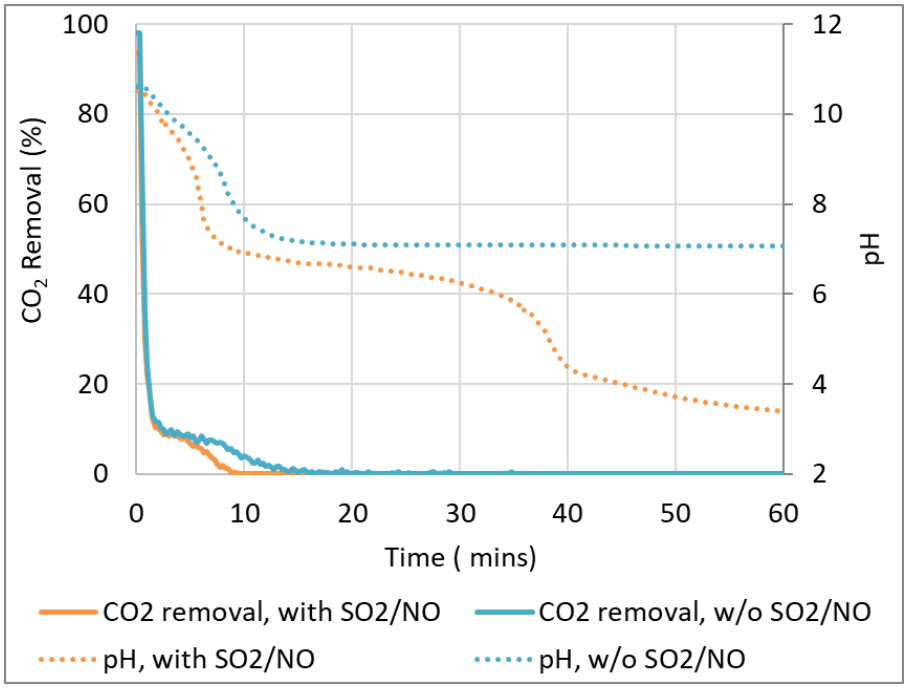

Figure 5-4: Removal (%) for CO_2 using sodium chlorite in a counter-current wet scrubber, with CO_2 in the exhaust gas.
Experimental conditions shown in Table 5-1, No. 2-3.

From all the observations seen above, it can be surmised that the presence of CO_2 in the exhaust gas has a positive effect in NO_x removal if the pH of the aqueous solution is in the alkaline range. This was because the absorption of CO_2 decreased the pH and promoted the conversion of the chlorite oxidant into ClO_2, its more powerful variant. However, this may not always be advantageous as the latter is also more volatile and may result in a higher loss of reactant. If the wet scrubber needs to be operated in the alkaline range, alkaline chemicals such as NaOH will have to be dosed continuously at a higher rate to counter the acidification caused by the absorption of CO_2, on top of the acidification caused by SO_2 and NO. If the wet scrubber is operated in the acidic pH range, then the presence of CO_2 in the exhaust gas will have no effect on SO_2 and NO removal, since CO_2 does not appear to interact with the aqueous phase at all below pH 7. As for the removal of SO_2, the acidification caused by CO_2 absorption seem to have very little effect based on the conditions of this study, owing to the high solubility of SO_2 in water.

5.2. Effect of pH adjustment with sodium hydroxide

In this section, the starting pH of the wet scrubber liquid with the sodium chlorite oxidant was adjusted by the addition of different amounts of NaOH. From Figure 5-5, it can be seen that the

removal of CO_2 was proportional to the amount of NaOH added. Comparing the CO_2 removal and the pH further corroborated the finding in the previous section that its absorption only occurred in alkaline conditions but stopped when the pH dipped into the acidic range. The addition of NaOH prolonged the aqueous phase in the alkaline range longer, allowing for more CO_2 absorption.

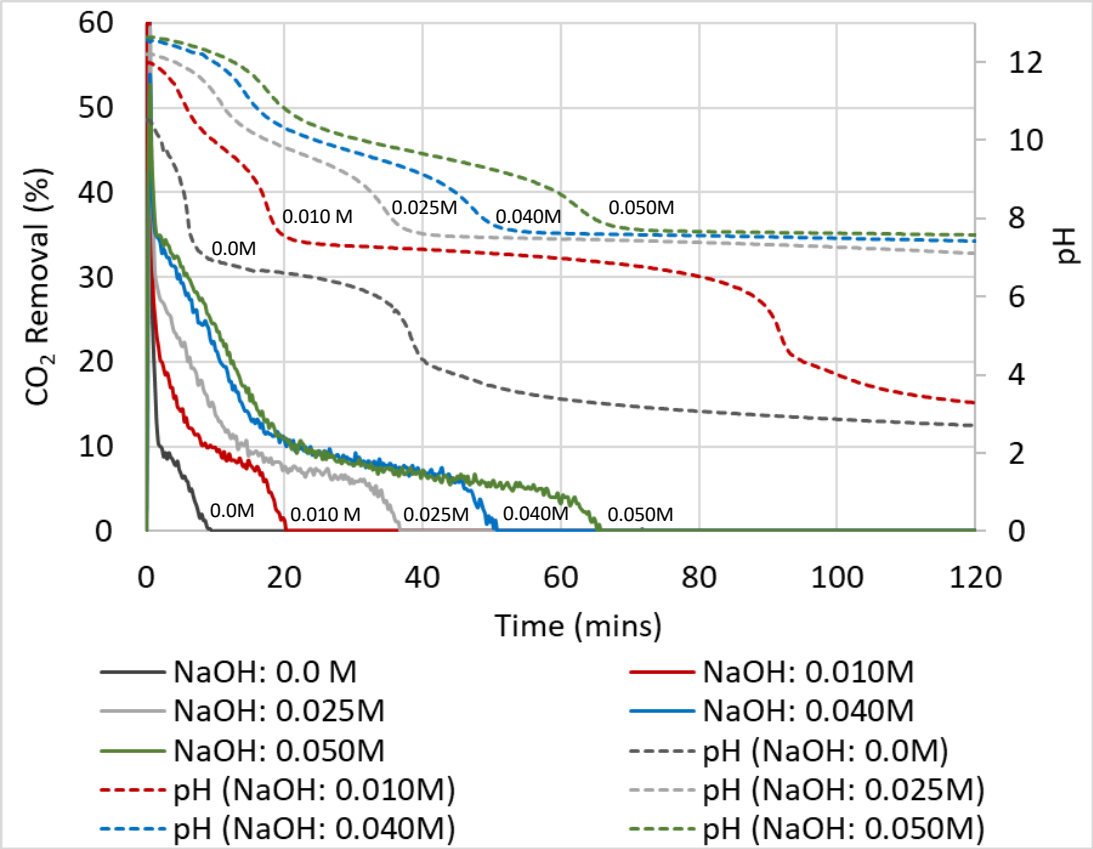

Figure 5-5: Removal of CO_2 from the simulated exhaust gas during the reaction between sodium chlorite with SO_2 and NO in the counter-current wet scrubber. Experimental conditions shown in Table 5-1, No. 1, 4-7.

As for SO_2 removal, no visible difference was observed as the amount of NaOH added was varied, since this gas has a very high solubility in water (Figure 5-6). For NO removal (Figure 5-7), it can be seen that the reaction rate was inversely proportional to the concentration of NaOH added. These differences were in accordance with their pH profiles (shown in Figure 5-5) where around 100% NO removal was achievable only when the pH of the scrubbing liquid dropped from the alkaline range to around the region of 8. This occurrence was due to the decomposition of chlorite to its more active chlorine dioxide form and was consistent with all previous observations so far.

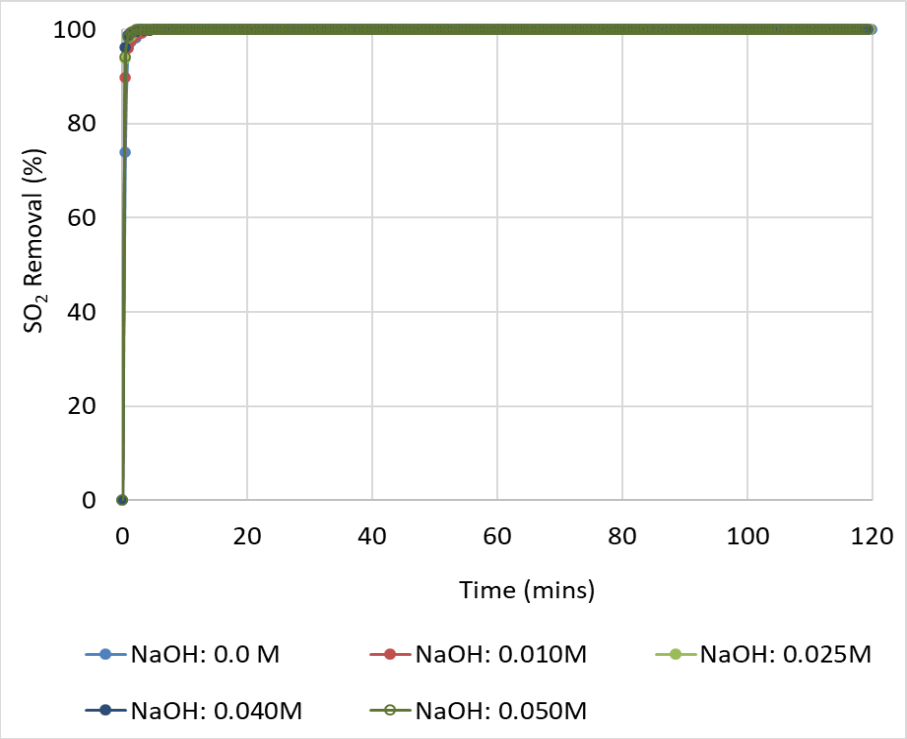

Figure 5-6: Removal (%) of SO_2 using sodium chlorite in a counter-current wet scrubber, with variation in NaOH addition.
Experimental conditions shown in Table 5-1, No. 1, 4-7.

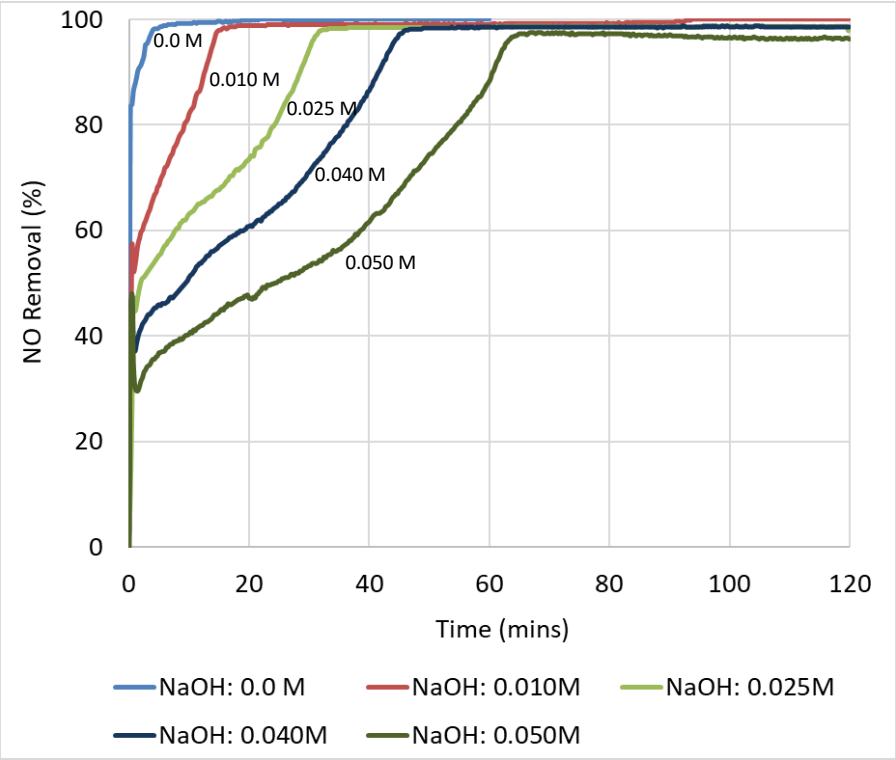

Figure 5-7: Removal (%) for NO using sodium chlorite in a counter-current wet scrubber, with variation in NaOH addition.
Experimental conditions shown in Table 5-1, No. 1, 4-7.

5.3. Improving the removal of NO_2 in the counter-current wet scrubber

In this section, various ways to increase the removal of NO_2 formed from the oxidation of NO were explored. Most of the studies carried out eventually hit a roadblock after oxidation of NO to NO_2 because the latter turned out to be harder to remove than expected. Although NO_2 is about 5 times more soluble in water than NO under atmospheric conditions, only partial removal could be achieved usually (Chin *et al.*, 2022). Subsequent studies conducted to overcome this can be summarised into two approaches – further oxidising NO_2 to even more soluble compounds or using a reducing agent to remove NO_2. The first approach involved further oxidising NO_2 to form high valency intermediates such as N_2O_3, N_2O_4 and N_2O_5 as these have higher solubility in aqueous solution (Lin *et al.*, 2016; Shao *et al.*, 2019). However, most of the gaseous nitrogen-based pollutants would end up in the aqueous phase, leading to high concentrations of nitrates. This would not be ideal for ship-based applications since the scrubber wastewater might have to be discharged into the ocean during voyage.

Table 5-2: A summary of potential reducing agents and their associated stabilizing agents for reaction with NO_2 gas.
Summary was interpreted from the NFPA 704: Standard System for the Identification of the Hazards of Materials for Emergency Response and the Globally Harmonized System of Classification and Labelling of Chemicals.

Chemical type	**Chemical formula**	**Reaction with NO_2**	**Stability in Aqueous Phase**	**Safety Issues**	**Environmental Issues**
Sodium sulfide	Na_2S	STRONG	UNSTABLE *Unless in high pH, otherwise will decomposes to H_2S)*	DANGEROUS *Toxic, corrosive, harmful*	HAZARDOUS
Sodium sulfite	Na_2SO_3	MODERATELY STRONG	UNSTABLE *Oxidizes to sulfate in the presence of O_2*	RELATIVELY SAFE	RELATIVELY SAFE
**Formaldehyde*	CH_2O	--	--	DANGEROUS *Toxic, corrosive, carcinogenic, health hazard*	--
**Hydroquinone*	$C_6H_4(OH)_2$	--	--	DANGEROUS *Corrosive, harmful, health hazard*	HAZARDOUS
Sodium thiosulfate	$Na_2S_2O_3$	MODERATE	STABLE	RELATIVELY SAFE	RELATIVELY SAFE

The second approach involving the usage of reducing agents has been studied widely in recent years due to its potential of converting the harmful nitrogen-based pollutants into its harmless gaseous N_2 form so that it does not end up as soluble nitrogen in the wastewater. The vast

majority of this focused on the usage of sodium sulfide (Na_2S) and sodium sulfite (Na_2SO_3) as reducing agents (Chang *et al.*, 2004; Mok and Lee, 2006; Kuroki *et al.*, 2008; Wu *et al.*, 2008; Chen *et al.*, 2011; Hao *et al.*, 2017; Kim *et al.*, 2018; Yamasaki *et al.*, 2019; Lian *et al.*, 2020; Zhang *et al.*, 2020; Gan *et al.*, 2021; Zhang *et al.*, 2021; Li *et al.*, 2022; Liu *et al.*, 2022; Schmid *et al.*, 2022; Zhang *et al.*, 2022a; Zhang *et al.*, 2022b). However, there are several stability, safety and environmental issues with these two reductants that posed challenges for commercial application (Table 5-2). While the decomposition of Na_2S to H_2S can be minimized by keeping it at very high pH, Na_2SO_3 is much less stable in aqueous conditions and typically require stabilizing agents which in itself can be hazardous as well (Lian *et al.*, 2020; Li *et al.*, 2022).

5.3.1. Removal of NO_2 using various types of chemical compounds

In this section, various types of chemicals were reacted with a simulated exhaust gas that was rich in NO_2 but also containing small amounts of NO. Such a condition may exist after an initial oxidation stage have converted most of the NO to NO_2 but could not further absorb the latter. The smaller setup involving the gas bubbling reaction shown in Figure 4-1 was used here before proceeding to use the larger counter-current wet scrubber in the next section. Sodium sulfite (Na_2SO_3), thiosulfate ($Na_2S_2O_3$), Urea ($CO(NH_2)_2$), sodium chlorite ($NaClO_2$) and deionised water (DI water) were compared, and their experimental conditions can be found in Table 5-3.

Table 5-3: A summary of experimental conditions for NO_2 removal carried out using the gas bubbling reactor.
Liquid volume: 150ml; gas flowrate: 1.50L/min; O_2: 14%; ambient temperature.

No	Scrubbing solution	Conc. (M)	pH	ORP (mV)	Exhaust Gas Concentration			
					SO_2 (ppmv)	NO (ppmv)	NO_2 (ppmv)	CO_2 (%)
1	Sodium chlorite ($NaClO_2$)	0.05	10.6	298	--	200	400	4
2	Sodium sulfite (Na_2SO_3)	0.05	9.6	-7	--	200	400	4
3	Urea ($CO(NH_2)_2$)	0.05	6.3	210	--	200	400	4
4	Deionised water (DI water)	--	5.8	361	--	200	400	4
5	Sodium thiosulfate ($Na_2S_2O_3$)	0.05	6.4	118	--	200	400	4
6	Sodium thiosulfate with 0.05ml NaOH (1M)	0.05	10.0	55.6	--	200	400	4
7	Sodium thiosulfate with 0.10ml NaOH (1M)	0.05	10.3	9.6	--	200	400	4
8	Sodium thiosulfate (0.025M) + Sodium sulfite (0.025M) + 0.10ml NaOH (1M)	0.025/ 0.025	10.0	-24.2	--	200	400	4

The results of the NO, NO_2 and NO_x removal are shown in Figure 5-8. From the middle of Figure 5-8, it can be seen that sodium sulfite was the most effective in removing NO_2, followed

by sodium thiosulfate. Sodium sulfite was able to achieve complete removal of NO_2, but this was not sustained after a period of time and the absorption eventually dropped to a level similar to using deionised water. This could have been because the reactant was unstable or could have been fully utilised after a short period of time. Although sodium thiosulfate could only achieve about 80% of NO_2 removal, this was sustained for the entire duration or the experiment. As for sodium chlorite and urea, both did not contribute to any significant increase of NO_2 removal compared to deionised water.

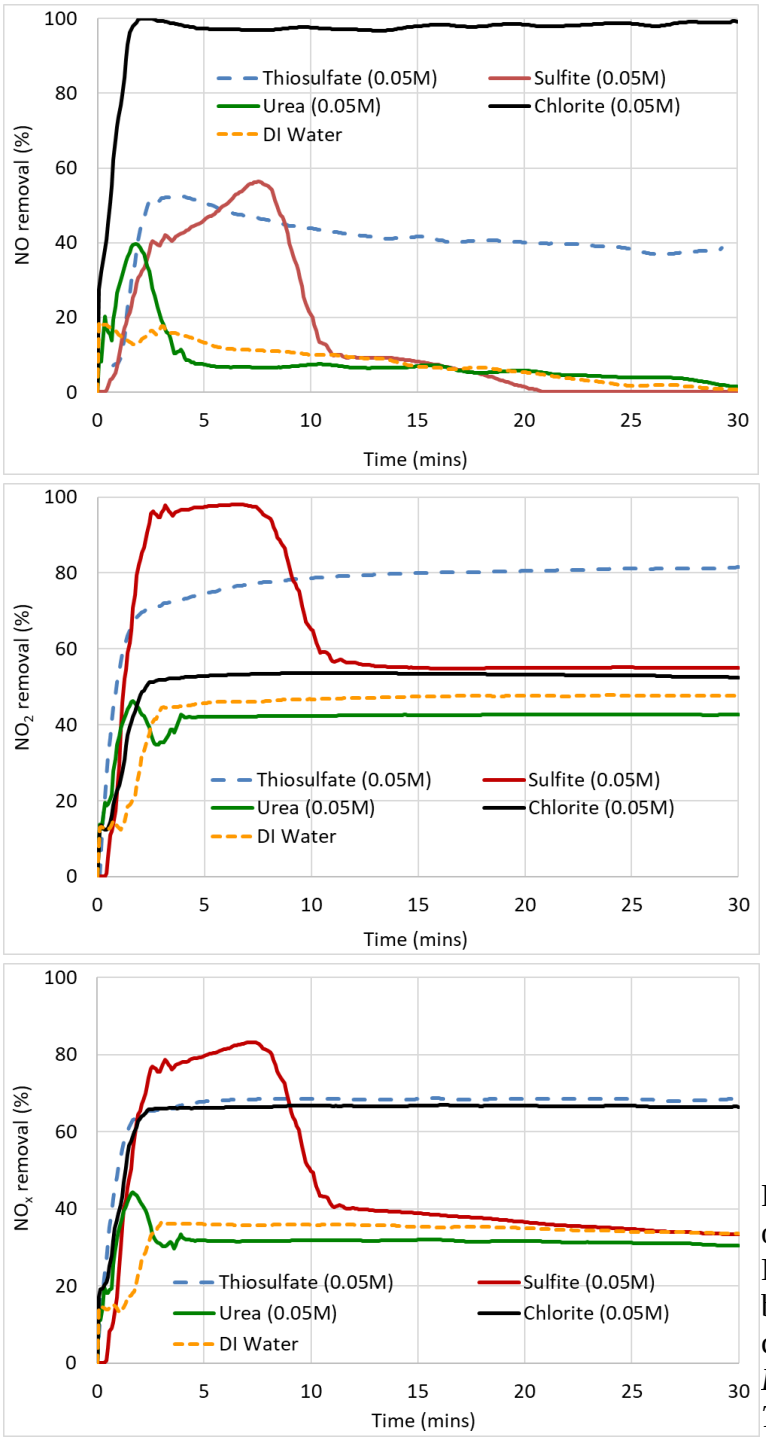

Figure 5-8: Outlet concentrations of NO (top), NO_2 (middle) and NO_x (bottom) exiting the gas bubbling reactor with variation of chemical compounds, *Experimental conditions found in Table 5-3, No. 1-5.*

Interestingly, both sodium sulfite and sodium thiosulfate also helped to improve NO removal compared to deionised water although they are both reducing agents (Figure 5-8, top). It is possible that both of these reactants were able to react with NO under these experimental conditions and this will be discussed more thoroughly in Section 5.3.2. For sodium sulfite, this removal could not be sustained after about 7 minutes of reaction and dropped to levels similar with deionised water, which was the same case observed for its removal of NO_2. As for sodium thiosulfate, its NO removal level was sustained throughout the whole duration. This again suggested that sodium thiosulfate was more stable than sodium sulfite.

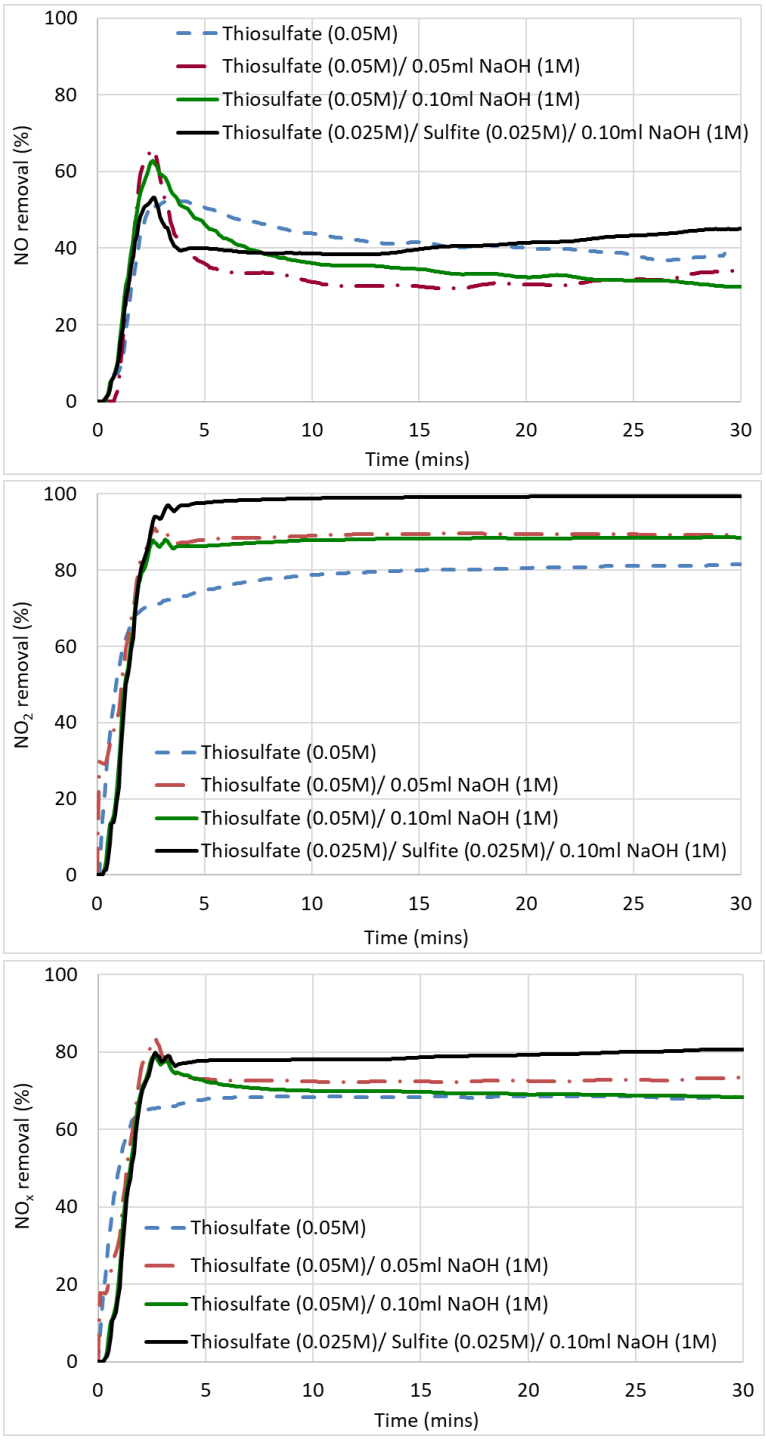

Figure 5-9: Outlet concentrations of NO (top), NO_2 (middle) and NO_x (bottom) exiting the gas bubbling reactor with variation of NaOH addition to sodium thiosulfate.
Experimental conditions found in Table 5-3, No. 6-8.

The usage of sodium thiosulfate was further investigated with the addition of NaOH and by combining it with sodium sulfite. It can be seen that for NO_2 removal (Figure 5-9, middle), addition of NaOH increased its removal, indicating that sodium thiosulfate was more efficient in NO_2 removal at high pH. The combination of sodium thiosulfate and sodium sulfite with NaOH achieved almost complete removal of NO_2 for the entire duration of the experiment. This could have been possible because the addition of sodium thiosulfate and sodium hydroxide to sodium sulfite made it more stable and slowed down its deterioration. In order to confirm this, the aqueous solution before and after the reaction were analysed with the ion chromatograph and the results shown in Figure 5-10.

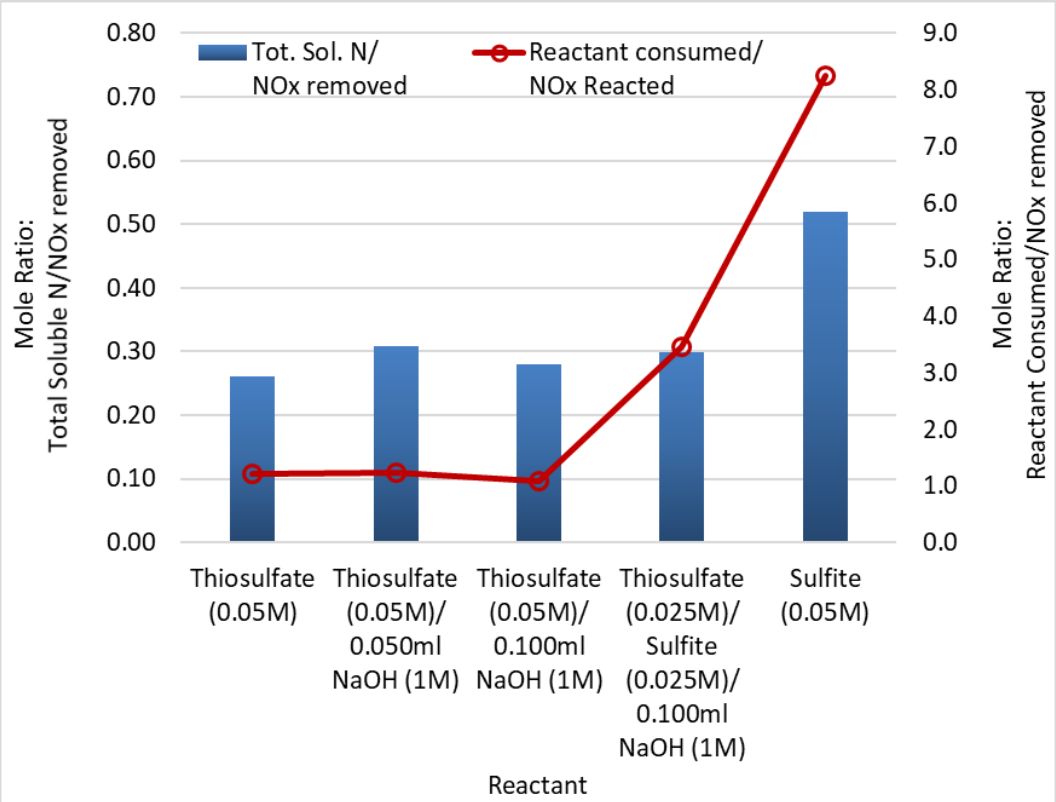

Figure 5-10: The mole ratios of soluble nitrogen formed over total NO_x removed, and reactant consumed over gaseous pollutant (NO_x) removed, with variation of reactant used in the glass bubbling reactor.
Experimental conditions found in Table 5-3, No. 6-8.

It can be seen from the results of the aqueous phase that the sulfite anion deteriorated more significantly compared to thiosulfate during the reaction. Approximately 8.3 moles of sulfite anion were consumed per mole of gaseous pollutant removed compared with just around 1.2 moles of thiosulfate consumed. In fact, no sulfite anion was detected in the aqueous scrubbing liquid that the end of reaction, indicating that it could have been completely absent at some point during reaction. This explained the sharp drop in NO and NO_2 removal by sodium sulfite after about 7 minutes of reaction time as observed in Figure 5-8 previously. This excessive

consumption of the reactant suggested that sulfite was unstable under these reaction conditions and could have been oxidised by the excess oxygen in the exhaust gas instead of being utilised by the NO_x molecules.

When thiosulfate was added to sulfite at a 1:1 ratio, the reactant consumption per mole of gaseous pollutant removed dropped to about 3.5 as the former was more stable. Apart from thiosulfate being more stable in itself, its presence could also have stabilised the sulfite anion and slowed down its deterioration. It has been previously reported that the presence of thiosulfate is able to inhibit the oxidation of sulfite by scavenging up the free radicals responsible for triggering sulfite oxidation (Shen and Rochelle, 1998).

5.3.2. Reaction mechanisms of NO_2 in the presence of reducing agents

In this section, the NO_2 removal mechanisms by reducing agents are explored further, with particular focus on sodium sulfite and sodium thiosulfate, which were shown to be among the more effective chemical compounds in the previous section.

It is well known that the presence of a strong reducing agent such as sulfite is able to reduce nitrogen dioxide to either nitrite anions or N_2 gas, as shown below (Chang *et al.*, 2004; Lian *et al.*, 2020; Zhang *et al.*, 2020):

$$2NO_2 + SO_3^{2-}(aq) + H_2O \rightarrow 2NO_2^-(aq) + SO_4^{2-} + 2H^+ \qquad \dots (5.4)$$

$$2NO_2 + 4SO_3^{2-}(aq) \rightarrow N_2(g) + 4SO_4^{2-} \qquad \dots (5.5)$$

However, the reduction of nitrogen dioxide using sodium thiosulfate is much less documented. Therefore, these reactions were predicted using a thermodynamic software (*Metso Outotec HSC Chemistry Version 7*) and other known generic thiosulfate reactions. The plausible reaction mechanisms are presented here, along with their Gibbs Free Energies which indicate the feasibility of the forward reactions (Table 5-4).

Table 5-4: Reaction mechanisms of sodium thiosulfate in the aqueous phase with NO_2 and their associated Gibbs Free Energy values, based on thermodynamic modelling software (Metso Outotec HSC Chemistry Version 7).

No	Reaction	Gibbs Free Energy, ΔG (kJ/mol of reductant) (25°C)	(55°C)
1	$S_2O_3^{2-}(aq) + 8NO_2(g) + 10\ OH^-(aq) \rightarrow 8NO_2^-(aq) + 2SO_4^{2-} + 5H_2O$	-1,289.4	-1,278.7
2	$S_2O_3^{2-}(aq) + 2NO_2(g) + 2OH^-(aq) \rightarrow N_2(g) + 2SO_4^{2-} + 2H_2O$	-995.0	-988.2

3	$S_2O_3^{2-}(aq) + 4NO(g) + 2OH^-(aq) \rightarrow 2N_2(g) + 2SO_4^{2-} + 2H_2O$	-1,239.1	-1,227.2
4	$S_2O_3^{2-}(aq) + 2NO_2(g) + H_2O \rightarrow 2NO_2^-(aq) + H_2SO_4(aq) + S$	-110.7	-106.4
5	$S_2O_3^{2-}(aq) + 2H^+(aq) \rightarrow S + SO_2(g) + H_2O$	-18.6	-27.6
6	$S_2O_3^{2-}(aq) + O_2(g) + 2OH^-(aq) \rightarrow 2SO_3^{2-}(aq) + H_2O$	-377.0	-369.8
7	$S_2O_3^{2-}(aq) + 2O_2(g) + 2OH^-(aq) \rightarrow 2SO_4^{2-}(aq) + H_2O$	-892.6	-882.2

Similar to sulfite, reaction of nitrogen dioxide with thiosulfate is a competition between the formation of nitrites and nitrogen gas, as shown here:

$$S_2O_3^{2-}(aq) + 8NO_2 + 10\ OH^-(aq) \rightarrow 8NO_2^-(aq) + 2SO_4^{2-} + 5H_2O \quad \ldots (5.6)$$

$$S_2O_3^{2-}(aq) + 2NO_2 + 2OH^-(aq) \rightarrow N_2(g) + 2SO_4^{2-} + H_2O \quad \ldots (5.7)$$

An alkaline aqueous condition is preferred for the reduction of nitrogen dioxide since the reaction consumes hydroxide ions (Equations 5.6 and 5.7). This is because under acidic conditions, the thiosulfate anion tends to dissociate to elemental sulfur and sulfur dioxide, which is undesirable due to unnecessary loss of the reductant and formation of precipitates:

$$S_2O_3^{2-}(aq) + 2NO_2(g) + H_2O \rightarrow 2NO_2^-(aq) + H_2SO_4(aq) + S \quad \ldots (5.8)$$

$$S_2O_3^{2-}(aq) + 2H^+(aq) \rightarrow S + SO_2(g) + H_2O \quad \ldots (5.9)$$

On top of the reactions mentioned above, thiosulfate may also have possibly reacted with NO to form N_2 via the following pathway shown here:

$$S_2O_3^{2-}(aq) + 4NO + 2OH^-(aq) \rightarrow 2N_2(g) + 2SO_4^{2-} + H_2O \quad \ldots (5.10)$$

Lastly, the possibility of thiosulfate breaking down to form sulfites and sulfates during reaction are proposed below:

$$S_2O_3^{2-}(aq) + O_2(g) + 2OH^-(aq) \rightarrow 2SO_3^{2-}(aq) + H_2O \quad \ldots (5.11)$$

$$S_2O_3^{2-}(aq) + 2O_2(g) + 2OH^-(aq) \rightarrow 2SO_4^{2-}(aq) + H_2O \quad \ldots (5.12)$$

5.3.3. Removal of NO_2 with variation of sodium thiosulfate concentration

In this section, sodium thiosulfate was selected as the main reducing agent for the removal of NO_2 using a counter current wet scrubbing with the experimental setup described in Figure 4-13. Its concentration was varied from 0.01 to 0.20 M and the experimental conditions can be found inTable 5-5, No. 1.

Table 5-5: A summary of experimental conditions for NO_2 removal carried out using the counter-current wet scrubber.
Liquid volume: 2.5 litres; liquid flowrate: 1.2 L/min; gas flowrate: 10 L/min; O_2: 14%; ambient temperature.

No	Scrubbing solution	Conc. (M)	Starting pH	Exhaust Gas Concentration			x_{NO2}*
				NO (ppmv)	NO_2 (ppmv)	NO_x (ppmv)	
1	Sodium thiosulfate ($Na_2S_2O_3$)	0.00 – 0.20	5.9 – 6.4	0	250	250	--
2	Sodium thiosulfate ($Na_2S_2O_3$)	0.05	6	250	0	250	0
3	Sodium thiosulfate ($Na_2S_2O_3$)	0.05	6	200	50	250	0.2
4	Sodium thiosulfate ($Na_2S_2O_3$)	0.05	6	150	100	250	0.4
5	Sodium thiosulfate ($Na_2S_2O_3$)	0.05	6	125	125	250	0.5
6	Sodium thiosulfate ($Na_2S_2O_3$)	0.05	6	100	150	250	0.6
7	Sodium thiosulfate ($Na_2S_2O_3$)	0.05	6	50	200	250	0.8
8	Sodium thiosulfate ($Na_2S_2O_3$)	0.05	6	0	250	250	1.0

** x_{NO2} refers to the mole fraction of NO_2, define as the mole of NO_2 divided by the total amount of NO_x (comprising of NO + NO_2).*

As can be seen from Figure 5-11, the NO_2 removal by various concentrations of sodium thiosulfate was quite stable, after an initial unsteady state period during the first minute of the reaction. This observed stability was quite consistent with the results seen using the gas bubbling reactor discussed in the previous section, comparing with sodium sulfite. As such, the average NO_2 removal values could be easily plotted vs. the concentration of the reducing agent on the *x*-axis (see Figure 5-12). It can be seen that NO_2 removal increased significantly as the sodium thiosulfate concentration progressively becomes higher, but this improvement slowed and eventually plateaued when the reducing agent concentration reached around 0.20M. This is further evidence that NO_2 can be effectively removed by sodium thiosulfate in a counter current wet scrubber setting on a closed loop liquid system.

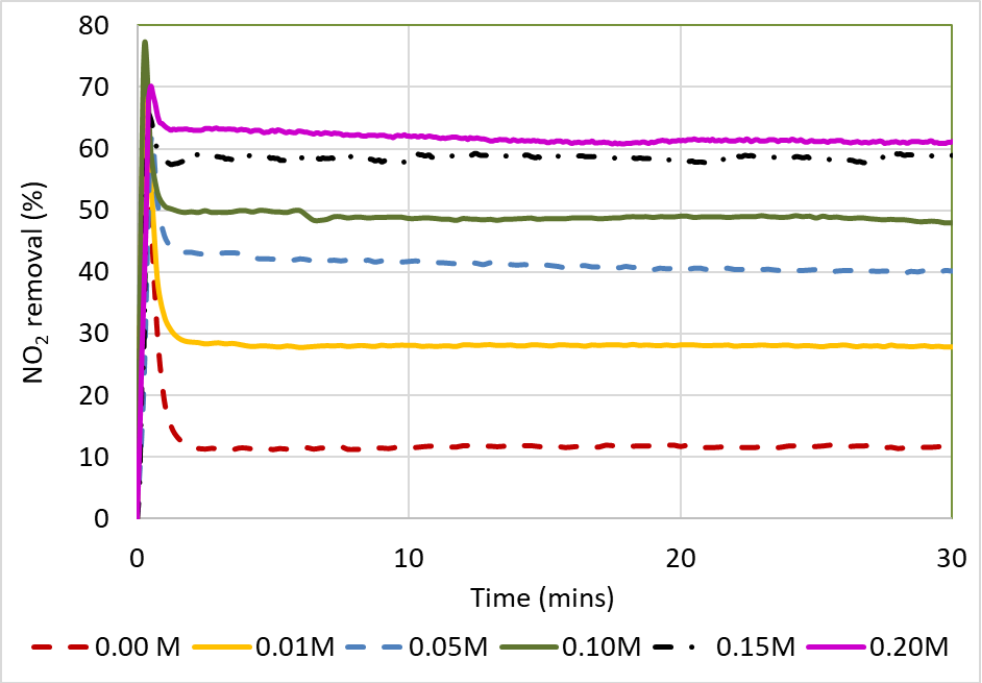

Figure 5-11: Removal of NO_2 with variation of sodium thiosulfate concentration using the counter-current wet scrubber,
Experimental conditions described in Table 5-5, No.1.

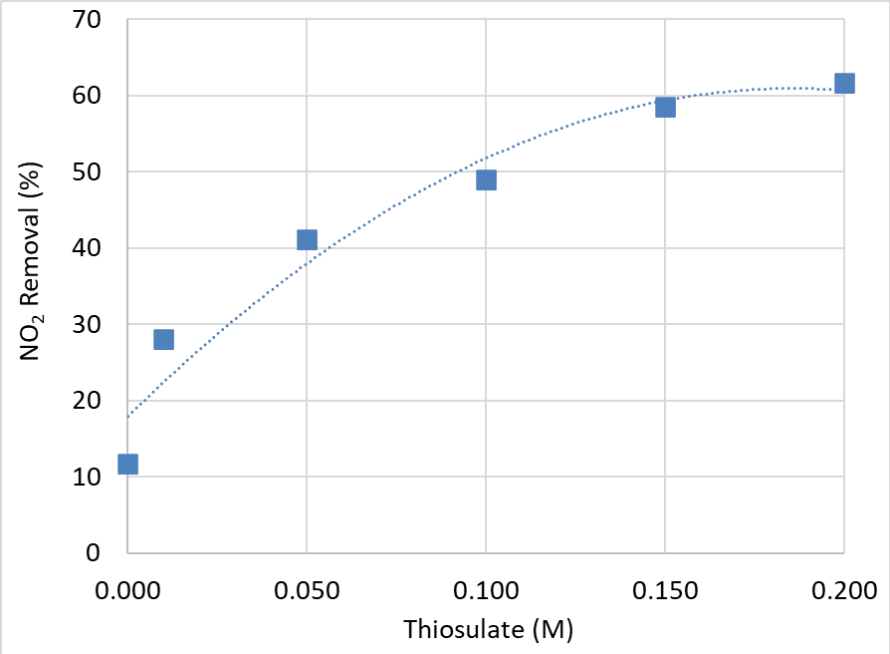

Figure 5-12: Removal of NO_2 with variation of sodium thiosulfate (average values without reaction time shown) using the counter current wet scrubber.
Experimental conditions shown in Table 5-5, No. 1.

The change of scrubbing liquid pH and ORP during the reaction can be seen in Figure 5-13 and Figure 5-14 respectively. It can be seen in Figure 5-13, that in the absence of sodium thiosulfate, the pH of the scrubbing liquid quickly dropped as the reaction progressed (from ~ 6.5 to 4.0).

This was to be expected as the absorption of the acidic NO_2 led to the formation of protons, as shown in Equations 4.7 and 4.8. However, in the presence of thiosulfate, the drop in pH during reaction was less. This buffering presence could have been provided by the decomposition of sodium thiosulfate according to the reaction shown in Equation 5.9, leading to the formation of sulfur precipitates. This decomposition was undesirable and should be avoided if thiosulfate is to be used as the reducing agent.

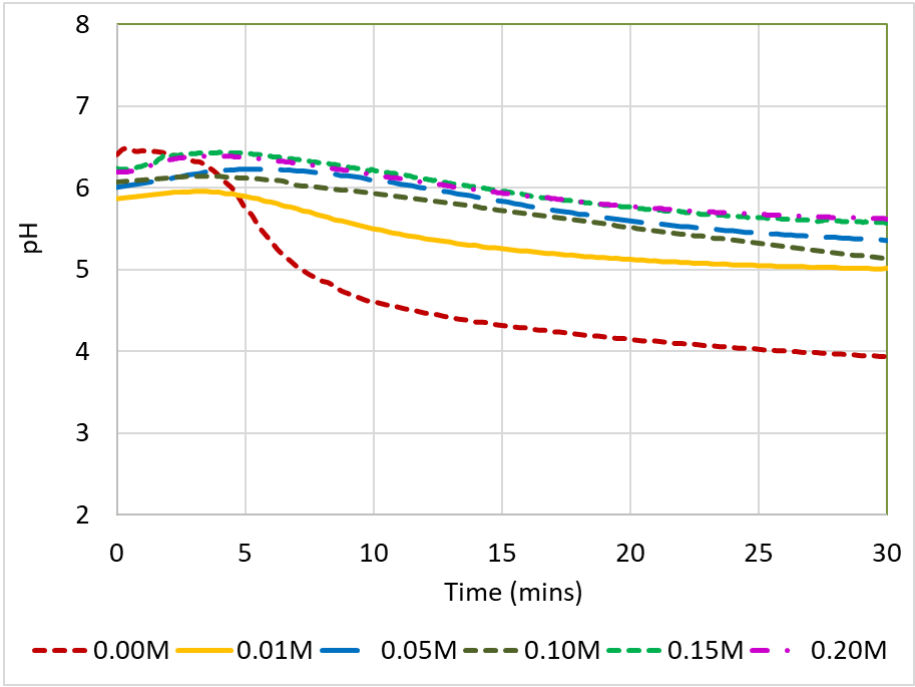

Figure 5-13: pH of scrubbing liquid used for NO_2 removal with variation of sodium thiosulfate using a counter-current wet scrubber.

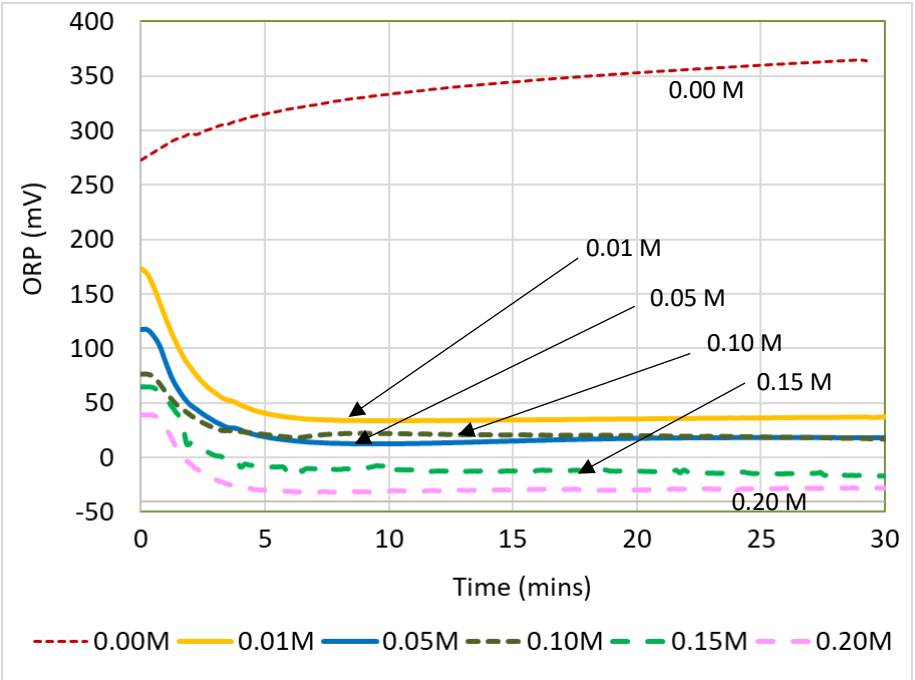

Figure 5-14: ORP of scrubbing liquid used for NO_2 removal with variation of sodium thiosulfate using a counter-current wet scrubber.

As for the redox potential of the scrubbing liquid during reaction (Figure 5-14), it can be seen that in the absence of sodium thiosulfate, the ORP increased as the reaction progressed. This was likely due to the increasing acidity of the aqueous phase from the absorption of NO_2. The redox potential of the scrubbing liquid decreased with increasing concentration of sodium thiosulfate, which was expected since it is a reducing agent.

5.3.4. Variation of NO to NO_2 ratio in the exhaust gas

In this study, the mole ratio of NO/NO_2 in the simulated exhaust gas was varied according to the experimental conditions described in Table 5-5, No. 2-8. The overall NO_x concentration, which was made up of NO and NO_2 gases, were kept at 250 ppm(v) for all runs. The overall NO_x removal with time is shown in Figure 5-15 and the legend shown at the bottom refers to x_{NO2}, the mole fraction of NO_2 gas. This is defined as the amount of NO_2 gas divided by the amount of NO_x (which is made up of NO and NO_2).

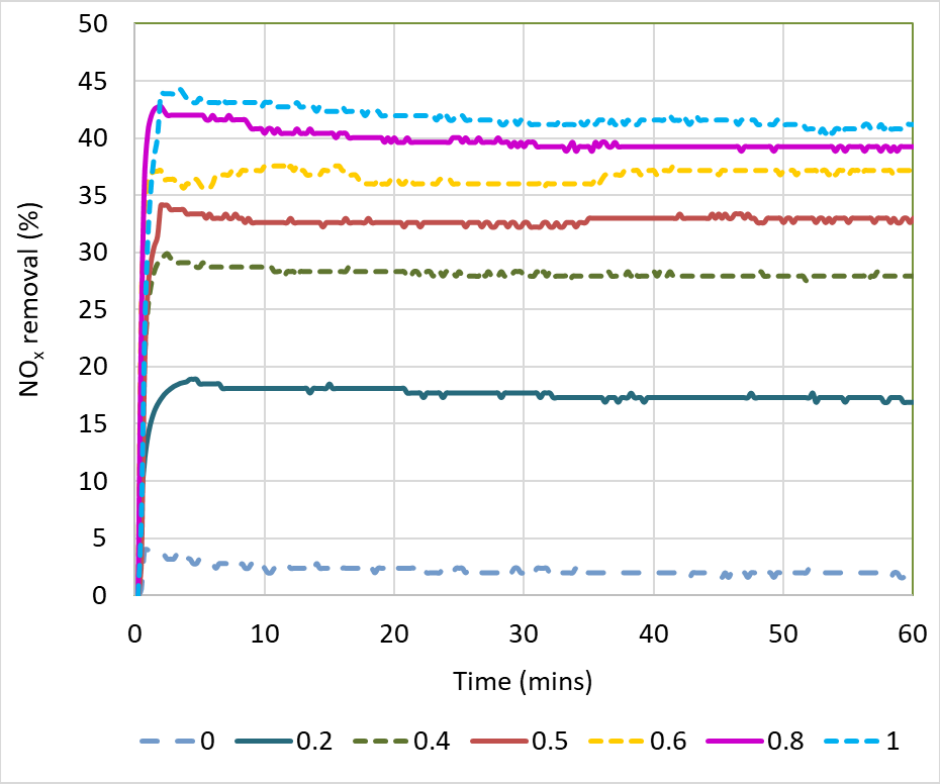

Figure 5-15: Removal of NO_x in the counter-current wet scrubber with variation of x_{NO2}, the mole fraction of NO_2.
Experimental conditions are shown in Table 5-5, No. 2-8.

When x_{NO2} was zero, the NO_x in the simulated exhaust gas was fully made up of NO gas. It was therefore unsurprising that NO_x removal was close to zero as it was discussed previously that sodium thiosulfate was not very effective in removing NO gas. This small removal of NO by thiosulfate could be in accordance with Equation 5.10. At the other end of the scale, when

x_{NO2} was 1.0, the NO_x in the simulated exhaust gas was fully made up of NO_2, and sodium thiosulfate was able to remove between 40 – 45% of it in the counter-current wet scrubber.

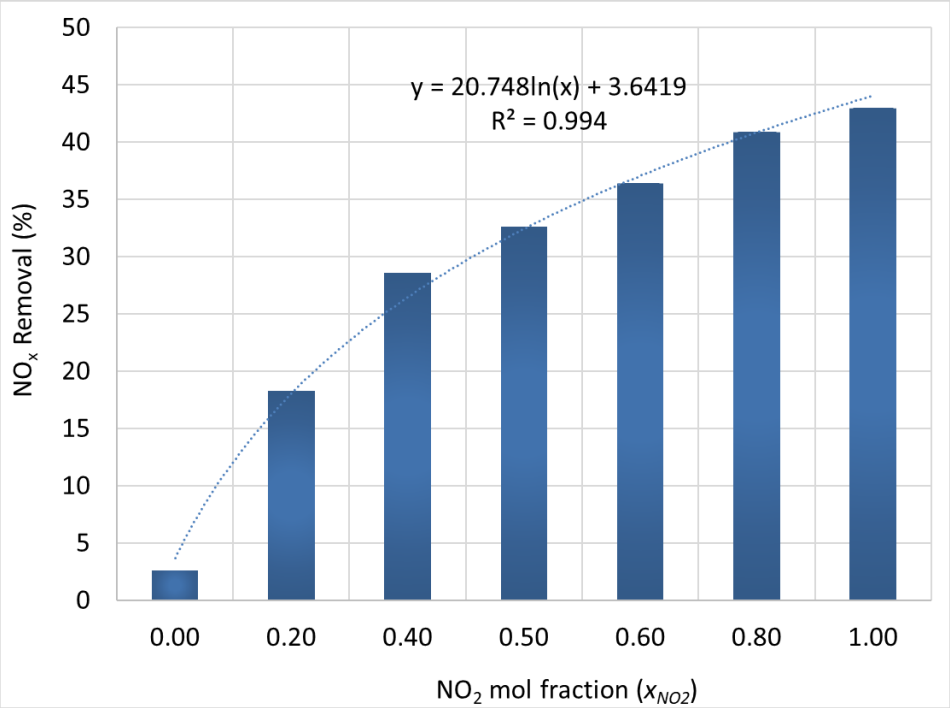

Figure 5-16: Overall NO_x removal with variation of x_{NO2}, the mole fraction of NO_2

The overall NO_x removal was stable for all runs during the duration of the experiment and their average removal values were plotted against x_{NO2}, the mole fraction of NO_2 (Figure 5-16). It can be seen from the figure that when the mole fraction of NO_2 increased from 0.0 to 0.20, the NO_x removal improved by about 16%. In the next increment of NO_2 mole fraction from 0.20 to 0.40, the NO_x removal improved only by a smaller amount, about 10%. The improvement seen in NO_x removal with increasing NO_2 mole fraction continued to decrease before coming close to a plateau when the mole fraction of NO_2 was at 1.0.

The NO_x removal with variation of the NO_2 mole fraction followed a logarithmic pattern as described in Equation 5.13, with a R^2 value of 0.99:

$$y = 20.748 ln x_{NO2} + 3.6419 \qquad \ldots (5.13)$$

Where:

y – removal of NO_x (%)

x_{NO2} – mole fraction of NO_2

This logarithmic function described above suggested that the presence of NO_2 gas had a positive effect on NO removal. This occurrence could have been possible as NO and NO_2 were able to react to form the higher valency N_2O_3 gas, which is slightly more soluble in water. In general, solubility of nitrogen in water increases with increasing nitrogen valency (Lin *et al.*, 2016). This could have resulted in more absorption of NO in the aqueous phase than it would otherwise have been (refer to Equations 4.9 and 4.11 described previously).

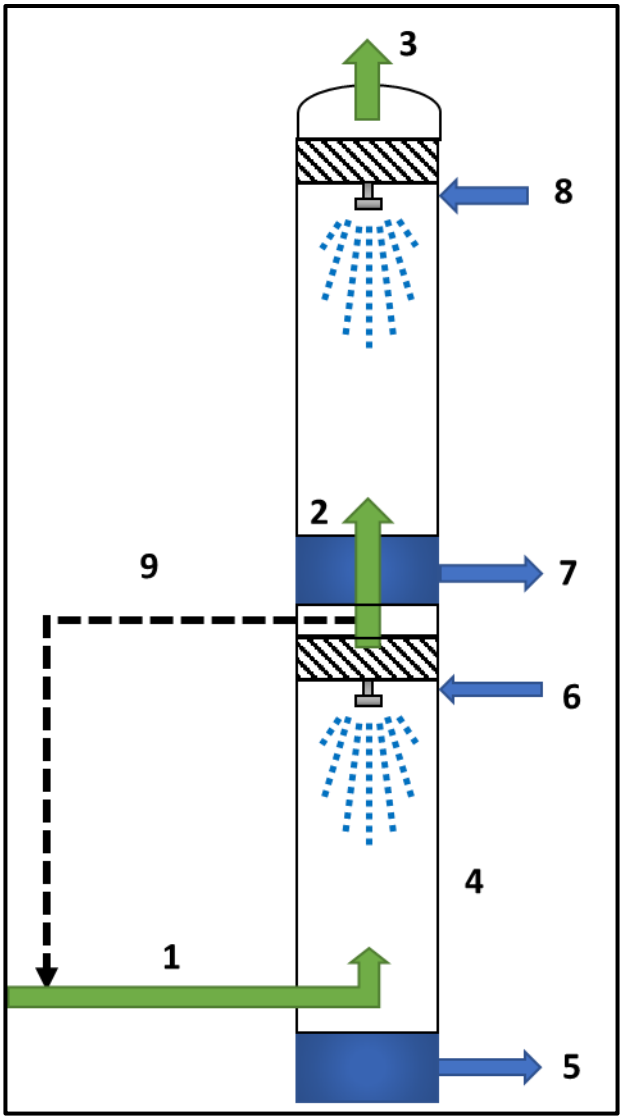

Figure 5-17: Possible conceptual design for a wet scrubber incorporating the partial recirculation of exhaust gas to increase NO removal. Bottom section of wet scrubber is oxidising while the top section is reducing. (1) exhaust gas inlet; (2) exhaust gas exiting bottom section of scrubber; (3) exhaust gas outlet; (4) wet scrubber; (5) Bottom section liquid outlet; (6) Bottom section liquid inlet; (7) Top section liquid outlet; (8) Top section liquid outlet; (9) exhaust gas recycling stream.

Although the reaction between NO and NO_2 to form N_2O_3 was only partial, given the short residence time in the wet scrubber, this positive effect on improving NO removal could be helpful in providing a boost if combined with a primary NO_x removal technology. One such manner this concept can possibly be applied is depicted in a wet scrubbing system shown in Figure 5-17. Here the wet scrubber is split into a bottom half consisting of an oxidising section and a top half consisting of a reducing section. As the exhaust from the oxidising section of the wet scrubber would be NO_2 rich, part of it can be recirculated back to the inlet in order to increase the NO_2 mole fraction in the exhaust gas composition and promote NO absorption.

This concept is not unlike the Exhaust Gas Recirculation (EGR) approach, except that in EGR, the exhaust gas is recirculated all the way back to the engine air intake instead of the inlet of the wet scrubber.

5.4. Summary

In this chapter, it was shown that the presence of CO_2 in the exhaust gas has a positive effect on NO_x removal if the pH of the aqueous solution is in the alkaline range. This was because the absorption of CO_2 decreased the pH and promoted the conversion of the chlorite oxidant into ClO_2, its more powerful variant. However, this may not always be advantageous as the latter is also more volatile and may result in a higher loss of reactant. If the wet scrubber needs to be operated in the alkaline range, alkaline chemicals such as NaOH will have to be dosed continuously at a higher rate to counter the acidification caused by the absorption of CO_2, on top of the acidification caused by SO_2 and NO. If the wet scrubber is operated in the acidic pH range, then the presence of CO_2 in the exhaust gas will have no effect on SO_2 and NO removal, since CO_2 does not appear to interact with the aqueous phase at all below pH 7. As for the removal of SO_2, the acidification caused by CO_2 absorption seem to have very little effect based on the conditions of this study, owing to the high solubility of SO_2 in water.

The usage of a reducing agent to improve the removal of NO_2 that was formed from the oxidation of NO was explored and it was shown that both sodium sulfite and sodium thiosulfate were effective in this. Among these two reducing agents, sodium sulfite was more effective in reducing NO_2 but it was less stable and likely decomposed in the presence of oxygen. Addition of alkalinity help to improve the effectiveness of sodium thiosulfate. Combining sodium sulfite and sodium thiosulfate at a 1:1 ratio plus sodium hydroxide showed some improvement in sodium sulfite stability. The reaction mechanisms for the reaction between sodium thiosulfate with NO and NO_2 were proposed based on experimental observations and thermodynamic calculations.

The relationship between sodium thiosulfate concentration and NO_2 removal in the counter-current wet scrubber was determined – increase of thiosulfate concentration also improved its removal before a plateau was reached. By varying the NO and NO_2 ratio in the simulated exhaust gas, it was demonstrated that the presence of NO_2 promoted the removal of NO gas by the thiosulfate reducing agent. This occurrence could have been possible as NO and NO_2 are able to react to form the higher valency N_2O_3 gas, which is slightly more soluble in water.

Chapter 6. Wet scrubbing with oxidation and reduction in series

In the work presented here, a novel wet scrubber comprising of an oxidation and a reducing section arranged in series was used for the removal of SO_2 and NO_x from simulated ship emissions. In the oxidizing section, sodium chlorite was used as it was previously shown to be very effective compared to many of the oxidants studied so far, as shown in Chapter 4. In the reducing section, both sodium sulfite (Na_2S0_3) and sodium thiosulfate ($Na_2S_2O_3$), which were explored and found to be suitable in Chapter 5, were utilized. Sodium thiosulfate, which is also a well-known reducing agent, has so far only been used as an additive to slow down the decomposition of sodium sulfite (Gan *et al.*, 2021; Li *et al.*, 2022; Schmid *et al.*, 2022). Rarely any attention has been given so far in its utilisation as the main reductant for NO_2. This is partly because it has been dismissed as being inferior to Na_2S and Na_2SO_3 for having lower reaction rates with NO_2 (Shen and Rochelle, 1998; Lee *et al.*, 2022). It will be shown in this study that sodium thiosulfate can be an effective reducing agent for the removal of NO_2, is comparable or superior to sodium sulfite in some aspects and is worthy of further developmental work.

6.1. Experimental procedure

A schematic diagram for the experimental setup is shown in Figure 6-1 and Figure 6-2. Two schematic representations are shown to reflect the two different configurations used in this study. Unless otherwise indicated, the simulated flue gas composition used is a representative of the typical flue gas conditions for large 2-stroke marine diesel engines, shown in Table 6-1.

Table 6-1: The composition of the simulated exhaust gas used in this study, unless otherwise indicated
Source: (EGCSA Handbook 2012: A practical guide to exhaust gas cleaning systems for the maritime industry, 2012).

Gas Type	**Concentration**
Sulfur dioxide, SO_2	500 ppm(v)
Nitric oxide, NO	900 ppm(v)
Carbon dioxide, CO_2	4%
Oxygen, O_2	14%
Nitrogen, N_2	Balance

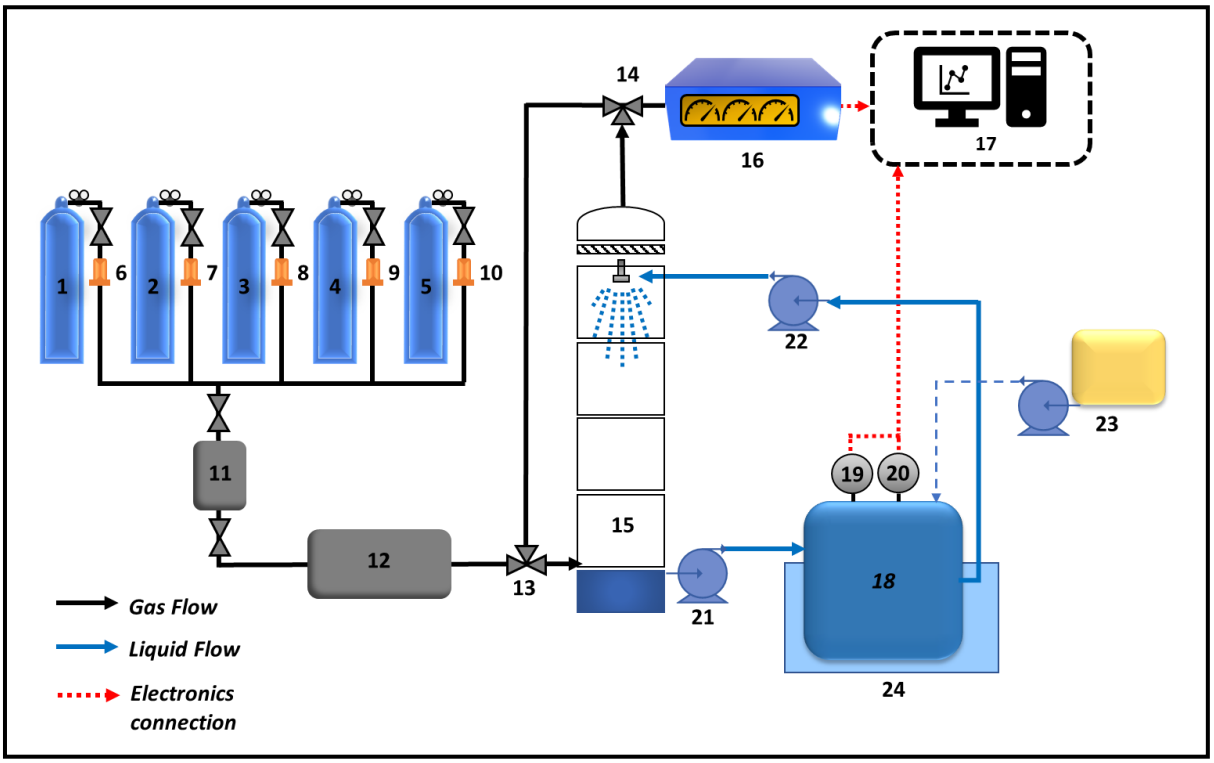

Figure 6-1: Schematic diagram for Configuration 1:
(1 – 5) Gas cylinders; (6 – 10) mass flow controllers; (11) gas mixer; (12) gas heater; (13 – 14) three way valves; (15) wet scrubber (height either 300 or 600mm); (16) flue gas analyzer; (17) computer (18) scrubbing liquid tank; (19) pH meter; (20) ORP meter; (21 – 22) peristaltic pumps for liquid in and out of scrubber; (23) peristaltic pump for alkaline dosing.

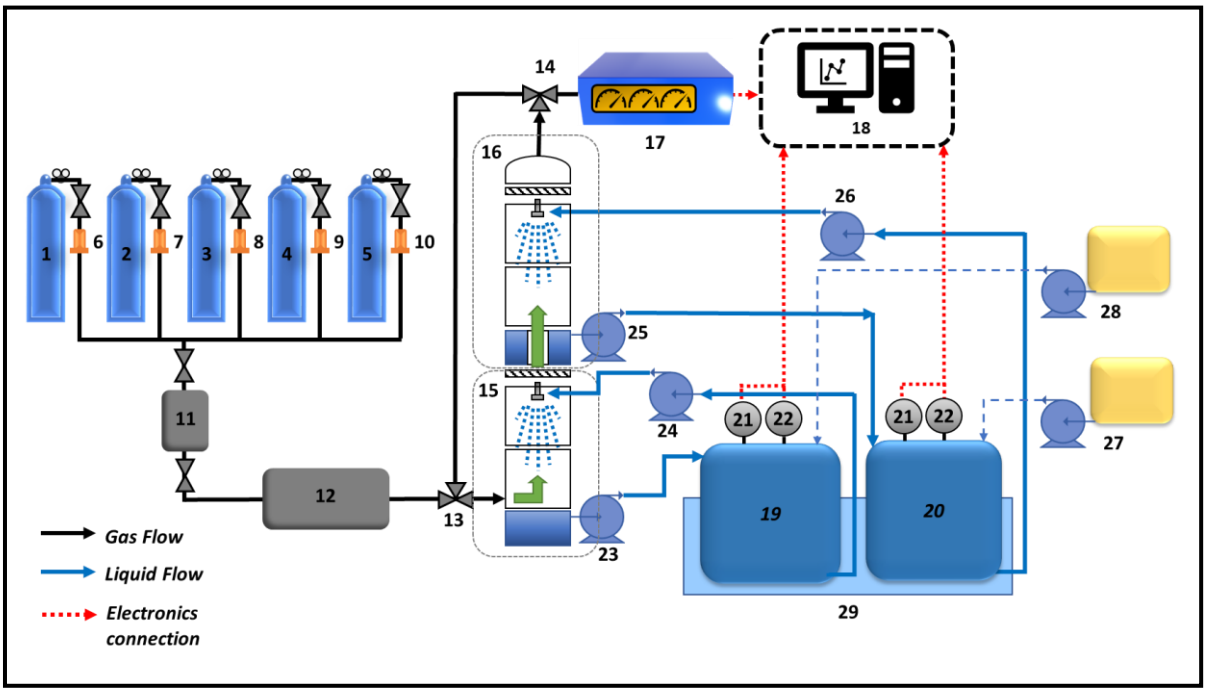

Figure 6-2: Schematic diagram for Configuration 2:
(1 – 5) Gas cylinders; (6 – 10) mass flow controllers; (11) gas mixer; (12) gas heater; (13 – 14) three way valves; (15) wet scrubber (oxidation half, 300mm); (16) wet scrubber (reducing half, 300mm); (17) flue gas analyzer; (18) computer; (19) scrubbing liquid tank for oxidation section of wet scrubber; (20) scrubbing liquid tank for reducing section of wet scrubber; (21) pH meters; (22) ORP meters; (23 – 24) peristaltic pumps for liquid in and out of oxidation half of scrubber; (25 – 26) peristaltic pumps for liquid in and out of reducing half of scrubber; (27 – 28) peristaltic pumps for alkaline dosing.

In general, all equipment used in these two configurations have already been described in Chapter 3 under Section 3.2. For the counter-current wet scrubber, the optimal full height required 4 of such modules, giving its reaction zone a height of 600 mm. Following from that, a half-height scrubber has two modules, giving its reaction zone a height of 300 mm. For brevity, the height of reaction zone will simply be referred to as 'scrubber height'. Unless otherwise indicated, all experiments were conducted using the spray chamber configuration, where the nozzles used was the Promax Quick Fulljet from Spray Systems Co., with the QPHA-1 for 0.38 L/min and QPHA-2 for 0.76 L/min. For the packed column configuration, the reaction zone of the wet scrubber was packed with 16 mm diameter polypropylene Pall Rings.

Before going into the wet scrubber, the simulated exhaust gas was channelled by a three-way ball valve into a flue gas analyser so that its composition could be measured. For background measurement, the simulated flue gas was channelled into the empty scrubber (without any liquid) and its composition measured at the exit. The MGA Luxx flue gas analyser was used for all gaseous measurements. All pH adjustments were carried out by dosing NaOH (1M) with a peristaltic pump using manual adjustment.

The study conducted here was arranged into 4 different areas consisting of two separate configurations:

i) Reaction in the oxidation half

In this section, the oxidant, sodium chlorite, was used to scrub the simulated exhaust gas using the Configuration 1 setup shown in Figure 6-1 with the scrubber height halved to 300 mm. The flue gas composition used is according to Table 6-1. Here, the NO in the gas would mostly be converted to NO_2 by the oxidant and then partially absorbed.

ii) Reaction in the reducing half

In this section, the reducing agent (mainly sodium thiosulfate), was used to scrub the simulated exhaust gas (NO: 200 ppmv, NO_2: 400 ppmv, CO_2: 4%, O_2: 14%, balance N_2) using the Configuration 1 setup shown in Figure 6-1 with the scrubber height halved to 300mm. Since the reducing reaction was meant to take place after the oxidation stage and mainly for the purpose of NO_2 removal, the simulated exhaust gas composition was adjusted to include more NO_2 and without SO_2. The simulated exhaust gas concentration here was chosen to reflect the typical concentration range seen exiting from the oxidation half.

iii) Reaction in a full height wet scrubber with oxidation only

In this section, the oxidant, sodium chlorite, was used to scrub the simulated exhaust gas using the Configuration 1 setup shown in Figure 6-1 with the wet scrubber at the full height of 600 mm. The flue gas composition used is according to Table 6-1. This was carried out in order to provide a simple basis of comparison with the scrubbing system comprising of an oxidation and reduction sections arranged in series.

iv) Reaction in a full height wet scrubber with oxidation and reduction in series

Here, the simulated flue gas shown in Table 6-1 was scrubbed using an oxidation stage followed by the reduction stage, with each stage comprising of a 300 mm height scrubber, therefore making the total scrubber height equivalent to a full height wet scrubber at 600 mm. Since two separate scrubbing liquids required two separate liquid tanks and additional peristaltic pumps and probes, the configuration was altered to Configuration 2 shown in Figure 6-2. A summary of experimental details can be found in Table 6-2.

Table 6-2: A summary of the experimental parameters used in this study. Unless otherwise indicated, the duration for all experimental runs in this study was 30 minutes.

Set No.	Scrubber Config.	Oxidation						Reduction						Total Scb. Ht. (m)	Total gas flow rate (L/min)	Total Liquid flow rate (L/min)	*L/G* Ratio (L/m^3)	Temp. (°C)
		Type	Conctn. (M)	pH	Liq. vol. (L)	Liq. flow rate (ml/min)	Scb. Section	Type	Conctn. (M)	pH	Liq. vol. (L)	Liq. flow rate (ml/min)	Scb. Section					
1	Config.1	$NaClO_2$	0.01	4-10	3.0	0.38	2	--	--	--	--	--	--	0.30	20	0.38	19	RT
2	Config.1	$NaClO_2$	0.005-0.03	10	3.0	0.38	2	--	--	--	--	--	--	0.30	20	0.38	19	RT
3	Config.1	--	--	--	--	--	--	$Na_2S_2O_3$	0.01-0.15	6	3.0	0.38	2	0.30	20	0.38	19	RT
4	Config.1	--	--	--	--	--	--	$Na_2S_2O_3$	0.05	4-12	3.0	0.38	2	0.30	20	0.38	19	RT
5	Config.1	--	--	--	--	--	--	Na_2SO_3	0.05	12	3.0	0.38	2	0.30	20	0.38	19	RT
6	Config.1	--	--	--	--	--	--	$Na_2S_2O_3$*	0.05	12	3.0	0.38	2	0.30	20	0.38	19	RT
7	Config.1	$NaClO_2$	0.02	10	6.0	0.76	4	--	--	--	--	--	--	0.60	10-50	0.76	15.2 – 76	RT
8	Config.2	$NaClO_2$	0.02	10	3.0	0.38	2	$Na_2S_2O_3$	0.05	12	3.0	0.38	2	0.60	10-50	0.76	15.2 – 76	RT
9	Config.2	$NaClO_2$	0.02-0.06	10	3.0	0.38	2	$Na_2S_2O_3$*	0.05	12	3.0	0.38	2	0.60	50	0.76	15.2	RT
10	Config.1	$NaClO_2$	0.02	10	3	0.38	2	--	--	--	--	--	--	0.30	20	0.38	19	25-55
11	Config.1	--	--	--	--	--	--	$Na_2S_2O_3$	0.05	12	3.0	0.38	2	0.30	20	0.38	19	25-55
12	Config.2	$NaClO_2$	0.02	10	3.0	0.38	2	$Na_2S_2O_3$	0.05	12	3.0	0.38	2	0.60	50	0.76	15.2	25, 55

** Packed scrubber configuration*

6.2. Thermodynamic Analysis

Before considering the experimental data obtained from this study, a thermodynamic analysis was first conducted for the chemical compounds that were present in the wet scrubbing gas-liquid system. The thermodynamic calculations and models here were built using the Metso Outotec HSC Chemistry version 7 software. Prior to this chapter, this software was also used to predict the viability of some of the many chemical reactions going on in the wet scrubber system on an individual basis. In this section, the thermodynamic models created applies to the whole system instead of individual chemical reactions. Two functions of the software used in the analysis here are the *Eh-pH* function and the *Equilibrium Compositions* function.

As seen from the experimental results so far, the wet scrubber is a complicated multiphase and multicomponent system and the availability of this powerful software allowed important predictions to be made in a complex system and enabled theoretical boundaries to be known. Nevertheless, the thermodynamic results presented here were interpreted with caution since reaction kinetics and mass transfer limitations also play a large role in determining whether a predicted reaction will actually take place.

6.2.1. Oxidation reduction potential versus pH diagrams

In this section, the thermodynamic software was used to create the redox potential (E_h) vs pH diagrams to help predict the outcomes of the various systems involved in the gas-liquid reactions in the wet scrubber. The Eh-pH Diagram function of the software was used to generate the redox potential vs pH diagrams for four main elements, namely, sulfur, nitrogen, carbon and chlorine. The first three elements were present in the system due to the presence of SO_2, NO_x and CO_2 in the exhaust gas while chlorine was present due to the usage of chlorine-based oxidising agents. The usage of sulfur-based reducing agents also contributed to the presence of sulfur. For the sake of simplicity, the four main elements of S, N, C and Cl present in the model were fixed at equal amounts of 1.0 kmol each. The individual species belonging to the four main elements that were selected to be present in the model can be seen in Table 6-3. In the E_h-pH diagrams shown from Figure 6-3 to Figure 6-10, the blue dotted lines represent the water stability limits. Beyond these limits, the water molecule is not stable and will either be oxidised into O_2 or reduced to H_2.

Table 6-3: Species included in the sulfur, nitrogen, carbon and chlorine systems used for the E_h-pH diagram model.

State	Sulfur	Nitrogen	Carbon	Chlorine
Gases	H_2S (g) SO_2 (g) SO_3 (g)	N_2 (g) N_2O (g) NO (g) NO_2 (g) NO_3 (g) N_2O_2 (g) N_2O_3 (g) N_2O_4 (g) N_2O_5 (g) NH_3 (g)	CO_2 (g)	Cl_2 (g) ClO_2 (g) Cl_2O_6 (g)
Aqueous Ions	HSO_3^- (aq) HSO_4^- (aq) HS^- (aq) SO_3^{2-} (aq) SO_4^{2-} (aq) S^{2-} (aq) $S_2O_3^{2-}$ (aq)	NO_2^- (aq) NO_3^- (aq) NH_4^+ (aq)	HCO_3^- (aq) CO_3^{2-} (aq)	Cl^- (aq) ClO^- (aq) ClO_2^- (aq) ClO_3^- (aq) ClO_2^+ (aq) ClO_4^- (aq)
Aqueous Neutrals	SO_2 (aq)		CO_2 (aq) H_2CO_3 (aq)	ClO_2 (aq) HOCl (aq)

6.2.2. Sulfur system

The sulfur system's redox potential vs pH diagram, shown in Figure 6-3, was important not only because of the presence of sulfur dioxide in the exhaust gas but also due to the usage of sulfur based reducing agents in the wet scrubbing process. The model showed that in an oxidative aqueous environment (E_h > 0V), the sulfur in the system will tend to form SO_4^{2-} ions, as expected. Under reducing conditions (E_h < 0V), care should be taken to avoid the acidic pH zone to prevent the formation of H_2S, preferable with the pH staying above 8.

From the diagram, it can also be seen that the precipitation of sulfur from the aqueous system can also happen under certain conditions. Under low E_h values, care should be taken to keep the pH high. Theoretically, the formation of sulfur precipitates can be avoided altogether above the pH of 8.4 no matter the ORP value. This model will be shown to be in agreement with experimental results discussed later in Section 6.4.2, where the turbidity of the aqueous solution decreased as the pH was increased due to less sulfur precipitation.

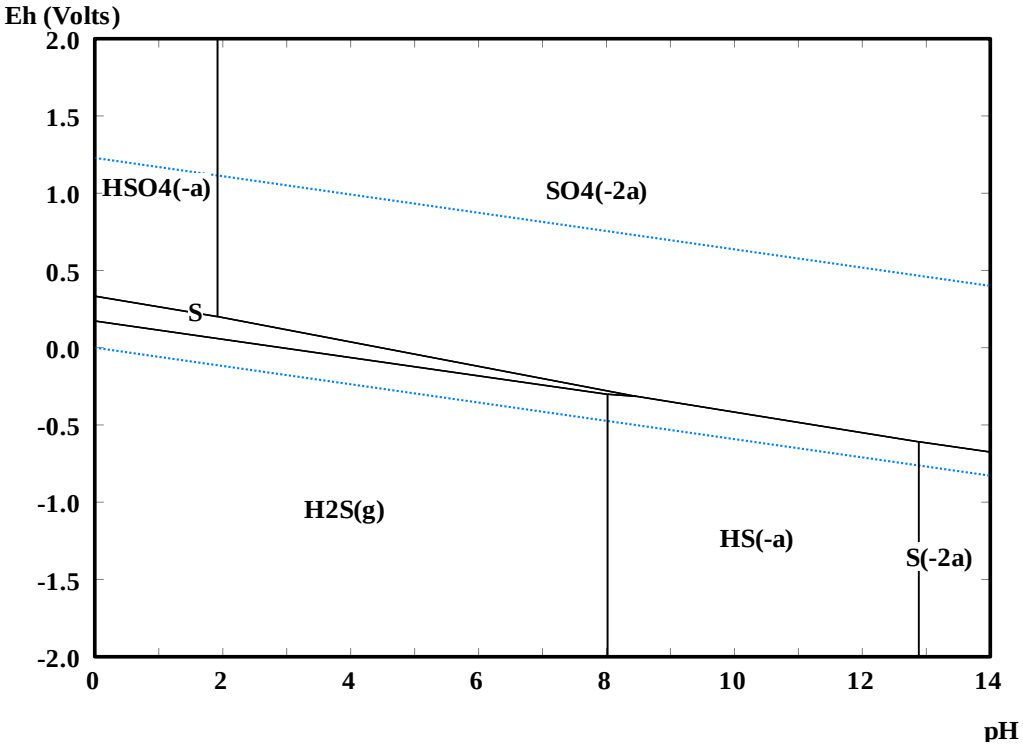

Figure 6-3: The E_h – pH diagram of the sulfur system at 25°C.

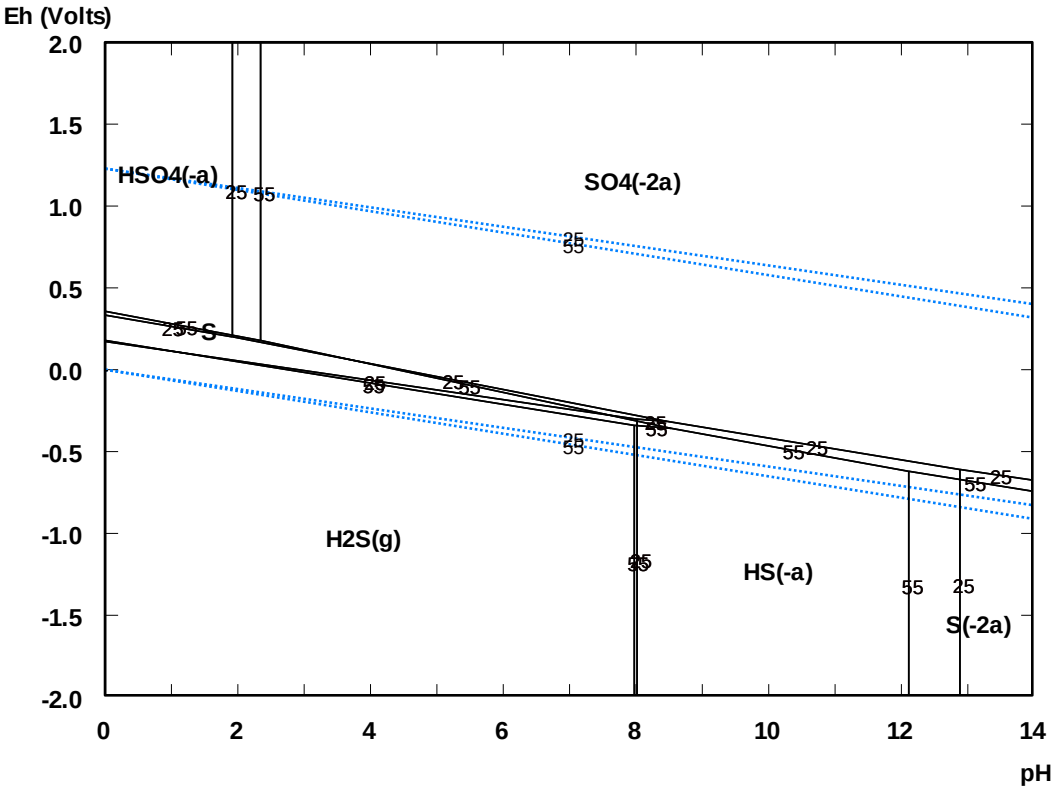

Figure 6-4: Comparison of the E_h – pH diagram of the sulfur system at 25°C and 55°C.

When the model was compared between 25°C and 55°C, it can be seen from Figure 6-4 that no significant changes occurred, especially in relation to the formation of H_2S and the avoidance of sulfur precipitation. The most significant change observed due to the difference in

temperature was in the boundary between HS^- and S^{2-} in the aqueous phase, which shifted from the pH of 13 to 12 in the negative redox potential zone.

6.2.3. Nitrogen system

The redox potential versus pH diagram for the Nitrogen system is shown in Figure 6-5. It can be seen that under high redox potential conditions, nitrogen tended to form nitrates in the aqueous phase while lower redox potential conditions would lead the formation of N_2 gas instead. In even lower redox potential environments, the nitrogen tended to form ammonium ions in the aqueous phase or ammonia in the gas phase. It could also be seen that both the NO_3^- – N_2 boundary and N_2 – Ammonia boundary were strongly influenced by pH.

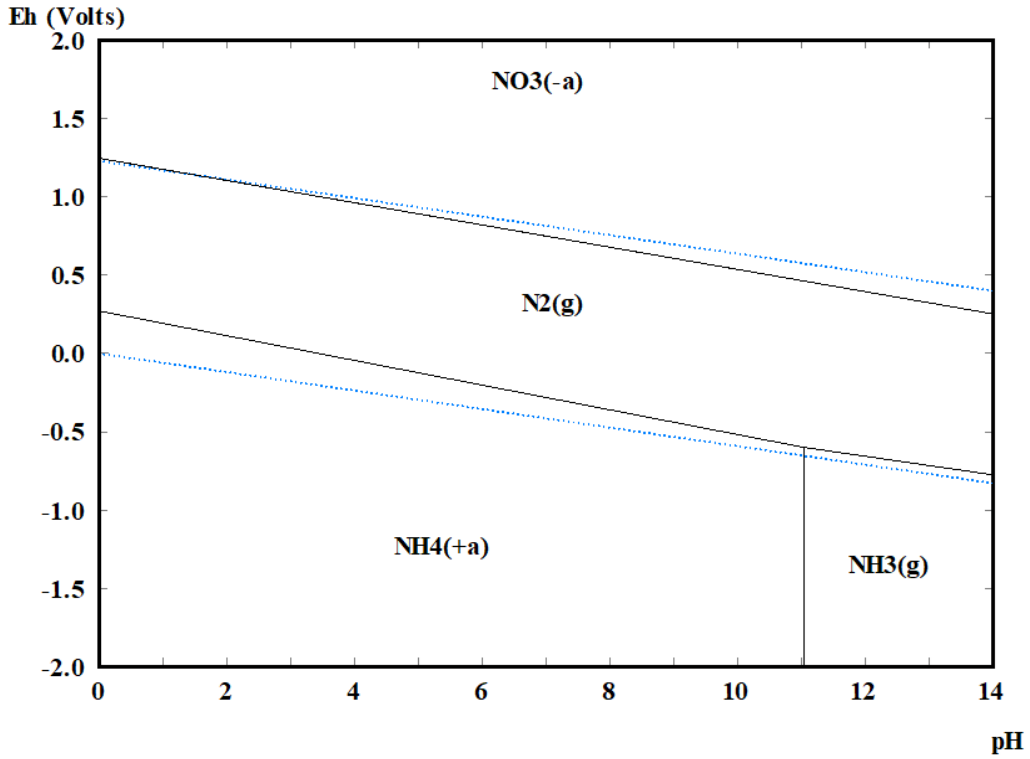

Figure 6-5: The E_h – pH diagram of the nitrogen system at 25°C.

For instance, an increase in pH in the system favoured the formation of nitrate ions instead of N_2 gas. This will be shown to be entirely consistent with the observed experimental data where increase in pH of the wet scrubber utilising a reducing agent resulted in higher total soluble nitrogen per mole of gaseous pollutant removed (Section 6.4.2, Figure 6-22). It should be noted that when the chlorite oxidant was used, this same trend will not be observed in the experimental results because the oxidative power of chlorite happened to be strongly dependent on pH as well – any pH increase would also reduce the system's redox potential and the tendency to form nitrates at the same time (to be discussed more thoroughly in Section 6.3.1, Figure 6-13).

Naturally, the pH of the aqueous scrubbing liquid should be kept low in order to favour N_2 gas and avoid the formation of soluble nitrogen for the reducing section of the wet scrubber. However, lowering the pH would also mean an increase in sulfur precipitates and the formation of toxic H_2S gas, as seen in the sulfur system previously. Therefore, a balance has to be struck in order to best meet these competing interests.

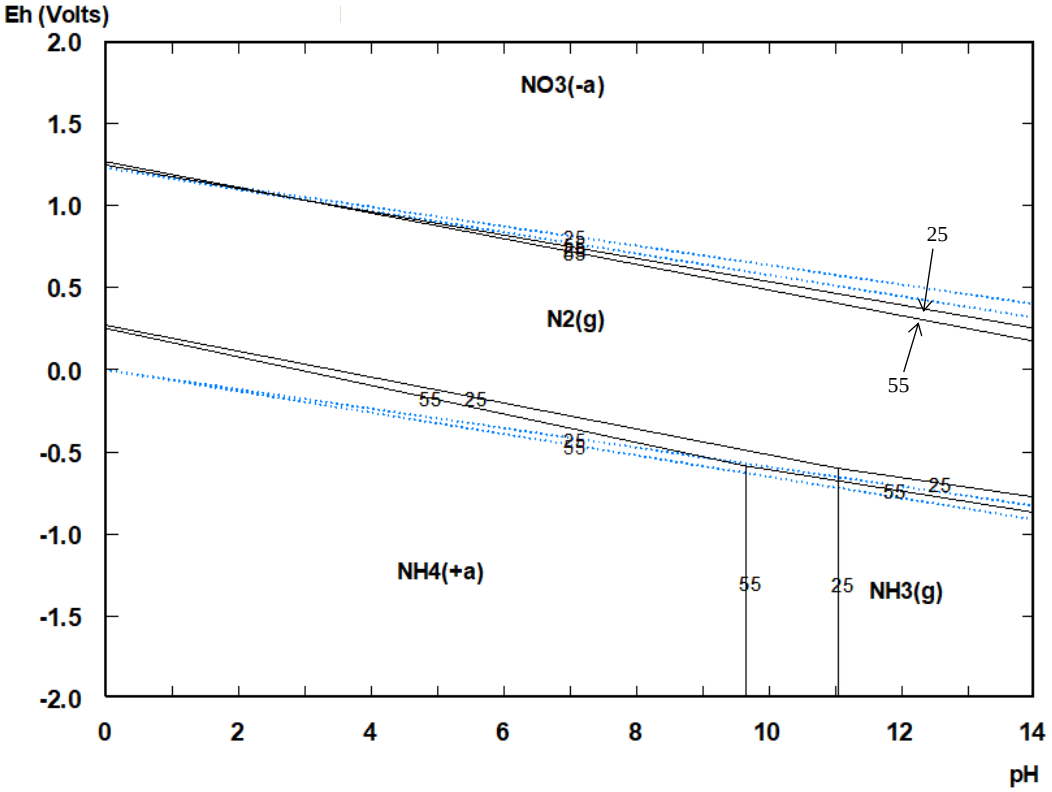

Figure 6-6: Comparison of the E_h – pH diagram of the nitrogen system at 25°C and 55°C.

When comparing the nitrogen system at different temperatures, it can be seen from Figure 6-6 that increasing the temperature from 25°C and 55°C shifted the boundaries of the stable N_2 gas region downwards on the redox potential scale. Although this shift was not large, it was more pronounced in the region of high pH. This showed that formation of nitrate was thermodynamically favoured over N_2 when temperature was increase in the high pH zone. This will be shown to be in agreement with the experimental results later when it was observed that the total soluble nitrogen formed in the aqueous phase increased in both the oxidation and reduction half of the wet scrubber when temperature was increased (Section 6.7). Apart from this, a difference was also observed between the ammonia – ammonium boundary, which shifted to a lower pH at 55°C.

6.2.4. Chlorine System

From the E_h-pH diagram of the chlorine system shown in Figure 6-7, it can be seen that chlorine had the tendency to exist as chloride ions in the aqueous phase when it is at equilibrium. Under very strong oxidative environment, the zone for ClO_3^- formation layed outside the stability region of the water molecule and is therefore unstable.

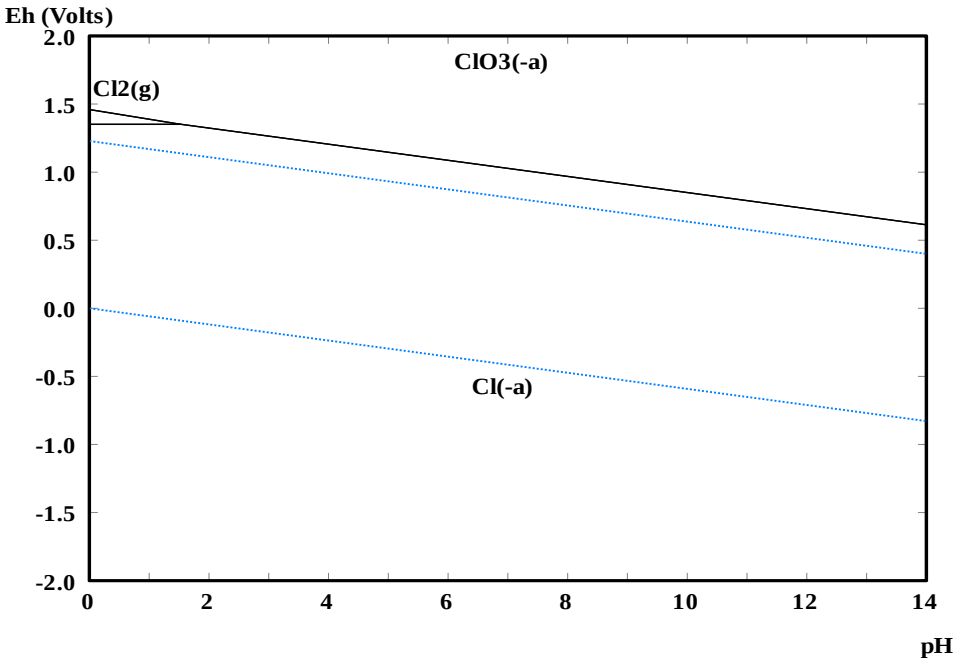

Figure 6-7: The E_h – pH diagram of the chlorine system at 25°C.

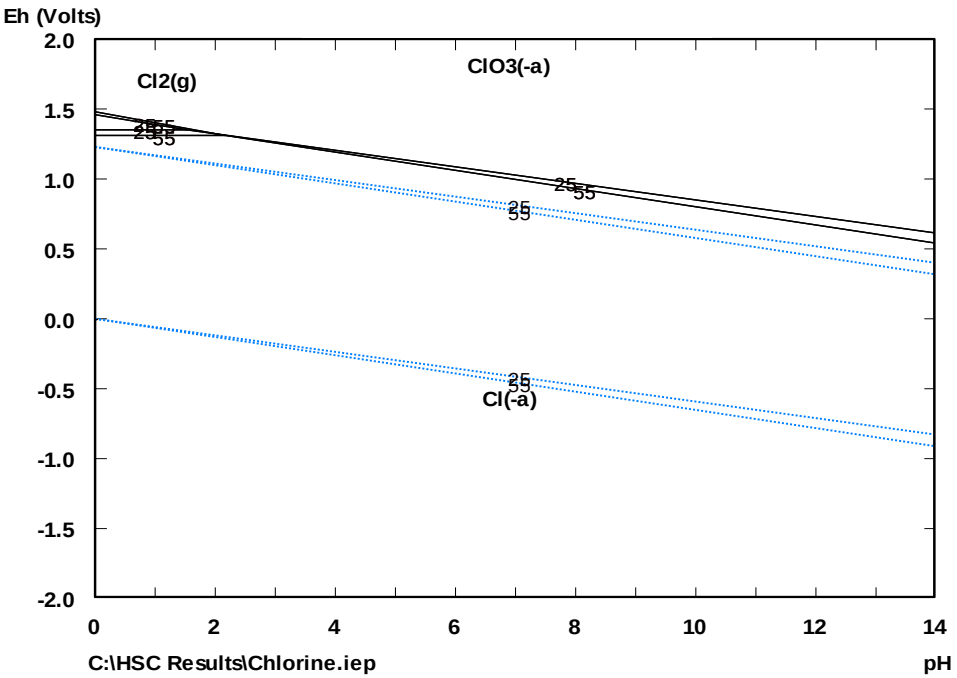

Figure 6-8: Comparison of the E_h – pH diagram of the chlorine system at 25°C and 55°C.

Formation of chlorine gas, which is poisonous and undesirable, would be unlikely as it can only occur under very acidic conditions (pH < 2) and would be unstable since it is outside the water stability region. Increase of temperature from 25°C to 55°C had minimal impact on the E_h-pH boundaries.

6.2.5. Carbon system

The E_h – pH diagram for the carbonate system is shown in Figure 6-9. It can be seen that the carbonic acid or CO_2 (aq) boundary with HCO_3^-, and the HCO_3^- – CO_3^{2-} boundaries occurred at pH 6.4 and 10.3 respectively, which was similar to the carbonic system represented in the Bjerrum plot format shown in Figure 5-3. Unlike the sulfur system, carbon is unlikely to precipitate out of the aqueous system as the C region lies outside the water stability limit. When the temperature was increased from 25°C to 55°C, the most significant change observed was the shifting of the CO_2 (aq) – HCO_3^- boundary from pH 6.4 to 7.2 (see Figure 6-10). This implied that at a higher temperature, a higher pH in the aqueous system was required in order to capture the carbon dioxide from the gas phase and convert it to its more stable bicarbonate or carbonate form in the aqueous phase.

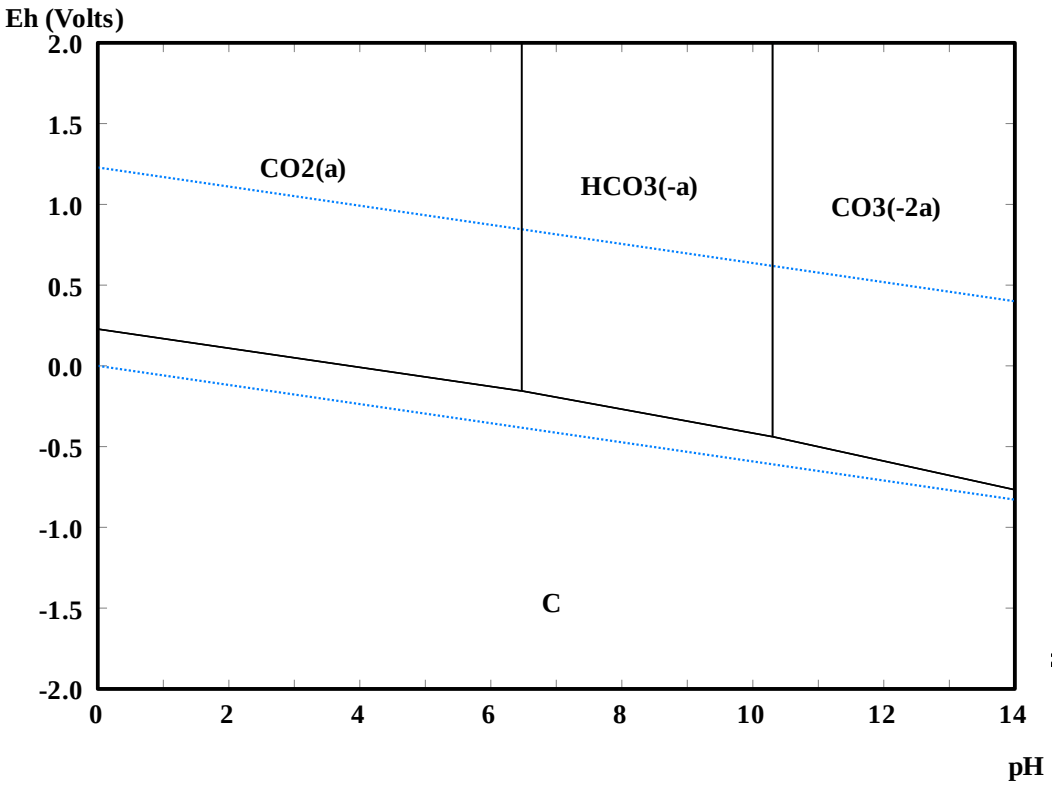

Figure 6-9: The E_h – pH diagram of the chlorine system at 25°C.

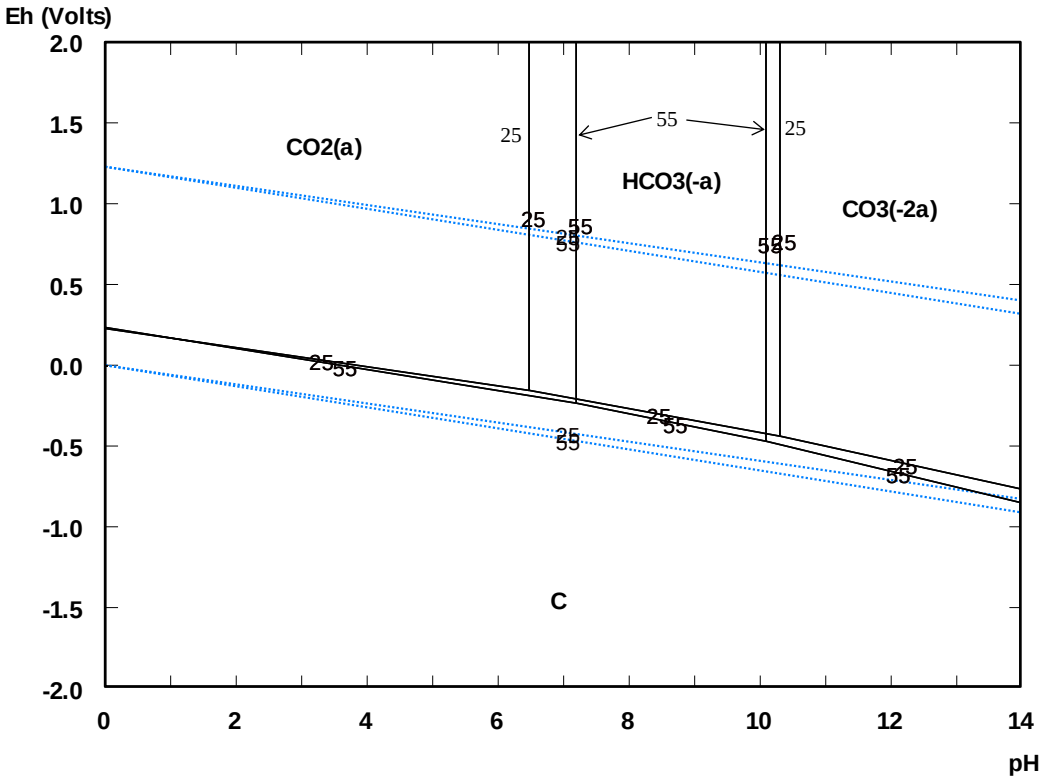

Figure 6-10: Comparison of the E_h – pH diagram of the chlorine system at 25°C and 55°C.

6.3. Oxidation in a half-height wet scrubber

In this section, the simulated exhaust gas was oxidized with sodium chlorite in a wet scrubber that had a height of 300 mm. This was half the height of the optimal scrubber design. The pH and concentrations of the oxidant were varied according to the conditions shown in Table 6-2 (Set 1 and 2).

6.3.1. Variation in pH

As can be seen from Figure 6-11, the removal of SO_2 was complete at >99% for all the pHs studied. Owing to high SO_2 solubility in the aqueous phase, its complete absorption in the wet scrubber was expected. Removal of NO (via oxidation to NO_2) by the sodium chlorite oxidant was pH dependent, with gradual increment with reducing pH. As the pH was reduced, the rate of chlorite anion decomposition to ClO_2 according to Equations 4.15 and 4.16 increased due to the increasing availability of protons. As ClO_2 has a stronger oxidation potential, the oxidation rate of NO to NO_2 would increase as well. This is consistent with the observations here.

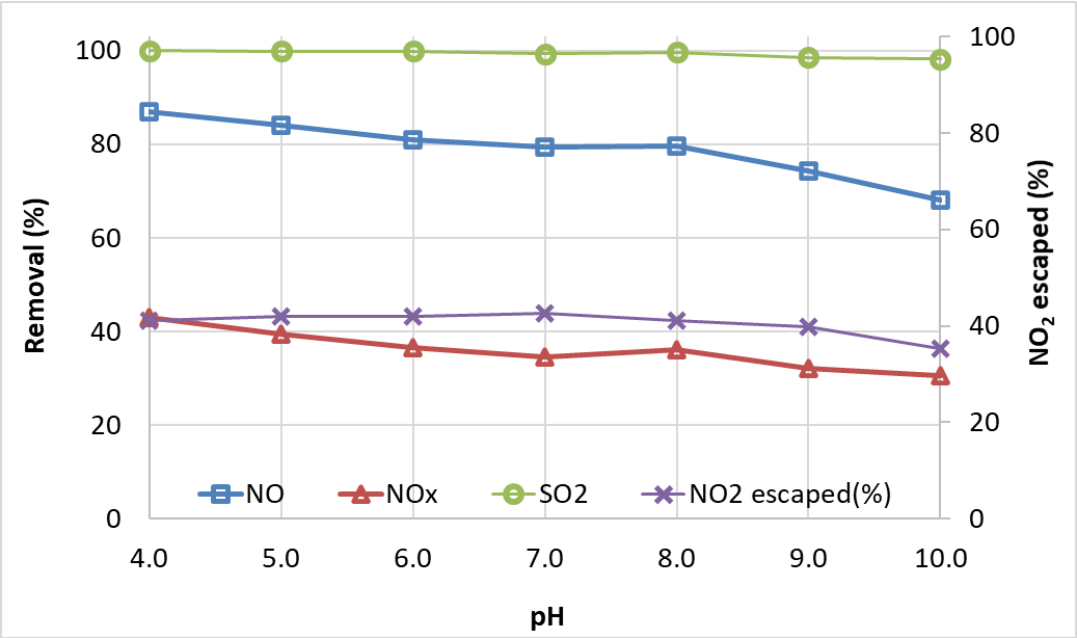

Figure 6-11: Removal of SO_2, NO, NO_x and the amount of N escaping the scrubber in the form of NO_2, with variation in the sodium chlorite oxidant pH in the oxidation half-height wet scrubber.
Experimental conditions described in Table 6-2 (Set 1).

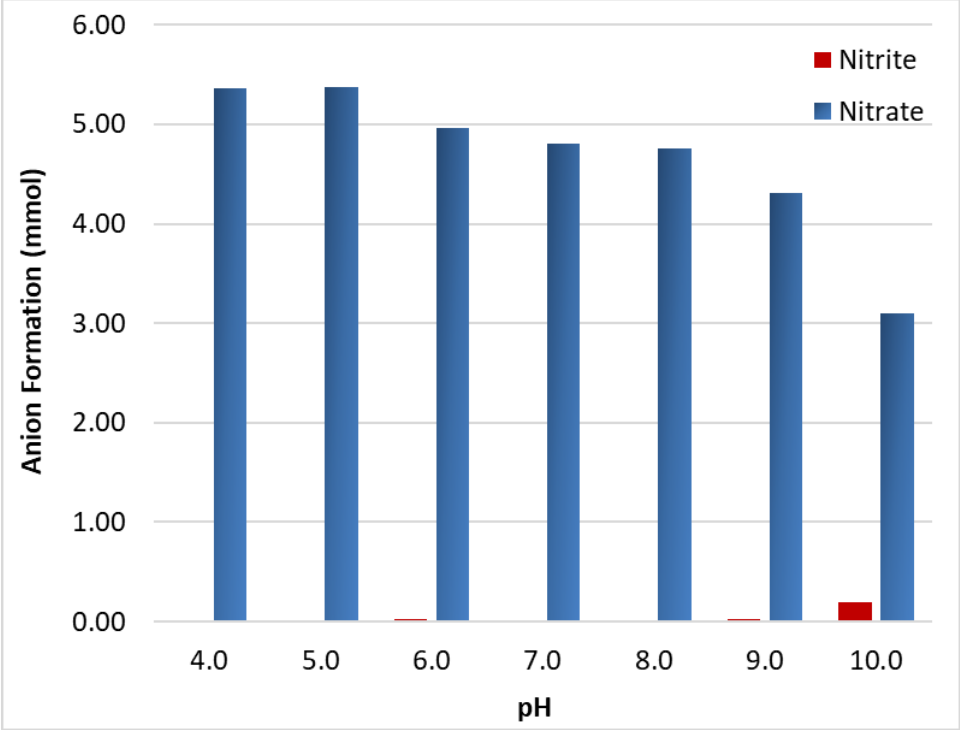

Figure 6-12: Formation of soluble nitrogen in the form of nitrites (NO_2^-) and nitrates (NO_3^-) in the aqueous scrubbing liquid of the oxidation half-height wet scrubber, with variation in pH.
Experimental conditions described in Table 6-2 (Set 1).

A significant amount of N escaped the wet scrubber in the form of NO_2. This was around 40% of the total NO in the inlet. The sodium chlorite oxidant was effective in oxidising NO to NO_2 but not very effective in absorbing the NO_2. From pH 4 to 7, the change in the amount of N escaping the scrubber in the form of NO_2 was insignificant and remained stable (with a fluctuation of less than 1.5%). However, there was a drop in this value as the pH was increased beyond pH 7. This was because less NO_2 was formed when the pH was increased. The overall NO_x removal by sodium chlorite slightly reduced with increasing pH, simply because more of it escaped the scrubber as NO without being oxidised to NO_2.

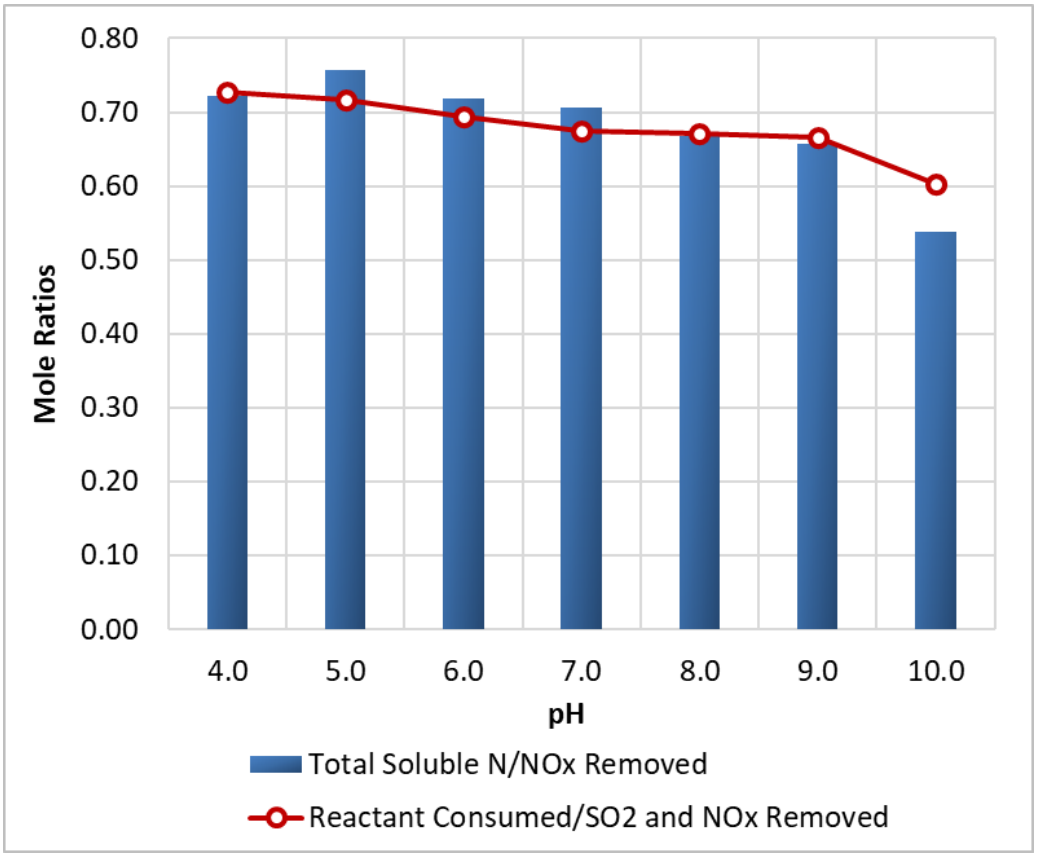

Figure 6-13: The mole ratios of soluble nitrogen formed over total NO_x removed, and reactant (chlorite) consumed over gaseous pollutant (SO_2 and NO_x) removed, as the pH of the chlorite oxidant was varied in the oxidation half-height wet scrubber.
Experimental conditions described in Table 6-2 (Set 1).

The results of the aqueous analysis of the scrubbing liquid with ion chromatography are shown in Figure 6-12 and Figure 6-13. It can be seen from Figure 6-12 that the absorption of N in the aqueous phase resulted in the formation of predominantly nitrate, while the presence of nitrite was only observed from pH 9 onwards. In Figure 6-13, it can be seen that the mole ratio of soluble nitrogen formed (consisting of nitrites and nitrates) over the total NO_x that was removed in the wet scrubbing process was dependent on pH, with its value generally decreasing with

increasing pH. As mentioned previously, this observation of decreasing nitrate formation with increasing pH was contradictory to the thermodynamic equilibrium model discussed previously in Section 6.2.3, which showed that increasing pH favoured the formation of nitrates. This was because sodium chlorite, which was the main oxidant in the system, also happened to be pH sensitive – any pH increase would also reduce the system's redox potential and the tendency to form nitrates according to the reactions shown in Equations 4.20 and 4.21. At pH 10, only 0.54 mole of soluble nitrogen was formed (mostly as nitrate) for every mole of N gas pollutant removed. For ocean discharge, low soluble nitrogen content is preferred as the presence of this nutrient in water bodies causes eutrophication (algae bloom).

In addition to lower soluble nitrogen formation, a higher pH also showed another advantage – as the pH of the scrubbing liquid was increased, less reactant was consumed for the removal of SO_2 and NO_x. As explained earlier, the higher the pH, the less decomposition of chlorite to the volatile chlorine dioxide. At pH 10, the removal of every mole of SO_2 and NO_x consumed 0.61 mole of chlorite anion. The choice of the operating pH therefore depends on whether emphasis is given to achieving a high NO oxidation rate versus achieving low soluble nitrogen formation and reactant consumption, since they are in competition with each other.

6.3.2. Variation of oxidant concentration

When the concentration of the $NaClO_2$ oxidant was increased from 0.005 to 0.030M, the absorption of SO_2 increased slightly from 96.2% at 0.005M and reaching 100% from 0.020M and beyond (see Figure 6-14). The presence of the oxidant likely helped the absorption of SO_2 by oxidising the sulfites and bisulfites formed to sulfates, as seen in Equations 4.4 and 4.5 and consistent with previous observations. The oxidation of NO to NO_2 also increased with increasing oxidant concentration, as expected. The amount of NO_x removed likewise also increased with increasing concentration. The amount of nitrogen escaping the wet scrubber in the form of NO_2 increased with increasing oxidant concentration. This was likely because at higher chlorite concentrations, more NO was oxidised to NO_2, and the aqueous phase had difficulty absorbing the latter.

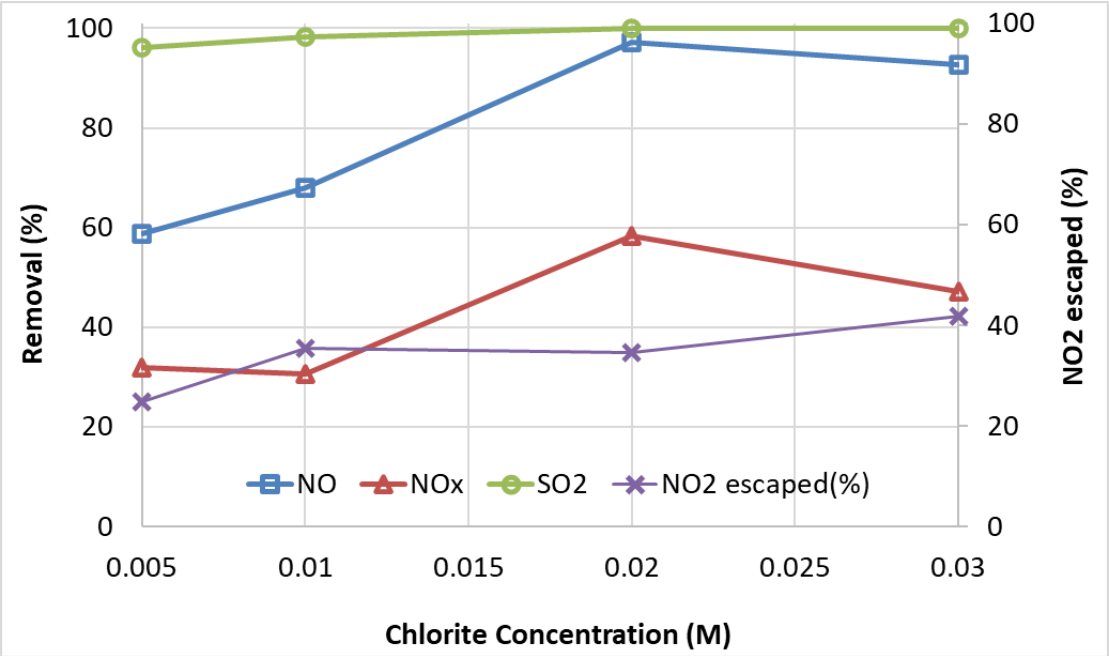

Figure 6-14: Removal of SO_2, NO, NO_x and the amount of N escaping the scrubber in the form of NO_2, with variation in the sodium chlorite oxidant concentration in the oxidation half-height wet scrubber.
Experimental conditions described in Table 6-2 (Set 2).

Referring to Figure 6-15, the increase of chlorite concentration from 0.005M to 0.030M slightly increased the ratio of soluble nitrogen formed per mole of NO_x removed, but this increase was not significant. However, the increase of reactant consumed per mole of gaseous pollutant was more significant, rising from 0.47 at 0.005M to 0.88 at 0.030M. This showed that achieving a higher reaction rate by using a higher oxidant concentration comes at the cost of a higher reactant utilisation rate. The chlorite concentration of 0.02M was chosen for subsequent experimental runs as a balance between achieving decent reaction rates while maintaining low reactant consumption rates. It was observed that the variation of reactant consumed per gaseous pollutant removed followed a quadratic trend in the range of chlorite concentration that was studied here, according to Equation 6.1.

$$y = -632.39[A]^2 + 38.54[A] + 0.29 \qquad \ldots (6.1)$$

Where:

y = mole ratio (chlorite reactant consumed per mole of gaseous pollutant removed)

$[A]$ = chlorite concentration, M

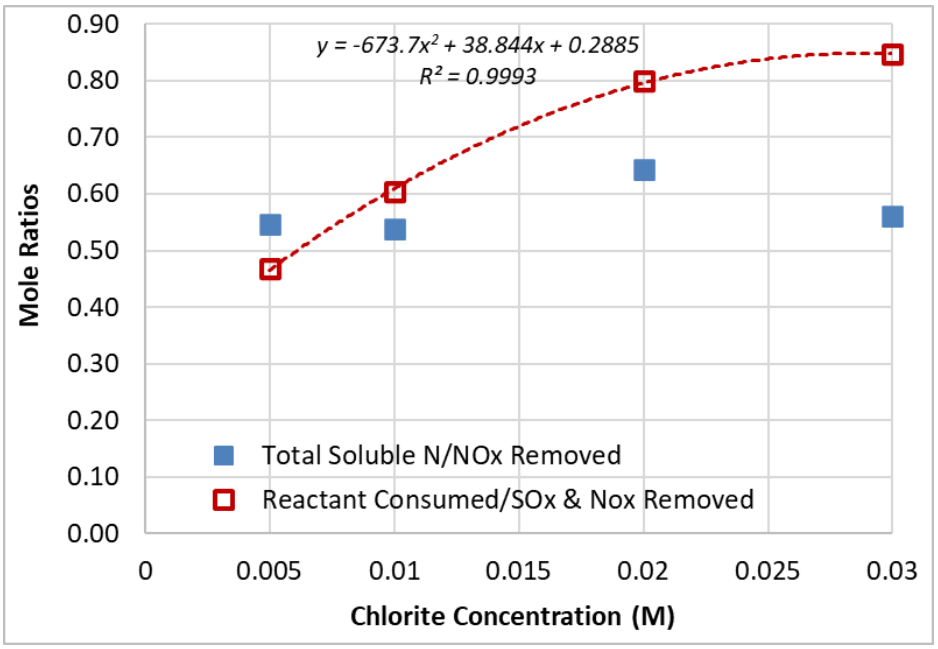

Figure 6-15: The mole ratios of soluble nitrogen formed over total NO_x removed, and reactant (chlorite) consumed over pollutant (SO_2 and NO_x) removed, as the concentration of the oxidant was varied in the oxidation half-height wet scrubber.
Experimental conditions described in Table 6-2 (Set 2).

6.3.3. Variation of oxidation reduction potential (ORP)

In general, the increase of redox potential of the scrubbing liquid corresponded with higher removal of SO_2, oxidation of NO to NO_2, overall removal of NO_x, and the amount of N escaping as NO_2 (see Figure 6-16). All these were consistent with the reasons described in the previous section. Of all the mentioned reactions, it could be clearly seen that the oxidation of NO to NO_2 was most affected by the change in oxidation potential values, judging by the gradient of the change – increasing the amount of NO being oxidised to NO_2 required the scrubbing liquid to have a stronger oxidation potential. The influence of oxidation potential for chlorite and also other common oxidants were discussed more thoroughly in a previous work in Section 4.2.3 (Chin *et al.*, 2022).

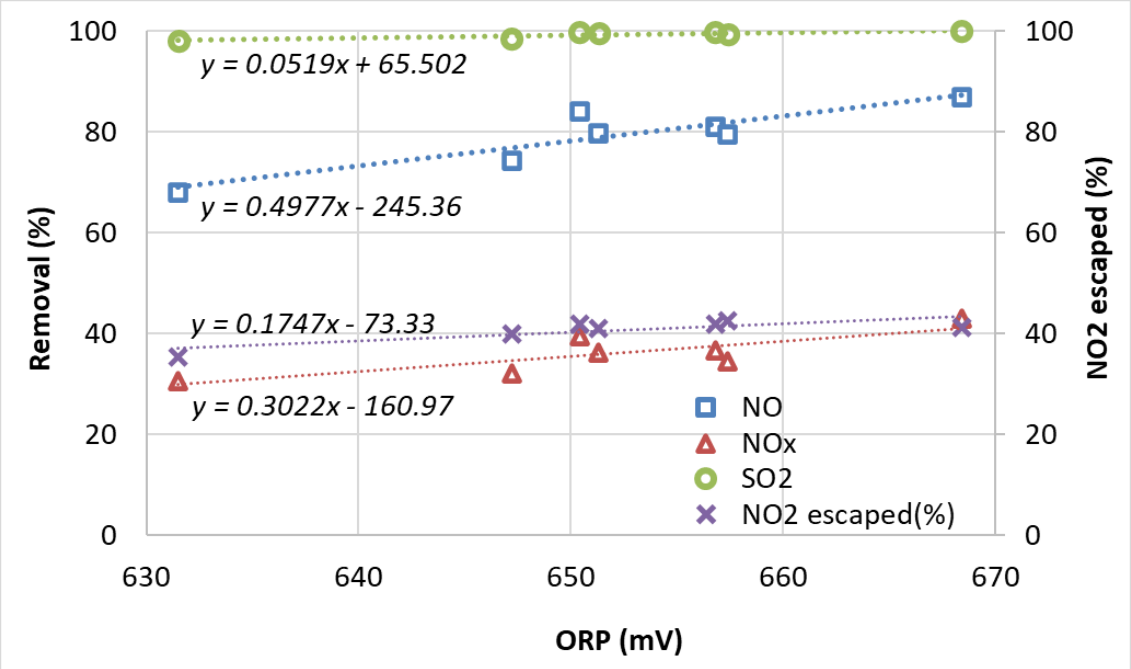

Figure 6-16: Removal of SO_2, oxidation of NO to NO_2, overall removal of NO_x, and the amount of N escaping as NO_2 with variation of the scrubbing liquid's oxidation potential in the oxidation half-height wet scrubber.
Experimental conditions described in Table 6-2 (Set 1).

6.4. Reduction with a half-height scrubber

In this section, the simulated exhaust gas (NO: 200 ppmv, NO_2: 400 ppmv, CO_2: 4%, O_2: 14%, balance N_2) was reacted with mainly sodium thiosulfate in a wet scrubber that had a height of 300 mm. This was half the height of the optimal scrubber design. The new simulated exhaust gas concentration contains significantly more amounts of NO_2 compared to NO – this reflected the typical exhaust gas concentration exiting the first half (or oxidation half) of the wet scrubber where most of the NO were already oxidised into NO_2. The purpose of the second half (or reduction half) of the wet scrubber was mainly to deal with the NO_2 that was formed. The pH and concentrations of the oxidant were varied according to the conditions shown in Table 6-2 (Sets 3 – 6).

6.4.1. Variation on reductant concentration

Without the presence of any thiosulfate, deionised water itself could only remove around a third of the NO_2 present (see Figure 6-17), through absorption of the latter in the aqueous phase as described in Equations 4.7 and 4.8. As for NO, it was totally insoluble in water, as expected. The adding of thiosulfate increased the removal of both NO and NO_2. Reaction of thiosulfate with NO_2 to form nitrites or N_2 gas likely took place as described earlier in Equations 5.6 and 5.7. Direct reaction between thiosulfate and NO was much more limited and likely took place according to the reaction described in Equation 5.10.

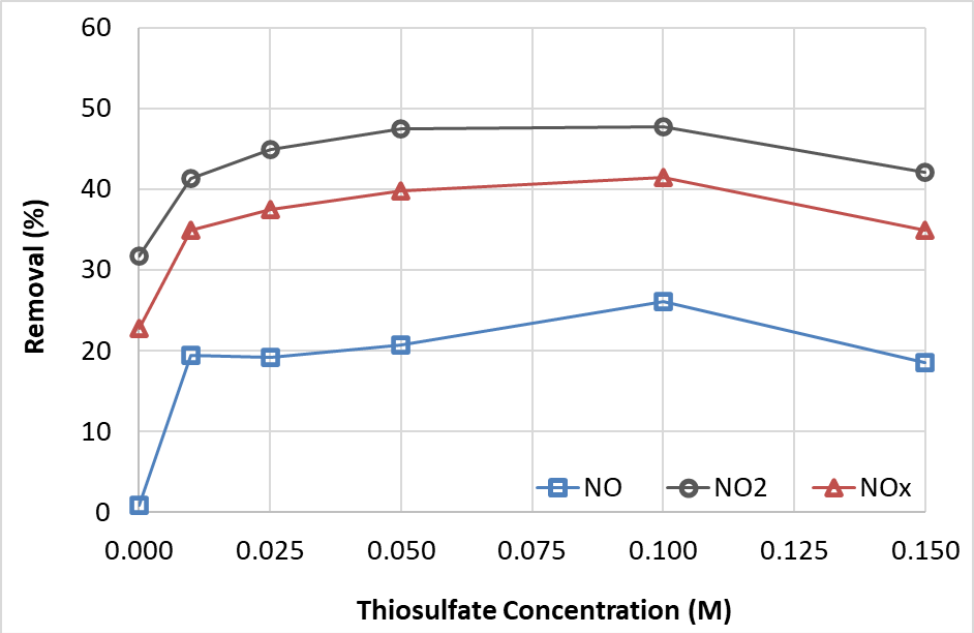

Figure 6-17: Removal of NO, NO_2 and NO_x with variation of sodium thiosulfate concentration in the reducing half-height wet scrubber.
Experimental conditions described in Table 6-2 (Set 3).

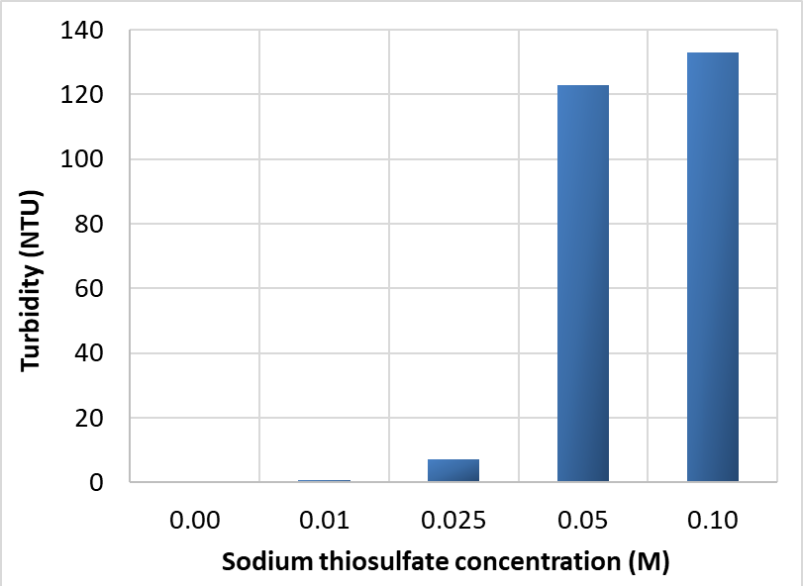

Figure 6-18: Turbidity of the scrubbing liquid in the reducing half-height wet scrubber at the end of the experiment (30 mins), with variation of thiosulfate concentration.
Experimental conditions described in Table 6-2 (Set 3).

The removal of NO and NO_2 increased with higher thiosulfate concentration before starting to plateau around 0.05 to 0.10M and began dropping again at 0.15M. This decrease of reaction at higher thiosulfate concentrations was likely due to the formation of significant amounts of white-yellowish precipitates as the reaction progressed, resulting in loss of reactant. This was consistent with the reactions described earlier in Equations 5.8 and 5.9. From the turbidity values of the aqueous phase as shown in Figure 6-18, it can be seen that even at the ideal

concentrations of 0.05 to 0.10M, significant amounts of precipitation have already occurred. Without resolving this issue, the precipitation of sulfur will render this approach impractical.

The results of the aqueous analysis of the scrubbing liquid with ion chromatography are shown in Figure 6-19 and Figure 6-20. As can be seen from Figure 6-19, the presence of the thiosulfate reducing agent increased the presence of nitrite in the aqueous phase significantly, mainly through the reaction described in Equation 5.6. The lowering of ORP due to increasing thiosulfate concentration from 0.0 to 0.10M favoured the formation of nitrites instead of nitrates. Beyond this concentration (at 0.15M), the slight increase in ORP value could be due to the reductant being precipitated out as sulfur (Equations 5.8 and 5.9).

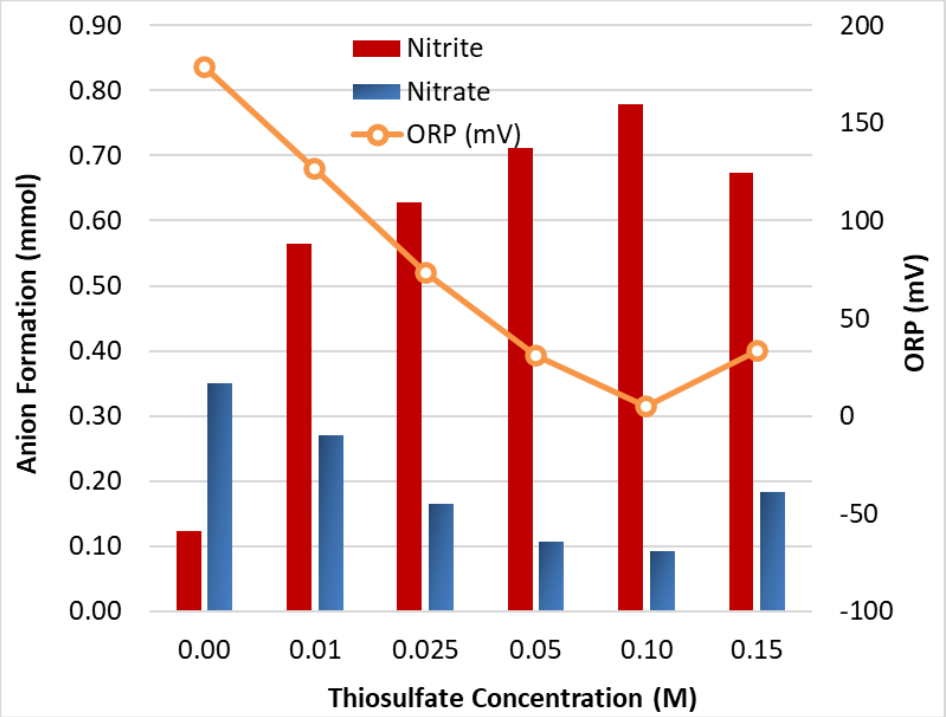

Figure 6-19: Formation of nitrites (NO_2^-) and nitrates (NO_3^-) and its corresponding ORP values in the aqueous scrubbing liquid, with variation in thiosulfate concentration, in the reducing half-height wet scrubber. *Experimental conditions described in Table 6-2 (Set 3).*

As seen in Figure 6-20, the mole ratio values of the total soluble nitrogen formed for every mole of NO_x removed was in a range that was considerably lower compared to the oxidation half of the wet scrubber. In all experimental conditions studied here, these mole ratios were all below 0.18 – less than 18% of the removed NO_x ended up in the aqueous solution as nitrite or nitrate. The unaccounted N was very likely reduced to harmless N_2 gas and released in the exhaust (via Equation 5.7). In the reaction between thiosulfate and NO_2, there was a competition to form nitrites, nitrates and N_2 gas. In the experimental parameters studied here (at pH 6), the ideal

condition for the formation of the least soluble nitrogen was achieved with a thiosulfate concentration of 0.05 M (Figure 6-19).

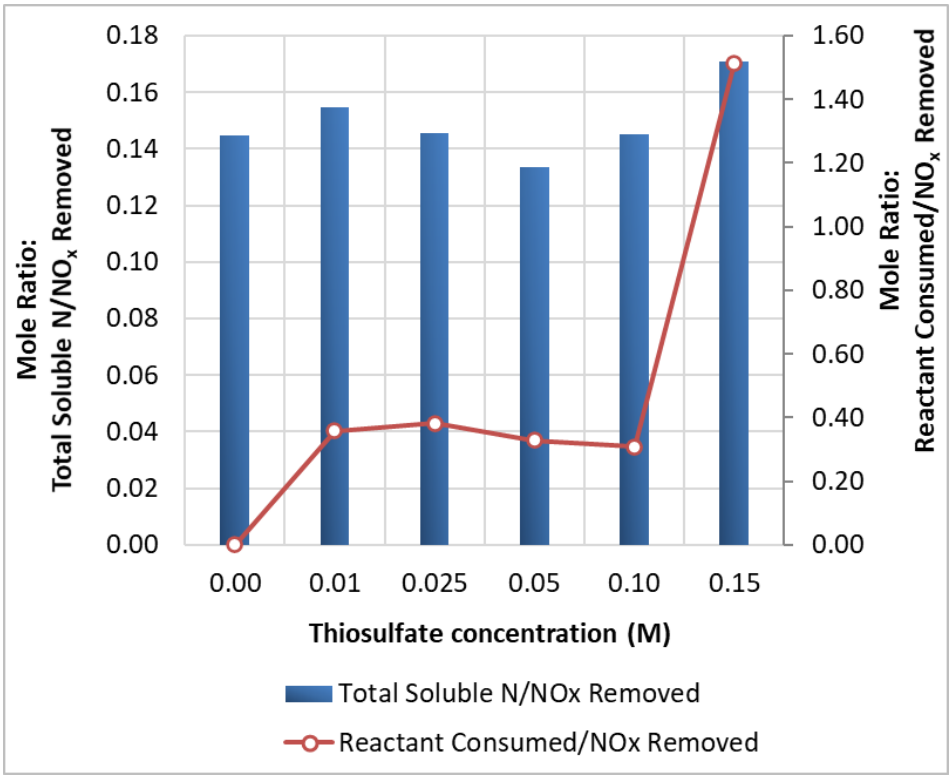

Figure 6-20: The mole ratios of soluble nitrogen formed over total NO_x removed, and reactant (thiosulfate) consumed over gaseous pollutant (NO_x) removed, as thiosulfate concentration was varied in the reducing half-height wet scrubber.
Experimental conditions described in Table 6-2 (Set 3).

The thiosulfate consumption rate per mole of gaseous pollutant removed was consistently low, below 0.40 for thiosulfate concentrations up to 0.10M (Figure 6-20). This low reactant consumption rate was consistent with the reactions suggested previously in Equations 5.6 and 5.7 where each mole of thiosulfate could theoretically oxidise 8 moles of NO_2 to nitrite and or 2 moles of NO_2 to N_2 gas. The sharp increase of reactant consumption at thiosulfate concentration of 0.15M was likely to higher loss of the reductant due to precipitation as discussed earlier.

6.4.2. Variation of pH

The pH of the aqueous scrubbing liquid in the reducing half of the wet scrubber was varied between 4 – 12 and the results of the reaction are shown in Figure 6-21. It could be seen that the removal of NO by thiosulfate improved slightly when the pH was increased from 8 to 12,

increasing from around 20 – 26%. This was likely because the presence of higher concentrations of OH^- anions likely helped to shift the reaction shown in Equation 5.10 to the right. However, this effect by the pH was only minimal. As for NO_2 removal by thiosulfate, it can be seen that the change of pH from 4 – 12 had no effect on the reaction although Equations 5.6 and 5.7 does suggest that a higher pH should improve the reaction.

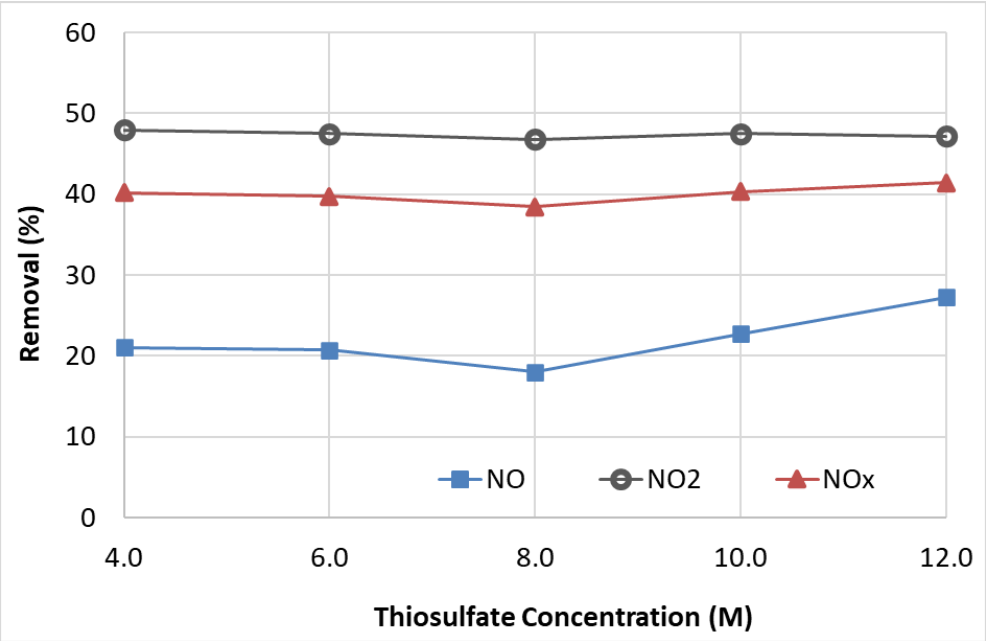

Figure 6-21: Removal of NO, NO_2 and NO_x with variation in pH, in a reducing half-height wet scrubber.
Experimental conditions described in Table 6-2 (Set 4).

The amount of total soluble nitrogen formed in the scrubbing liquid increased with increasing pH, reaching 0.16 mol per mole of NO_x removed when the pH was 12 (Figure 6-22). A higher pH seemed to have favoured the formation of nitrites rather than N_2 gas. It is possible that the conversion of NO_2 to nitrite by thiosulfate required a higher consumption of alkalinity compared to the conversion of NO_2 to N_2 gas. This observation was consistent with the reactions shown in Equations 5.6 and 5.7, where one mole of NO_2 required 1.25 moles of hydroxide anion to form nitrites but just 1 mole of it to form N_2 gas. As for reactant consumption, the amount of thiosulfate consumed per mole of gaseous pollutant (NO_x) removed was highest at pH 4 and dropped significantly when the pH was increased to 6, and gradually decreased further as pH was increased. This observation is further evidence that the precipitation reaction observed here is in accordance with Equation 5.9 and has a higher tendency to occur at a lower pH where there are more protons available to react with the thiosulfate. At pH 12, it can be seen that the formation of precipitates was negligible (Figure 6-23). This observation was also entirely consistent with the thermodynamic model prediction shown previously in Section 6.2.2.

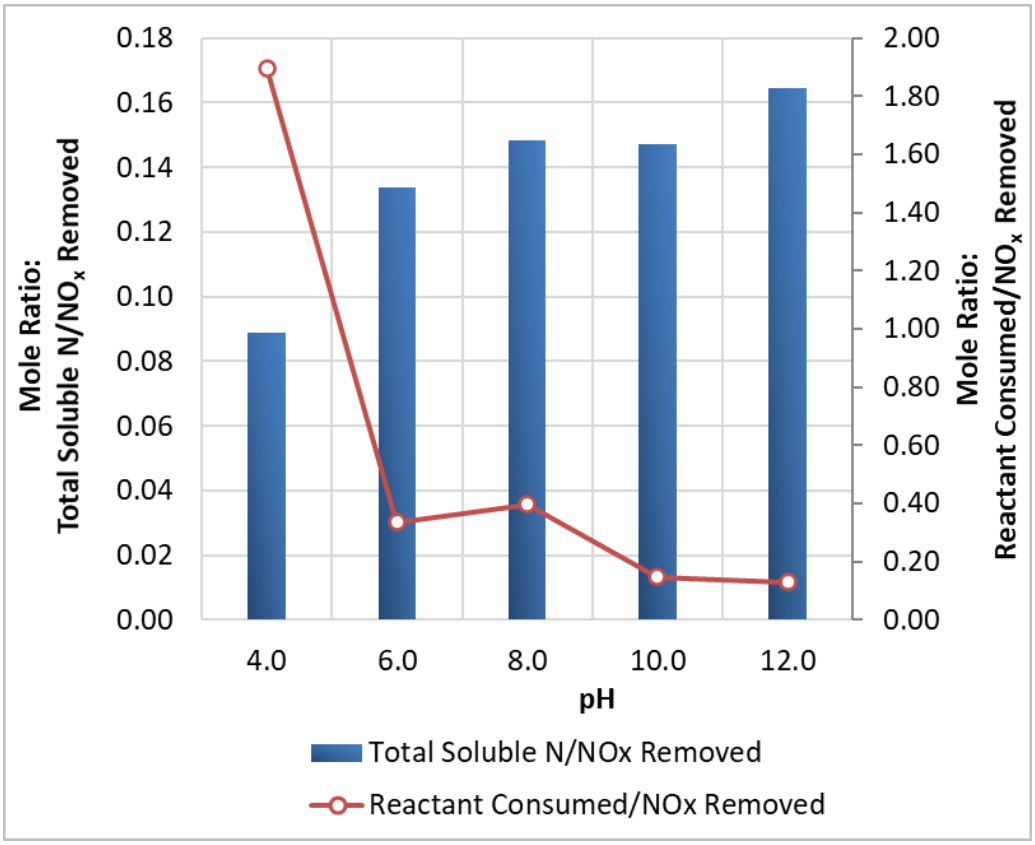

Figure 6-22: The mole ratios of soluble nitrogen formed over total NO_x removed, and reactant (thiosulfate) consumed per mole of gaseous pollutant (NO_x) removed, with variation of pH in a reducing half-height wet scrubber.
Experimental conditions described in Table 6-2 (Set 4).

It would seem that in selecting the optimal pH for the application of thiosulfate for reducing nitrogen dioxide gas in the reducing half wet scrubber, the goal of achieving low soluble nitrogen formation and low reactant consumption seemed to be at opposing ends. However, it would be more reasonable to opt for a higher pH. Although increasing pH caused more soluble nitrogen to be formed, the amount was still quite low – even at pH 12, only about 0.16 mols of soluble nitrogen were formed per mole of NO_x removed. However, the reduction in thiosulfate consumption was more considerable and precipitation due to sulfur formation can largely be avoided at pH 12.

In the reaction involving the removal of NO and NO_2 with thiosulfate, all experimental observations were in good agreement with the thermodynamic prediction shown in Table 5-4 earlier. This differed from the reaction mechanisms postulated by Kim et. al. (Kim *et al.*, 2016) and Lee et. al (Lee *et al.*, 2022) which suggested that the removal of NO_2 by thiosulfate involved the formation of disulfur as a by-product.

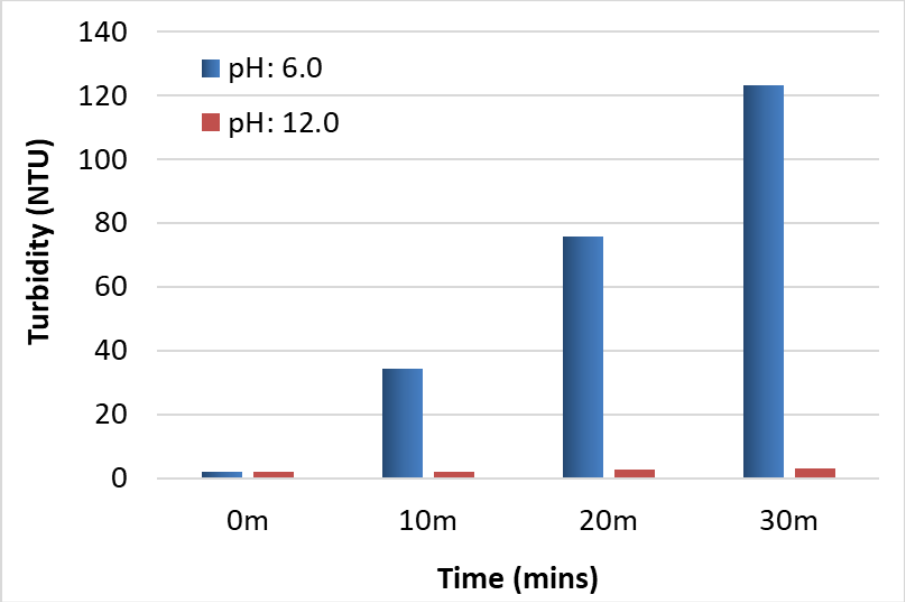

Figure 6-23: Turbidity of the scrubbing liquid in the reducing half-height wet scrubber at pH 6 and 12 respectively, with variation of reaction time.
Experimental conditions described in Table 6-2 (Set 4).

6.4.3. Effect of using a packed column configuration

In general, spray columns are preferred over the packed column configurations for ship-based scrubbers. This is because post-combustion ship emissions contain high amounts of soot and particulate matter (PM) and may end up clogging the packing material and increase the differential pressure. However, by splitting the wet scrubber into two halves consisting of an oxidation half followed by a reducing half in series, most of the soot and PM are expected to be removed in the oxidation half. This therefore may possibly free-up the reducing half to have some form of packing without severe clogging and pressure drop issues.

As can be seen from Figure 6-24, the addition of packing material in the wet scrubber significantly increased its performance in all areas – a 17% increase in NO conversion, 15% for NO_2 removal and 16% in overall NO_x removal. This was not surprising as the presence of packing material increases the surface area for the gas-liquid reaction to take place. The addition of packing material did not significantly alter the soluble nitrogen formation or the reactant consumption rate (Figure 6-25).

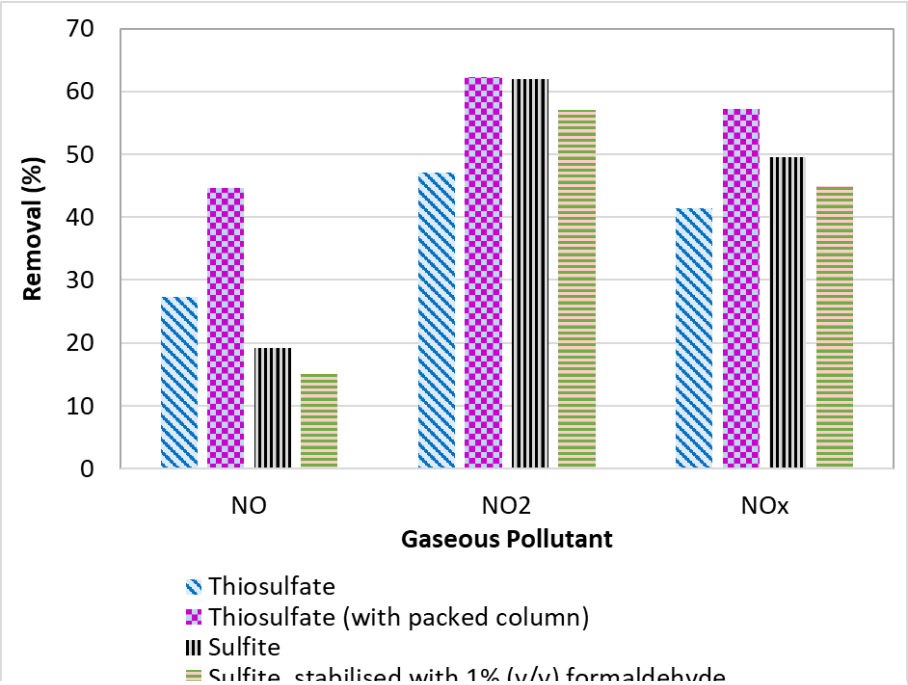

Figure 6-24: Comparison of NO, NO_2 and NO_x removal in the reducing half-height wet scrubber using 0.05M of thiosulfate (with and without packing) and 0.05M sulfite (with and without stabilisation using 1% (v/v) formaldehyde).
Experimental conditions described in Table 6-2 (Sets 4 – 6).

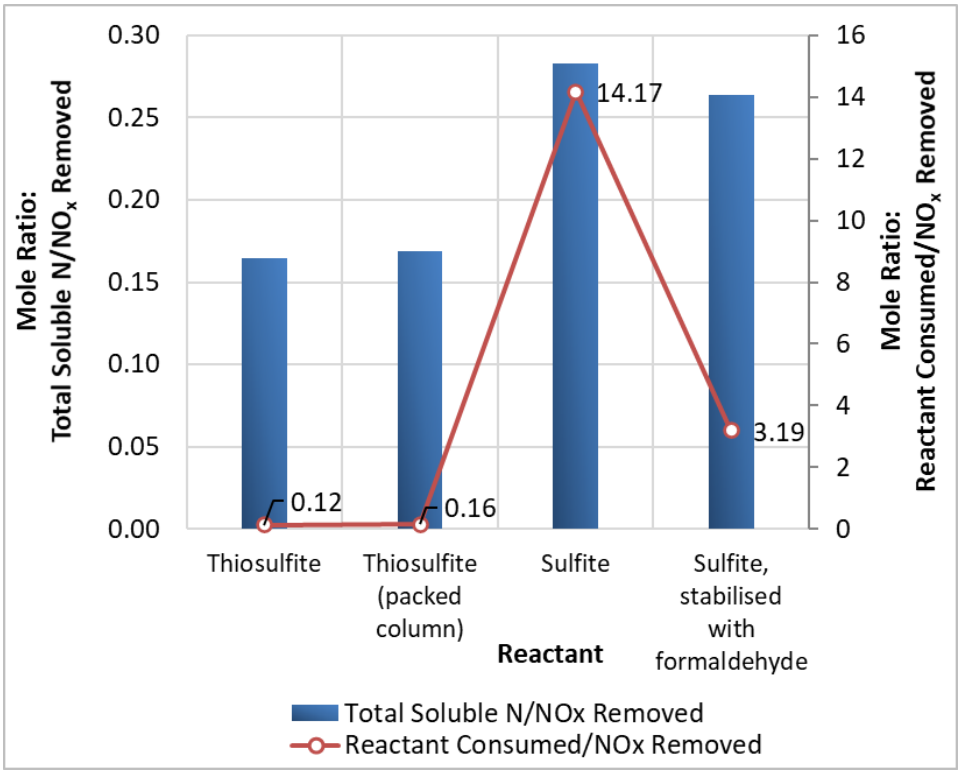

Figure 6-25: The mole ratios of soluble nitrogen formed over total NO_x removed, and reactant consumed over gaseous pollutant (NO_x) removed, in the reducing half-height wet scrubber, using 0.05M of thiosulfate (with and without packing) and 0.05M sulfite (with and without stabilisation using 1% (v/v) formaldehyde).
Experimental conditions described in Table 6-2 (Sets 4 – 6).

6.4.4. Comparison between thiosulfate and sulfite as reducing agents

The performance of sulfite was compared with thiosulfate in the reducing half wet scrubber and the results are shown in Figure 6-24. It can be seen that although sulfite was slightly more inferior in its conversion of NO, it was about 15% and 8% more effective in NO_2 and overall NO_x removal respectively, compared to thiosulfate. Nevertheless, this higher effectiveness came at a price as the reactant consumption for sulfite was about 118 times more compared to thiosulfate – about 14.2 mols of sulfite is consumed for each mole of pollutant removed (Figure 6-25). This showed the extent of sulfite instability as a significant amount of unreacted sulfite was oxidised to sulfate due to the high oxygen content of the exhaust gas.

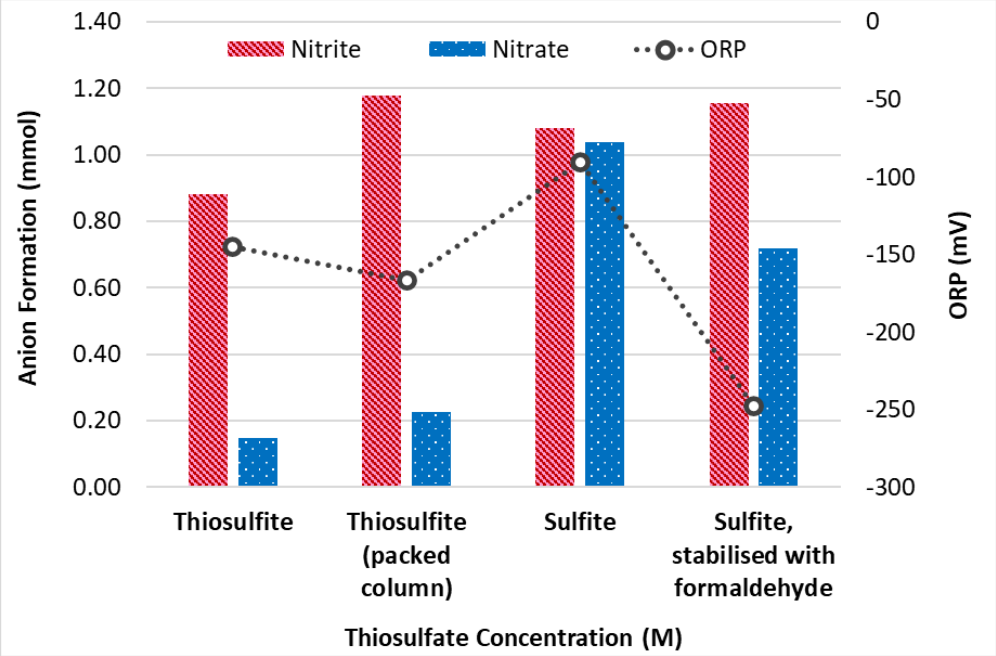

Figure 6-26: Formation of nitrites (NO_2^-) and nitrates (NO_3^-) in the aqueous scrubbing liquid at the end of the experiment, in the reducing half-height wet scrubber using 0.05M of thiosulfate (with and without packing) and 0.05M sulfite (with and without stabilisation using 1% (v/v) formaldehyde). The ORP values of the scrubbing liquid are also shown here.
Experimental conditions described in Table 6-2 (Sets 4 – 6).

The addition of 1% (v/v) formaldehyde to the sulfite reductant slightly reduced its effectiveness in NO, NO_2 and NO_x removal but significantly improved its stability – the sulfite consumption dropped from 14.2 to 3.2 mol per mole of pollutant removed. However, this was still about 27 times more than the thiosulfate consumption. Furthermore, the formation of soluble nitrogen was between 1.6 to 1.8 times more when sulfite was used compared to thiosulfate.

Further observation showed that when thiosulfate was used for the removal of NO_2, the soluble nitrogen formed was predominantly in the form nitrite instead of nitrate (Figure 6-26). However,

significantly more nitrates were formed when sulfite was used. When it comes to the formation of soluble nitrogen, nitrates are of course much less desirable than nitrites because it is the former that is actually regulated in the washwater discharge to the ocean instead of the latter (MEPC.259(68), 2015).

6.4.5. Absorption of carbon dioxide

It was observed that some CO_2 absorption in the reducing half of the wet scrubber was possible, especially when operating at high pH (Figure 6-27). The initial spike of CO_2 absorption was ignored as this was when the aqueous solution was still very unsaturated with CO_2 during the unsteady-state period. After the reaction reached a steady state several minutes later, it can be seen that the absorption of CO_2 was pH dependant – the higher the pH, the higher the CO_2 absorption on a continual basis. The reaction taking place are described earlier in Equations 5.1 – 5.3 where CO_2 gas was continually being converted to carbonate ions, with the reaction driven by high concentrations of hydroxide ions in the scrubbing liquid.

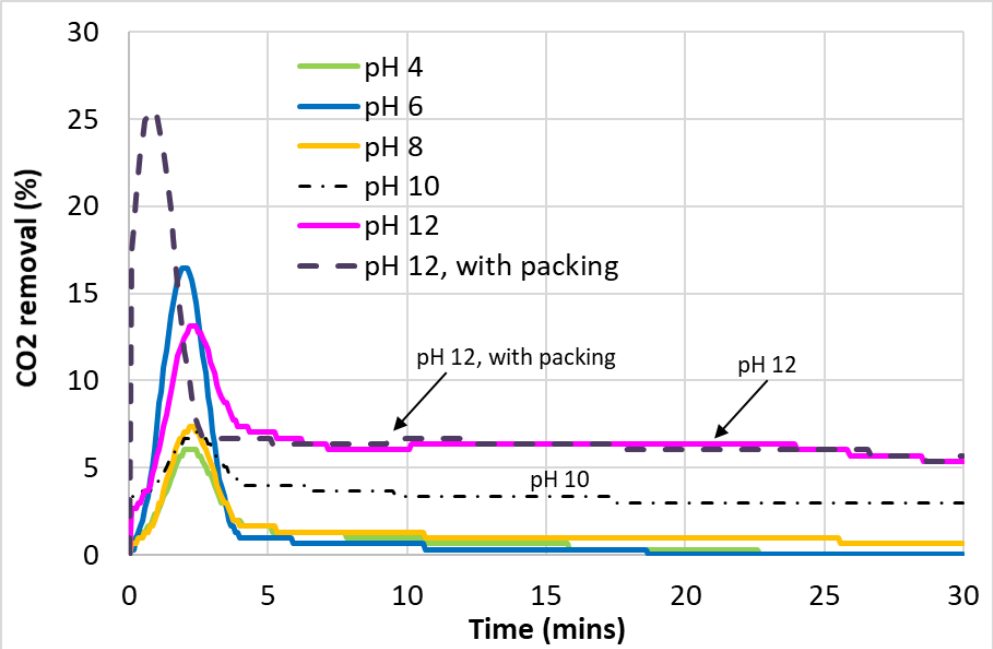

Figure 6-27: Removal of CO_2 with the variation of pH of 0.05M of thiosulfate in the reducing half-height wet scrubber.
Experimental conditions described in Table 6-2 (Set 4).

At pH 12, an absorption rate of around 5 – 6% of CO_2 could be sustained. Although this may seem little, it adds up significantly over the long term due to the large volumes and high CO_2 content (around 4%) in ship exhaust emissions. For a typical slow speed large diesel engine, this amount can possibly translate between 200 – 250 tons of CO_2 captured for a 2-week journey (Appendix B). However, if pH adjustment of washwater is carried out to bring its pH down from highly alkaline to levels closer to seawater pH before ocean discharge, the amount of CO_2

captured would be lower as some of it would escape from the aqueous phase back to the atmosphere. The necessity of doing so, however, is arguable as current IMO MARPOL Annex VI regulations prevent acidic washwater discharge but seem to allow alkaline discharge (*EGCSA Handbook 2012: A practical guide to exhaust gas cleaning systems for the maritime industry*, 2012). Nevertheless, the regulation does contain a catchall clause which stipulates that further assessment of the washwater is needed when it contains chemicals and additives, which would presumably include the sodium hydroxide used for pH adjustment.

6.5. Reaction in a full height wet scrubber with oxidation only

In this section, a full height wet scrubber was used for the treatment of the simulated exhaust emissions, with chlorite as the scrubbing liquid. The liquid flowrate was fixed while the simulated gas flowrate was increased from 10 to 50 litres/min, resulting in a range of *L/G* values. The lower the *L/G* ratio, the higher the gaseous flowrate into the scrubber, with the liquid flowrate remaining constant.

6.5.1. Gaseous pollutant removal

As can be seen from Figure 6-28 (solid lines), the complete removal of SO_2 was achieved for the entire range of *L/G* ratios. With the liquid flowrate remaining constant, the increase in gaseous flowrate did not reduce the absorption of SO_2, owing to its high solubility in water, especially at a high pH.

As the *L/G* ratio was lowered, both the oxidation of NO to NO_2 and the overall removal of NO_x reduced accordingly. This was expected as the gas-liquid reaction taking place could not cope with the higher gaseous flowrate, showing that this reaction is limited by mass transfer. From the *L/G* of 76.0 L/m^3 to 15.2 L/m^3, the amount of NO oxidation dropped from 100% to around 83%, thereby roughly reducing about 17%. However, the NO_2 escaping the wet scrubber increased by a much larger magnitude, from 20% to 58%. This showed that the oxidation of NO to NO_2 was less affected by the limitations of mass transfer, unlike the absorption of NO_2 – it was easier to achieve high oxidation rates of NO to NO_2 even at low *L/G* values but harder to absorb the NO_2 that was subsequently formed. As the rate of NO_2 absorption in the gas-liquid reaction could not keep up with the rate of NO_2 formation, a need for a more effective mechanism for dealing with the NO_2 being formed is needed.

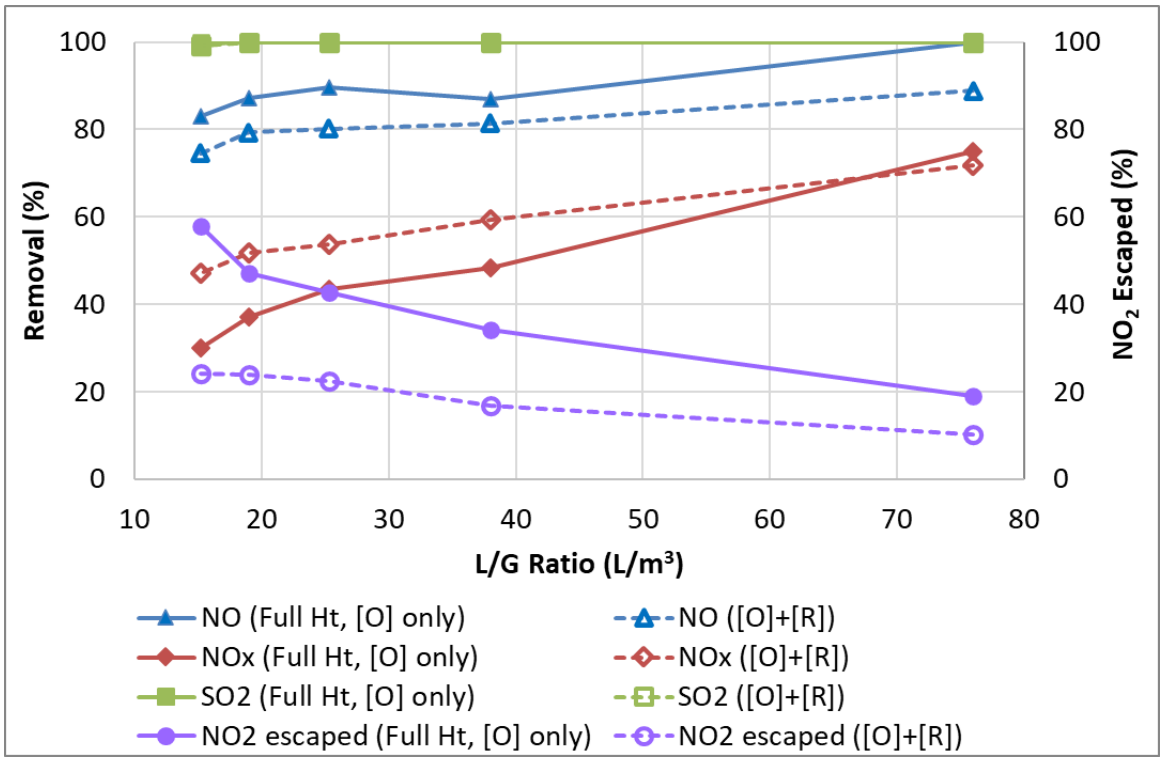

Figure 6-28: Removal of SO_2, NO, NO_x, and the amount of N escaping the scrubber in the form of NO_2, with variation of the L/G ratio in a full height wet scrubber.
Experimental conditions described in Table 6-2 (Sets 7 and 8). Line and markers for SO_2 [O]+[R] overlapped with SO_2 [O] only.

6.5.2. Aqueous Analysis

The formation of nitrites, nitrates and the ORP values of the scrubbing liquid can be seen in Figure 6-29. As expected, the reaction with the chlorite oxidant favoured the formation of nitrates over nitrites. The ratio of soluble nitrogen formation per mole of NO_x removed was mostly within the expected range of 0.48 – 0.64 (Figure 6-30). Apart from the datapoint at the *L/G* ratio of 76, it can be seen that higher gaseous flowrates tended to increase the amount of soluble nitrogen formed – at the *L/G* ratio of 15.2, about 0.64 mol of soluble nitrogen was formed for every mole of NO_x removed.

It can be seen from Figure 6-31 that the reactant consumed per mole of gaseous pollutant removed increased as the *L/G* ratio reduced, in general. This showed that higher gaseous flowrates will cause a drop in reactant utilisation efficiency in the wet scrubber. At the *L/G* ratio of 15.2, around 0.87 mol of chlorite were consumed for every mole of pollutant removed. In both the formation of soluble nitrogen and reactant consumption, the datapoint at the *L/G* ratio of 76, which had the lowest gaseous flowrate, did not follow the overall trend. It is possible that at a lower gaseous flowrate, the gas-liquid reactions were more controlled by the various chemical reaction rates instead of the gas-liquid mass transfer rates, thereby following a

different behaviour altogether. A more thorough discussion on these is covered in Chapter 7 (Section 7.2), demonstrated that higher gas flowrate which increased turbulence and mixing led to higher nitrate formation.

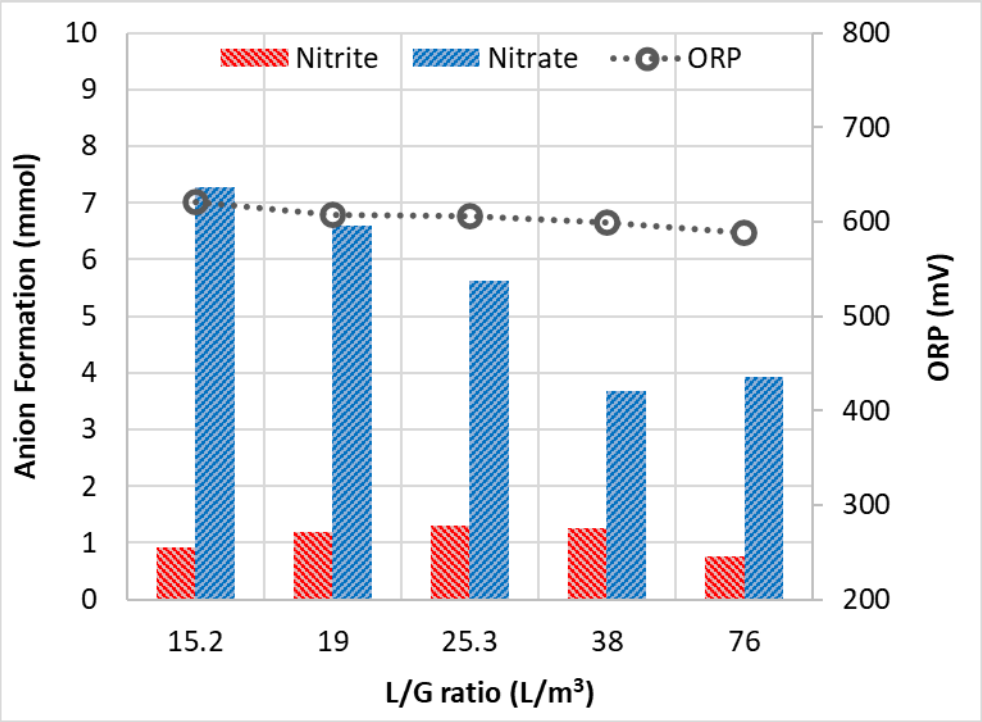

Figure 6-29: Formation of nitrites (NO_2^-) and nitrates (NO_3^-) in the aqueous scrubbing liquid at the end of the experiment, in the full height wet scrubber with oxidation only. The ORP values of the scrubbing liquid are also shown here.
Experimental conditions described in Table 6-2 (Sets 7).

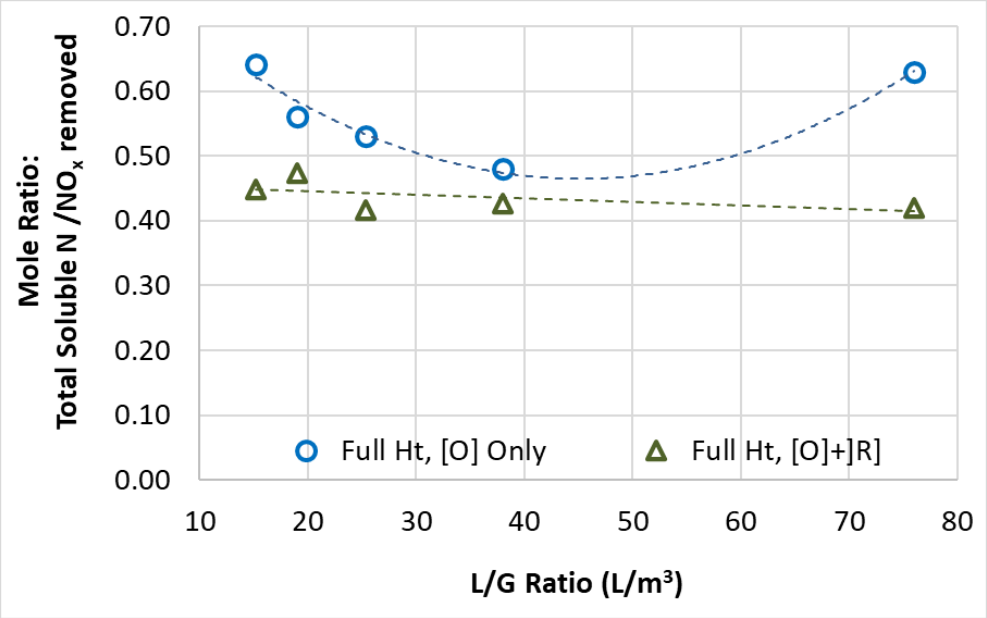

Figure 6-30: The mole ratios of soluble nitrogen formed over total NO_x removed in the full height wet scrubber, with variation of the L/G ratio. In the full height [O] only scrubber, chlorite was used as the oxidant. In the oxidant and reduction wet scrubber, the full height scrubber was split into an oxidation half and reduction half.
Experimental conditions described in Table 6-2 (Sets 7 – 8).

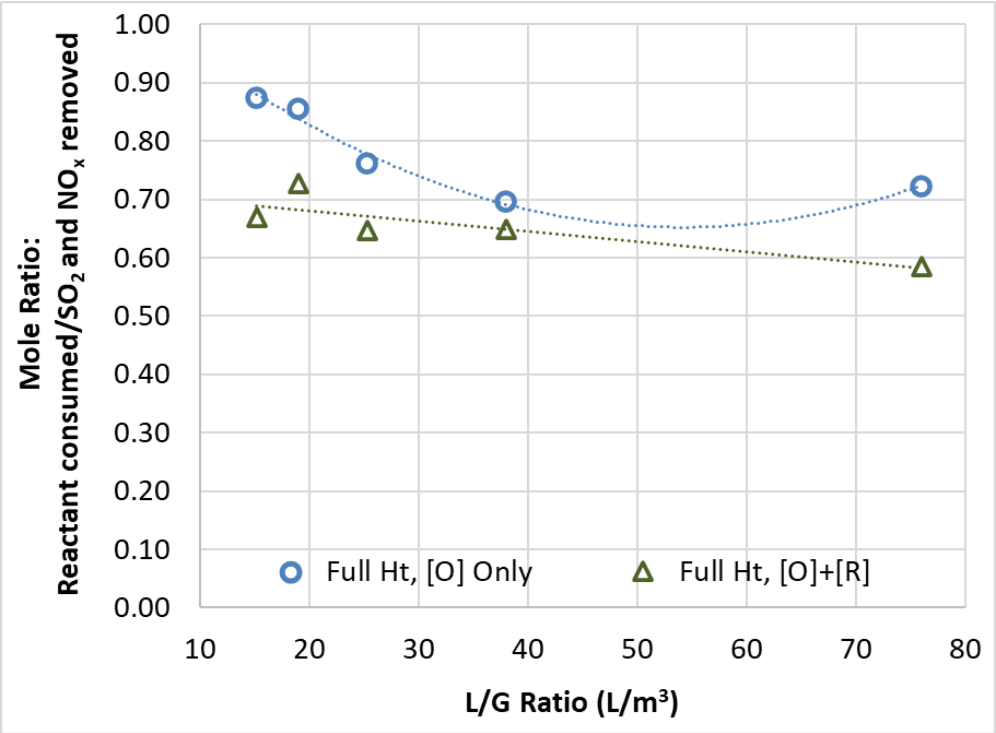

Figure 6-31: The mole ratios of the reactant consumed per mole of gaseous pollutant removed the full height wet scrubber, with variation of the *L/G* ratio. In the full height [O] only scrubber, chlorite was used as the oxidant. In the oxidant and reduction wet scrubber, the full height scrubber was split into an oxidation half and reduction half.
Experimental conditions described in Table 6-2 (Sets 7 – 8).

6.6. Reaction in a full height wet scrubber with oxidation and reduction in series

In this section, the simulated exhaust gas was passed through a full height wet scrubber that was made up of two halves – the first being the oxidation half with $NaClO_2$ and the second being the reduction half using $Na_2S_2O_3$. The liquid flowrate was fixed while the simulated exhaust gas flowrate was increased from 10 to 50 litres/min, resulting in a range of *L/G* values. The experimental conditions used in this section are shown in Table 6-2 (Set 8). The results from here were compared with the reaction from a full height wet scrubber (equivalent scrubber height) with oxidation only.

6.6.1. Gaseous pollutant removal

It was discussed previously that the full height wet scrubber with oxidation only was very effective in oxidation of NO to NO_2 but the rate determining step was in removing the NO_2 that was subsequently formed. It can be seen that in the oxidation/reduction wet scrubber, the removal of NO_2 formed was remarkably improved – gaseous N escaping from the wet scrubber in the form of NO_2 drastically dropped by around 34% when the *L/G* was 15.2 (Figure 6-28). The introduction of a reducing half in the wet scrubbing process enabled more of the NO_2 to be reduced into nitrite ions or harmless N_2 gas. In this new configuration, the oxidation of NO to

NO_2 step was not too much affected although there was only half a scrubber left to carry out the oxidation. This was because the oxidation of NO to NO_2 was the faster step. Additionally, a limited amount of NO removal also took place in the reducing half of the wet scrubber (as discussed previously). At the *L/G* ratio of 15.2, its capacity to oxidise NO to NO_2 compared to the oxidation only full height wet scrubber diminished by less than 10%.

When it came to the overall NO_x removal, it was clear that the full height oxidation/reduction scrubber had significant advantages over the equivalent scrubber with oxidation only. When the *L/G* ratio was at the highest value of 76, the difference in NO_x removal between these two scrubber configurations was insignificant. However, as the *L/G* ratio was decreased (ie. higher flowrate in the system, with all else remaining constant), the advantage of the oxidation/reduction configuration for NO_x removal became more and more significant. At the *L/G* value of 15.2, the difference between these two configurations for NO_x removal was around 17%. This was likely because at lower *L/G*, the amount of NO_2 formed by the oxidation of NO was much higher and the scrubber with only oxidation could not cope with its absorption due to mass transfer limitations. Having a reduction part in the wet scrubber allowed more of the NO_2 formed to be absorbed, therefore increasing the overall NO_x removal.

6.6.2. Aqueous analysis

As illustrated in Figure 6-30, the formation of soluble nitrogen per mole of NO_x gaseous pollutant removed in the oxidation/reduction full height wet scrubber was significantly lower compared to the oxidation only wet scrubber of equivalent height for the entire range for the *L/G* ratios studied. At the *L/G* ratio of 15.2, only about 0.45 mols of soluble nitrogen was formed per mole of NO_x removed in the oxidation/reduction system compared with about 0.64 mols in the oxidation only wet scrubber. This lower amount of soluble nitrogen formation in the system was achieved because the reducing portion in the oxidation/reducing wet scrubber had a higher tendency to reduce the NO_2 formed to its harmless N_2 form according to Equation 5.7. The soluble nitrogen that was formed in the oxidation/reduction system was mainly contributed by the oxidation half (around 70%) of the wet scrubber in the form of nitrates (Figure 6-32).

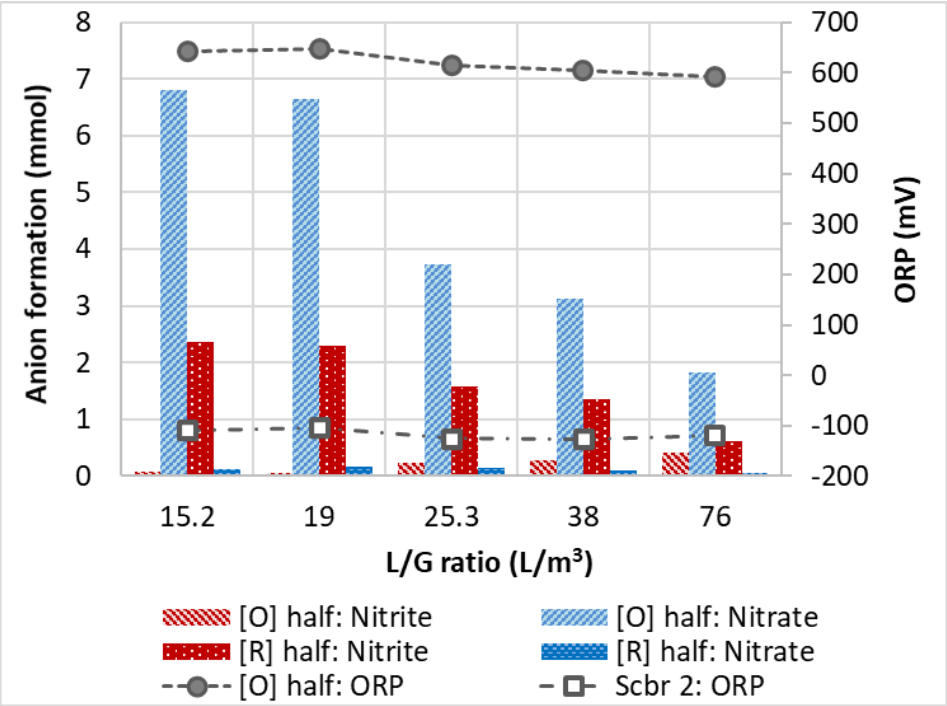

Figure 6-32: Formation of nitrites (NO_2^-) and nitrates (NO_3^-) in the aqueous scrubbing liquid at the end of the experiment, in the full height wet scrubber consisting of an oxidation half and a reducing half arranged in series. The ORP values of the scrubbing liquid in both halves are also shown here.
Experimental conditions described in Table 6-2 (Set 8).

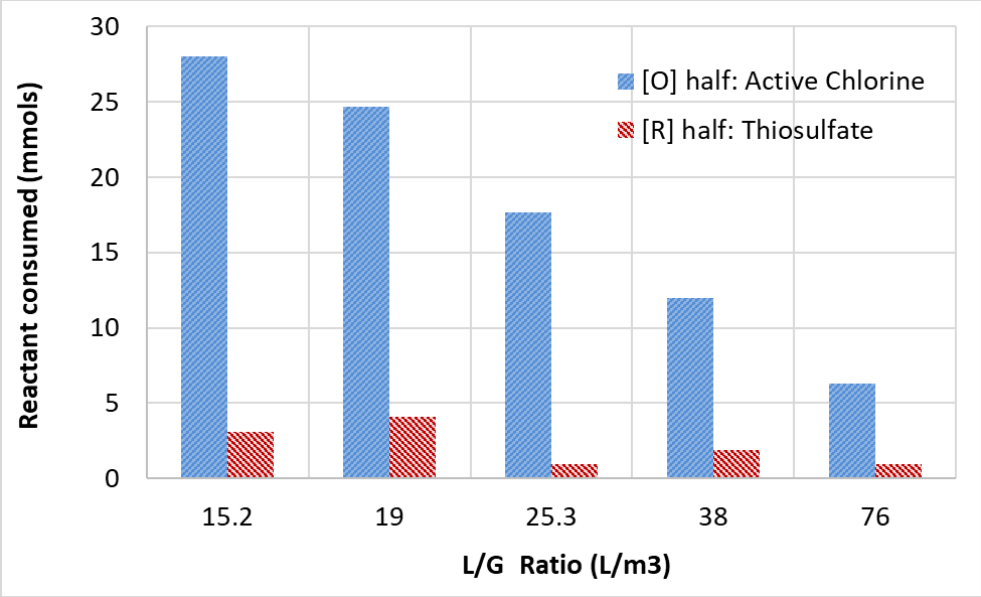

Figure 6-33: Reactants consumed in the oxidation and reduction halves of the full height wet scrubber with the oxidation/reduction configuration, with variation of L/G ratio.
Experimental conditions described in Table 6-2 (Set 8).

The reactant utilisation in the oxidation/reduction system was also significantly lower compared to the oxidation only system – at a *L/G* ratio of 15.2, this ratio was around 0.67 for the former compared to about 0.87 for the latter (Figure 6-31). This was because the reducing half of the wet scrubber was able to achieve a much higher efficiency compared to the oxidation half (Figure 6-33), thereby contributing to the overall lower utilisation rate of the oxidation/reduction system.

6.6.3. Improving the removal efficiency of the oxidation and reduction system

The pollutant removal efficiency of the oxidation and reduction in series wet scrubbing system can be further enhanced by reducing the pH of the oxidant, increasing the oxidant concentration or the usage of a packed column in the reducing half. This was carried out at a low *L/G* ratio of 15.2 and the results can be seen in Figure 6-34. Doubling the oxidant concentration to 0.04M while remaining at pH 10 led to significantly more NO conversion and overall NO_x removal compared to decreasing the pH to 8 while maintaining oxidation concentration. At the chlorite concentration of 0.06M at pH 10 in the oxidation half, the oxidation of NO to NO_2 reached 96% and the overall NO_x removal reached 73%. This could be further improved with more optimisation if needed.

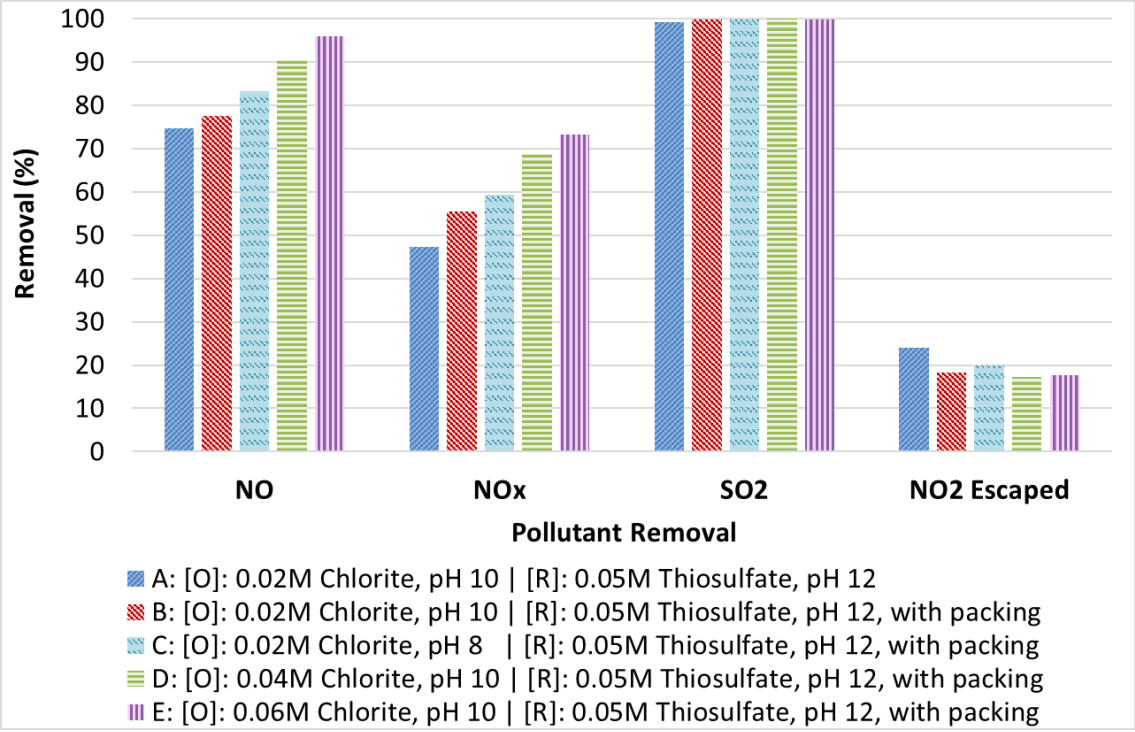

Figure 6-34: Gaseous pollutant removal carried out by the oxidation/reduction full height wet scrubber, enhanced with higher oxidant concentration in the first half or using a packed column the second half.
Experimental conditions described in Table 6-2 (Sets 8 and 9).

As can be seen from Figure 6-35, decreasing the pH or increasing the concentration of the oxidant used in the oxidation half carried a slight penalty with more soluble nitrogen formed per mole of NO_x removed, although they were still within the 0.40 – 0.60 range. The penalty for reaction losses were higher – as can be seen from the ratio of reactant consumed per mole of gaseous pollutant removed, increasing the chlorite concentration to 0.04 and 0.06M also increased this ratio from 0.67 to between 0.80 – 0.90.

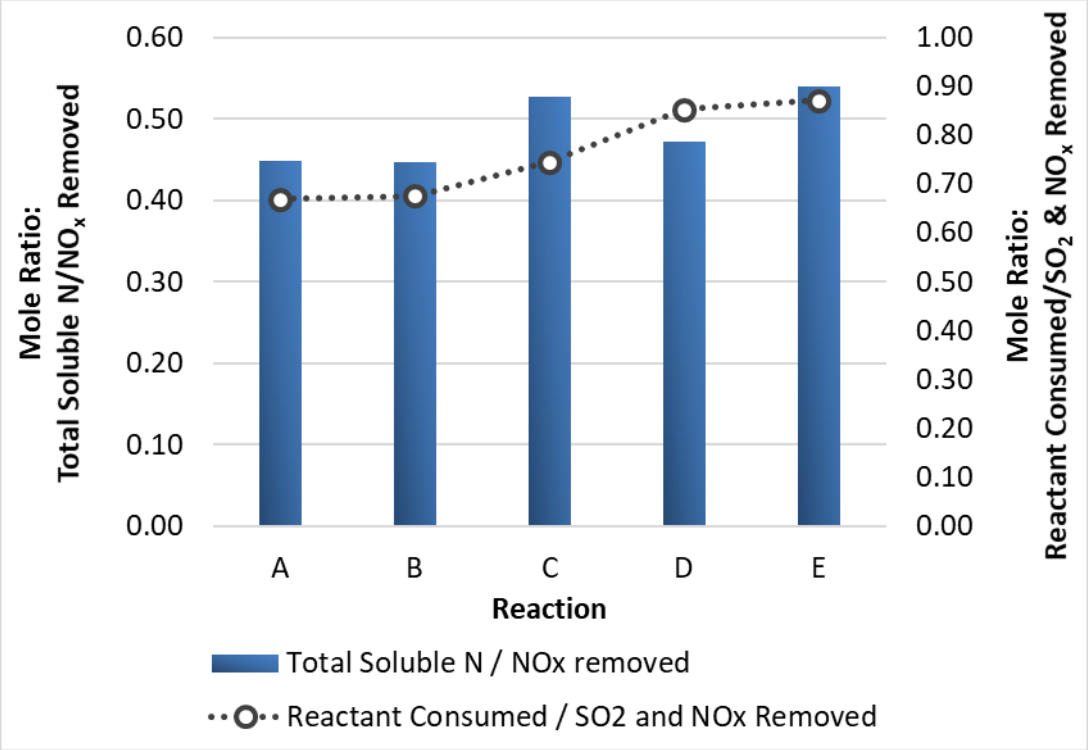

Figure 6-35: The mole ratios of soluble nitrogen formed over total NO_x removed, and reactant consumed over gaseous pollutant (SO_2 & NO_x) removed, using the full height wet scrubber with oxidation and reduction configuration with further enhancements made.
Reaction A – [O]: 0.02M Chlorite, pH10 | [R]: 0.05M Thiosulfate, pH 12
Reaction B – [O]: 0.02M Chlorite, pH10 | [R]: 0.05M Thiosulfate, pH 12, with packing
Reaction C – [O]: 0.02M Chlorite, pH8 | [R]: 0.05M Thiosulfate, pH 12, with packing
Reaction D – [O]: 0.04M Chlorite, pH10 | [R]: 0.05M Thiosulfate, pH 12, with packing
Reaction E – [O]: 0.06M Chlorite, pH10 | [R]: 0.05M Thiosulfate, pH 12, with packing
Experimental conditions described in Table 6-2 (Sets 8 and 9).

6.6.4. Absorption of carbon dioxide

The removal of CO_2 from the simulated exhaust gas was compared between the full height scrubbers of oxidation only configuration versus the configuration with oxidation and reduction in series (Table 6-4). The reaction in the oxidation only configuration did not result in CO_2 removal. Comparatively, some CO_2 removal was achieved in the oxidation/reduction configuration. As discussed in the previous section, this absorption of CO_2 was mainly

contributed by the reduction half of the wet scrubber. As the *L/G* ratio decreased, the amount of CO_2 absorbed also steadily decreased. This was because lower *L/G* ratios meant that the wet scrubber has to handle higher gaseous flowrates, causing absorption to be lowered by mass transfer limitations. At the *L/G* ratio of 15.2, the oxidation/reducing configuration still managed to achieve about 4% of CO_2 absorption. When a packed column was used in the reducing half, the absorption of CO_2 was increased to 5%.

Table 6-4: The CO_2 absorbed from the simulated exhaust gas between the two full height scrubber configurations – oxidation only configuration versus the oxidation and reduction in series configuration.

***L/G* ratio**	**CO_2 removal (%)**	
(L/m^3)	**Full height scrubber, [O] only**	**Full height scrubber, [O]+[R]**
76.0	0.0	13.0
38.0	0.0	10.2
25.3	0.0	7.0
19.0	0.0	4.9
15.2	0.0	4.0
15.2*	0.0	5.0

** With packed column configuration in the reduction half*

6.7. Effect of temperature

The reaction temperature was varied between 25°C to 55°C for the various configurations studied here. In the oxidation half-height wet scrubber (Figure 6-36), it can be seen that higher temperatures helped push the removal NO from 85.7% at 25°C to 96.2% at 55°C. The amount of nitrogen pollutant escaping the wet scrubber as NO_2 also reduced, leading to a significant overall improvement in NO_x removal from 40.3% to 55.5%. Higher reaction temperatures likely increased the gas-liquid mass transfer rates and also the chemical reaction rates of the various reactions taking place in the wet scrubbing system. These increases likely exceeded the diminishing solubility of NO_2 in water due to higher liquid temperatures (Zhao *et al.*, 2016; Yang *et al.*, 2018). Furthermore, elevation in temperature could also have increased the decomposition of chlorite to form ClO_2 (Equations 4.15 and 4.16), thereby promoting NO_x removal (Zhao *et al.*, 2010). Removal of SO_2 was unchanged and remained at 100% at all temperatures.

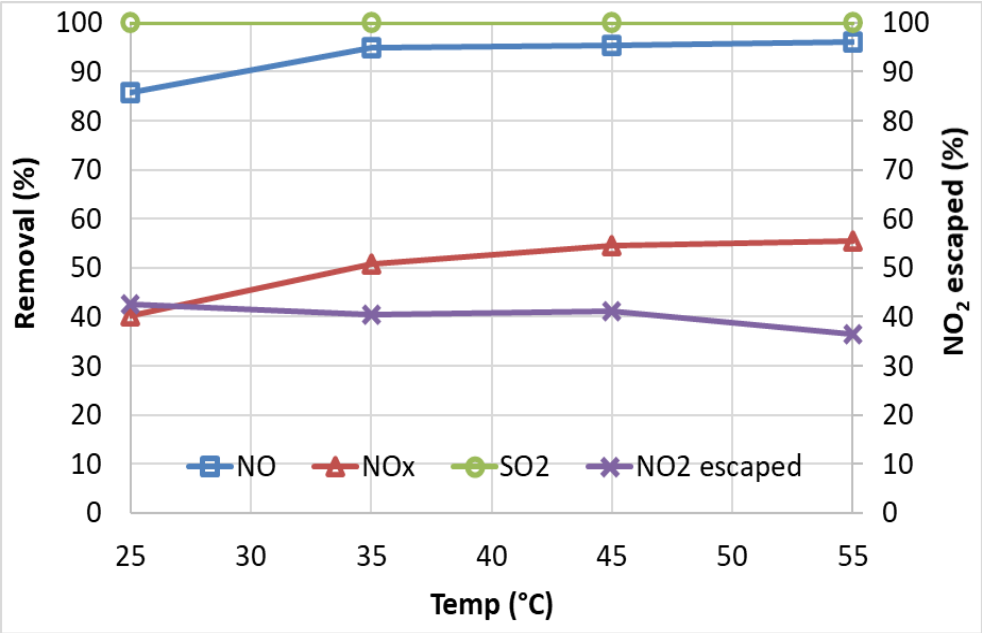

Figure 6-36: Removal of SO_2, NO, NO_x and the amount of N escaping the scrubber in the form of NO_2, with variation of reaction temperature in the oxidation half-height wet scrubber.
Experimental conditions described in Table 6-2 (Set 10).

In the aqueous phase, increase of temperature corresponded to a slight increase in the amount of soluble nitrogen formed per mole of NO_x removed, from 0.46 at 25°C to around 0.58 at 55°C, but this was not very significant (Figure 6-37). This was consistent with the thermodynamic modelling results discussed previously in Section 6.2.3, which showed that an increase of temperature from 25°C to 55°C slightly favoured the formation of nitrates over nitrogen. Change in temperature had minimal effect the reactant consumption, with the mole ratio of reactant consumed per mole of gas pollutant removed fluctuating between 0.72 to 0.79.

In the reducing half-height wet scrubber, increase in reaction temperature slightly lowered the removal of NO from 25.4% at 25°C to 21.3% at 55°C (Figure 6-38). Because of this, the overall NO_x removal was slightly lowered as well, as no discernible change was observed in the NO_2 removal. All in all, change in temperature here had little overall effect on pollutant gas removal – any increases in diffusion and chemical reaction rates due to elevation of temperature seemed to have been balanced out by loss in solubility in a warmer aqueous phase.

One area of significant change that was observed, however, was in CO_2 removed – this increased from about 6.3% at 25°C to 24.3% at 55°C. This was mainly because elevation of the liquid temperature also increased ionisation and the formation of H^+ ions, as pH of a solution is slightly inversely proportional with temperature. Due to this phenomenon, an increase of

NaOH addition was needed at higher temperatures in order to keep the pH at 12. Therefore, more CO_2 will be captured in the aqueous phase as well.

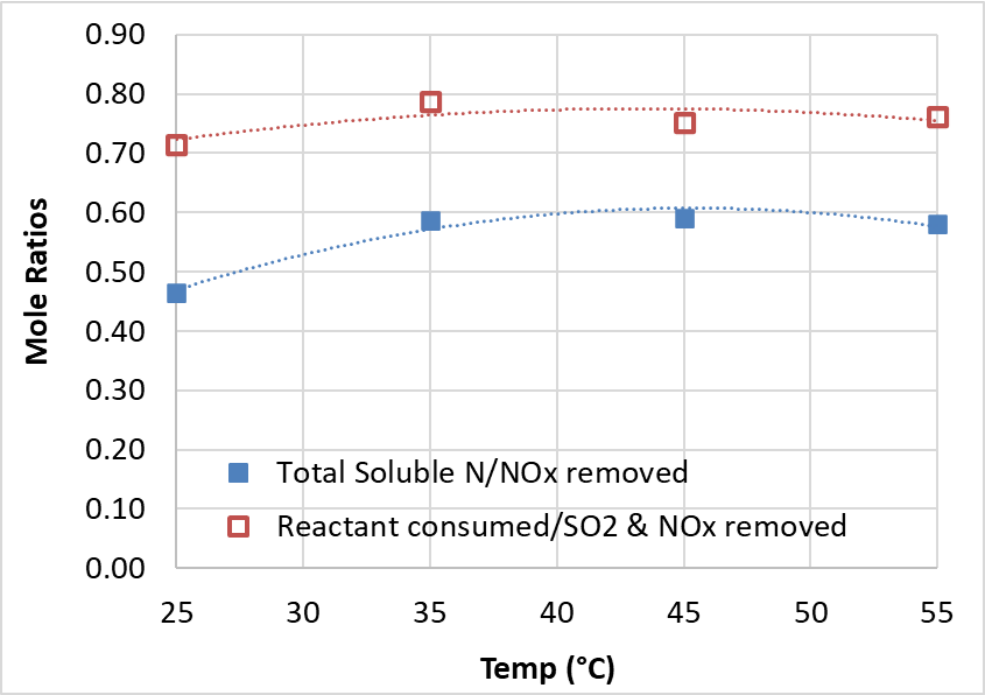

Figure 6-37: The mole ratios of soluble nitrogen formed over total NO_x removed, and reactant (chlorite) consumed over pollutant (SO_2 and NO_x) removed, as the reaction temperature was varied in the oxidation half-height wet scrubber.
Experimental conditions described in Table 6-2 (Set 10).

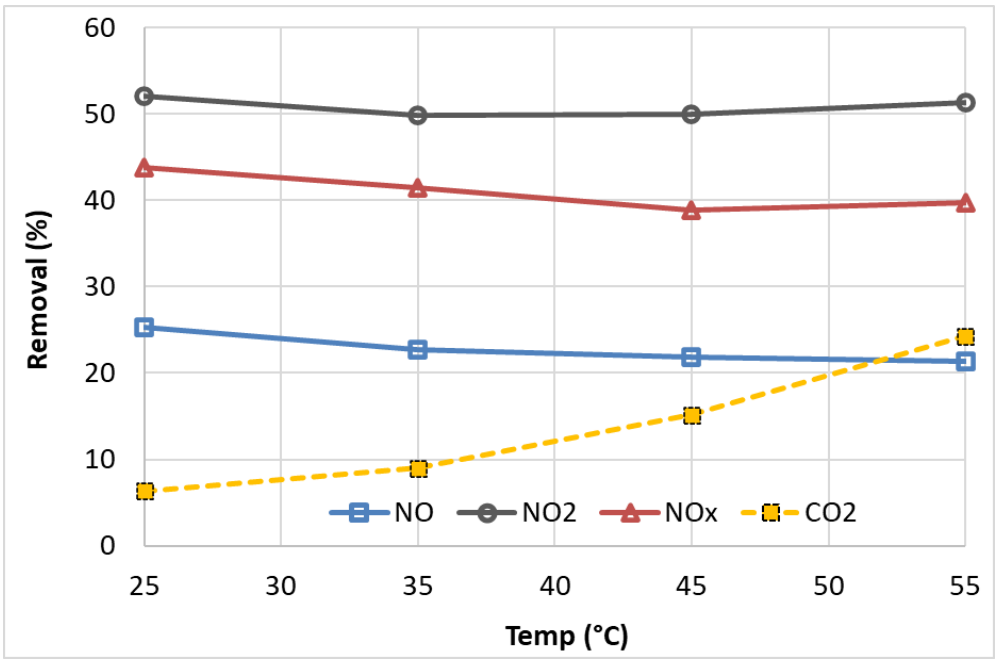

Figure 6-38: Removal of NO, NO_2, NO_x and CO_2 with variation of reaction temperature in the reducing half-height wet scrubber.
Experimental conditions described in Table 6-2 (Set 11).

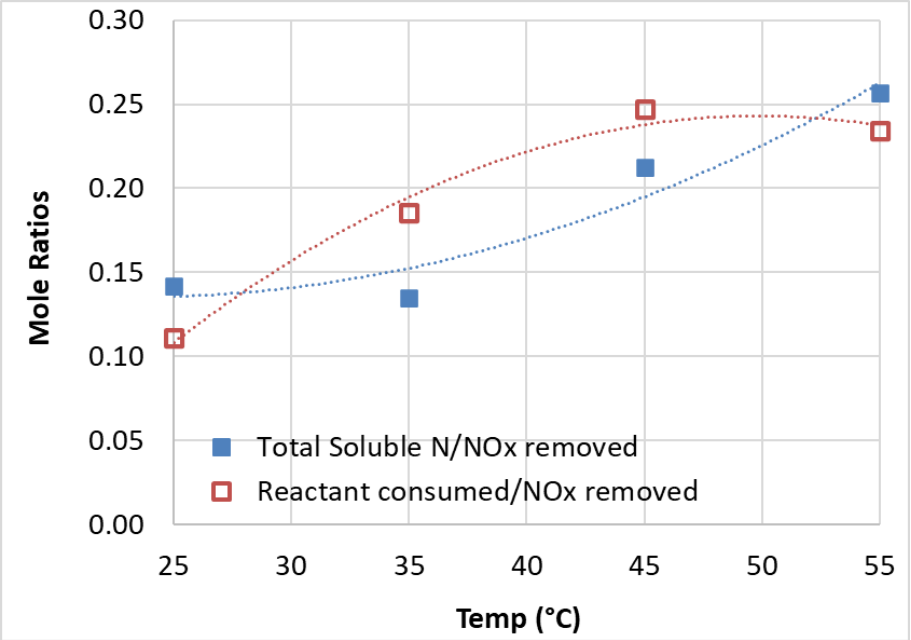

Figure 6-39: The mole ratios of soluble nitrogen formed over total NO_x removed, and reactant (thiosulfate) consumed over pollutant (NO_x) removed, as the reaction temperature was varied in the reducing half-height wet scrubber.
Experimental conditions described in Table 6-2 (Set 11).

In the aqueous phase of the reducing half scrubber, increase of temperature caused more soluble nitrogen to be formed for every mole of NO_x removed (Figure 6-39). This was consistent with the thermodynamic modelling results in Section 6.2.3, as discussed previously. A similar increase in the formation of soluble nitrogen in the aqueous phase was also observed by Zhang and co-researchers during the removal of NO_2, when the reaction temperature was increase from 40°C to 60°C (Zhang *et al.*, 2022b).

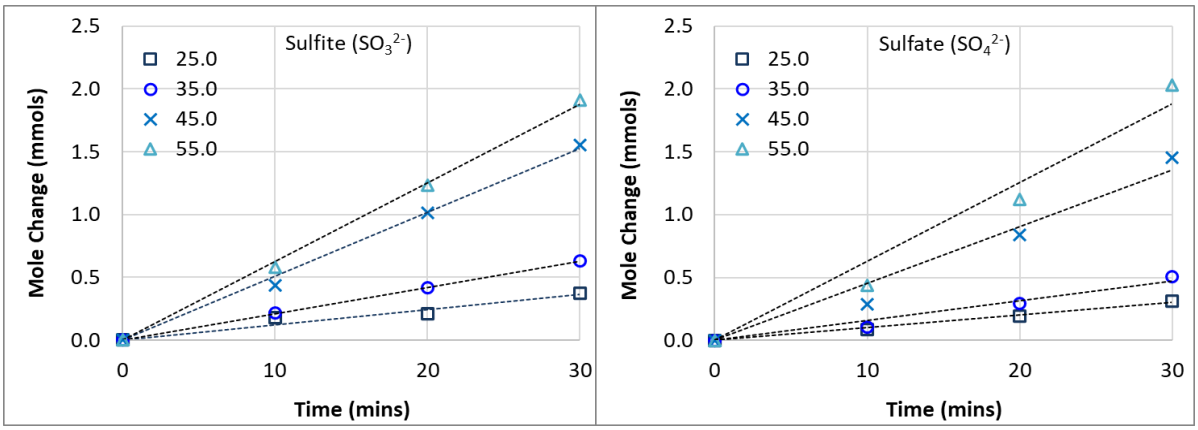

Figure 6-40: Formation of sulfites and sulfates during reaction in the reducing half-height wet scrubber, with variation in reaction temperature.
Experimental conditions described in Table 6-2 (Set 11).

As for reactant consumption, it can be seen that the increase of temperature also increased the mole ratio of thiosulfate consumption per mole of NO_x removed. This could possibly be due to the decomposition of thiosulfate to form sulfites and sulfates, as described in Equations 5.11 and 5.12. This decomposition was not significant at lower temperatures but increased when the reaction temperatures were raised (Figure 6-40). Nevertheless, even with increasing soluble nitrogen formation and reaction consumption due to rising temperatures, the mole ratios for these values per mole of NO_x removed were still quite low and were well within 0.30 at 55°C.

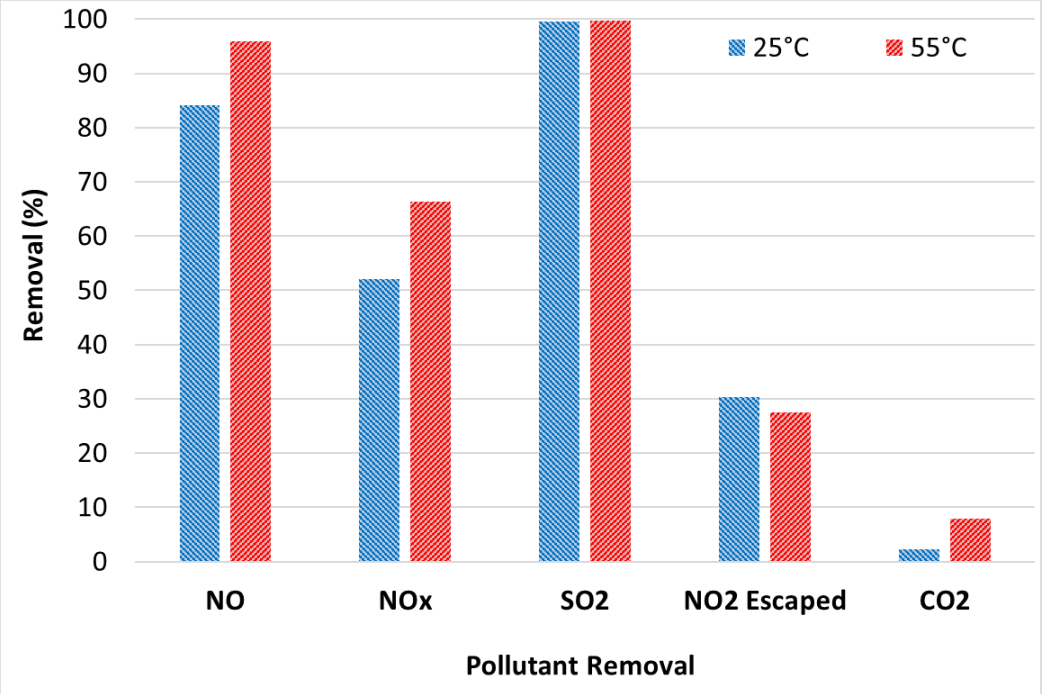

Figure 6-41: Gaseous pollutant removal carried out by the oxidation/reduction full height wet scrubber, with comparison between reaction temperatures of 25°C and 55°C.
Experimental conditions described in Table 6-2 (Sets 12).

The reaction carried out using the full height wet scrubber with oxidation/reduction configuration were compared at 25°C and 55°C and the results are shown in Figure 6-41. It can be seen that the increase of temperature improved the removal of NO and reduced the NO_2 escaping, thereby increasing the overall NO_x removal by about 14.3%. No change was observed in SO_2 removal. As discussed previously, this was likely due to the increase of mass transfer diffusion and chemical reaction rates exceeding the loss of solubility due to temperature increase in the oxidation half of the scrubbing system. Removal of CO_2 also increased with increasing temperature due to the additional NaOH dosing needed to maintain the pH at 12 at the reducing half of the scrubbing system when the temperature was elevated, as discussed previously.

In the aqueous phase, increases were seen in soluble nitrogen formed (30%) and reactant consumed (19%) when the temperature was increased (Figure 6-42). The magnitude of these increases was consistent with the adding up of the individual changes observed from the oxidation and reduction sections when temperature was increased. The increase of soluble nitrogen formed in the aqueous phase was likely contributed by both the oxidation and reduction sections while the increase in reactant consumption was mainly contributed by the reduction section of the scrubber.

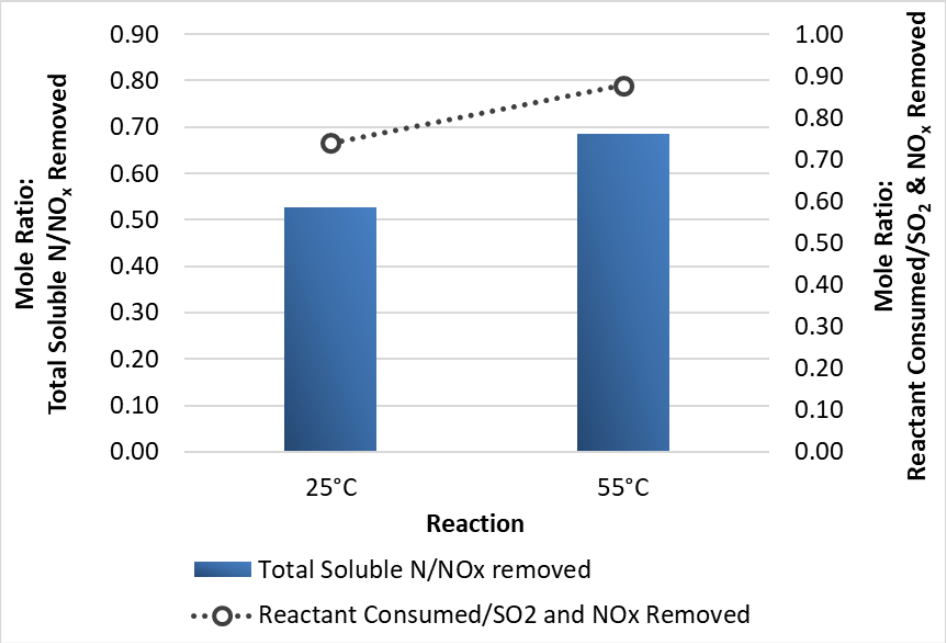

Figure 6-42: The mole ratios of soluble nitrogen formed over total NO_x removed, and reactant consumed over gaseous pollutant (SO_2 & NO_x) removed, using the full height wet scrubber with oxidation and reduction configuration, with comparison between reaction temperatures of 25°C and 55°C.
Experimental conditions described in Table 6-2 (Sets 12).

6.8. Considerations for scrubber washwater discharge in the ocean

As mentioned earlier, one of the main issues preventing any discharge of liquid wastewater from the scrubber into the ocean is the high nitrate content. In order to consider whether the wastewater from the scrubber system proposed here is suitable for ocean discharge, a simple calculation was carried out and shown in Appendix C. The premise for this theoretical consideration is to linearly scale up the oxidation and reduction scrubber system to scrub the exhaust of a slow-speed, 2-stroke, large diesel engine, based on the experimental data obtained here. Although soluble nitrogen in water consists of both nitrites and nitrates, it was assumed that all nitrites will eventually be oxidised into nitrates over time in the natural environment.

The typical washwater discharge from commercial freshwater closed-loop scrubbers utilising chemicals to scrub SO_2 from in ships typically range from 0.1 – 0.3 m^3/MWh – the upper limit of this range was used in this calculation here (*Exhaust Gas Scrubber Washwater Effluent*, 2011).

It can be seen that the nitrate discharge limit of 60mg/l (normalised for a washwater discharge rate of 45 tons/MW discharge) translates to 1,804 mols of nitrate per hour. The rate of nitrate accumulation in the reducing half's scrubbing liquid was at 1,306 mols/hour, below the permissible rate of nitrate discharge. This implies that the washwater from the reducing half of the scrubber can be discharged on a continuous basis without exceeding the regulatory limit. In the scrubbing liquid of the oxidation half, nitrates accumulated at a faster rate than the allowed nitrate discharged rate, so ocean discharge alone cannot be relied on entirely. However, partial discharge of the washwater from the oxidation half is still possible, by mixing it with a portion of washwater from the reducing half. This would also help to cancel out the high and low oxidation potential of the oxidizing and reducing scrubbing liquids to a more moderate level suitable for ocean discharge.

This system can be further optimised to reduce the rate of soluble nitrogen forming in the scrubbing liquid, thereby allowing for more of the washwater to be discharged to the ocean on a continuous basis. It should also be noted although nitrate discharge is regulated because of its potential to cause algae blooms in the ocean, its tendency to do so in the open seas is low due to the lack of phosphorus there (*EGCSA Handbook 2012: A practical guide to exhaust gas cleaning systems for the maritime industry*, 2012). However, since phosphorus is more abundant in parts of the sea that is closer to shore, concern of algae blooms due to nitrate discharge in those areas are certainly not overstated.

6.9. Mass balance considerations

In this section, the mass balance of the species entering and leaving the system were analysed, in particular for chlorine, sulfur and nitrogen, for the experiments carried out in this chapter. This was carried out to check for discrepancies and to better understand the wet scrubber system.

6.9.1. Chlorine balance

Chlorine entered the wet scrubber in the form of ClO_2^- in the aqueous phase as the main oxidant. After reaction, Cl^-, ClO_2 (aq), ClO^- and ClO_3^- would be formed. In this set of data, all of these compounds were quantified at various reaction times except for ClO^-. However, the formation of hypochlorite as a by-product was expected to be small, similar to ClO_3^- which was less than

5% of total chloride. The data for chlorite consumed and soluble chlorine-based compounds formed (minus hypochlorite) is shown in Figure 6-43, with the gradients of the trendlines displayed as well. Data from the half-height reduction scrubber setup was left out as there was no chlorite input.

For chlorine compounds to be perfectly accounted between input and output, the gradient of the linear trendlines should be near to 1, since 1 mol of chlorite will form 1 mol of any of the chlorine-based products . It can be seen from the gradients of the linear trendlines in Figure 6-43 that around 22 – 28% of chlorine was unaccounted for. The fact that hypochlorite was left out would not account for this missing chlorine as the amount of this by-product formed was expected to be low. The missing chlorine compound could have been due to its losses in the form of ClO_2 which had partitioned into the gas phase and exited into the atmosphere along with the exhaust gas. The gradients obtained for the different scrubber configurations were quite similar, indicating consistency in the chlorine-related reactions across the system.

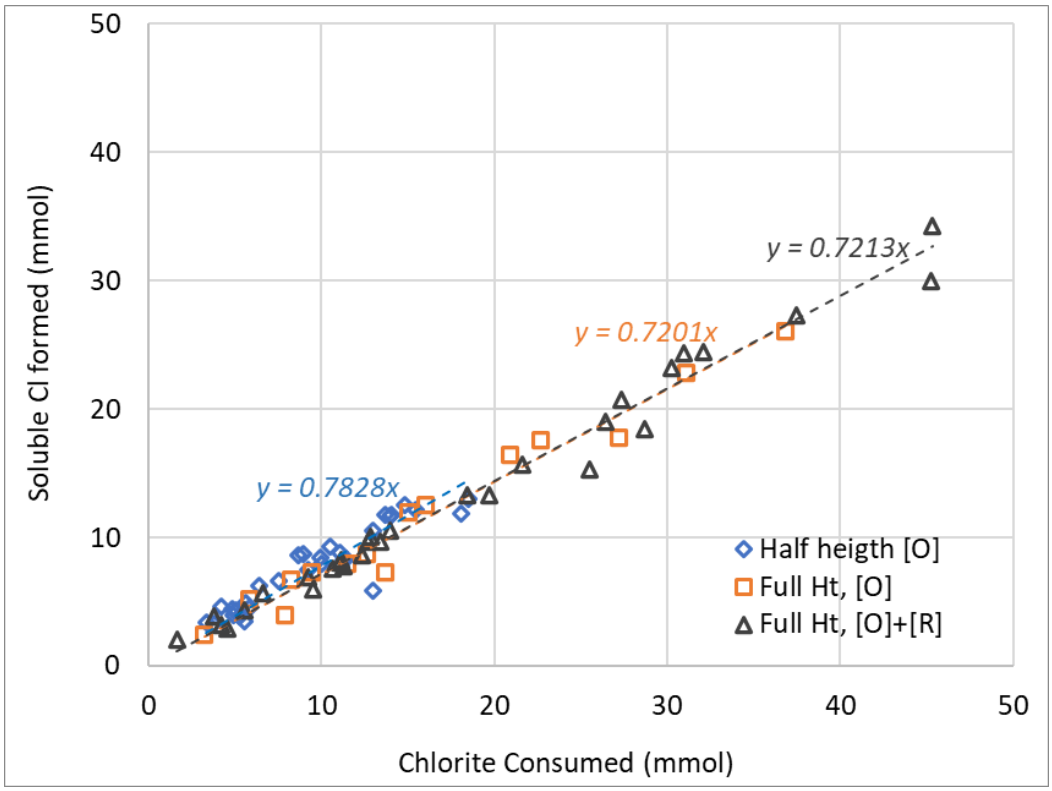

Figure 6-43: Chlorite consumed (in) versus soluble chlorine compounds formed in the aqueous phase (out).

6.9.2. Nitrogen balance

The nitrogen element entered the system as NO_x gas and formed nitrites and nitrates in the aqueous phase and N_2 in the gas phase. The experimental data for the removal of NO_x was plotted against the soluble nitrogen formed in the aqueous phase and shown in Figure 6-44.

As 1 mol of NO_x would form 1 mol of either nitrite or nitrate anion, the gradient of the respective trendlines would be 1 if none were reduced to N_2, which cannot be measured directly because its amount is small compared to the N_2 present in the bulk simulated exhaust gas. Unlike the case of chlorine mass balance which had similar gradients for the various wet scrubber configurations, the nitrogen balance gradients were quite dissimilar among different setups. The setups with the highest linear trendline gradients were for the half-height and full-height oxidation only wet scrubber configurations. This was because these two setups would have the least amount of N_2 formed from the reduction of NO_2, owing to the high redox potential environment in their aqueous phase. The gradient of the full height oxidation/reduction wet scrubber configuration was in the middle while the half-height scrubbers with reduction only had the lowest gradient. Comparing the half-height configuration with reduction only, the gradient obtained when thiosulfate was used was lower compared to sulfite, confirming an earlier observation that the former was more effective in reducing NO_2 to the harmless N_2 (Section 6.4.4).

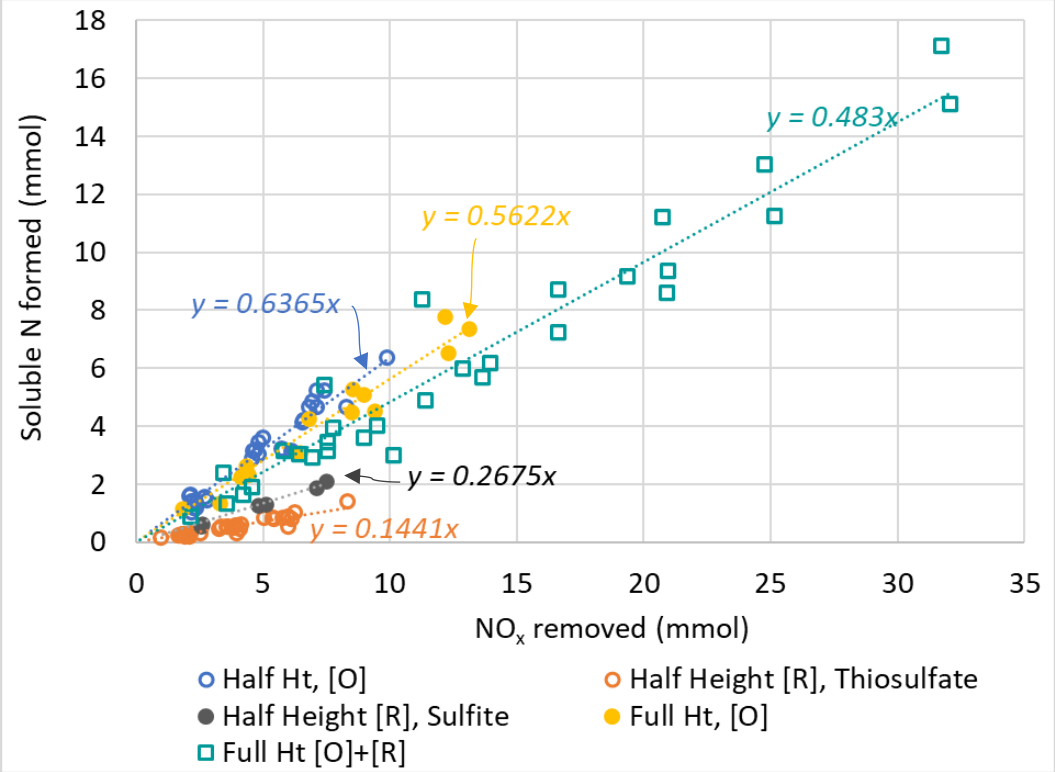

Figure 6-44: NO_x removed (in) versus soluble nitrogen compounds formed in the aqueous phase (out).

6.9.3. Sulfur balance

The sulfur element entered the system as SO_2 gas and formed sulfites and sulfates in the aqueous phase. The experimental data for the removal of SO_2 were plotted against the amount of soluble sulfur formed in the aqueous phase and shown in Figure 6-45. It can be seen that the respective gradients of the linear trendline from the various scrubber configurations were in the region of 1. This was because each mole of SO_2 removed resulted in the formation of either 1 mol of SO_3^{2-} or SO_4^{2-}. This was unlike the case of chlorine or nitrogen where losses occurred in the system when $ClO_2(g)$ or $N_2(g)$ were formed and escaped into the atmosphere without being detected.

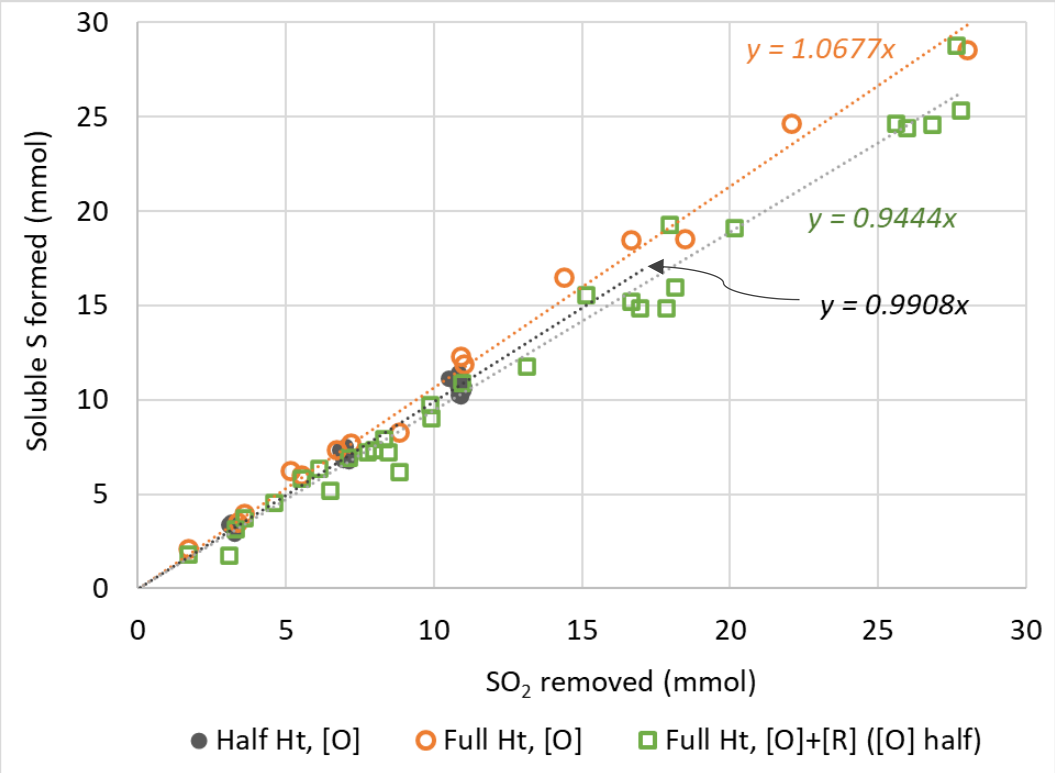

Figure 6-45: SO_2 removed (in) versus soluble sulfur compounds formed in the aqueous phase (out).

6.10. Summary

The experimental results demonstrated that a wet scrubbing process comprising of an oxidation and a reducing section arranged in series can be a viable option for the simultaneous removal of SO_2 and NO in ship exhaust gas. This configuration showed clear advantages in comparison with other wet scrubbing processes being studied, in terms of a having less soluble nitrogen formed (especially nitrates) and a low reactant consumption rate. Partial wastewater discharge in the ocean is also possible as the washwater from the reducing half of the wet scrubber has significantly less soluble nitrogen formed and can be discharged to the ocean on a continuous basis without the need for nitrate removal. Portions of the washwater from the oxidation and

reducing halves can be mixed to adjust the oxidation potential before discharge. Partial removal of CO_2 from the exhaust gas was also achieved.

Typically, the usage of chlorine-based oxidants may result in accidental release of chlorine dioxide or chlorine gas from the wet scrubber exhaust. However, this configuration prevents accidental release of dangerous gaseous compounds as any active chlorine escaping in the gaseous phase from the oxidation half will be removed in the reducing half of the wet scrubber, preventing any accidental discharge into the atmosphere. To improve the gas-liquid mass transfer, the addition of packing materials in the reducing half of the wet scrubber should also be viable without causing a significant pressure drop as most of the particulate matter in the exhaust would have been removed in the oxidation half.

Although the usage of a reducing agent such as sodium sulfide or sodium sulfite for the removal of NO_2 gas has been studied extensively before, sodium thiosulfate has rarely been considered as a viable reducing agent for this gaseous pollutant removal. Unlike sodium sulfide, it is not hazardous. It also does not require the addition of hazardous or environmentally dangerous substances such as formaldehyde or hydroquinone to stabilise it (like in the case of sodium sulfite). The results here showed the precipitation issue of thiosulfate due to the formation of sulfur can be avoided by increasing the operating pH to 12. At this pH, the by-product formed was sulfate ions, thereby requiring just a simple pH adjustment before discharge to the ocean, if necessary. The results here showed that thiosulfate consumption per mole of gaseous pollutant removed is very low, owing to its high stability. The reactant consumed is about 118 times less than sulfite or 27 times less than formaldehyde-stabilised sulfite.

It was seen that the thermodynamic modelling results obtained were largely in agreement with the experiment results conducted. Amongst other things, it was learnt that under low redox potential ($E_h > 0V$), the pH of the aqueous phase should be above 8 to avoid the formation of H_2S and 8.4 to avoid the precipitation of sulfur. However, increasing the pH would also favour the formation of soluble nitrogen in the aqueous phase instead of N_2 gas when NO_x was removed. Therefore, balance need to be struck between these competing interests.

Finally, a mass balance analysis was performed between the input and output in both the gaseous and liquid phases. The analysis showed that Cl and N-based compound were likely lost in the system in the form of ClO_2 (g) and N_2 gas as they could not be quantified, while S-based compound were fully accounted for by quantitative analysis in the input and output of the system.

Chapter 7. Reaction kinetics and mass transfer considerations

7.1. Reaction kinetics considerations

The oxidation, reduction and absorption of SO_2 and NO with sodium chlorite and sodium thiosulfate turned out to be a very complicated process, with multiple independent or competing reactions occurring concurrently. Although it is difficult to calculate the rate constant of each reaction due to this complexity, certain important information about the nature of reactions that took place here could still be obtained through the analysis of the experimental results from the kinetics point of view.

7.1.1. Wet scrubbing with oxidation

In this section, the experimental data for the use of sodium chlorite as the oxidant to remove SO_2 and NO in the half height wet scrubber configuration was analysed (Section 6.2). In order to simplify this complicated system, all reactions were lumped together into a single equation shown in Equation 7.1, although it is known that there were various different types of reactions occurring simultaneously as previously discussed.

$$a\mathrm{ClO_2^-(aq)} + b\mathrm{SO_2(g)} + c\mathrm{NO(g)} \rightarrow d\mathrm{Cl^-} + e\mathrm{NO_2^-} + f\mathrm{NO_3^-} + g\mathrm{N_2(g)} + h\mathrm{SO_3^{2-}} + i\mathrm{SO_4^{2-}} \quad \ldots (7.1)$$

The integers *a* to *i* represent the unknown coefficients of the various reactants. For the case of the oxidation in the half height wet scrubber, the *L/G* ratio was kept constant for all the experimental runs carried out. Therefore, it can be assumed that the mass transfer rate occurring between the gas-liquid boundaries were similar for all runs and the difference in the reaction rates were purely attributed to the reaction kinetics.

The rate of reaction can be represented by the rate of change of the main chlorite oxidant, as shown in Equation 7.2 (Brady *et al.*, 2000):

$$Rate = -\frac{d[ClO_2^-]}{dt} = -\frac{d[SO_2]}{dt} = -\frac{d[NO]}{dt} = k_1[ClO_2^-]^x[SO_2]^y[NO]^z \quad \ldots (7.2)$$

where k_1 refers to the rate constant and *x*, *y* and *z* refers to the exponents of ClO_2^-, SO_2 and NO respectively. Here, it was also assumed that the reaction between the chlorite oxidant with SO_2 and NO gases were more substantial than the subsequent reaction with NO_2 gas was formed – therefore NO_2 was not featured in the reaction equations here. Also, it was assumed that CO_2 did not interact with the chlorite oxidant but was removed purely by the alkalinity of water.

i) Variation of chlorite starting concentration

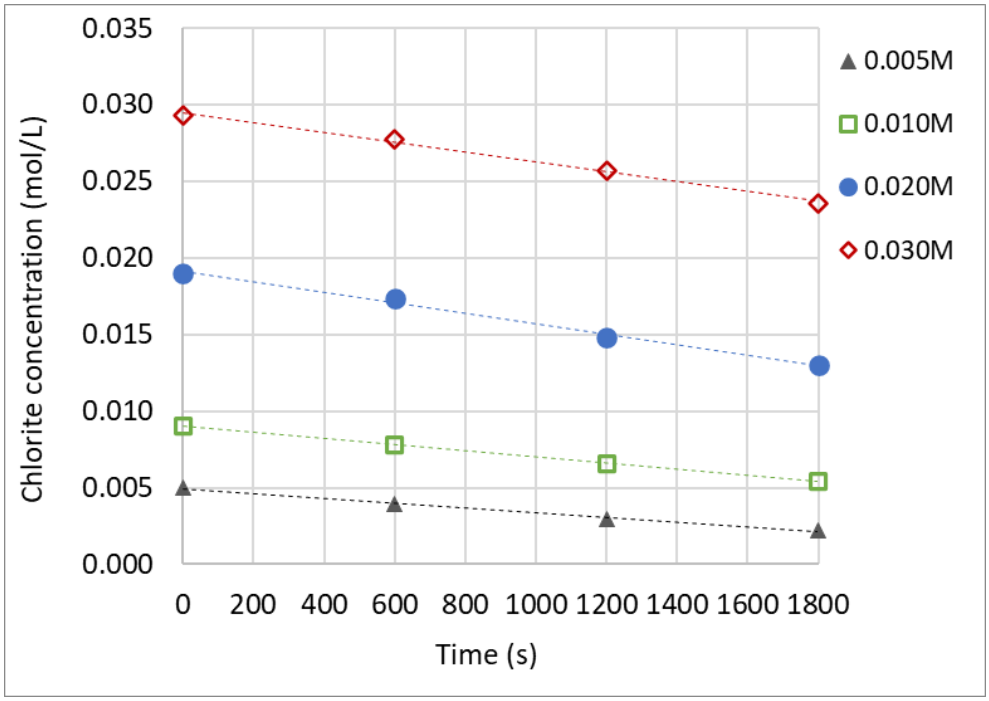

Figure 7-1: Chlorite concentration in the aqueous phase with time, in the half height oxidation wet scrubber, with variation in chlorite starting concentration.
Experimental conditions described in Table 6-2 (Set 2).

The graph of chlorite concentration versus time for the reaction carried out in the half height wet scrubber configuration in shown in Figure 7-1, with variation in the starting chlorite concentration. It is known that the change of reactant concentration with time can be an indication of the order of the reaction, for reactions that are zero order with respect to a reactant will usually have a linear trend, while first and second order reactions will usually show up as a continuously diminishing curve that eventually reaches a horizontal plateau (Brady *et al.*, 2000). As the concentration of chlorite with time appeared to linear, the reaction shown in Equation 7.2 was assumed to be zero order, i.e., the exponents *x*, *y* and *z* are all zero, then the following is obtained:

$$Rate = -\frac{d[ClO_2^-]}{dt} = k_1 \qquad \ldots (7.3)$$

where k_1 has a unit of mol/L.s. Rearranging and integrating both sides of the above equation will yield the following:

$$\mathrm{d}[\mathrm{ClO_2^-}] = -k_1 \mathrm{dt}$$

$$\int_{[ClO_2^-]_0}^{[ClO_2^-]_t} d[ClO_2^-] = -\int_{t_0}^{t} k_1 dt$$

where $[ClO_2^-]_0$ is the initial concentration of chlorite at time 0 and $[ClO_2^-]_t$ is the chlorite concentration at time *t*.

$$[ClO_2^-]_t - [ClO_2^-]_0 = -k_1 t$$

$$[ClO_2^-]_t = -k_1 t + [ClO_2^-]_0 \qquad \ldots (7.4)$$

It can be seen that Equation 7.4 is a linear equation ($y = mx + c$), with $[ClO_2^-]_t$ as the *y*-axis, $-k_1$ being the gradient of the slope, *t* being the *x*-axis and $[ClO_2^-]_0$ as the *y*-intercept, proving that the concentration of chlorite with time would appear to be linear if the reaction is zero order. In order to check for the degree of linearity, linear trendlines were added for the various chlorite concentrations shown in Figure 7-1 and their linear equations, linear regression value (R^2) and rate of reaction, k_1 are shown in Table 7-1. From the table, it can be seen that the R^2 values for the various concentrations showed a high degree of linearity (>0.99), suggesting that the data fitted a straight line and this reaction was indeed zero order.

Table 7-1: The linear equations, linear regression values (R^2) and reaction rate constants obtained from adding a linear trendline to the chlorite concentration versus time graph in Figure 7-1, with variation in starting chlorite concentration.

$[ClO_2^-]_0$ (M)	Equation	R^2	k_1 (mol/L.s)
0.005	*y = -1.58E-06x + 0.0049*	0.9924	1.585×10^{-06}
0.010	*y = -2.00E-06x + 0.0090*	0.9999	2.001×10^{-06}
0.020	*y = -3.43E-06x + 0.0191*	0.9945	3.431×10^{-06}
0.030	*y = -3.20E-06x + 0.0294*	0.9948	3.208×10^{-06}

It was shown in previous sections that the oxidation of NO gas was dependent on the concentration of the sodium chlorite reaction, with higher oxidant concentration resulting in higher NO oxidation (Section 6.3.2). This seemingly contradicts with the observation here that the reaction depicted in Equation 7.1 is zero order with respect to the sodium chlorite oxidant. This complication is most probably due to the tendency of chlorite reactant to decompose to ClO_2, its more reactive form (via Equations 4.15 and 4.16).

As the results shown here were carried out at a high pH of 10, the chlorite reactant would be quite stable and the fraction of ClO_2 would be small in the bulk liquid, possibly only increasing in concentration as an intermediate near the gas-liquid interface when it came into contact with the acidic gas. A check on the concentration of ClO_2 at pH 10 showed that its concentration

remained below 2% in the bulk liquid throughout the entire reaction (Figure 7-2). In all likelihood, the small fraction of the reactive ClO_2 would continue to be replenished from the larger pool of chlorite as the reaction progressed. This would give the appearance that the reaction was independent of the concentration of chlorite oxidant.

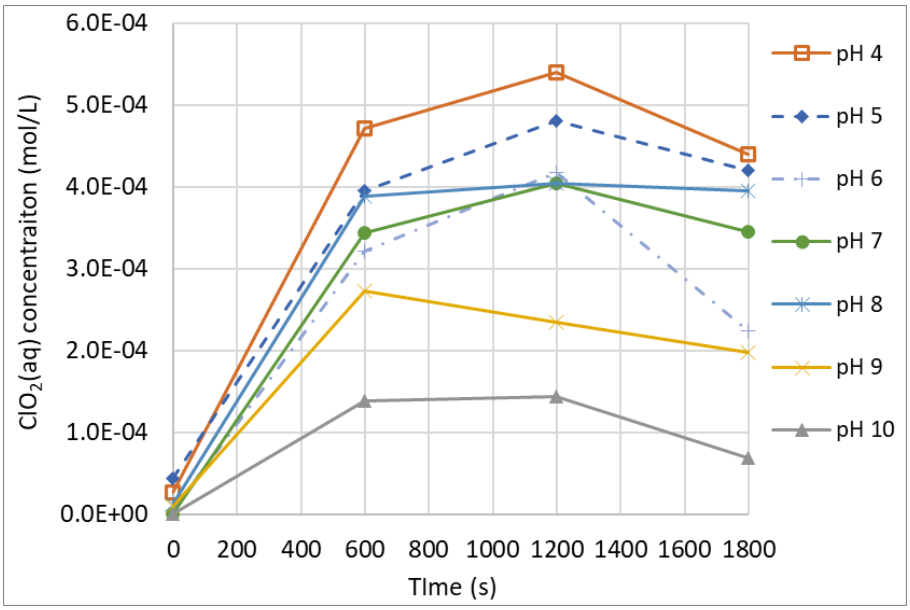

Figure 7-2: Concentration of ClO_2 in the scrubbing liquid with time, in the half-height oxidation wet scrubber, with variation in pH.
Experimental conditions described in Table 19 (Set 1).

As for the other two reactants in the system, SO_2 and NO were not only present at much greater concentrations compared to the chlorite oxidant but was also supplied into the system at a fix concentration and on a continuous basis, making them constantly replenished throughout the entire duration of the experiment. It is known that reactions would typically appear to be zero-order for reactants that are present in greater excess (Brady *et al.*, 2000). The reaction would therefore also appear to be zero order with respect to SO_2 and NO.

Although the reaction depicted in Equation 7.1 appeared to be zero order and therefore independent of the actual chlorite concentration during reaction, it was dependent on the *starting* chlorite concentration ($[ClO_2^-]_0$ at t = 0s). From Table 7-1, it can be observed that the reaction rates, k_1, obtained from the gradients of the linear equations were different for the different staring chlorite concentrations.

A plot of the reaction rate obtained from the zero-order reaction rate constant (k_1) versus starting chlorite concentration showed that the reaction rate increased with increasing starting chlorite concentration (Figure 7-3). The equation defining this relationship between the reaction rate and starting chlorite concentration was derived and shown in Equation 7.5.

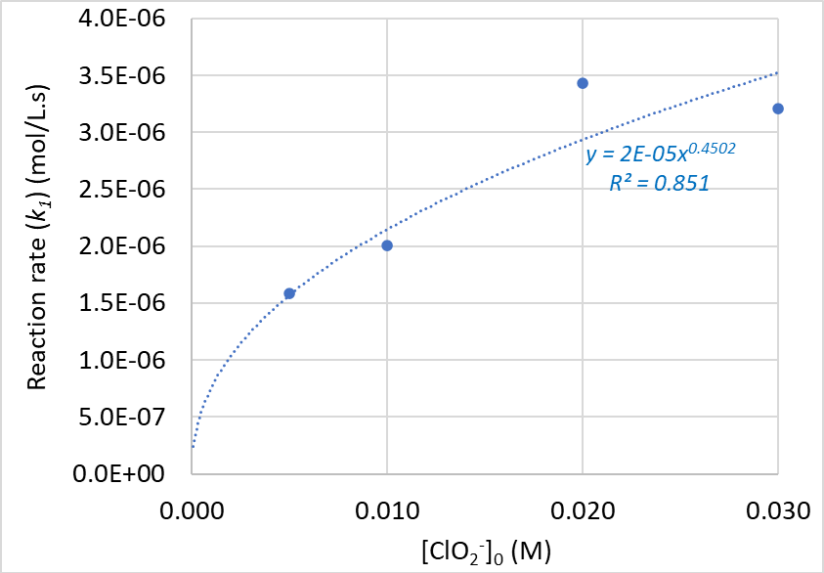

Figure 7-3: Overall reaction rate obtained from the rate constant, k_1, with variation in starting chlorite concentration, assuming zero-order reaction.
Experimental conditions described in Table 19 (Set 2).

Based on the limited data points available here, the relationship possibly followed the power equation showed in Equation 7.5. However, as the R^2 value was not optimal due to limited data points, having more data points would improve the accuracy of this predictive relationship.

$$k_1 = 2E^{-05}[ClO_2^-]_0^{0.4502} \qquad \dots (7.5)$$

In a final validation, the rates of SO_2, NO and NO_2 removal were derived (Table 7-2) in order to compare them with the reaction rates obtained from the zero-order assumption used. For ease of comparison, this set of data was plotted together with the reaction rate of chlorite obtained previously and shown in Figure 7-4.

Table 7-2: The rate of change of NO, NO_2 and SO_2 removal with variation of starting chlorite concentration.
Experimental conditions described in Table 6-2 (Set 2). Refer to Appendix D for more details in calculation methods used.

$[ClO_2^-]_0$ (M)	$\frac{d[NO]}{dt}$ (mol/L.s)	$\frac{d[NO_2]}{dt}$ (mol/L.s)	$\frac{d[SO_2]}{dt}$ (mol/L.s)
0.005	2.17×10^{-06}	1.40×10^{-06}	2.52×10^{-06}
0.010	2.71×10^{-06}	1.47×10^{-06}	2.61×10^{-06}
0.020	3.97×10^{-06}	2.38×10^{-06}	2.62×10^{-06}
0.030	3.76×10^{-06}	2.00×10^{-06}	2.61×10^{-06}

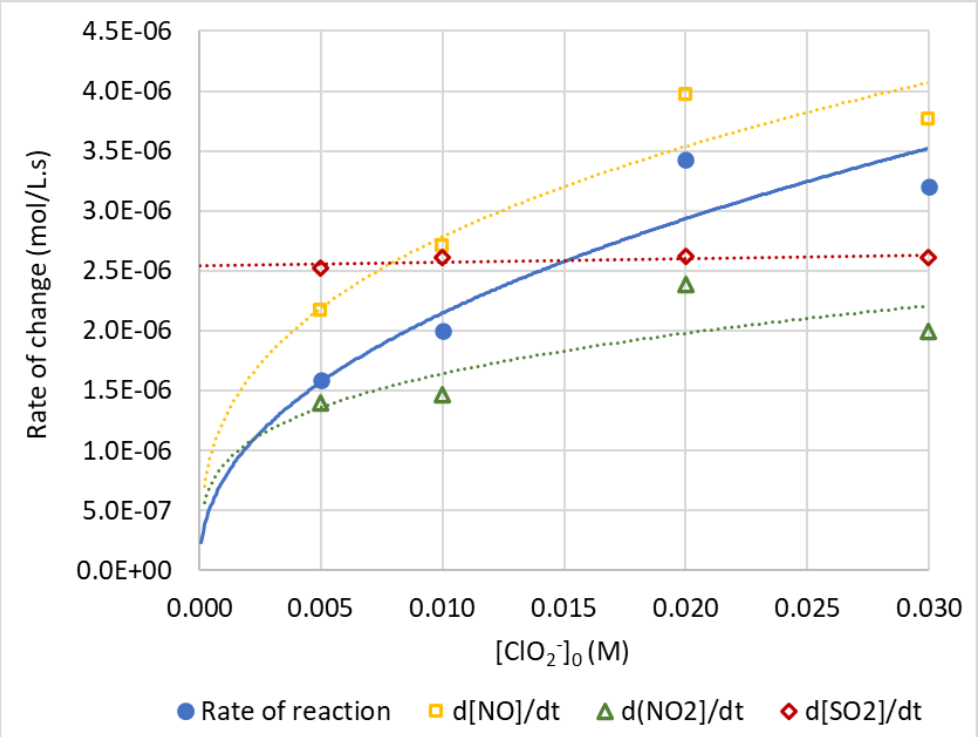

Figure 7-4: The rate of change of NO, NO_2 and SO_2, compared with the calculated reaction rate, with variation of starting chlorite concentration. *Experimental conditions described in Table 19 (Set 2).*

It can be seen that the rate of change of NO and NO_2 removal followed the trend displayed by the overall reaction rate obtained from the change of chlorite concentration while the rate of change of SO_2 removal seemed to be linear and independent of the starting chlorite concentration. This was so because SO_2 can be removed by physical absorption and the alkalinity of in the water. The contribution of chlorite in oxidising the HSO_3^- and SO_3^{2-} that were formed in the absorption process to SO_4^{2-} was probably minimal compared chlorite consumption by NO. Similarly, it is known from previous discussion (Section 4.2.3, Part C) that more NO_2 was removed by its absorption with water (Equations 4.7 and 4.8) instead of reacting with chlorite (Equations 4.25 and 4.26). Due to these reasons, it can be reasonably stated that chlorite was chiefly utilised for the oxidation of NO.

Bearing in mind the stoichiometric of the reaction (Equations 4.18 and 4.19) where 1 mol of chlorite can oxidise anywhere from 1 to 2 mols of NO, it can be seen from Figure 7-4 that the reaction rate obtained from this exercise fell within expectation when comparing with the rate of NO removal ($\frac{d[NO]}{dt}$). Therefore, it can be concluded that the assumptions made in calculating the reaction rate based on chlorite consumption were reasonable.

Due to the fact that SO_2 and NO_2 were mainly absorbed by water and hydroxide ions without significant consumption of chlorite, the overall Equation 7.2 for chlorite removal of SO_2 and NO could more accurately be rewritten as follows:

$$Rate = -\frac{d[ClO_2^-]}{dt} = -\frac{d[NO]}{dx} = k_1[ClO_2^-]^x[NO]^z$$

$$Rate = -\frac{d[ClO_2^-]}{dt} = -\frac{d[NO]}{dx} = k_1 \quad \ldots (7.6)$$

where the reaction rate, k_1, is dependent on the starting concentration of chlorite, $[ClO_2^-]_0$.

ii) Variation of chlorite pH

The change of chlorite concentration in the aqueous phase with time during the experiment carried out with variation of pH values was examined (see Figure 7-5). Using the zero-order assumption in accordance with the previous discussion, and the overall reaction rate can be represented by Equation 7.6. Linear trendlines were added to the experimental data in Figure 7-5 and the linear equations, linear regression value (R^2) and reaction rate constant, k_{pH} were derived and shown in Table 7-3. From the table, it can be seen that the R^2 values for the various concentrations displayed a decent degree of linearity, as expected.

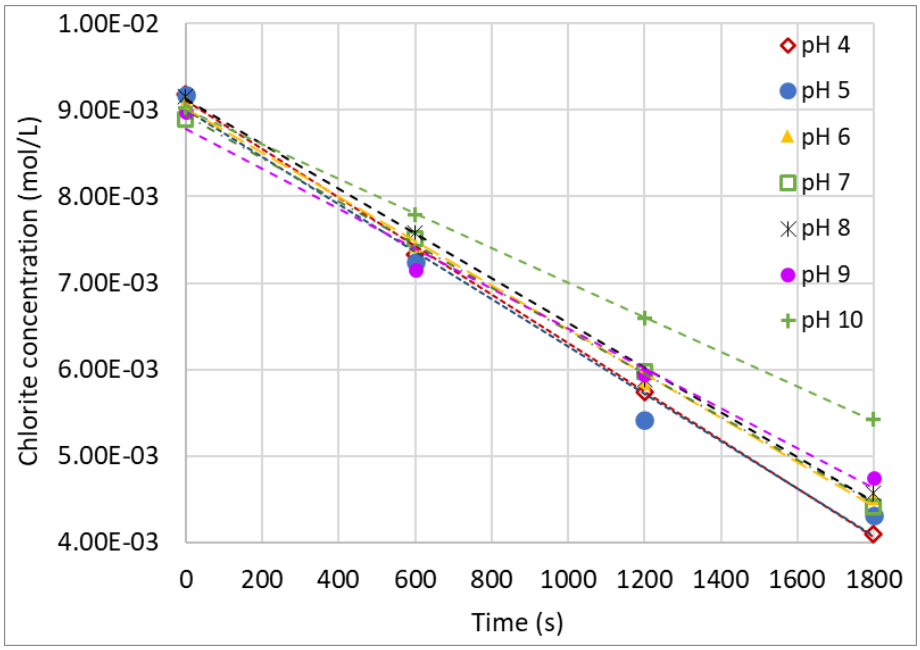

Figure 7-5: Chlorite concentration in the aqueous phase with time, in the half height oxidation wet scrubber, with variation in pH.
Experimental conditions described in Table 6-2 (Set 1).

Table 7-3: The linear equations, linear regression values (R^2) and reaction rate constants obtained from adding a linear trendline to the chlorite concentration versus time graph in Figure 7-5, with variation in pH.

pH	Equation	R^2	k_{pH}
4	*y = -2.804E-06x + 0.009114*	0.9988	2.804 x 10^{-06}
5	*y = -2.736E-06x + 0.009001*	0.9860	2.736 x 10^{-06}
6	*y = -2.554E-06x + 0.009018*	0.9975	2.554 x 10^{-06}
7	*y = -2.492E-06x + 0.008944*	0.9992	2.492 x 10^{-06}
8	*y = -2.578E-06x + 0.009118*	0.9974	2.578 x 10^{-06}
9	*y = -2.312E-06x + 0.008787*	0.9879	2.312 x 10^{-06}
10	*y = -2.001E-06x + 0.009008*	0.9999	2.001 x 10^{-06}

For validation purposes, the rates of SO_2, NO and NO_2 removal were derived (see Table 7-4) in order to compare them with the reaction rates calculated here. For ease of comparison, this set of data was plotted together with the calculated reaction rates obtained from the reaction rate constant, k_{pH}, and shown in Figure 7-6. It was known from previous discussion that the chlorite oxidant was chiefly consumed by the oxidation of NO to NO_2. From the figure, it can be seen that the trend of the calculated reaction rate was fell within expectation when compared to the rate of change of NO removal, suggesting that the approached use and assumptions made were reasonable.

Table 7-4: The rate of change of NO and SO_2 removal with variation of liquid pH.
Experimental conditions described in Table 6-2 (Set 1). Refer to Appendix D for more details in calculation methods used.

pH	$\frac{d[NO]}{dt}$ (mol/L.s)	$\frac{d[NO_2]}{dt}$ (mol/L.s)	$\frac{d[SO_2]}{dt}$ (mol/L.s)
4	3.552 x 10^{-06}	1.789 x 10^{-06}	2.636 x 10^{-06}
5	3.502 x 10^{-06}	1.708 x 10^{-06}	2.599 x 10^{-06}
6	3.398 x 10^{-06}	1.667 x 10^{-06}	2.651 x 10^{-06}
7	3.379 x 10^{-06}	1.639 x 10^{-06}	2.605 x 10^{-06}
8	3.412 x 10^{-06}	1.713 x 10^{-06}	2.645 x 10^{-06}
9	3.186 x 10^{-06}	1.590 x 10^{-06}	2.621 x 10^{-06}
10	2.709 x 10^{-06}	1.470 x 10^{-06}	2.611 x 10^{-06}

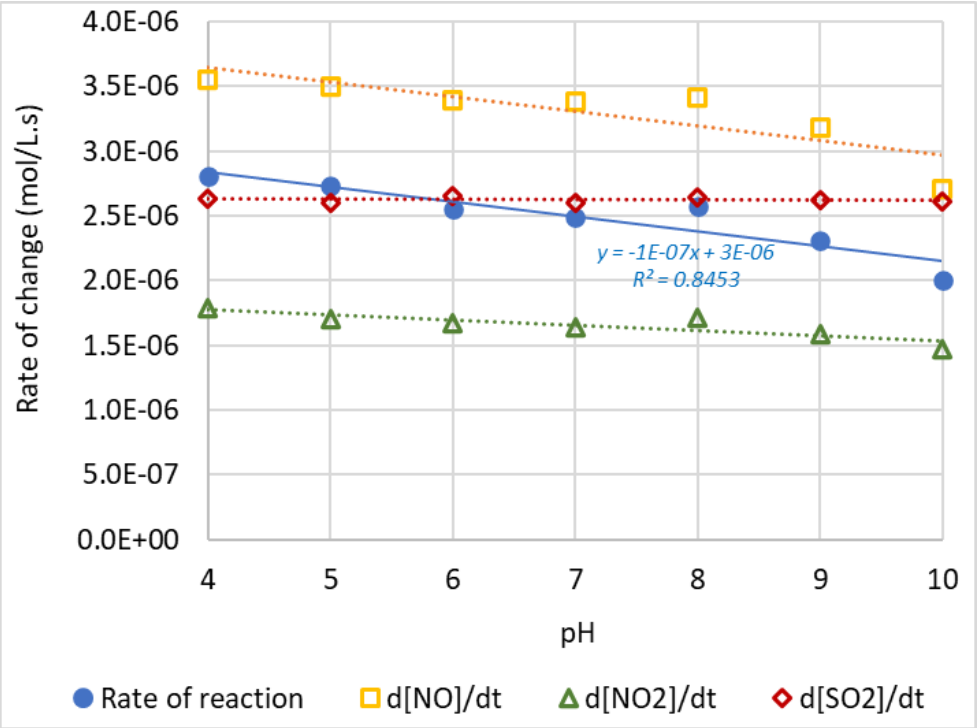

Figure 7-6: The rate of change of NO, NO_2 and SO_2 compared with the calculated reaction rate, with variation of pH.
Experimental conditions described in Table 19 (Set 1).

Additionally, it can be seen that an increase of liquid pH resulted in the lowering of all rates of change, except for SO_2. This was because chlorite decomposition to the reactive ClO_2 decreased with increasing pH, as discussed previously and also consistent with experimental observation (Figure 7-2). On the other hand, the rate of change of SO_2 had minimal change with pH – it was not dependent on the ability of chlorite to form ClO_2 and its removal was based on physical absorption due its high solubility in water.

The relationship between the reaction rate constant with pH can be predicted by the following equation:

$$k_{pH} = 1.154 \times 10^{-7}[pH] + 3.3045 \times 10^{-6} \qquad \dots (7.7)$$

7.1.2. Wet scrubbing with reduction

In this section, the experimental data of the half scrubber with reduction were analysed (see Section 6.4 for more details).

i) Thiosulfate as reducing agent

Unlike the oxidation part of the wet scrubber, SO_2 was not present in the simulated exhaust gas. The encounter between thiosulfate with NO and NO_2 gases can be simplified by Equation 7.8:

$$aS_2O_3^{2-}(aq) + bNO(g) + cNO_2(g) \rightarrow dNO_2^- + eNO_3^- + fN_2(g) + gSO_3^{2-} + hSO_4^{2-} \quad \dots (7.8)$$

where the integers *a* to *h* represent the unknown coefficients of the various reactants. Similar to the case of the oxidation half height scrubber, the *L/G* ratio was also kept constant for all the experimental runs carried out, thereby keeping the mass transfer rate between the gas-liquid boundaries constant and allowing for the changes to be attributed to chemical reaction kinetics. The rate of reaction for Equation 7.8 can be represented by the rate of change of the main thiosulfate reductant, as shown in here:

$$Rate = -\frac{d[S_2O_3^{2-}]}{dt} = -\frac{d[NO]}{dt} = -\frac{d[NO_2]}{dt} = k_2[S_2O_3^{2-}]^x[NO]^y[NO_2]^z \quad \dots (7.9)$$

where k_2 refers to the rate constant and *x*, *y* and *z* refers to the exponents of $S_2O_3^{2-}$, NO and NO_2 respectively. Similar to the previous case, it was assumed that CO_2 did not interact with the reducing agent but was removed purely by absorption with water.

The starting thiosulfate concentration in the reducing wet scrubber was varied and the thiosulfate concentration in the aqueous phase with time is shown in Figure 7-7. As the concentration of thiosulfate with time appeared to linear, the reaction shown in Equation 7.9 was assumed to be zero order, i.e., the exponents *x*, *y* and *z* are all zero. The following is obtained:

$$Rate = -\frac{d[S_2O_3^{2-}]}{dt} = k_2 \quad \dots (7.10)$$

where k_2 has a unit of mol/L.s. Rearranging and integrating both sides of the above equation would eventually yield the following:

$$[S_2O_3^{2-}]_t = -k_2t + [S_2O_3^{2-}]_0 \quad \dots (7.11)$$

where $[S_2O_3^{2-}]_0$ is the initial concentration of thiosulfate at time 0s. It can be seen that Equation 7.11 is a linear equation ($y = mx + c$), with $[S_2O_3^{2-}]_t$ as the *y*-axis, $-k_2$ as the gradient of the slope, *t* being the *x*-axis and $[S_2O_3^{2-}]_0$ as the *y*-intercept. Hence, if this reaction is zero-order, the change of thiosulfate concentration with time in Figure 7-7 would be linear as well. The linear equations, linear regression values (R^2) and reaction rate constants, k_2 obtained from Figure 7-7 are shown in Table 7-5. It can be seen that the linear regression values obtained were

satisfactory, suggesting a decent fit of the experimental data with the linear trendline and this reaction was indeed zero order.

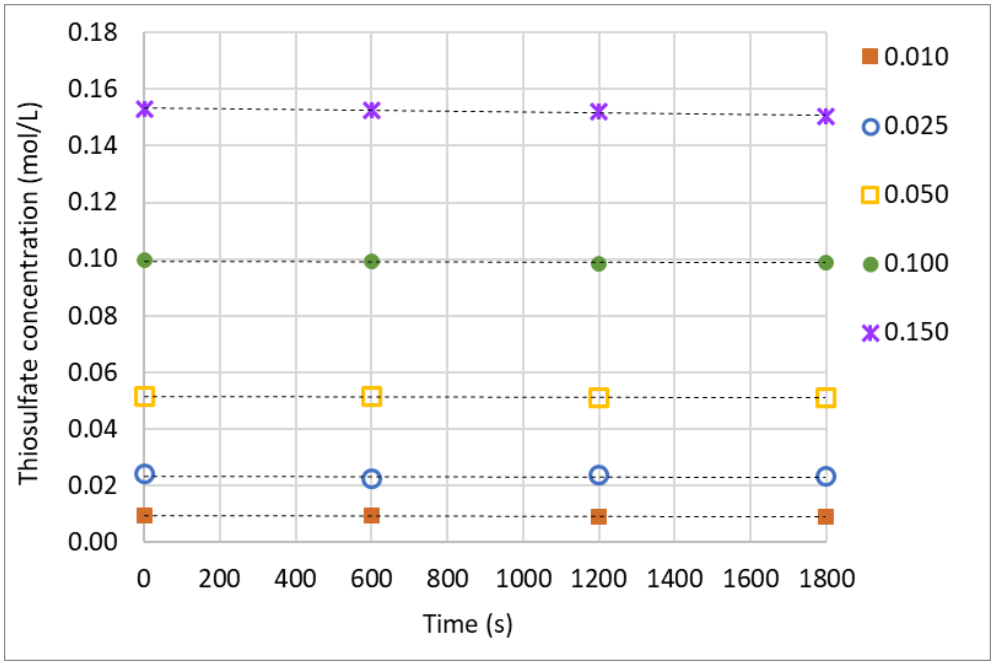

Figure 7-7: Thiosulfate concentration in the aqueous phase with time, in the half height reduction wet scrubber, with variation in thiosulfate starting concentration (M).
Experimental conditions described in Table 6-2 (Set 3).

Table 7-5: The linear equations, linear regression values (R^2) and reaction rate constants obtained from adding a linear trendline to the thiosulphate concentration versus time graph in Figure 7-7, with variation in starting thiosulfate concentration.

$[S_2O_3^-]_0$ (M)	Equation	R^2	k_2 (mol/L.s)
0.010	*y = -3.503E-07x + 0.0095*	0.9952	3.503×10^{-7}
0.025	*y = -3.660E-07x + 0.0241*	0.9996	3.660×10^{-7}
0.050	*y = -3.790E-07x + 0.0516*	0.9392	3.790×10^{-7}
0.100	*y = -3.383E-07x + 0.0995*	0.9959	3.383×10^{-7}
0.150	*y = -1.354E-06x + 0.1532*	0.9458	1.354×10^{-6}

Table 7-6: The rate of change of NO and NO_2 removal, with variation of thiosulfate starting concentration.
Experimental conditions described in Table 6-2 (Set 2). Refer to Appendix D for more details in calculation methods used.

$[S_2O_3^{2-}]_0$ (M)	$\frac{d[NO]}{dt}$ (mol/L.s)	$\frac{d[NO_2]}{dt}$ (mol/L.s)
0.010	2.156×10^{-7}	1.082×10^{-6}
0.025	1.966×10^{-7}	1.120×10^{-6}
0.050	2.194×10^{-7}	1.256×10^{-6}
0.100	2.660×10^{-7}	1.184×10^{-6}
0.150	2.008×10^{-7}	1.010×10^{-6}

Since the reaction was zero-order, the reaction rate constant, k_2, is also equivalent to the rate of reaction. The obtained rate of reaction at different starting thiosulfate concentration were compared to the rates of change of NO and NO_2 removal (Table 7-6) and shown in Figure 7-8. In this system, NO_2 gas was the dominant pollutant as it was present at a much higher concentration compared to NO. Looking at the rate of change of NO_2, it can be seen that it was several times higher than the reaction rate obtained from thiosulfate consumption.

This was in accordance with expectations for two reasons – firstly, even without any thiosulfate present, about 30% of NO_2 could be absorbed by water via Equations 4.7 and 4.8 (Figure 6-17). Secondly, each mole of thiosulfate was expected to react with anywhere from 2 to 8 mols of NO_2, according to the stoichiometry of the reaction (Equations 5.6 and 5.7). As such, the rate of change of NO_2 removal was expected to be several times higher than rate of reaction derived from thiosulfate consumption. Therefore, the reaction rates estimated in the exercise here can be considered to be reasonable, up to the thiosulfate starting concentration of 0.10M. Beyond this concentration, a spike in the reaction rate can be seen (0.15M). This was probably due to the precipitation issue encountered at high thiosulfate concentrations (as discussed in Section 6.4.1), causing the calculated reaction rate to be inaccurate.

The reaction of thiosulfate with NO and NO_2 appeared as zero-order mostly likely because thiosulfate was a very stable reducing agent and was consumed at a very slow rate, as discussed previously in Section 6.4. As the amount of starting thiosulfate present in scrubbing liquid would be considerably larger, the rate of thiosulfate change would appear flat as the gradient is very small (Figure 7-7). This would cause the reaction to appear as zero-order where the concentration of thiosulfate in the system did not seem to affect the rate of reaction much. As for NO and NO_2 gases, the reaction would appear to be zero-order to these two reactants as well

because there were present in greater excess and continually replenished in the inlet throughout the entire duration of the experiment.

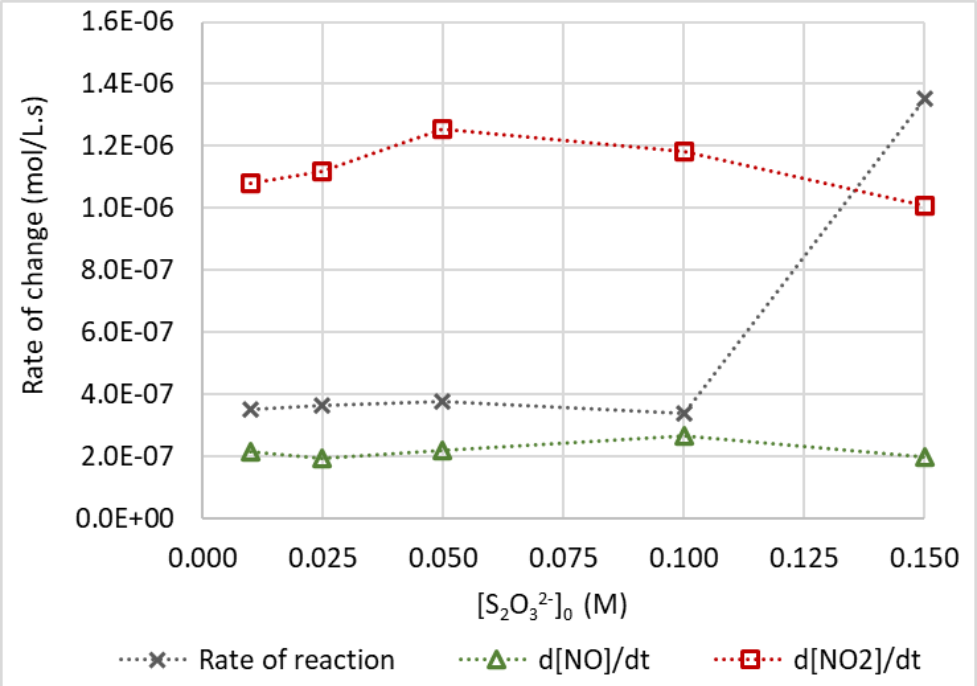

Figure 7-8: The rate of change of NO and NO_2 removal compared with the calculated reaction rate, with variation thiosulfate concentration.
Experimental conditions described in Table 19 (Set 3).

Therefore, the reaction rate, k_2, can be represented by Equation 7.10. Unlike the case of chlorite previously where the reaction rate was at least correlated to the starting concentration of chlorite, the reaction rate here does not appear to be significantly affected by the thiosulfate starting concentration, up to the concentration of 0.10M. However, it should be noted that in a different experimental setting, this reaction may not appear as zero-order, especially if the starting thiosulfate concentration is lower or the amount of scrubbing liquid used per reaction batch is smaller.

ii) Sulfite as reducing agent

The rate of reaction using sulfite as the reducing agent for the removal of NO and NO_2 in the wet scrubber was examined here. Replacing the thiosulfate with sulfite, the rate of reaction can be represented here in Equation 7.12:

$$Rate = -\frac{d[SO_3^{2-}]}{dt} = -\frac{d[NO]}{dt} = -\frac{d[NO_2]}{dt} = k_3[SO_3^{2-}]^x[NO]^y[NO_2]^z \qquad \dots (7.12)$$

where k_3 refers to the rate constant and x, y and z refers to the exponents of SO_3^{2-}, NO and NO_2 respectively. The change of sulfite concentration with time was plotted for both the case with and without stabilisation by formaldehyde and shown in Figure 7-9. Unlike the previous two

cases when chlorite or thiosulfate was used, it can be clearly seen that the change of sulfite concentration with time was not linear but curved in shape, with the concentration of sulfite slowly reducing to a plateau. This showed that the reactions here cannot possibly be zero-order.

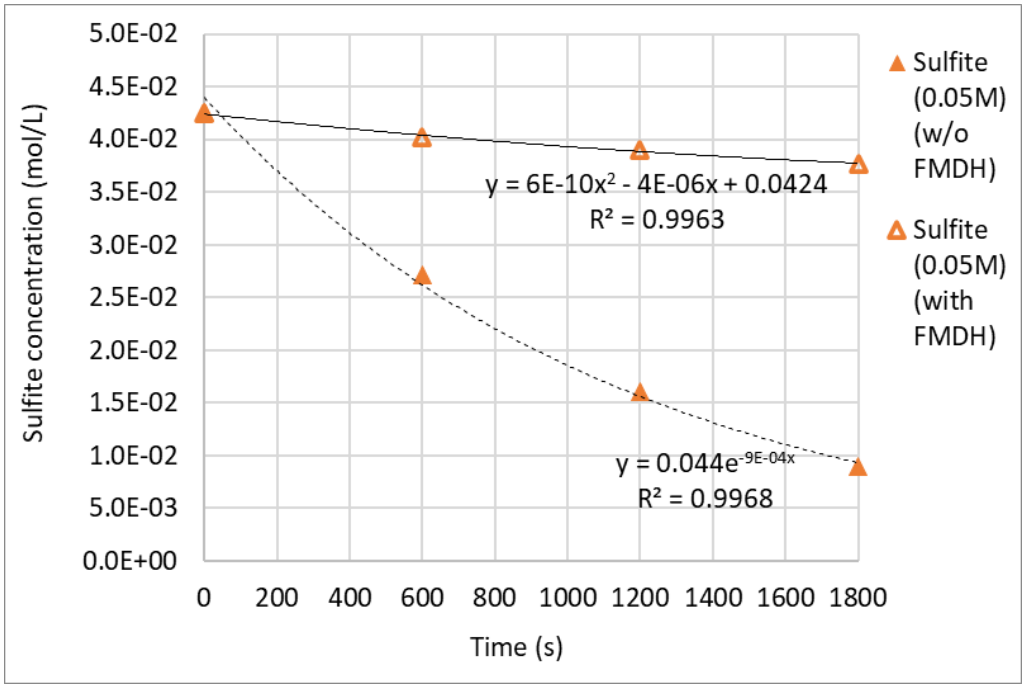

Figure 7-9: Sulfite concentration in the aqueous phase with time, in the half height reduction wet scrubber, with and without formaldehyde stabilisation. *Experimental conditions described in Table 6-2 (Set 5).*

Assuming a first-order reaction, the exponent *x* would be 1 while *y* and *z* would remain as zero, and the following can then be obtained:

$$Rate = -\frac{d[SO_3^{2-}]}{dt} = k_3[SO_3^{2-}] \qquad \ldots (7.13)$$

where k_3 has a unit of 1/s. Rearranging and integrating both sides of the above equation will yield the following:

$$\frac{d[SO_3^{2-}]}{[SO_3^{2-}]} = -k_3 \mathrm{dt}$$

$$\int_{[SO_3^{2-}]_0}^{[SO_3^{2-}]_t} \frac{1}{[SO_3^{2-}]} d[SO_3^{2-}] = -\int_{t_0}^{t} k_3 dt$$

where $[SO_3^{2-}]_0$ is the initial concentration of sulfite at the initial time 0s.

$$ln[SO_3^{2-}]_t - ln[SO_3^{2-}]_0 = -k_3 t$$

$$ln[SO_3^{2-}]_t = -k_3 t + ln[SO_3^{2-}]_0 \qquad \ldots (7.14)$$

It can be seen that Equation 7.14 is linear ($y = mx + c$), with $ln[SO_3^{2-}]_t$ as the y-axis, $-k_3$ the gradient of the slope, t the x-axis and $ln[SO_3^{2-}]_0$ as the y-intercept. Therefore, if the reaction shown in Equation 7.12 is first order, the plotting of the experimental data in the form of Equation 7.14 would yield a straight line with k_3 as the gradient. This plot was carried out and shown in Figure 7-10, with linear trendlines fitted to check for linearity.

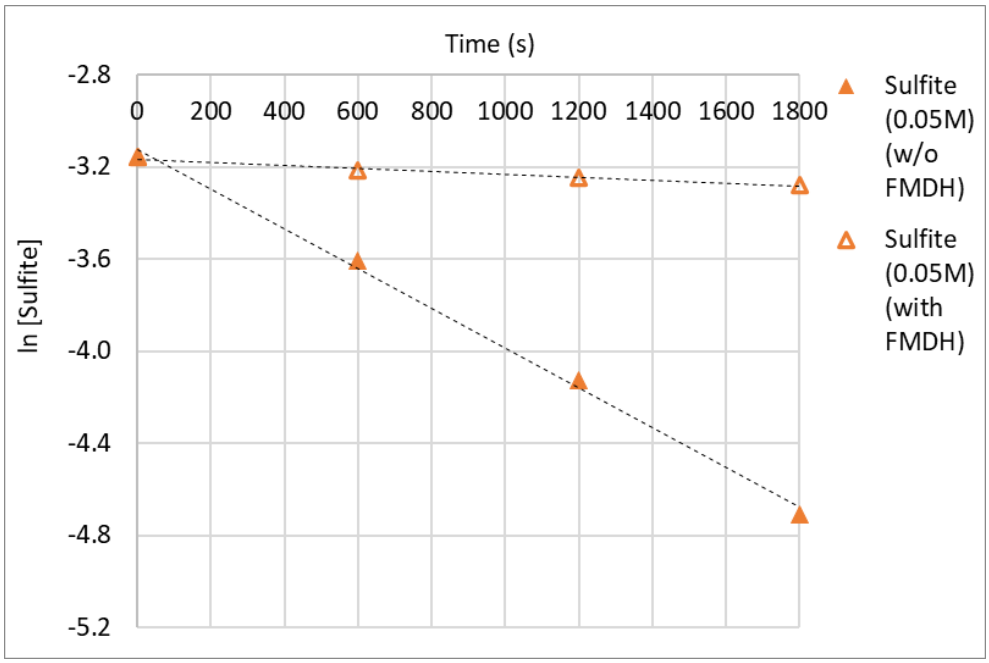

Figure 7-10: The natural logarithm of sulfite concentration in the aqueous phase with time, in the half height reduction wet scrubber.
Experimental conditions described in Table 6-2 (Set 5).

The linear equations, linear regression values (R^2) and rates of reaction, k_3 obtained from Figure 7-10 are shown in Table 7-7. As the fitting of the natural logarithm data to a straight line was satisfactory, it can be assumed that this reaction appeared to be first-order with respect to sulfite. For first-order reactions, the reaction rate can be obtained by the multiplication of the rate constant with the actual concentration of sulfite at a specific time ($[SO_3^{2-}]_t$). These values were calculated and shown in Table 7-8.

Table 7-7: The equation, linear regression value (R^2) and reaction rate constant obtained from adding a linear trendline to the natural logarithmic value of sulfite concentration versus time graph in Figure 7-10.

$[SO_3^-]_0$ (M)	**Equation**	**R^2**	**k_3 (1/s)**
0.05 – w/o formaldehyde	*y = -8.637E-04x - 3.1238*	0.9969	8.637×10^{-4}
0.05 – with formaldehyde	*y = -6.480E-05x - 3.1653*	0.9842	6.480×10^{-5}

Table 7-8: Calculation of the reaction rate of sulfite, obtained by the multiplication of the rate constant that was obtained with the $[SO_3^{2-}]_t$.

Time	*Without stabilisation*			*With stabilisation*		
	k	**$[SO_3^{2-}]$**	**Reaction rate**	**k**	**$[SO_3^{2-}]$**	**Reaction rate**
(s)	**(1/s)**	**(mol/L)**	**(mol/L.s)**	**(1/s)**	**(mol/L)**	**(mol/L.s)**
0	8.637×10^{-4}	0.0426	3.678×10^{-5}	6.480×10^{-5}	0.0425	2.751×10^{-6}
600	8.637×10^{-4}	0.0271	2.339×10^{-5}	6.480×10^{-5}	0.0403	2.609×10^{-6}
1200	8.637×10^{-4}	0.0161	1.391×10^{-5}	6.480×10^{-5}	0.0390	2.526×10^{-6}
1800	8.637×10^{-4}	0.0090	7.775×10^{-5}	6.480×10^{-5}	0.0377	2.443×10^{-6}

The reaction rate of sulfite obtained in Table 7-8 were compared with the rate of change of NO and NO_2 removal with time during the reaction (Table 7-9) and plotted in Figure 7-11. It can be seen that for the case of sulfite without formaldehyde stabilisation, the reaction rate as determined by sulfite consumption was significantly above the rate of removal of NO and NO_2 gases. This was likely because most of the sulfite was lost through oxidation instead of reacting with the gas pollutants, as shown in Section 6.4.4. The rate of decomposition reduced with time as the concentration of sulfite in the system dropped over time. For the case of sulfite with formaldehyde stabilisation, it can be seen that the reaction rate as determined by sulfite consumption was much closer to the rate of removal of NO and NO_2. With stabilisation, the loss of sulfite to oxidation by the presence of O_2 in air could not be ruled out but this would be much less significant compared with the case without formaldehyde stabilisation.

Table 7-9: The rate of change of NO and NO_2 removal for sulfite reducing agent with and without formaldehyde stabilisation.
Experimental conditions described in Table 6-2 (Set 2). Refer to Appendix D for more details in calculation methods used.

Sulfite stabilisation	$\frac{d[NO]}{dt}$	$\frac{d[NO_2]}{dt}$
	(mol/L.s)	**(mol/L.s)**
Without formaldehyde	-2.057	-1.571E-06
With formaldehyde	-1.568	-1.499E-06

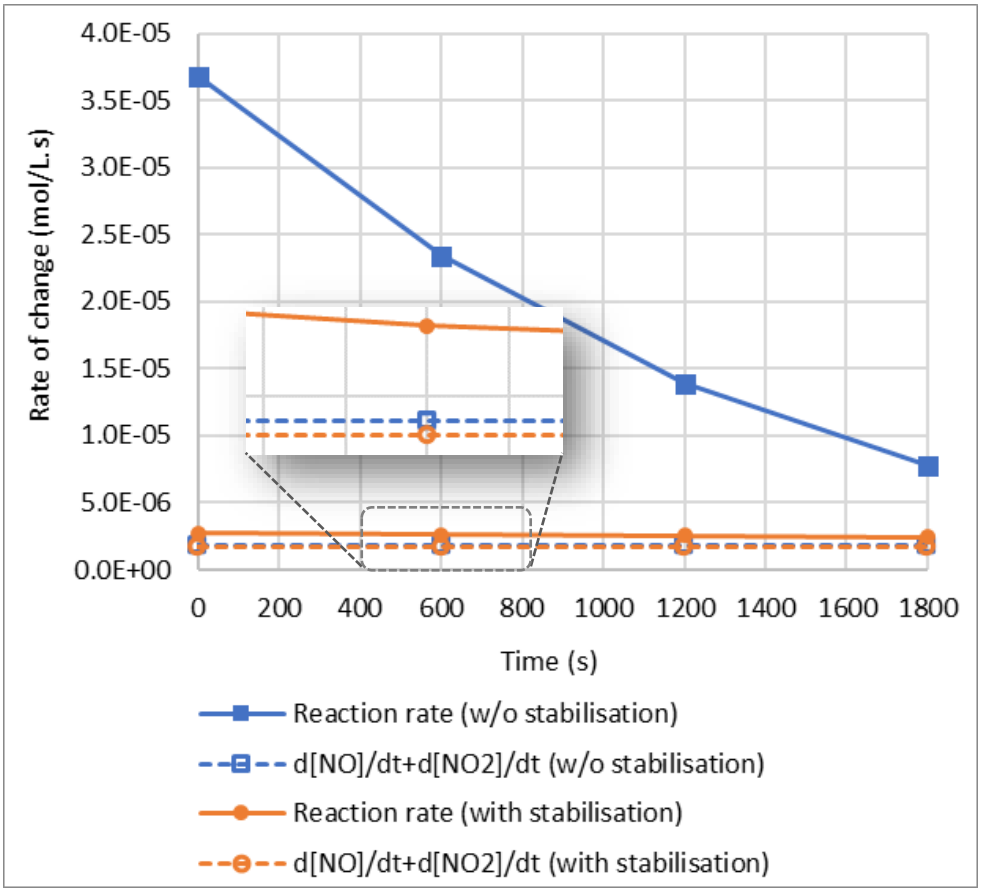

Figure 7-11: Comparison between the calculated reaction rate from sulfite consumption and the rate of change of NO and NO_2 gases, with and without formaldehyde stabilisation.
Experimental conditions described in Table 6-2 (Set 5).

7.2. Mass transfer considerations

In this section, the mass transfer characteristics of the full height wet scrubbers for both the oxidation only and oxidation and reduction in series systems were analysed (see Sections 6.5 and 6.6 for experimental data). In this analysis, the two-film theory for absorption followed by chemical reaction was applied as both SO_2 and NO were expected to undergo chemical reactions in the liquid film after diffusing past the gas-liquid interface (*Perry's Chemical Engineer's Handbook*, 2007). For both the full height wet scrubbers, when the *L/G* ratio was varied, all other parameters such gas concentrations, temperature and pH were kept constant. As such, it was assumed that changes in the rate of reaction were mostly affected by mass transfer instead of reaction kinetics. This would be especially true as the *L/G* ratio was reduced – with increasing gas flowrates and constant liquid flowrates, the reaction would increasingly be limited by the transfer of gases between the gas film and liquid film boundaries instead of the rates of chemical reactions taking place.

7.2.1. Full height scrubber with oxidation only

The average amount of gaseous pollutant being removed during reaction (in mol/s) were plotted against the *L/G* ratio and shown in Figure 7-12. It can be seen that highest rate of change was attributed to NO, followed by SO_2, which corresponded with their input gas concentrations in the simulated exhaust gas composition. The NO_2 that was removed in the system was formed from the oxidation of NO within the wet scrubber, as there was no NO_2 present in the simulated exhaust gas entering the system. The calculation methods and assumptions made can be found in Appendix E.

The overall rate of mass transfer of gas A through the gas film into the liquid film and subsequently entering into the bulk liquid can be represented by the following equation (*Coulson and Richardson's Chemical Engineering*, 2017):

$$N'_A = K_G(P_{AG} - P_{Ae}) = K_L(C_{Ae} - C_{AL}) \qquad \dots (7.15)$$

Where N_A' is the overall rate of mass transfer of gas A (mol/area.time), K_G is the overall gas phase coefficient, K_L is the overall liquid phase coefficient, P_{AG} is the partial pressure of gas A in the bulk gas, C_{AL} is the concentration of A in the bulk liquid, P_{Ae} is the partial pressure of gas A in equilibrium with C_{AL} and C_{Ae} is the concentration of A in liquid in equilibrium with P_{AG}.

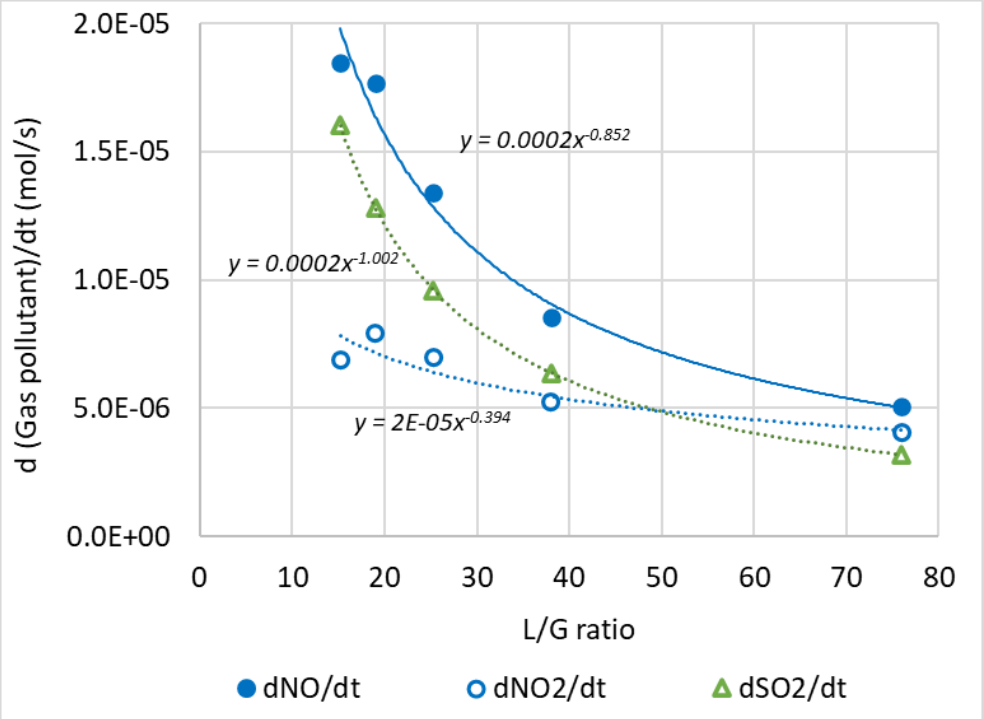

Figure 7-12: Change in amount of gas pollutant removed with time (averaged value) at different L/G ratio, using the full height oxidation only wet scrubber. *Experimental conditions described in Table 6-2 (Set 7).*

Mass transfer of sulfur dioxide

With a high Henry's Law constant of $1.3 \times 10^{-2}\ \frac{mol.m^3}{Pa}$ (Table 4-4) and from the observation that complete absorption in the wet scrubber was achieved for almost all experimental runs conducted here, SO_2 was considered to be a highly soluble gas. When diffusing across the gas-liquid interface, it would encounter a much lower resistance in the liquid phase compared to the gas-phase, which suggest that it would be gas phase controlled. The equation obtained from the trendline of the rate of mass transfer of SO_2 from Figure 7-12 was combined with Equation 7.15 to obtain the following:

$$N'_{SO_2}A = K_{G(SO_2)}A\left(P_{SO_2,G} - P_{SO_2,e}\right) = 0.00024481x^{-1.002}\ \left(\frac{mol}{s}\right) \qquad \ldots (\ 7.16\ )$$

where *x* represents the *L/G* ratio and *A* represents the total area where the mass transfer took place.

$$K_{G(SO_2)}A = 0.00024481x^{-1.002}/\left(P_{SO_2,G} - P_{SO_2,e}\right)$$

The concentration of SO_2 at 500ppmv is equivalent to 0.02047 $\frac{mol}{m^3}$ and $P_{SO_2,e}$ was assumed to be zero due to the high solubility of SO_2 and large liquid reservoir use ($P_{SO_2,e} \approx C_{SO_2,L} \approx 0$). The following can therefore be obtained:

$$K_{G(SO_2)}A = 9.771E^{-03}x^{-1.002}$$

$$\frac{1}{K_{G(SO_2)}A} = 83.61076x^{1.002} \qquad \ldots (\ \ 7.17\ \ )$$

Equation 7.17 was plotted on a graph (Figure 7-13, see data for full height wet scrubber with oxidation only). The experimental data points for SO_2 removal were also converted accordingly to this form and plotted on the graph. It can be seen that the experimental data closely fitted the calculated equation, showing that the latter was a good approximation for the overall mass transfer coefficient.

Another observation that can be made is that the overall gas phase mass transfer coefficient, K_{GA}, was inversely proportional with the *L/G* ratio – when the *L/G* ratio was lowered (gas flowrate increased), K_{GA} would increase, implying that the mass transfer of SO_2 gas into the liquid phase was improved. The increase of gas flowrate could have intensified the turbulence in the system, thereby increasing mixing and lowering the gas-film resistance (Wang *et al.*, 2015).

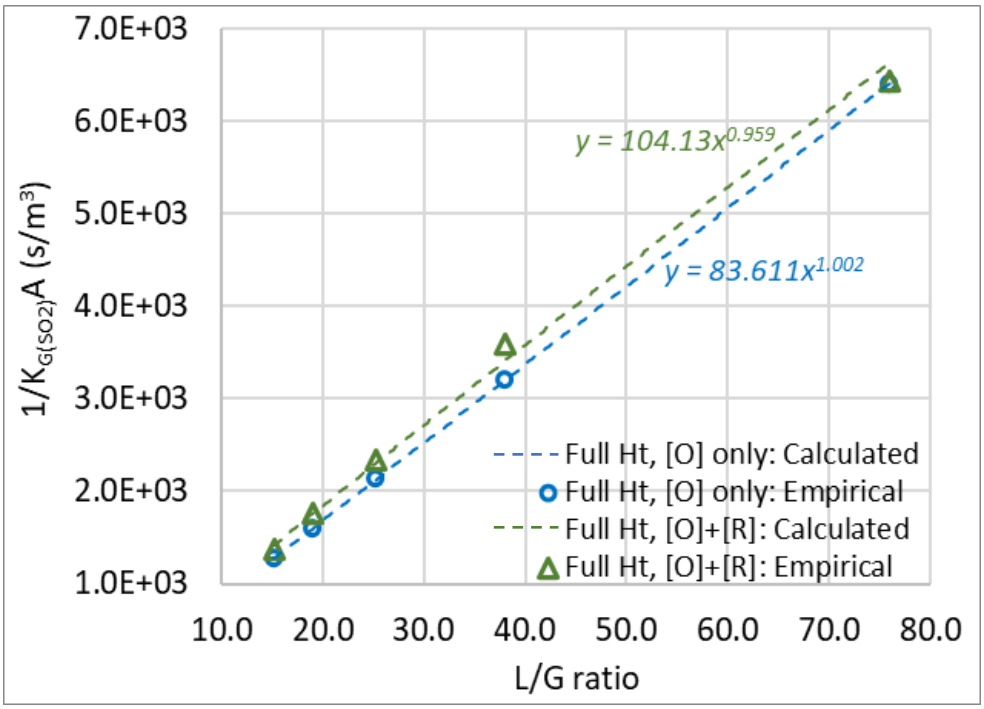

Figure 7-13: The relationship between the overall gas phase mass transfer coefficient for SO_2 and *L/G* ratio,with variation in the full height wet scrubber arrangement.
Experimental conditions described in Table 6-2 (Set 7-8).

Mass transfer of nitric oxide

Unlike SO_2, NO gas is a highly insoluble gas. As such, when diffusing across the gas-liquid interface, it would encounter a much lower resistance in the gas phase compared to the liquid phase, suggesting it would be liquid-phase controlled instead. The equation obtained from the trendline of the rate of mass transfer of NO obtained from Figure 7-12 was combined with Equation 7.15 to give the following:

$$N'_{NO} = K_{L(NO)}A\left(C_{NO,e} - C_{NO,L}\right) = 0.00020105x^{-0.852}\ \left(\frac{mol}{s}\right) \qquad \ldots (\ 7.18\ )$$

where *x* represents the *L/G* ratio and *A* represents the total area where the mass transfer took place.

$$K_{L(NO)}A = 0.00020105x^{-0.852}/\left(C_{NO,e} - C_{NO,L}\right)\ \left(\frac{mol}{s}\right)$$

As NO is a highly insoluble gas, it was assumed that $C_{NO,L} \approx 0$. Using the Henry's Law constant of NO gas ($1.9 \times 10^{-5}\ \frac{mol.m^3}{Pa}$, see Table 4-4), the concentration of $C_{NO,e}$ was calculated to be at 1.7327 x 10^{-06} mol/L, based on the NO inlet gas of P_{NO} = 900ppmv in the simulated exhaust gas (more details in Appendix F). Therefore, the following can be obtained:

$$\frac{1}{K_{L(NO)}A} = 8.61825E^{-03}x^{0.852}\ (\frac{s}{mol}) \qquad \ldots (7.19)$$

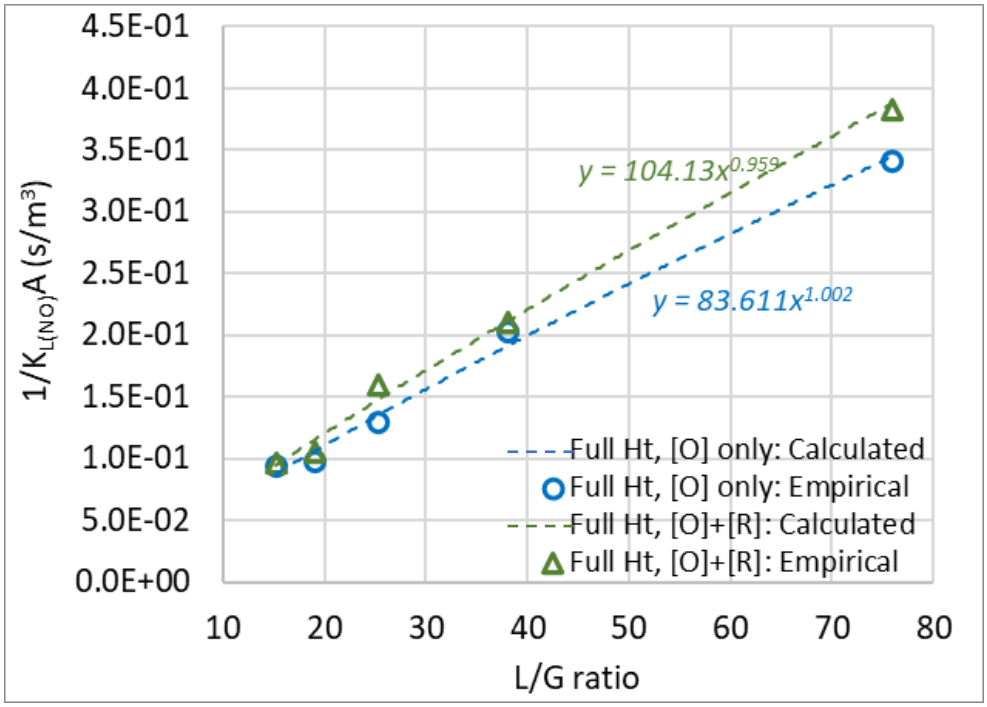

Figure 7-14: The relationship between the overall liquid phase mass transfer coefficient for NO and *L/G* ratio,with variation in the full height wet scrubber arrangement.
Experimental conditions described in Table 6-2 (Set 7-8).

Equation 7.19 was plotted on a graph (Figure 7-14, see data for full height wet scrubber with oxidation only). The experimental data points for NO removal were also converted to a similar form and included in the plot. It can be seen that the experimental data fitted the calculated equation quite well, which indicated that the latter was a good approximate for the relationship between the mass transfer rate of NO with the *L/G* ratio. Similar to the case of SO_2, the rate of mass transfer of NO was inversely proportional to the *L/G* ratio. There was due to the possibility that increasing gas flowrate (decrease of *L/G* ratio) also increased the amount of turbulence and mixing across both sides of the gas-liquid interface, thereby lowering not only the gas film resistance but also the liquid film resistance.

Mass transfer of nitrogen dioxide

Nitrogen dioxide gas is more soluble in water than NO but less soluble than SO_2. Comparing the Henry's Law constants of the 3 gases (Table 4-4), in can be seen that the solubility of NO_2 lied much closer to NO instead of SO_2. As such, for the mass transfer consideration here, NO_2 was treated similarly with NO and liquid-phase control was assumed. Therefore, the equation

obtained from the trendline of the rate of mass transfer of NO_2 in Figure 7-12 could be combined with Equation 7.15 to give the following:

$$N'_{NO_2} = K_{L(NO_2)}A\left(C_{NO_2,e} - C_{NO_2,L}\right) = 0.000022899x^{-0.394}\ \left(\frac{mol}{s}\right) \qquad \ldots (\ 7.20\ )$$

where x represents the L/G ratio and A represents the total area where the mass transfer took place. Since there was no NO_2 in the inlet exhaust gas, the partial pressure of NO_2 (P_{NO2}) in the system was estimated to be at 89.3% of the NO concentration in the inlet of the simulated exhaust gas, based on the average conversion rate of NO to NO_2 in the wet scrubber (more details in Appendix F). Similar to the treatment discussed for NO gas, $C_{NO_2,e}$ was calculated to be 1.5478 x 10^{-06} mol/L and Equation 7.20 can be simplified to the following:

$$\frac{1}{K_{L(NO_2)}A} = 0.06759x^{0.394}\ \left(\frac{s}{mol}\right) \qquad \ldots (\ 7.21\ )$$

Equation 7.21 was plotted on a graph (in Figure 7-15, see data for full height wet scrubber with oxidation only). The experimental data points for NO_2 removal were also converted accordingly to a similar form and included in the plot. It can be seen that the experimental data generally fitted the calculated equation, which indicated that the latter was a good approximate for the relationship between the mass transfer rate of NO_2 with the L/G ratio. Similar to SO_2 and NO, the decrease of L/G ratio due to increasing gas flowrate likely increased the amount of turbulence in the system and lowered both the gas film and liquid film resistance, thereby increasing the mass transfer rate of NO_2 gas.

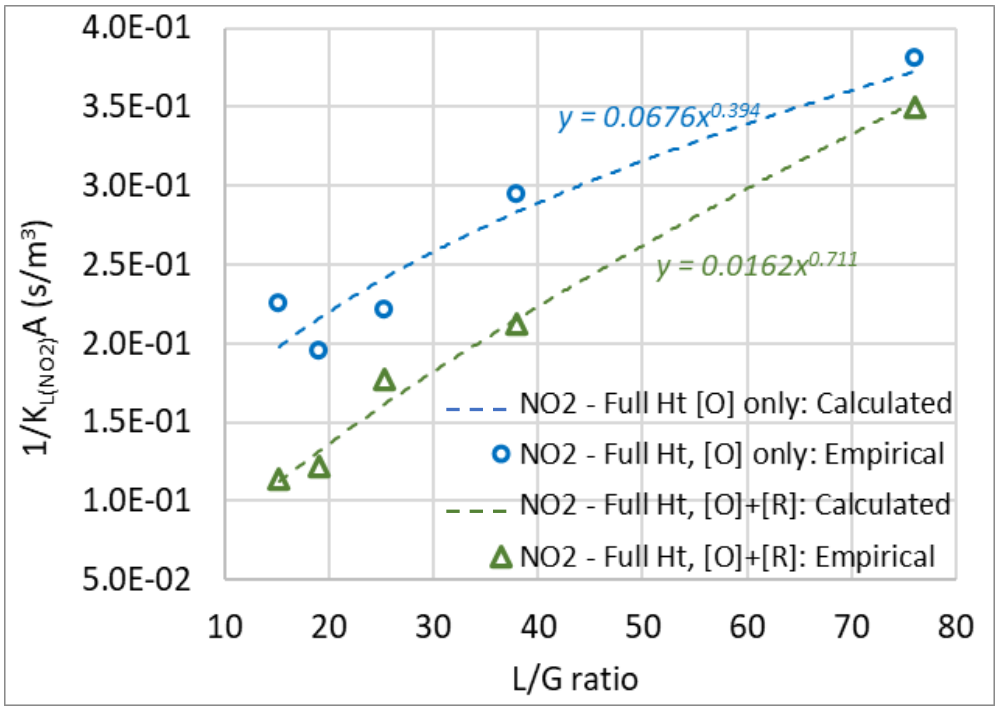

Figure 7-15: The relationship between the overall liquid phase mass transfer coefficient for NO_2 and *L/G* ratio, with variation in the full height wet scrubber arrangement.
Experimental conditions described in Table 6-2 (Set 7-8).

7.2.2. Full height scrubber with oxidation and reduction in series

A similar treatment for the SO_2, NO and NO_2 mass transfer rates was conducted for the full height wet scrubber with oxidation and reduction in series. The change in the amount of gas pollutant with time for this wet scrubber configuration showed a similar profile with the full height wet scrubber system with oxidation only that was discussed in the previous section (Figure 7-16).

Using a similar approach, the following relationships between the mass transfer rates and the L/G ratio were obtained for SO_2, NO and NO_2 (see Equations 7.22 to 7.24). The corresponding comparison between the calculated and empirical data can be found within Figure 7-13, Figure 7-14 and Figure 7-15).

SO_2: $$\frac{1}{K_{G(SO_2)}A} = 104.1296x^{0.959}\ (\frac{s}{mol}) \quad \ldots (7.22)$$

NO: $$\frac{1}{K_{L(NO)}A} = 8.658E^{-03}x^{0.878}\ (\frac{s}{mol}) \quad \ldots (7.23)$$

NO_2: $$\frac{1}{K_{L(NO_2)}A} = 0.016224x^{0.711}\ (\frac{s}{mol}) \quad \ldots (7.24)$$

For the case of SO_2, it can be seen from Figure 7-13 that the overall mass transfer coefficients of SO_2 were very similar between the two wet scrubber configurations, with the full height with oxidation only configuration slightly edging out the configuration with oxidation/reduction. For the case of NO gas (Figure 7-14), it can be seen that the full height wet scrubber with oxidation only configuration performed better, especially at high *L/G* values. Although both full height configurations had the same scrubbing area, the configuration with oxidation only performed better because it had the entire length of the scrubber dedicated to the oxidation of NO while the oxidation/reduction configuration only had the first half of the scrubber as the second half was dedicated to reduction instead. This advantage, however, seemed to slowly erode as the *L/G* ratio was lowered. Low *L/G* values, which had much higher gas flowrates, seem to favour the oxidation of NO in the oxidation/reduction scrubber configuration, probably by increasing turbulence and promoting diffusion across the gas-liquid interface.

The largest difference between the two scrubber configurations occurred for NO_2 removal (Figure 7-15) where the oxidation/reduction setup had a distinct advantage in achieving higher mass transfer for NO_2. The difference in the NO_2 mass transfer here demonstrated the advantage of dedicating the second half of the wet scrubber for reduction. In the oxidation only configuration, the removal of NO_2 was achieved mainly by its absorption in water (Equations 4.7 and 4.8), whereas in the oxidation/reduction configuration, it had the advantage of being

reacted with a reducing agent (via reactions shown in Equations 5.6, 5.7 and 5.10) on top of being absorbed by water.

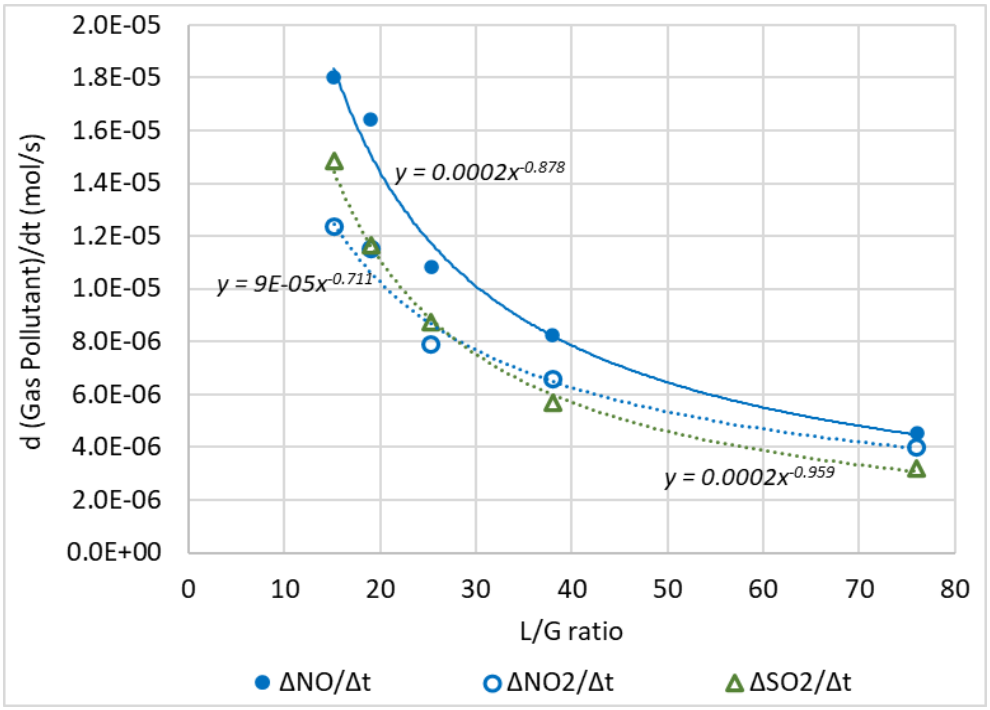

Figure 7-16: Change in amount of gas pollutant removed with time (averaged value) at different *L/G* ratio, using the full height wet scrubber with oxidation and reduction in series.
Experimental conditions described in Table 6-2 (Set 8).

Lowering of the *L/G* ratio by increasing the gas flowrate widened the gulf of the NO_2 mass transfer rate between the two scrubber configurations even further. When *L/G* ratio was high (low gas flowrate), the rate of reaction was probably more influenced by the rate of chemical reaction and the differences between these two scrubber configurations was not very large. As the *L/G* values were decreased (higher gas flowrate), the reaction rate likely shifted to be more limited by mass transfer. The high gaseous flowrate and resulting higher turbulence likely helped with the diffusion of NO_2 gas, allowing it to react faster with the reducing agent and also to be absorbed by water in the oxidation/reduction wet scrubber. Unlike the oxidation/reduction configuration, the oxidation only configuration only had the benefit of NO_2 absorption by water – although the increase in gas flowrate also likely resulted in exactly the same amount of increase in turbulence and mixing, the same rate of NO_2 diffusion may not have been achieved because of the hold-up in the reaction to convert it into another form, since only the absorption route is available. The observations here were entirely consistent with previous discussion in Section 6.5 (Figure 6-28).

7.3. Summary

In this section, the experimental data were analysed from the reaction kinetics and mass transfer and point of view based on the experiments carried out in Chapter 6. Analysis of the reaction kinetics showed that the removal of SO_2 and NO using the chlorite in the oxidation only wet scrubber configuration appeared to be zero order in the experimental conditions used in this study. Most of the chlorite oxidant was consumed for the reaction to oxidise NO to NO_2 and less so for the absorption of SO_2 and NO_2. The equations governing relationship between the reaction rate constant with starting chlorite concentration and pH were postulated here. As for the reduction wet scrubber configuration for the removal of NO and NO_2, the reaction appeared to be zero-order for sodium thiosulfate and first-order when sodium sulfite was used, based on the experimental conditions in this study.

In the mass transfer analysis using the two-film theory, the equations governing the relationships between the overall mass transfer coefficients for SO_2, NO and NO_2 gases with the L/G ratio were postulated based on the experimental data. When comparing the mass transfer of gas pollutants between the full height oxidation only with the oxidation/reduction scrubber configuration, it was shown that the mass transfer rates were slightly higher for SO_2 and NO in the former but was more inferior when it came to NO_2. At low L/G values, the advantage of the oxidation/reduction configuration became more prominent – this was because at high gas flowrates, the overall reaction likely shifted from reaction kinetics controlled to mass transfer controlled. In the oxidation/reduction configuration, after diffusing across the gas-liquid interface into the liquid film, NO_2 could depend on two reaction pathways to ease its passage into the bulk liquid – a reduction reaction with a reducing agent and an absorption reaction with water, resulting in less congestion within this zone. As for the oxidation only configuration, NO_2 that has managed to diffuse into the liquid film could only be cleared by a single pathway involving the absorption with water, resulting in more congestion and making it harder to complete the diffusion process into the bulk liquid.

Chapter 8. Conclusions and Recommendations

8.1. Conclusions

In the first phase of study where a broad range of widely reported substances were systematically compared, it was observed that in the reaction with SO_2, full removal of this pollutant was achieved by nearly all the different types of scrubbing mixtures that were tested. This is because SO_2 gas is very soluble in the aqueous phase. The absorption of SO_2 in the aqueous phase by the various gas-liquid reactions were likely influenced by three factors, namely pH, the ionic concentration in the scrubbing mixture in terms of both its overall ionic strength and concentration of sulphate ions, and oxidation potential. Results from this study showed that an effective scrubbing liquid for the effective removal of SO_2 gas should have high pH or alkalinity, low in ionic strength and sulphate ions, and oxidative in nature.

As for NO_x removal, the effectiveness of various chemical compounds used can be ranked as follows, from least to most effective: Seawater, NaOH, H_2O_2 < NaClO < $KMnO_4$ < $NaClO_2$. The first three, seawater, NaOH and H_2O_2 had little or no effect. NaClO was somewhat effective when the pH was lowered to 9 and below, when the hypochlorite ions shifted to its oxidative form, HOCl. Following that was $KMnO_4$ which was moderately effective, while $NaClO_2$ was the most effective, especially when the pH was below 10. When the L/G ratio was reduced from 100 L/m^3 to 15 L/m^3, $NaClO_2$ showed no changed in its effectiveness for NO_x removal while NaClO and $KMnO_4$ showed a reduction in 80% and 40% respectively. This showed that $NaClO_2$ is the most reactive and suitable for scaling up to industrial size (higher gas flowrate, lower liquid flowrate conditions) while NaClO and $KMnO_4$ would probably require higher concentrations to make up for their limitation.

In the subsequent phase, the application of $NaClO_2$ was further developed in a counter-current wet scrubber using a representative exhaust gas concentration from typical ship exhaust, which included carbon dioxide. It was shown that the presence of CO_2 in the exhaust gas had a positive effect in NO_x removal if the pH of the aqueous solution was in the alkaline range. This was because the absorption of CO_2 decreased the pH and promoted the conversion of the chlorite oxidant into ClO_2, its more powerful variant. However, this may not always be advantageous as ClO_2 is also more volatile and may result in higher reactant losses. When the wet scrubber was operated in the acidic pH range, the presence of CO_2 in the exhaust gas had no effect on SO_2 and NO removal, since CO_2 did not appear to interact with the aqueous phase at all below

pH 7. As for the removal of SO_2, the acidification caused by CO_2 absorption seem to have very little effect based on the conditions of this study, owing to the high solubility of SO_2 in water.

It was also discovered that successful oxidation of NO to NO_2 did not necessarily translate to high NO_x removal as the absorption of NO_2 proved to be a challenge although it is approximately 5 times more soluble than NO in the aqueous phase. Alkalinity was not a factor for the absorption of NO_2 into the aqueous phase as increasing the NaOH concentration had no effect on it. Rather, NO_2 absorption showed an inverse relationship with oxidation potential in this study. Results also showed that increasing the oxidising potential in an attempt to convert NO_2 to higher valency nitrogen intermediates which have higher solubility such as N_2O_3, N_2O_4 and N_2O_5 did not work.

Therefore, the application of reducing agents to improve NO_2 removal was explored and it was shown that sulfite and thiosulfate were both able to remove NO_2. Among these two reducing agents, sodium sulfite was more reactive in reducing NO_2 but it was less stable and likely decomposed in the presence of oxygen. Addition of alkalinity help to improve the effectiveness of sodium thiosulfate. Combining sodium sulfite and sodium thiosulfate at a 1:1 ratio with sodium hydroxide showed some improvement in sodium sulfite stability. By varying the NO and NO_2 ratio in the simulated exhaust gas, it was demonstrated that the presence of NO_2 promoted the removal of NO gas by the thiosulfate reducing agent. This occurrence could have been possible as NO and NO_2 are able to react to form the higher valency N_2O_3 gas, which is slightly more soluble in water.

In the final experimental phase, a novel wet scrubber comprising of an oxidation and a reducing section arranged in series was used. In the oxidizing section, sodium chlorite was used while in the reducing section, both sodium sulfite (Na_2S0_3) and sodium thiosulfate ($Na_2S_2O_3$), were compared. The experimental results demonstrated that this scrubber design is a viable option for the simultaneous removal of SO_2 and NO in ship exhaust gas. This configuration showed clear advantages in comparison with other wet scrubbing processes being studied, in terms of a having less soluble nitrogen formed (especially nitrates) and a low reactant consumption rate. Partial wastewater discharge in the ocean is also possible as the washwater from the reducing half of the wet scrubber has significantly less soluble nitrogen formed and can be discharged to the ocean on a continuous basis without the need for nitrate removal. Partial removal of CO_2 from the exhaust gas was also achieved.

Typically, the usage of chlorine-based oxidants may result in accidental release of chlorine dioxide or chlorine gas from the wet scrubber exhaust. However, this configuration prevents

accidental release of dangerous gaseous compounds as any active chlorine escaping in the gaseous phase from the oxidation half will be removed in the reducing half of the wet scrubber, preventing any accidental discharge into the atmosphere. The results also showed that the precipitation issue of thiosulfate due to the formation of sulfur can be avoided by increasing the operating pH to 12. At this pH, the by-product formed was sulfate ions, thereby requiring just a simple pH adjustment before discharge to the ocean, if necessary. It was shown that although sulfite was around 15% more effective than thiosulfate in NO_2 removal, its consumption rate was more by a factor of 100 when compared to thiosulfate – this was because sulfite was unstable in a high oxygen environment and a significant amount was lost through oxidation to sulfate.

In the final phase, the experimental data were analysed from the thermodynamics, reaction kinetics, mass transfer and mass balance point of view. From the thermodynamics model results, it was learnt that under low redox potential ($E_h > 0V$), the pH of the aqueous phase should be above 8 to avoid the formation of H_2S and 8.4 to avoid the precipitation of sulfur. However, increasing the pH would also favour the formation of soluble nitrogen in the aqueous phase instead of N_2 gas when NO_x was removed. A balance between these two competing interests is therefore needed. Analysis of the reaction kinetics showed that the reaction of SO_2 and NO with chlorite in the oxidation only wet scrubber configuration appeared to be zero order based on the experimental conditions used in this study. As for the reduction wet scrubber configuration for the removal of NO and NO_2, the reaction appeared to be zero-order for sodium thiosulfate and first-order when sodium sulfite was used.

In the mass transfer analysis using the two-film theory, the equations governing the relationships between the overall mass transfer coefficients for SO_2, NO and NO_2 gases with the L/G ratio were postulated based on the experimental data. When comparing the mass transfer of gas pollutants between the full height oxidation only with the oxidation/reduction scrubber configuration, it was shown that the mass transfer rates were slightly higher for SO_2 and NO in the former but was more inferior when it came to NO_2. At low L/G values, the advantage of the oxidation/reduction configuration became more prominent – this was because at high gas flowrates, the overall reaction likely shifted from reaction kinetics controlled to mass transfer controlled. In the oxidation/reduction configuration, after diffusing across the gas-liquid interface into the liquid film, NO_2 could depend on two reaction pathways to ease its passage into the bulk liquid – a reduction reaction with a reducing agent and an absorption reaction with water, resulting in less congestion within this zone. As for the oxidation only configuration, NO_2 that has managed to diffuse into the liquid film could only be cleared by a

single pathway involving the absorption with water, resulting in more congestion and making it harder to complete the diffusion process into the bulk liquid.

8.2. Recommendations for future work

There are several potential areas for future work in order to further the discoveries made here and strengthen the case for commercial application. Firstly, additional optimisation can be done to increase the NO_x removal efficiency and further push the nitrogen by-product formation to favour the harmless N_2 in gaseous form instead of nitrites and nitrates in aqueous form. This will help to allow for more washwater discharge into the ocean for marine-based applications or to avoid having a soluble nitrogen treatment unit for land-based applications.

A more thorough study can be carried out in the washwater discharge from the scrubber. This includes the mixing of the washwater from the oxidation and reduction halves at various ratios, pH adjustments, stability and aging studies, application of wastewater treatment methods, etc, in order to determine the potential and limitations of washwater discharge into the ocean during operation. Any improvement to the amount wastewater percentage that can be discharged safety into the ocean will go a long way to reduce the logistical constraint for on-board operations.

For the oxidation/reduction wet scrubber configuration, non-chemical oxidation methods like UV and ozone can be considered. Partial recirculation of exhaust gas coming out of the oxidation half back to its inlet will help to increase the NO_2 content in this section and may reduce the amount of oxidants needed. On the reducing half, a mixture of thiosulfate with sulfite at an optimised ratio may also yield some increase in efficiency. The wet scrubber height of the oxidation and reduction half also does not need to be exactly the same – variation of the height ratio between these two sections may improve efficiency as well.

Last but not least, the chemical reaction rates and mass transfer data obtained can be used to build a database in Aspen Hysys so that a meaningful simulation can be performed. On the costing aspect, the simple cost analysis performed in Section 4.2.4 can be expanded to the oxidation/reduction scrubber system, to include both capital and operating cost. The Aspen Hysys simulation would not only help with design optimisation but can also provide a more reliable basis for the cost analysis.

References

ABS Advisory On Exhaust Gas Scrubber Systems (2018). American Bureau of Shipping (ABS).

Al-Enezi, G., Ettouney, El-Dessouky, H. and Fawzi, N. (2001) 'Solubility of Sulfur Dioxide in Seawater', *Industrial & Engineering Chemistry Research*, 40(5), pp. 1434-1441.

An, S. and Nishida, O. (2003) 'New Application of Seawater and Electrolysed Seawater in Air Pollution Control of Marine Diesel Engine', *Japanese Society of Mechanical Engineers*, JSME Series B(46), pp. 206-213.

Andreasen, A. and Mayer, S. (2007) 'Use of Seawater Scrubbing for SO2 Removal from Marine Engine Exhaust Gas', *Energy & Fuels*, 21(6), pp. 3274-3279.

Brady, J.E., Russell, J.W. and Holum, J.R. (2000) *Chemistry : Matter and Its changes*. Wiley, New York.

Brogren, C., Karlsson, H.T. and Bjerle, I. (1997) 'Absorption of NO in an Alkaline Solution of KMnO4', *Chemical Engineering & Technology*, 20, pp. 396-402.

Brogren, C., Karlsson, H.T. and Bjerle, I. (1998) 'Absorption of NO in an Aqueous Solution of NaClO2', *Chemical Engineering & Technology*, 21, pp. 61-70.

Chang, M.B., Lee, H.M., Wu, F. and Lai, C.R. (2004) 'Simultaneous Removal of Nitrogen Oxide/Nitrogen Dioxide/Sulfur Dioxide from Gas Streams by Combined Plasma Scrubbing Technology', *Journal of the Air & Waste Management Association*, 54, pp. 941-949.

Chen, L., Lin, K.F. and Yang, C.L. (2011) 'Pilot study of absorption of NO2 with Na2S aqueous solutions', *Environmental Progress & Sustainable Energy*, 30(4), pp. 632-639.

Chien, T.W. and Chu, H. (2000) 'Removal of SO2 and NO from flue gas by wet scrubbing using an aqueous NaClO2 solution', *Journal of Hazardous Materials*, B80, pp. 43-57.

Chien, T.W., Chu, H. and Li, Y.C. (2005) 'Absorption Kinetics of Nitrogen Oxides Using Sodium Chlorite Solutions in Twin Spray Columns', *Water, Air, and Soil Pollution*, 166, pp. 237–250.

Chin, T., Tam, I.C.K. and Yin, C.Y. (2022) 'Comparison of various chemical compounds for the removal of SO2 and NOx with wet scrubbing for marine diesel engines', *Environmental Science and Pollution Research*, 29(6), pp. 8873-8891.

Chu, H., Chien, T.W. and Li, S.Y. (2001) 'Simultaneous absorption of SO2 and NO from flue gas with KMnO4/NaOH solutions', *The Science of the Total Environment*, 275, pp. 127-135.

Chu, H., Chien, T.W. and Twu, B.W. (2003) 'Simultaneous Absorption of SO2 and NO in a Stirred Tank Reactor With NaClO2/NaOH Solutions', *Water, Air, and Soil Pollution*, 143, pp. 337–350.

Corporation, B.V. (2009) 'Chemistry of Aqueous Chlorine', in *White's Handbook of Chlorination and Alternative Disinfectants*. pp. 68-173.

Coulson and Richardson's Chemical Engineering (2017). 7th edn.

Deng, J., Wang, X., Wei, Z., Wang, L., Wang, C. and Chen, Z. (2021) 'A review of NOx and SOx emission reduction technologies for marine diesel engines and the potential evaluation of liquefied natural gas fuelled vessels', *Science of The Total Environment*, 766, p. 144319.

Deshwal, B.R., Lee, S.H., Jung, J.H., Shon, B.H. and Lee, H.K. (2008) 'Study on the removal of NOx from simulated flue gas using acidic NaClO2 solution', *Journal of Environmental Sciences*, 20(1), pp. 33-38.

EGCSA Handbook 2012: A practical guide to exhaust gas cleaning systems for the maritime industry (2012). Exhaust Gas Cleaning Systems Association Association, E.G.C.S. [Online]. Available at: https://www.egcsa.com/wp-content/uploads/EGCSA-Handbook-2012-A5-size-.pdf.

Exhaust Gas Scrubber Washwater Effluent (2011). United States Environmental Protection Agency.

Fang, P., Cen, C.-p., Wang, X.-m., Tang, Z.-j., Tang, Z.-x. and Chen, D.-s. (2013) 'Simultaneous removal of SO2, NO and Hg0 by wet scrubbing using urea+KMnO4 solution', *Fuel Processing Technology*, 106, pp. 645-653.

Fang, P., Cen, C., Tang, Z., Zhong, P., Chen, D. and Chen, Z. (2011) 'Simultaneous removal of SO2 and NOX by wet scrubbing using urea solution', *Chemical Engineering Journal*, 168(1), pp. 52-59.

Feng, S., Xu, S., Yuan, P., Xing, Y., Shen, B., Li, Z., Zhang, C., Wang, X., Wang, Z., Ma, J. and Kong, W. (2022) 'The Impact of Alternative Fuels on Ship Engine Emissions and Aftertreatment Systems: A Review', *Catalysts*, 12(2) [Online] DOI: 10.3390/catal12020138.

Furugen, M., Makino, T., Takahashi, T. and Takikawa, K. (2016) *Exhaust Gas Purification Device For Marine Diesel Engine That Uses Low Quality Fuel, EP3085910A1*.

Gan, Y., Ji, J., Li, K., Dai, W., Ye, L., He, M., Xia, D., Xie, Z., Luo, S., Cao, Y., Liang, W. and Huang, H. (2021) 'Synergistic Effects of a Combination of Vacuum Ultraviolet–Induced Oxidation and Wet Absorption Process on Removal of Nitric Oxide at Room Temperature', *Journal of Environmental Engineering*, 147(10), p. 04021040.

Global Exhaust Gas Scrubber Market 2020 Industry Future Trends, Growth, Strategies, Size, Share, Segmentation, In-depth Analysis Research Report by Foresight to 2025. Available at: https://www.marketwatch.com/press-release/global-exhaust-gas-scrubber-market-2020-industry-future-trends-growth-strategies-size-share-segmentation-in-depth-analysis-research-report-by-foresight-to-2025-2020-04-08.

Gong, P., Li, C. and Li, X. (2020) 'A novel method of pH-buffered NaClO(2)-NaCl system for NO removal from marine diesel engine', *Environ Sci Pollut Res Int*, 27(14), pp. 16963-16971.

Han, Z., Lan, T., Han, Z., Yang, S., Dong, J., Sun, D., Yan, Z., Pan, X. and Song, L. (2019) 'Simultaneous Removal of NO and SO2 from Exhaust Gas by Cyclic Scrubbing and Online Supplementing pH-Buffered NaClO2 Solution', *Energy & Fuels*, 33(7), pp. 6591-6599.

Hao, R., Yang, S., Zhao, Y., Zhang, Y., Yuan, B. and Mao, X. (2017) 'Follow-up research of ultraviolet catalyzing vaporized H2O2 for simultaneous removal of SO2 and NO: Absorption

of NO2 and NO by Na-based WFGD byproduct (Na2SO3)', *Fuel Processing Technology*, 160, pp. 64-69.

Hinke, J. and Hinke, T.V. (2000) *Flue Gas Scrubbing and Waste Heat Recovery, US 6063348*.
Hooper, R.G. (1992) *SOx NOx Pollution Control Composition, US 5,082,586*.
IMO (2015) *2015 Guidelines for Exhaust Gas Cleaning Systems, Resolution MEPC.259(68), Annex 1, Maritime Environmental Protection Committee*. International Maritime Organisation. [Online]. Available at: http://www.imo.org/en/OurWork/Environment/PollutionPrevention/AirPollution/Documents/MEPC.259(68).pdf.

Ito, K. and Naohiro, H. (2015) *Scrrubber, Exhaust Gas Treatment Apparatus, A Ship, JP6188033B2*.

Jin, D.S., Deshwal, B.R., Park, Y.S. and Lee, H.K. (2006) 'Simultaneous removal of SO2 and NO by wet scrubbing using aqueous chlorine dioxide solution', *J Hazard Mater*, 135(1-3), pp. 412-7.

Kaczur, J.J., Iacoviello, S.A. and Duncan, B.L. (1994) *Process for removal of NOx and SOx oxides from waste gases with chloric acid, US 5,328,673A*.

Kim, H., Han, B., Woo, C.G. and Kim, Y. (2018) 'NO<italic>x</italic> Removal Performance of a Wet Reduction Scrubber Combined With Oxidation by an Indirect DBD Plasma for Semiconductor Manufacturing Industries', *IEEE Transactions on Industry Applications*, 54(6), pp. 6401-6407.

Kim, J.-K., Lee, J.-Y., Park, B.-H. and Choi, J. (2016) 'A Study on Ammonia Substitutes in Wet Cleaning Method', *Journal of the Korean Society for Applied Science and Technology*, 33(1), pp. 110-117.

Kuang, M., Wang, J., Hu, X. and Yang, G. (2020) 'Seawater/Seawater Cascade-Scrubbing Desulfurization Performance for Exhaust Gas of a 162-kW Marine Diesel Engine', *Journal of environmental engineering*, 146(1), p. 04019090.

Kuroki, T., Fujishima, H., Otsuka, K., Ito, T., Okubo, M., Yamamoto, T. and Yoshida, K. (2008) 'Continuous operation of commercial-scale plasma–chemical aftertreatment system of smoke tube boiler emission with oxidation reduction potential and pH control', *Thin Solid Films*, 516(19), pp. 6704-6709.

Kurpoka, J. (2011) 'Removal of Nitrogen Oxides From Flue Gases in a Packed Column', *Environment Protection Engineering*, 37(1), pp. 13-22.

Lee, Y., Sung, J.-H., Han, B., Kim, Y.-J. and Kim, H.-J. (2022) 'Minimizing the consumption of reducing agents for NOx removal in a wet scrubber without H2S formation', *Separation and Purification Technology*, 282, p. 120101.

Li, H., Liu, F., Wang, S., Wang, F., Qian, X., Zhang, C., Ma, Y. and Wang, L. (2019) 'Oxidation and absorption of SO2 and NOx by MgO/Na2S2O8 solution at the presence of Cl−', *Fuel Processing Technology*, 194, p. 106125.

Li, S., Huang, W., Xu, H., Liu, K., Wang, J.-n., Sun, Y., Qu, Z. and Yan, N. (2022) 'Enhanced simultaneous absorption of NOx and SO2 in oxidation-reduction-absorption process with a compounded system based on Na2SO3', *Journal of Environmental Sciences*, 111, pp. 1-10.

Lian, Z., Guo, L., Zhang, S., Xiong, Y., Meng, F., Zeng, Y. and Zhong, Q. (2020) 'Using excess O3 to facilitate the NO2 absorption in a sulfite solution: Process conditions and mechanism', *Fuel Processing Technology*, 206, p. 106457.

Liémans, I. and Thomas, D. (2013) 'Simultaneous NOx and SOx Reduction from Oxyfuel Exhaust Gases using Acidic Solutions Containing Hydrogen Peroxide', *Energy Procedia*, 37, pp. 1348-1356.

Lin, C.-Y. (2013) 'Strategies for promoting biodiesel use in marine vessels', *Marine Policy*, 40, pp. 84-90.

Lin, F., Wang, Z., Ma, Q., He, Y., Whiddon, R., Zhu, Y. and Liu, J. (2016) 'N2O5 Formation Mechanism during the Ozone-Based Low-Temperature Oxidation deNOx Process', *Energy & Fuels*, 30(6), pp. 5101-5107.

Liu, M., Gurunthalingam, N.R., Thepsithar, P., Sin, C.W. and Foo, K.S. (2012) *Systems and methods for exhaust gas cleaning and/or ballast water treatment, WO 2012/128721 A2*. WO 2012/128721 A2.

Liu, Y., Wang, Q., Yin, Y., Pan, J. and Zhang, J. (2014) 'Advanced oxidation removal of NO and SO2 from flue gas by using ultraviolet/H2O2/NaOH process', *Chemical Engineering Research and Design*, 92(10), pp. 1907-1914.

Liu, Y., Zhou, J., Zhang, Y., Pan, J., Wang, Q. and Zhang, J. (2015) 'Removal of Hg0 and simultaneous removal of Hg0/SO2/NO in flue gas using two Fenton-like reagents in a spray reactor', *Fuel*, 145, pp. 180-188.

Liu, Y.X. and Zhang, J. (2011) 'Photochemical Oxidation Removal of NO and SO2 from Simulated Flue Gas of Coal-Fired Power Plants by Wet Scrubbing Using UV/H2O2Advanced Oxidation Process', *Industrial & Engineering Chemistry Research*, 50(7), pp. 3836-3841.

Liu, Z.-H., Xu, H.-Z., Li, Y.-B., Luo, Y., Zhang, L.-L. and Chu, G.-W. (2022) 'Nox removal from gas mixture intensified by rotating packed bed with NaClO2 preoxidation', *Chemical Engineering Journal*, 430, p. 132671.

Long, X.-l., Xin, Z.-l., Chen, M.-b., Xiao, W.-d. and Yuan, W.-k. (2007) 'Nitric oxide absorption into cobalt ethylenediamine solution', *Separation and Purification Technology*, 55(2), pp. 226-231.

Marine Scrubber Market Research Report (2022) 'Information by technology (Wet scrubbing, Dry Scrubbing), by fuel (MDO, MGO and Hybrid), by application (Commercial, Offshore, Recreational), and Region - Forecast till 2030'. Available at: https://www.marketresearchfuture.com/reports/marine-scrubber-market-10077 (Accessed: 23 Mar 2023).

McKinlay, C.J., Turnock, S.R. and Hudson, D.A. (2021) 'Route to zero emission shipping: Hydrogen, ammonia or methanol?', *International Journal of Hydrogen Energy*, 46(55), pp. 28282-28297.

Menon, M. and Ovrebo, D. (2014) *Method and Cleaning Apparatus for Removal of SOx and NOx From Exhaust Gas, WO 2014/114735 Al*. WO 2014/114735 Al.
MEPC.72/17/Annex11 (2018) *Initial IMO Strategy on Reduction of GHG Emissions from Ships*. IMO. [Online]. Available at: https://wwwcdn.imo.org/localresources/en/OurWork/Environment/Documents/Resolution%20MEPC.304%2872%29_E.pdf.

MEPC.259(68) (2015) *2015 Guidelines for Exhaust Gas Cleaning Systems*. [Online]. Available at: https://wwwcdn.imo.org/localresources/en/OurWork/Environment/Documents/MEPC.259(68).pdf (Accessed: 23 Jun 2022).

Metcalf & Eddy, Tchobanoglous, G. and Burton, F.L. (1991) *Wastewater Engineering Treatment, Disposal and Reuse*. McGraw-Hill, Inc.

Mohd Noor, C.W., Noor, M.M. and Mamat, R. (2018) 'Biodiesel as alternative fuel for marine diesel engine applications: A review', *Renewable and Sustainable Energy Reviews*, 94, pp. 127-142.

Mok, Y.S. and Lee, H.-J. (2006) 'Removal of sulfur dioxide and nitrogen oxides by using ozone injection and absorption–reduction technique', *Fuel Processing Technology*, 87(7), pp. 591-597.

Mölgaard, S. (2014) *Exhaust gas scrubber, system for treatment of scrubber water and use of an exhaust gas scrubber, EP2738364A1*.

Mondal, M.K. and Chelluboyana, V.R. (2013) 'New experimental results of combined SO2 and NO removal from simulated gas stream by NaClO as low-cost absorbent', *Chemical Engineering Journal*, 217, pp. 48-53.

Nevers, N.D. (2000) *Air Pollution Control Engineering*. 2nd edn. McGraw-Hill International Editions.

Ni, P., Wang, X. and Li, H. (2020) 'A review on regulations, current status, effects and reduction strategies of emissions for marine diesel engines', *Fuel*, 279, p. 118477.

Nitrogen Oxides (NOx) – Regulation 13 (2022). Available at: https://www.imo.org/en/OurWork/Environment/Pages/Nitrogen-oxides-(NOx)-%E2%80%93-Regulation-13.aspx (Accessed: 23 Jun 2022).

Okude, K., Iizuka, H., Kuroda, O., Doi, R., Ogawa, T., Yamashita, H., Azuhata, Y., Kitahara, S., Hiratsuka, N. and Shinotsuka, T. (2001) *Exhaust Gas Cleaning Apparatus and Method For Internal Combustion Engine, US 6,272,848 B1*.

Okude, K., lizuka, H., Kuroda, O., Doi, R., Ogawa, T., Yamashita, H., Azuhata, S., Kitahara, Y., Hiratsuka, T. and Shinotsuka, N. (1999) *Exhaust gas cleaning apparatus and method for internal combustion engine, EP0892159A2*.

Park, H.W., Choi, S. and Park, D.W. (2015) 'Simultaneous treatment of NO and SO2 with aqueous NaClO2 solution in a wet scrubber combined with a plasma electrostatic precipitator', *J Hazard Mater*, 285, pp. 117-26.

Peng, S. (2011) *Process and Device for Simultaneously Desulfurizing and Denitrating the Flue Gas With the Seawater, EP2347816A1*.

Perry's Chemical Engineer's Handbook (2007). 8th edn.

Pu, C.J. and Li, T. (2012) *Desulfurization and denitrification method and treatment device for marine exhaust gas, CN102463015A*.

Resnik, K.P., Yeh, J.T. and Pennline, H.W. (2004) 'Aqua ammonia process for simultaneous removal of CO2, SO2 and NOx', *International Journal of Environmental Technology and Management*, 4, pp. 89-103.

Roy Choudhury, A.K. (2011) '3 - Pre-treatment and preparation of textile materials prior to dyeing', in Clark, M. (ed.) *Handbook of Textile and Industrial Dyeing*. Woodhead Publishing, pp. 64-149.

Sander, R. (2015) 'Compilation of Henry's law constants for water as solvent', *Atmospheric Chemistry and Physics*, (15), pp. 4399-4981.

Schmid, D., Karlström, O., Kuvaja, V., Vuorinen, I., Paavola, M. and Hupa, M. (2022) 'Role of Sulfite Oxidation in NO2 Absorption in a pH-Neutral Scrubber Solution', *Energy & Fuels*, 36(5), pp. 2666-2672.

Shao, J., Yang, Y., Whiddon, R., Wang, Z., Lin, F., He, Y., Kumar, S. and Cen, K. (2019) 'Investigation of NO Removal with Ozone Deep Oxidation in Na2CO3 Solution', *Energy & Fuels*, 33(5), pp. 4454-4461.

Shen, C.H. and Rochelle, G.T. (1998) 'Nitrogen Dioxide Absorption and Sulfite Oxidation in Aqueous Sulfite', *Environmental Science & Technology*, 32(13), pp. 1994-2003.

Silic, F., Silic, G. and Silic, I. (2013) *Emission Control System, WO 2013/033763 Al*. WO 2013/033763 Al.

Skelley, A.P., McMichael, J.C., Cobb Jr, J.T., Rohrer Jr, W.M., Custer II, P.E. and Elsubki, T.M. (1993) *Process For Removing NOx and SOx From Exhaust Gas, US 5,206,002*.

Snoeyink, V.L. and Jenkins, D. (1980) 'Water Chemistry'.

Sulphur oxides (SOx) and Particulate Matter (PM) – Regulation 14 (2022). Available at: https://www.imo.org/en/OurWork/Environment/Pages/Sulphur-oxides-(SOx)-%E2%80%93-Regulation-14.aspx (Accessed: 23 Jun 2022).

Sun, C., Zhao, N., Wang, H. and Wu, Z. (2015) 'Simultaneous Absorption of NOx and SO2 Using Magnesia Slurry Combined with Ozone Oxidation', *Energy & Fuels*, 29(5), pp. 3276-3283.

Tchobanoglous, G., Stensel, H.D. and Burton, F.L. (2013) *Wastewater Engineering: Treatment and Resource Recovery*. 5th edn. McGraw-Hill Education.

Thepsithar, P. (2020) *Alternative Fuels For International Shipping*. Maritime Energy & Sustainable Development (MESD) Centre of Excellence NTU.

Tokumura, M., Baba, M., Znad, H.T., Kawase, Y., Yongsiri, C. and Takeda, K. (2006) 'Neutralization of the Acidified Seawater Effluent from the Flue Gas Desulfurization Process: Experimental Investigation, Dynamic Modeling, and Simulation', *Industrial & Engineering Chemistry Research*, 45(18), pp. 6339-6348.

Toma, Y. (2014) *Exhaust Gas Purification Device and Marine Engine System Provided with Same, WO 2014/041734 A 1*. WO 2014/041734 A 1.

Van Duc Long, N., Lee, D., Kim, M., Kwag, C., Lee, Y., Kang, K., Lee, S. and Lee, M. (2021) 'Desulfurization scrubbing in a squared spray column for a 720 kW marine diesel engine: Design, construction, simulation, and experiment', *Chemical Engineering and Processing: Process Intensification*, 161, pp. 108317-undefined.

Vidal B, F. and Ollero, P. (2001) 'A Kinetic Study of the Oxidation of S(IV) in Seawater', *Environmental Science & Technology*, 35(13), pp. 2792-2796.

Wang, Y., Cao, Q., Liu, L., Wu, Y., Liu, H., Gu, Z. and Zhu, C. (2022) 'A review of low and zero carbon fuel technologies: Achieving ship carbon reduction targets', *Sustainable Energy Technologies and Assessments*, 54, p. 102762.

Wang, Z., Peng, Y., Ren, X., Gui, S. and Zhang, G. (2015) 'Absorption of Sulfur Dioxide with Sodium Hydroxide Solution in Spray Columns', *Industrial & Engineering Chemistry Research*, 54(35), pp. 8670-8677.

Wang, Z., Zhou, J., Zhu, Y., Wen, Z., Liu, J. and Cen, K. (2007) 'Simultaneous removal of NOx, SO2 and Hg in nitrogen flow in a narrow reactor by ozone injection: Experimental results', *Fuel Processing Technology*, 88(8), pp. 817-823.

Wärtsilä (2023) *Methanol as marine fuel – is it the solution you are looking for?* Available at: https://www.wartsila.com/insights/article/methanol-fuel-for-thought-in-our-deep-dive-q-a (Accessed: 30 March 2023).

Wei, J., Luo, Y., Yu, P., Cai, B. and Tan, H. (2009) 'Removal of NO from flue gas by wet scrubbing with NaClO2/(NH2)2CO solutions', *Journal of Industrial and Engineering Chemistry*, 15(1), pp. 16-22.

Weissman, W., Dean, A.M. and Pink, H.S. (2002) *NO to NO2 Conversion Control in a Compression Injection Engine By Hydrocarbon Injection During the Expansion Stroke, EP1038099B1*.

Wen, Z., Shen, H., Li, Y., Wang, Z., Wang, G. and Cen, K. (2019) 'Experimental Study on the NOx Removal by Scrubbing with Urea–H2O2 Solution after NO Partial Preoxidation', *Energy & Fuels*, 33(7), pp. 6600-6605.

WLPGA (2021) *LPG for Marine Engines The Marine Alternative Fuel*. World LPG Association. [Online]. Available at: https://www.wlpga.org/wp-content/uploads/2018/02/LPG-for-Marine-Engines-2017-.pdf.

Wu, J.H.Z. and Dettling, J.C. (2004) *SOx Tolerant NOx Trap Catalyst and Methods of Making and Using The Same, US 6,699,448 B2*.

Wu, Z., Wang, H., Liu, Y., Jiang, B. and Sheng, Z. (2008) 'Study of a photocatalytic oxidation and wet absorption combined process for removal of nitrogen oxides', *Chemical Engineering Journal*, 144(2), pp. 221-226.

Xi, H., Zhou, S. and Zhang, Z. (2020) 'A novel method for the synchronous absorption of SO2 and NO from marine diesel engines', *Fuel Processing Technology*, 210, p. 106560.

Xia, D., Hu, L., He, C., Pan, W., Yang, T., Yang, Y. and Shu, D. (2015) 'Simultaneous photocatalytic elimination of gaseous NO and SO2 in a BiOI/Al2O3-padded trickling scrubber under visible light', *Chemical Engineering Journal*, 279, pp. 929-938.

Xie, W., Xu, C., Zhang, J., Liu, Y., Xi, J., Lv, J. and Gu, Z. (2019) 'Simultaneous Removal of SO2 and NO Using H2O2/Urea Activated by Vacuum Ultraviolet Light in a Pilot-Scale Spraying Tower', *Energy & Fuels*, 33(2), pp. 1325-1333.

Yamasaki, H., Koizumi, Y., Kuroki, T. and Okubo, M. (2019) 'Plasma–Chemical Hybrid NOx Removal in Flue Gas from Semiconductor Manufacturing Industries Using a Blade-Dielectric Barrier-Type Plasma Reactor', *Energies*, 12(14).

Yang, S., Han, Z., Pan, X., Yan, Z. and Yu, J. (2016) 'Nitrogen oxide removal using seawater electrolysis in an undivided cell for ocean-going vessels', *RSC Advances*, 6, pp. 114623-114631.

Yang, S., Pan, X., Han, Z., Zhao, D., Liu, B., Zheng, D. and Yan, Z. (2018) 'Removal of NOx and SO2 from simulated ship emissions using wet scrubbing based on seawater electrolysis technology', *Chemical Engineering Journal*, 331, pp. 8-15.

Ylinen , E. (2007) *Method and Arrangement for Treating the Inlet Air and Exhaust Gases of an Internal Combustion Engine, WO 2007 /045721 Al*. WO 2007 /045721 Al.

Ylinen, E. (2009) *Method and Arrangement for Cleaning the Exhaust Gases of an Internal Combustion Engine, EP1957181B1*.

Your options for emissions compliance: Guidance for shipowners and operators on the Annex VI SOx and NOx regulations (2015). Available at: https://issuu.com/lr_marine/docs/213-35826_your_options_for_emission.

Yu, G., Yu, Q. and Gu, N. (2010) *Method for synchronous desulfurization and denitrification of marine vessel exhaust, CN 101822937A*.

Yu, J. (2015) *Integrated De-SOx and De-NOx Process, WO 2015/176101 A1*. WO 2015/176101 A1.

Zannis, T.C., Katsanis, J.S., Christopoulos, G.P., Yfantis, E.A., Papagiannakis, R.G., Pariotis, E.G., Rakopoulos, D.C., Rakopoulos, C.D. and Vallis, A.G. (2022) 'Marine Exhaust Gas Treatment Systems for Compliance with the IMO 2020 Global Sulfur Cap and Tier III NOx Limits: A Review', *Energies*, 15(10).

Zhang, Z., Xi, H., Zhou, S., Zhou, W. and Shreka, M. (2022a) 'Efficient removal of NOx from simulated marine exhaust by using O3-Na2SO3: Experimental factors and optimization analysis', *Fuel*, 313, p. 122659.

Zhang, Z., Zhou, S., Xi, H. and Shreka, M. (2020) 'A Prospective Method for Absorbing NO2 by the Addition of NaHSO3 to Na2SO3-Based Absorbents for Ship NOx Wet Absorption', *Energy & Fuels*, 34(2), pp. 2055-2063.

Zhang, Z., Zhou, S., Xi, H. and Shreka, M. (2021) 'A prospective absorption system for marine NOx removal from simulated gas using Na2SO3/urea composite absorbents in bubble reactor', *Fuel*, 288, p. 119709.

Zhang, Z., Zhou, S., Xi, H. and Zhou, W. (2022b) 'Study on removing NO from simulated marine diesel engine exhaust gas using the novel composite system of Ozone-Na2SO3/(NH2)2CO', *Chemical Engineering Journal*, 430, p. 132707.

Zhao, M., Kuang, M., Wu, S., Hu, X. and Yang, G. (2021) 'Desulfurization performance of a large - scale marine diesel engine's scrubber with packing scrubbing: Validation of design parameters based on ASPEN PLUS simulations', *Asia-Pacific Journal of Chemical Engineering*, 16(3), pp. undefined-undefined.

Zhao, Y., Guo, T., Chen, Z. and Du, Y. (2010) 'Simultaneous removal of SO2 and NO using M/NaClO2 complex absorbent', *Chemical Engineering Journal*, 160(1), pp. 42-47.

Zhao, Y., Han, Y. and Chen, C. (2011) 'Simultaneous Removal of SO2 and NO from Flue Gas Using Multicomposite Active Absorbent', *Industrial & Engineering Chemistry Research*, 51(1), pp. 480-486.

Zhao, Y., Han, Y., Guo, T. and Ma, T. (2014) 'Simultaneous removal of SO2, NO and Hg0 from flue gas by ferrate (VI) solution', *Energy*, 67, pp. 652-658.

Zhao, Y., Hao, R.-L., Guo, Q. and Feng, Y.-N. (2015a) 'Simultaneous removal of SO2 and NO by a vaporized enhanced-Fenton reagent', *Fuel Processing Technology*, 137, pp. 8-15.

Zhao, Y., Hao, R. and Qi, M. (2015b) 'Integrative process of preoxidation and absorption for simultaneous removal of SO2, NO and Hg0', *Chemical Engineering Journal*, 269, pp. 159-167.

Zhao, Y., Hao, R., Wang, T. and Yang, C. (2015c) 'Follow-up research for integrative process of pre-oxidation and post-absorption cleaning flue gas: Absorption of NO2, NO and SO2', *Chemical Engineering Journal*, 273, pp. 55-65.

Zhao, Y., Hao, R., Yuan, B. and Jiang, J. (2016) 'Simultaneous removal of SO(2), NO and Hg(0) through an integrative process utilizing a cost-effective complex oxidant', *J Hazard Mater*, 301, pp. 74-83.

Zhou, J., Ma, J. and Wang, Z. (2022) 'Experimental study on removal performance of SO2 and NOx in marine exhaust gas using seawater/urea peroxide solution and analysis of ions concentration change', *Fuel Processing Technology*, 227, p. 107133.

Appendices

Appendix A: Conversion of NO_x emission limits from g/kWh to NO_x concentration based on ship engine type

Basis:

- Tier III of MARPOL Annex VI Regulation 13
- Assume that NO_x mainly consists of NO (Molecular Weight of NO = 30.01g/mol)

Case A: Small-Sized Engine, Fast Speed

Engine Specifications:

Model =	Caterpillar 1160	
n =	2800	rpm
Power =	225	hp
=	167.78	kW
Intake CFM =	410	cfm
Exhaust temp =	1050	°F
=	565.6	°C
Exhaust flowrate =	1146	cfm
	1,947.06	m^3/hr

Calculation:

NO_x limit =	2.00	g/kWh (from table)
	335.57	g/hr
	11.18	mol/hr

Using PV=nRT:

For 1 mol of gas, V = 0.068822278 m^3/mol

Therefore,

NO_x limit =	0.77	m^3 of NO/hr
	395.2	**ppm(v)**

Case B: Mid-Sized Engine, Medium Speed

Engine Specifications:

Model =	Caterpillar 3616	
n =	1000	rpm
Power =	6655	hp
=	4962.63	kW
Intake CFM =	14470	cfm
Exhaust temp =	800	°F
=	426.7	°C
Exhaust flowrate =	33763	cfm
	57,363.65	m^3/hr

Calculation:

NO_x limit =	$9n^{-0.2}$	g/kWh
	2.26	g/kWh
	11,219.01	g/hr
	373.84	mol/hr

Using PV=nRT

For 1 mol of gas, V = 0.057425371 m^3/mol

Therefore,

NO_x limit =	21.47	m^3 of NO/hr
	374.2	**ppm(v)**

Case C: Large-Sized Engine, Slow Speed

Engine Specifications:

Model =	MAN B&W 6G95ME-C9.2-TII	
n =	80	rpm
Power =	41,420	kW
Exhaust temp =	260	°C
Exhaust flowrate =	303,668	kg/hr
	10,529,404	mol/hr

Calculation:

NO_x limit =	3.40	g/kWh
	140,828.00	g/hr
	4,692.70	mol/hr

Using PV=nRT

For 1 mol of gas, V = m^3/mol

Therefore,

NO_x limit =		m^3 of NO/hr
	445.7	**ppm(v)**

Appendix B: Estimation of potential CO_2 that can be removed on a two-week journey based on a typical slow-speed, large diesel engine

Engine model	MAN B&W 6G95ME-C9.2-TII (Slow speed, Large-sized engine)
RPM	80
Power	41,420 kW
Exhaust flowrate	303,668 kg/h

Calculations

CO_2 concentration in engine exhaust = 4% wt (assumption)

= 303,668 kg/h x 0.04

= 12,146.7 kg/h

Duration of journey = 2 weeks

= 336 hours

Amount of CO_2 absorbed in wet scrubber = 5%

= 12,146 kg/h x 336 hrs x 0.05 x 1/1000

= **204.1 tonnes**

Amount of CO_2 absorbed in wet scrubber = 6%

= 12,146 kg/h x 336 hrs x 0.06 x 1/1000

= **244.9 tonnes**

Appendix C: Calculation related to discharge of washwater containing nitrate, based on a typical slow-speed large diesel ship engine

Based on MAN B&W 6G95ME-C9.2-TII, specifications indicated in Table 5.

Basis

- 60mg/L normalised for washwater discharge rate of 45 tons/MWh (MEPC.259(68))
- Wet scrubber with [O]+[R] in series configuration is scaled up linearly
- Washwater specification used for comparison is from Experiment E (Figure 26) ([O]:0.06M chlorite, pH 10 / [R]: 0.05M Thiosulfate, pH 12, with packing)

Assumptions

- Washwater discharge volume = 0.3 m^3/MWh
- Molecular weight of air = 28.9647

Washwater discharge volume = $0.3 \frac{m^3}{MWh}$ x $\frac{41420}{1000} MW$

= 12.43 m^3/h

Nitrate discharge limit = 60 mg/L x 45/0.3

= 9,000 mg/L

= 145.16 mol/m^3

Maximum nitrate discharge rate = 145.16 mol/m^3 x 12.43 m^3/h

= **1,803.8 mol/h**

Engine exhaust flowrate = 303668 kg/hr

= 10484071.99 mol/hr

Experimental exhaust flowrate = 50 L/min

= 68.5729 mol/hr

Scale-up factor = 10484071.99/68.5729

= 152,890

Oxidation half washwater

Soluble nitrogen accumulation rate = 12.86 mmol in 30 mins x 152890

= 25.72 mmol/hr x 152890

= **3,932 mol/h**

Reducing half washwater

Soluble nitrogen accumulation rate = 4.27 mmol in 30 mins x 152890

= 8.54 mmol/hr x 152890

= **1,306 mol/h**

Appendix D: Calculation of rate of change of SO_2, NO and NO_2 removal during wet scrubbing

Volume of reaction zone in wet scrubber, $V = \pi r^2 \times Ht$

$= \pi(\frac{0.099m}{2})^2 \times 0.30m$

$= 2.309 \times 10^{-3} m^3$

$= 2.309$ L

Change of concentration of species A with time, $\frac{d[A]}{dt} = \frac{A_{inlet} - A_{t,outlet}}{V \times \Delta t} (\frac{mol}{L.s})$

Where A_{inlet} is the amount of gaseous pollutant A entering the scrubber (in moles), which is fixed, and $A_{t,outlet}$ is amount of gaseous pollutant A existing the scrubber at time *t*. In this study, the data is recorded every 5 seconds so changes with time were tracked quite accurately.

Appendix E: Calculation of rate of change of SO_2, NO and NO_2 gases during wet scrubbing

Change of species A with time, $\frac{dA}{dt} = \frac{A_{inlet} - A_{t,outlet}}{\Delta t} (\frac{mol}{s})$

Where A_{inlet} is the amount of gaseous pollutant A entering the scrubber (in moles), which is fixed, and $A_{t,outlet}$ is amount of gaseous pollutant A existing the scrubber at time *t*. In this study, the data is recorded every 5 seconds so changes with time were tracked quite accurately.

Appendix F: Calculation of concentration of species A in the aqueous phase based on the equilibrium with its partial pressure using Henry's Law

Case: Concentration of NO in the aqueous phase in equilibrium with 900ppmv in gas phase, under atmospheric temperature and pressure.

$$\text{Partial pressure, } P_{NO,e} = 900 \text{ ppmv}$$

$$= \frac{900 m^3 of\ NO}{1 \times 10^6 m^3} \times 101325 Pa$$

$$= 91.19\ Pa$$

$$C_{A,e} = H_{NO} P_{NO,e}$$

$$= 1.9 \times 10^{-5} \frac{mol}{m^3 Pa} \times 91.19 Pa$$

$$= 1.727 \times 10^{-3} \frac{mol}{m^3}$$

$$= 1.727 \times 10^{-6} \frac{mol}{L}$$